COUNTERCURRENT COOLING OF BLOWN FILM

by Kurt F. Strater

A thesis submitted to the Faculty of Graduate Studies
and Research in partial fulfillment of the requirements
for the degree of Master of Engineering

Department of Chemical Engineering

McGill University

Montreal, Quebec

© 1985

ABSTRACT

Many blown film production lines are limited by cooling. Any attempt to increase throughput without exceeding the film blocking temperature must be accompanied by an increase in the amount of cooling. However, higher cooling air flow rates decrease bubble stability, and this is reflected in bubble deformations, corresponding dimensional variations in the film and an unacceptable product. In an attempt to generate stronger cooling conditions, air was drawn down along the film bubble in a countercurrent fashion, that is, in a direction opposite to that of film motion.

The position of cooling air withdrawl was found to have strong affect on bubble stability and shape. Surface temperatures, air velocities and cooling air temperatures were measured along the film bubble, and heat transfer coefficients were calculated as a function of distance from the die in order to compare the cooling ability of this type of operation with that of a standard single lip air ring. Lower surface temperatures were recorded over the portion of bubble where countercurrent cooling air flows were applied than were measured for standard cooling. This suggests the possibility of increasing polymer throughputs by means of countercurrent cooling.

ii

RESUME

Beaucoup de lignes de la production du film soufflé
sont limitées par la refroidissement. Tout essai d'augmenter
la production sans dépasser la température d'encombrement
du film doîtêtre accompagné par une augmentation du total
de refroidissement. Cependant, les rates d'écoutement d'air
refroidissant plus élevées diminuent la stabilité de la
bulle: les resultats sont des déformations dans la bulle,
des variations corréspondantes dans les dimensions du film,
et un produit inacceptable. Dans un effort de créer des
conditions de refroidissemênt plus fortes, l'air est tiré
à la long de la bulle du film dans une manière contre le
courant; c'est à dire, dans une direction qui oppose celle
du mouvement du film.

On a trouvé que la position de la retraite de l'air
refroidissant a eu un influence fort sur la stabilité et
la forme de la bulle. On a mesuré les températures de la
surface, la vélouité de l'air, et la température de l'air
refroidissant à le long de la bulle du film. On a aussi
calculé le coefficient du transport de chaleur comme une
fonction de la distance du coin pour comparet la capabilité
refroidissante de ce type d'opération avec celle du rond
d'air standard d'un bord simple. On a registré les
températures de la surface plus bas sur la portion de la
bulle où on a appliqué de sécoulements d'air refroidissant
contre le courant que celles où on a mé suré la refroidissement
standarde ce veut suggérer une possibilité d'augmenter la
production de polymère par la refroidissement contre le courant.

iii

ACKNOWLEDGEMENTS

TABLE OF CONTENTS

v

LIST OF TABLES

x

xi

LIST OF FIGURES

xiii

xiv

xv

Chapter 1

Introduction

1.1 Statement of Problem and Methods

Polymer processing involves the conversion of polymeric raw materials into finished products. Many processes require the polymer to be melted and pumped into a shape forming device. Extrusion for example, which is an integral part of fiber spinning, blow molding, flat film production and film blowing, is used to melt and convey molten polymer to a forming device. The heart of an extruder is a rotating screw in a heated barrel. Once in the molten state, the polymer is shaped into some form of product. Subsequent cooling solidifies the polymer and determines its final dimensions.

Plastic sheeting, 0.2 to 50 mils thick, is loosely referred to as film by the industry (1,2). Film products have a wide range of applications: thin films, less than 0.5 mils thick, are used by the garment industry as a protective covering, while construction and agricultural uses require a much thicker film, greater than 10 mils. The majority of films produced are in the 1.0 to 4.0 mil

thickness range and are used to fabricate bags or in packaging.

Blown film extrusion is a process to form film. It can be thought of as combining features of blow molding and flat film extrusion. An advantage of the film blowing process over flat film extrusion is that in the former a biaxially oriented film is produced, whereas the latter results in a uniaxially oriented film. Most polymeric film is manufactured by the blown film process.

In film blowing, molten polymer is extruded through a die and formed into a tube. An air duct within the die serves to inflate the tube, while nip rolls, downstream from the die, clamp the tube together, thus containing the air and forming a 'bubble'. Film passing through nip rolls is flattened and processed further to product specifications.

Between die and nip rolls the polymer is cooled and undergoes a phase change from the molten to the solid state. Cooling is accomplished by an air ring situated above the die, which directs air alongside the film bubble, that is in the same direction the film is moving. In one sense, cooling blown film can be thought of as a heat exchanger operating cocurrently. The cooling air is warmed from heat dissipated by the film and the temperatures of the two media approach each other as distance from the die increases. This warmed air tends to collect around the upper portion of

film bubble as the cooling stream slows with increasing distance from the die. Film being produced at temperatures just below the point where the film sticks to itself or 'blocks' when it is flattenned and clamped in the nip rolls can be adversely affected by the accumulation of warmed air in the upper region of the bubble. In summer months this problem is particularly troublesome and in some cases production lines have been slowed to allow for additional cooling.

Commercial blown film production is limited by cooling (2,3). Any attempt to increase throughput without exceeding the blocking temperature must necessarily be accompanied by an increase in the amount of cooling. However, greater quantities of cooling air increase bubble instabilities. This is reflected in deformations in the bubble, corresponding dimensional variations and an unacceptable product. Consequently, it is bubble instabilities which limit the amount of cooling air that may be applied against the bubble.

Many cooling methods have been proposed to increase blown film cooling, while preserving bubble stability. All proposed cooling schemes apply cooling air in a cocurent fashion along the bubble and use elaborate methods to maintain bubble stability. The complexity of these new

cooling methods is reflected in the high cost of the systems that have been commercially produced.

This work explores the possibility of improving blown film cooling by applying cooling air along the film bubble in a different manner. In a new approach to generate stronger cooling conditions, air was drawn down along the bubble in a countercurrent fashion, that is in an opposite direction to that in which the film travels. It was hypothesized that lower film surface temperatures would result with cooling air applied in this manner than under usual cocurrent cooling conditions and that greater cooling would allow for the possibility of an increase in polymer throughput. This work was not intended to be a definitive study on countercurrent blown film cooling, but rather to explore the feasibility of this type of cooling. If greater film bubble cooling was possible with the countercurrent cooling apparatus developed in this work, further research would have to follow in order to optimize the design and evaluate commercial feasibilty.

1.2 The Blown Film Extrusion Process

1.2.1 Description of Process

A schematic of the blown film process is shown in Figure 1.1. A hopper(1) is filled with resin(2), which is the polymeric raw material. A gravitational feed introduces the resin to the extruder(3). The extruder is fundamentally a variably cut screw(4) within a heated barrel(5). In the extruder the resin fills the space between the extruder screw flights and the barrel. As the screw rotates, the resin is compressed and conveyed toward the die(6). The screw is variably cut so that the channel depth diminishes as the resin goes from solid to melt. The mechanical energy derived from turning the extruder screw and shearing the melt supplies heat which, combined with heat from outside sources(8), melts the polymer. The extruder screw acting as a pump, pressurizes the molten material along the final portion of screw flghts. Under this pressure gradiant, melt flows through a connecting arm(7), elbow (8), adapter (9) and into the die. Blown film dies are annular and thus able to form a tubular extrudate. Within the die the polymer melt flows through a small annular gap experiencing, mainly shearing stresses along its course, before emerging from the die.
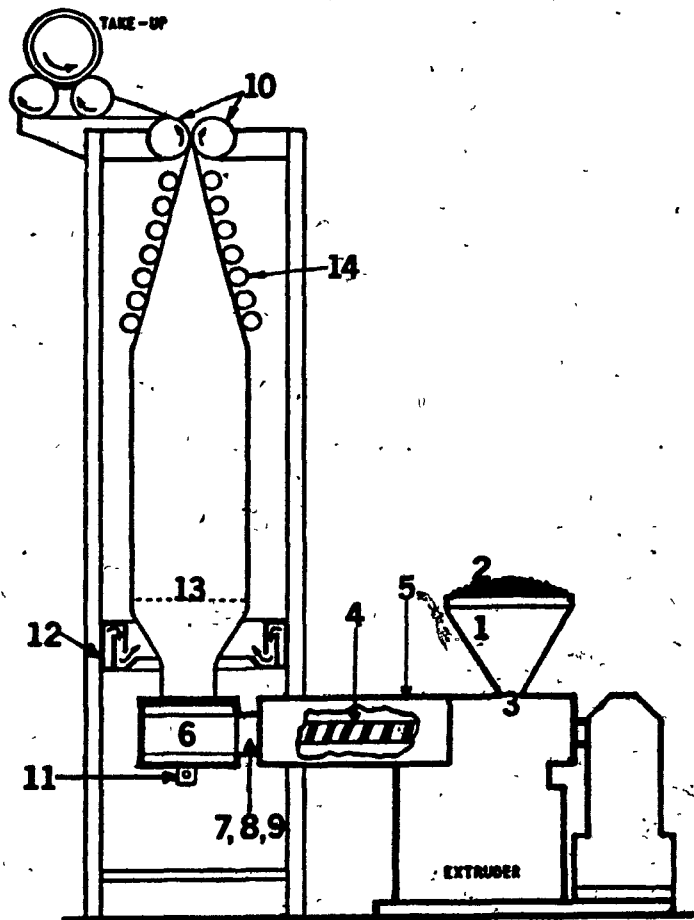
FIGURE 1.1   Diagram Showing the Tubular
             Blown Film Extrusion Process

For start-up, melt oozing from the annular die is bunched and hauled upward through open nip rolls(10). At the same time, air is admitted through an inlet duct(11) in the die distorting the shape of the elongating tube. Once the bunched section of polymer, which may be thought of as the knot of a balloon, passes through the opened nip rolls, the nip rolls are clamped together, trapping the air. Thus, the air within the film tube is contained between die and nip rolls.

Sequential photographs of a start-up procedure are shown in Figure 1.2. Polymer leaving the die is in the molten state and must be cooled before passing through the nip rolls. Insufficiently cooled film will stick together or 'block' when flattened. The temperature at which film blocks is termed the blocking temperature and establishes a lower temperature limit for the cooling process. An air ring(12) located just above the die provides the cooling. From the ring an annular stream of air is directed towards and alongside the bubble in the same direction the film is moving. The air entrains some ambiant air and cools the bubble. Downstream from the die there is a region of the bubble where the molten polymer is solidifying. When extruding a clear resin this demarcation line is white or cloudy and is usually referred to as the 'freeze-' or 'frostline'(13). In Figure 1.3 the frostline is pointed
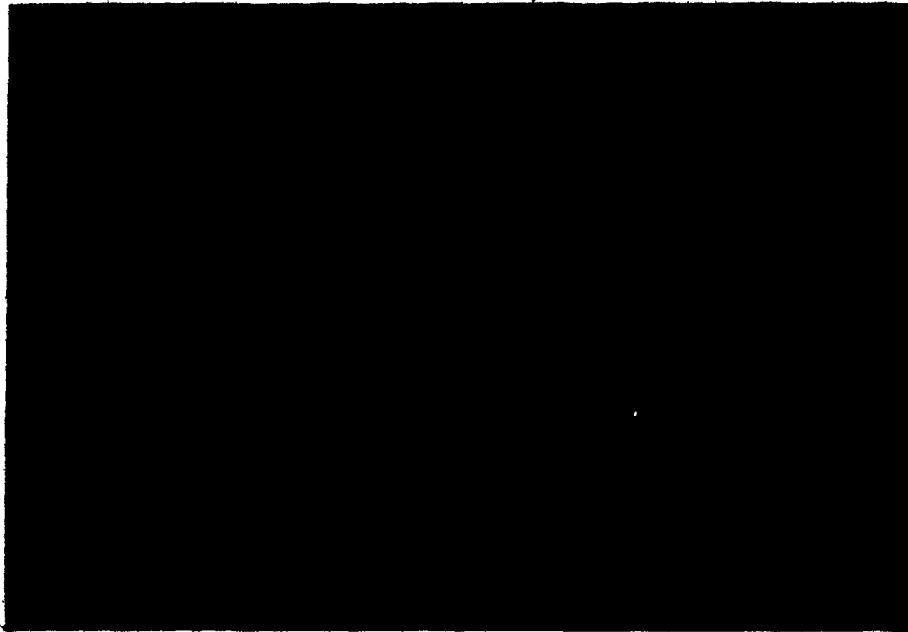
FIGURE 1.2 Start Up Procedure for Forming
a Blown Film Bubble
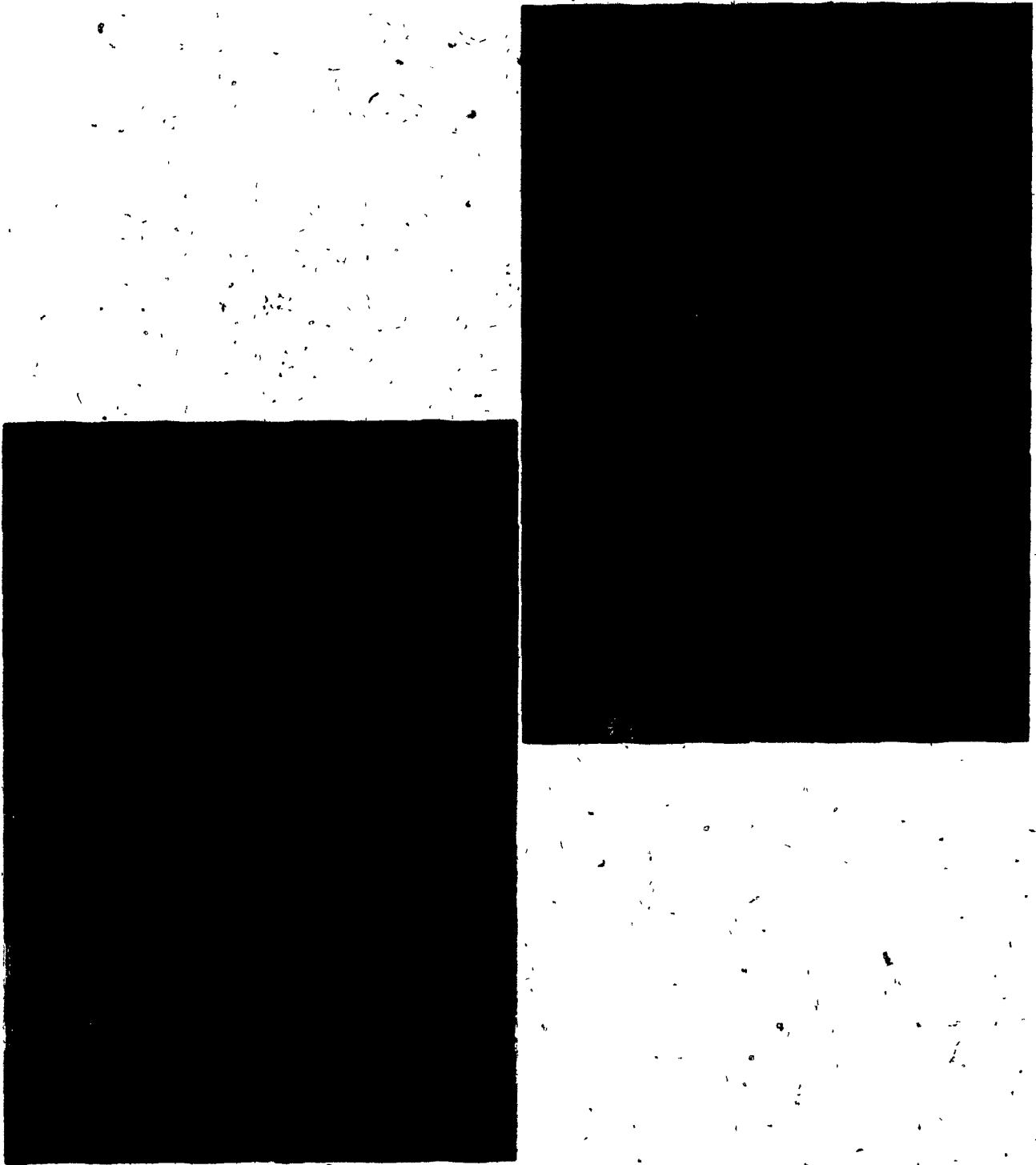
FIGURE 1.2 Start Up Procedure for Forming
a Blown Film Bubble

FIGURE 1.3 Photograph of Film Bubble Neck Region
with Frostline Indicated

out.

Low density polyethylene is a semi-crystalline material and partially crystallizes when cooled. Most of the crystallization occurs in the frostline region, although the amount of crystallization for a given polymer depends on a number of factors such as the rate of cooling, the type of deformation occurring and the magnitude of the deformation.

The tubular film shape is referred to as a 'balloon' or 'bubble'. The amount of air trapped within the bubble directly affects the bubble diameter and therefore the final dimensions of the film. Increases in the amount of air in the bubble cause greater stretching in the transverse direction, the direction normal to the path of film, and lead to larger bubble diameters. The ratio of bubble diameter to die diameter is termed the blow up ratio (BUR), and is commonly used to describe the size of a film bubble. Typical blow up ratios for low density polyethylene range from 2 to 5, while those for linear polyethylene are somewhat higher.

Blow up ratio and film thickness determine the final film dimensions. Film thickness is governed by nip roll speed at a given output. The turning rolls pull the film upward at a greater speed than the melt flows from the die gap. The result is a decrease in film thickness proportional to nip roll rotation. The ratio of die gap

width to final film thickness is termed drawdown. Typical drawdown values are in the 10 to 60 range. Such large values in comparison to blow up ratios indicate that greater stretching occurs in the machine direction, that is the direction in which the film travels, than in the tranverse direction. Also, the stretching being caused by the pulling action of the nip rolls may be thought of as a mainly extensional deformation.

The stretching in the machine direction attributed to the nip rolls and expansion in the transverse direction caused by inflating the bubble all occur in the area between die and frostline. These deformations occur over a relatively small portion of film bubble and in a short time period, while the temperature of the film is dropping rapidly and crystalline regions are beginning to form. The frostline can be thought of as 'freezing' whatever stresses are still present in the film. These so called 'frozen-in-stresses' impart an orientation to the film. Because both machine and transverse direction stretching occur, the orientation is biaxial unlike film produced from a slot die, which is simply pulled in the machine direction. Biaxially oriented films have more balanced properties* than uniaxially oriented films and thus have found more product applications. Blown film anisotropy is discussed more fully

* Film properties with similar values in the two principle blown film directions, that is the machine and transverse directions, are said to be balanced.

in Chapter 8.

Once the bubble is cooled to the solid state, above the frostline region, it is gradually collapsed in a frame(14) and then flattened by nip rolls. The flattened tubular film may be further processed on line for particualr product specifications or simply wound on a wind-up spool for shipping or secondary treatment. Thus, it is easily imagined how tubular blown film extrusion is particularly suitable for bag fabrication.

1.2.2 Independent and Dependent Variables

In blown film extrusion, parameters or variables may be organized into several categories: I) independent variables that are difficult to change; II) independent variables that are readily adjusted; III) dependent variables described with a single value; IV) dependent variables associated with phenomena occurring along the bubble; and V) film properties. Variables divided into these categories are presented in Table 1.1.

Table 1.1: Independent and Dependent Variables in Blown Film Extrusion

    I)   Independent Variables (fixed)

          Extruder power and heating
          Screw design
          Connecting arm, elbow and adapter design
          Die design
          Die gap
          Cooling system design

    II) Independent Variables (adjustable).

          Screen pack
          Extruder and die temperatures
          Screw speed
          Internal air pressure.
          Nip roll speed
          Cooling air temperature
          Cooling air flow rate
          Manner of cooling air application
          Height of countercurrent plenum

    III) Dependent Variables (single-valued)

          Extruder back pressure
          Film output
          Melt temperature
          Blow up ratio
          Layflat width
          Final film thickness

IV) Dependent Variables (position dependent)

Surface temperature
Film thickness
Bubble shape
Air temperature
Air velocity

Heat transfer coefficient
Crystallinity

V) Ultimate Film Properties

Mechanical

Tear resistence
Puncture resistance
Impact resistance
Tensile strength
Yield strength
Elongation percent
Elongation to break
Restrained shrinkage
Free shrinkage
Sonic velocity
Slip
Block

Optical

Haze
Gloss
Birefrigence

Independent variables in Part 1 of Table 1 are related to the design of the blown film equipment used. Part II independent variables are adjustable and depend on the extrusion system controls. Adjustments in control settings correspond to independent variable changes. The last three variables in Part III are exceptions, in that they are related to adjustments of the cooling apparatus.

Dependent variables are the result of a given set of independent variables and reflect occurrences happenning on and near the film surface. Dependent variables have been arranged in two major categories. In the first (Part III), variables that can be specified with a single value are listed. Establishment of these variables, along with adjustable independent variables (Part II), determine operating conditions. Consequently, single-valued dependent variables and adjustable independent variables are routinely reported by technicians. Furthermore, these variables provide a minimum basis of comparison for blown films produced on different extruders with correspondingly different independent variables. The second group of dependent variables (Part IV) are no longer single-valued, rather they depend on position. These variables give a detailed account of the occurrances along the film bubble. What links all the dependent variables together is that they are measured after the independent variables have been

established for a blown film system. The final two dependent variables, heat transfer coefficient and crystallinity, are exceptions to this generalization and must be calculated from other dependent variables and also from a thermal analysis of the polymer.

The most common film properties are listed in Part V. They are determined by industrial tests that have little fundamental physical significance. Their principal value is that they give information directly translatable into film characteristics of interest to the consumer.

Independent and dependent variables are interrelated in a complex manner. A dependent variable can be altered by changing any one of several independent variables. For example film thickness, a dependent variable, responds to changes in internal bubble pressure, nip roll speed and screw speed. Thickness can be affected to a lesser extent by altering die and extruder temperatures and the cooling conditions.

An independent variable change may also affect more than one dependent variable. For example, by increasing the screw speed while holding all other independent variables constant, output, film thickness and melt temperature increase. At the same time the cooling conditions become weaker, resulting in a higher frostline. Less cooling causes the blow up ratio to increase somewhat, thereby

affecting layflat width.

With these complex variable interrelationships, independent variables in any study of the blown film process must be strictly controlled, so that measured differences in dependent variables correspond to changing a particular independent variable. Otherwise, dependent variable measurements are an undistinguishable lumped sum of several independent varible changes. Some researchers have expressed this concern and maintained that only one design variable should be changed in a particular study to obtain meaningful measurements of the effects of the change. (4,5) The variables held constant in this study are discussed in Chapter 3.

Chapter 2

Methods of Cooling Blown Film

Molten plastic, extruded from a die and blown into a bubble, must be cooled before passing between the nip rolls. Cooling is accomplished by blowing air against and along the film bubble. The transition from molten to solid state occurs at the frostline. The frostline height is an indication of the cooling conditions. A lower frostline reflects greater cooling. Cooling conditions ultimately influence film properties, such as crystallinity and optical and mechanical properties. Also, cooling conditions are recognized as the limiting factor to greater throughputs on most blown film extrusion systems. In turn, bubble stability dictates the rate of cooling. Too much cooling causes bubble instabilities and a dimensionally unacceptable product. Thus, the maximum air flow rate which can be applied to the bubble, while controlling bubble stability, is desirable.

2.1 Single Lip Air Rings

Cooling air is directed at the bubble by means of an air ring. The air ring is located just over the die. It consists of several tangental air duct inlets, through which the air is fed by a blower. The swirling air flows through a series of baffles within the air ring, which serve to redirect the flow. In early air ring designs the cooling air was redirected so that it impinged directly on the bubble (6). This air struck the bubble just above the die, where the film is molten and thus easy to deform. To delay the onset of bubble instabilities, guide bars were positioned above the frostline. The guide bars were typically four straight aluminum bars or cardboard cores arranged in a square around the film bubble (7). They succeeded in damping small deformations to within acceptable dimensional limits. Nevertheless, the early cooling systems were limited to use at rather low air flow rates because of bubble instabilities. Thus the cooling conditions restricted output of film.

Improvements in air ring design led to a second generation of air rings that incorporated deflector plates at the orifice openning of the ring. These plates prevented the air stream from impinging directly on the bubble by deflecting it in a more parallel direction. Higher air flow rates were possible with this innovation than with the earlier impinging flow apparatus, as the film bubble was
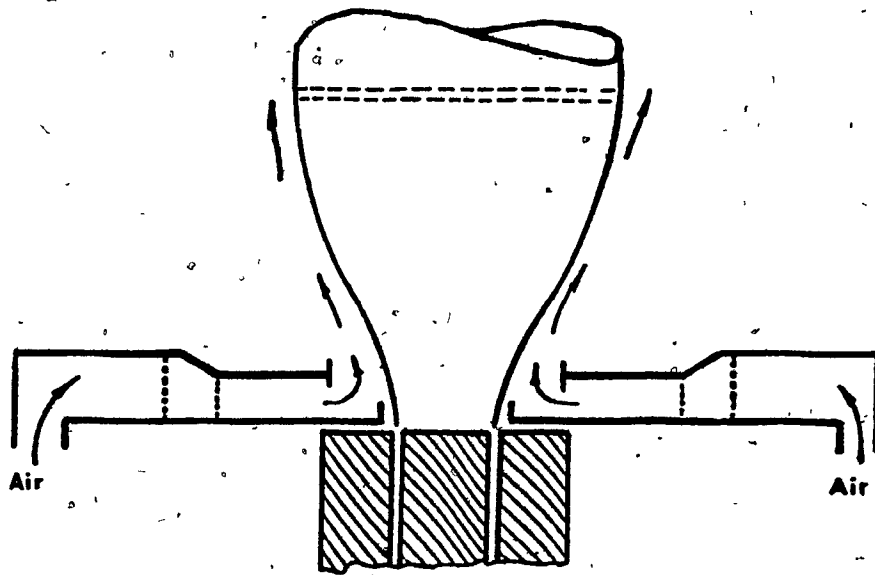
FIGURE 2.1 Single Lip Deflector Plate Air Ring

more stable under this flow. Greater overall cooling resulted, as demonstrated. by outputs larger than those previously obtained (8). A schematic of an air ring incorporating deflector plates is shown in Figure 2.1. This air ring was the industrial standard in blown film extrusion for nearly thirty years.

With this type of air ring air rushing mostly parallel to the film bubble creates a Venturi effect, pulling the film outward. Thus, the leading edge of the lower deflector plate can not be positioned too close to the molten tube nor can the height of the leading edge be too great, or else the expanding bubble will touch the plate. The consequence of these restrictions is a cooling air stream striking the bubble with a fan-type spray. The major velocity components of the air stream are neither perpendicular nor parallel to the bubble surface (9). Although this type of flow contributed to greater outputs than the impinging flow air ring, cooling conditions still controlled throughput (10).

2.1.1 Multiple, Single-Lip Air Rings

Nonuniformities in the die gap, resulting from a non-concentric central die core or weld lines within the die, are reflected in a film product of varying gauge. Gauge variations are not proportional to die gap

nonuniformities, as the thinner portions of film are cooled first; while the thicker sections undergo additional stretching and thus thinnning, before reaching the solid state. However, this self-adjusting process is incomplete and gauge variations persist when the die gap is nonuniform. The resulting film product will naturally have sections with very different properties. The thickness smoothing process, inherent to cooling blown film, was the basis of several cooling system designs to improve film properties (11,12).

An elaborate multi-level cooling scheme was proposed by Ebert et. al. (11) to control the shape of the film bubble. Strict control over film bubble shape and specifically over the neck region shape, would reduce gauge variations and, moreover, control stretching in the machine and transverse directions. This latter claim implies a greater degree of control over orientation of blown films than is now present. A schematic of Ebert's cooling system is shown in Figure 2.2. A low velocity fan-type spray air ring is located just over the die and provides mild cooling. Downstream from the air ring, the tubular film encounters a tiered pressure zone that prevents expansion. In the first portion of the pressure zone, heat is removed from the bubble by applying a slight negative pressure. Contact between the bubble and a roughened wall of the pressure zone occurs, but sticking is prevented by maintaining the wall at a low temperature by

Liquid
Cooled Wall

Expansion

Film
Bubble

Positive
Pressure

Liquid
Cooled Wall

Single Lip
Air Ring

Air

Air
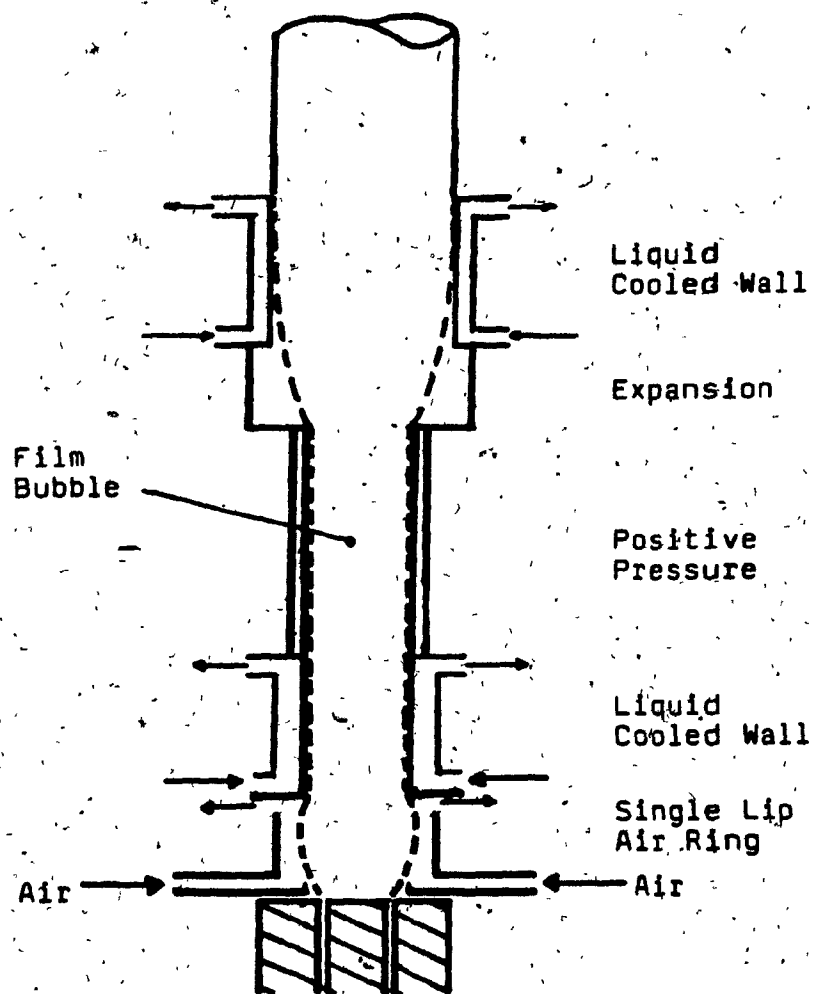
FIGURE 2.2   Cooling System Incorporating
             Elevated Cooling Zone (Reference 11)

circulating cooling liquid through a jacket around this section. The middle section of the pressure zone exerts a positive pressure on the film bubble to prevent expansion and contact with the tube wall. In the final section, the film tube is heated and then suddenly allowed to expand under a controlled environment to provide the 'desired amount of biaxial stretching'. The expanded film bubble contacts a restraining sleeve, which cools the film below its blocking temperature. In this elevated cooling zone, fluid circulating within the sleeve walls maintains the restraining sleeve at a low temperature. The goals of gauge uniformity and stretching control as measured by free shrinkage were only partially realized over a very limited range of blow up ratios (11).

Another method was proposed by Saint Eve et. al. (12) to improve film property balance, as measured by mechanical tests and shrinkage in the machine and transverse directions. In this scheme, bubble shape was controlled by mounting two standard air rings one on top of the other. The space between the two rings was sealed off and a negative pressure gradient applied to partially control bubble shape. The configuration, shown in Figure 2.3, resulted in film with more balanced mechanical properties and improved optical properties than film cooled with a single air ring.
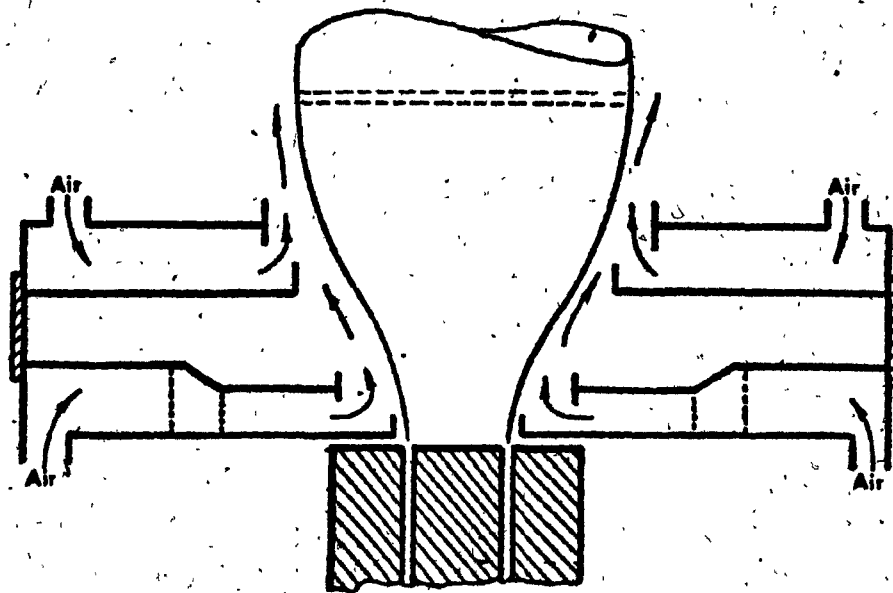
FIGURE 2.3 Stacked Single Lip Air Rings

The stacked air ring configuration of Figure 2.3 allows more air to be directed along the bubble than a single ring does. The stream of cooling air leaving the raised air ring contacts the bubble in an area where some cooling has occurred. Consequently, this partially cooled bubble can withstand larger air flows before bubble instabilities occur. Saint Eve (12) alludes to the possibilty of greater outputs due to stronger cooling conditions with this arrangement over those of a single air ring. However the possibility was not pursued.

An extension of the dual air ring concept is the use of multiple air rings stacked one on top of the other. Several proposals in the literature (13,14,15) incorporate this idea. Each configuration uses a fan-type spray air ring. Between the rings the previously applied air is withdrawn by an outside source. Thus, the film bubble is continuously quenched with new streams of cooling air. It is claimed that lower surface temperatures would result with this cooling system than with a single air ring and that output could be correspondingly increased.

2.2 Dual Lip Air Rings

The classic fan spray air ring and all the variations thereof, still contained a substantial impinging air stream component which limited the amount of air that could be applied to a film bubble. Increasing the air flow rate beyond a certain point caused bubble instabilities. A substantial improvement in blown film cooling technology, occurred by deflecting the cooling air stream in a much more parallel direction than was previously possible. With little or no impinging air stream component, bubble stability could be preserved under much higher flow rates. Earlier attempts to generate highly parallel flow rates were stymied by the Venturi-effect occurrence which drew the film into the deflector plate (9). With the introduction of a secondary air stream, below the contact point between bubble and high flow rate stream, the negative pressure was relieved. Thus, two deflector plates are incorporated in this air ring, and for this reason it is usually referred to as a dual-lip air ring, A schematic of a dual lip air ring is shown in Figure 2.4. The forming cone and adjustable deflector plates are the key to this design. They determine the manner in which air is applied to the bubble. A high volume of air is deflected parallel to the bubble surface by the forming cone. The air stream cools and supports the
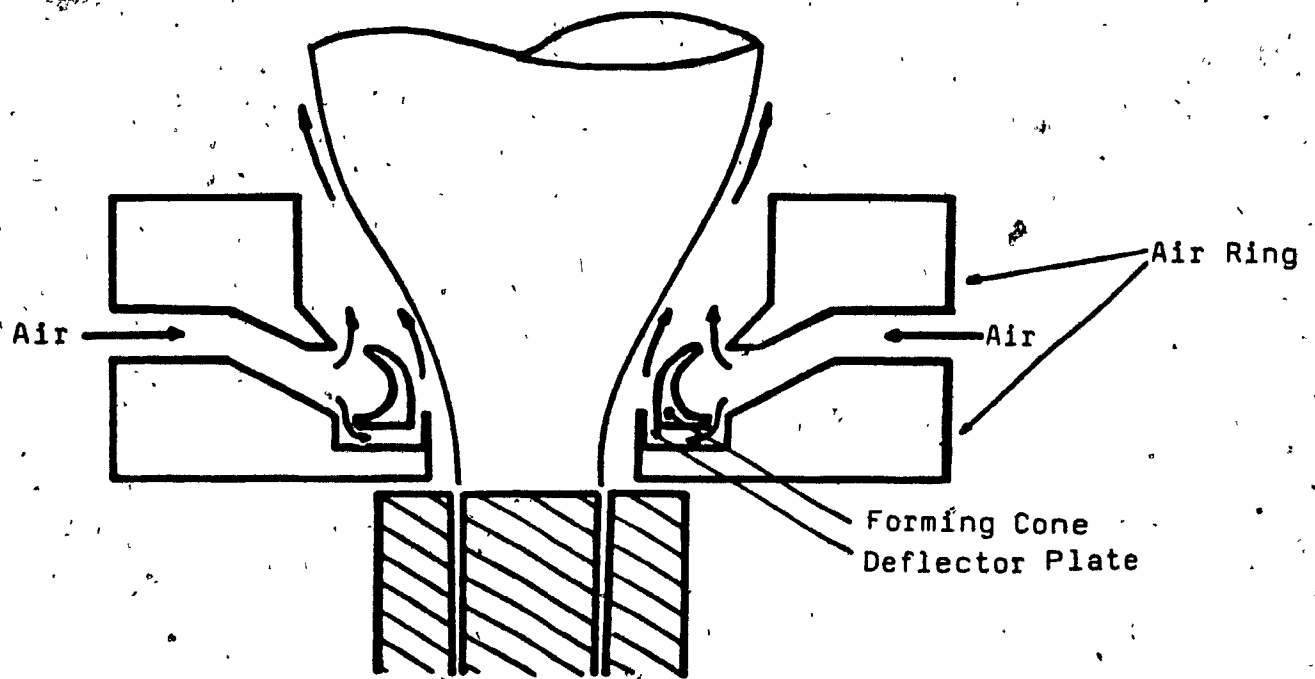
FIGURE 2.4   Dual Lip Air Ring

film bubble. This moving stream creates a negative pressure area between the forming cone and bubble, which is relieved by a secondary air stream introduced upstream from the high volume flow. The secondary stream also acts to partially cool the hottest section of film bubble.

The use of much greater flow rates with a dual lip air ring have resulted in cooling rates fifty percent greater than those of classical fan-type air rings (9,16,17). Greater cooling subsequently lead to sizeable throughput increases (18,19). For example, outputs of low density polyethylene in commercial blown film extruders equipped with a standard air ring are in the 6 to 8 pounds per hour per inch of die circumference range, while with cooling supplied by a dual lip air ring throughputs are in the 9 to 11 range (6). The most significant increases in film output have occurred with linear low density polyethylene and high density polyethylene, which are weaker in extension than low density polyethylene and thus especially susceptible to a fan-type cooling air spray. The parallel air flow from the dual lip ring is less disturbing to these resins weaker in extension (9,20).

A prototype of the commercial dual lip air ring first appeared in 1970 (21). Hinrich's proposal incorporated a conventional air ring housing and a complicated set of

deflector plates. After numerous redirections, the cooling air was applied to the bubble in two general streams. A secondary stream contacted the molten film just above the die, while a larger volume air stream was introduced further downstream, where the bubble had already partially cooled. Comparisons were carried out between this and classical air rings. In each case the maximum air flow rate for a stable bubble was used. Hinrich found that his invention had a greater cooling 'ability', as evidenced by lower bubble frostlines, than the classical air ring. Also the new ring could cool melts emerging from the die at higher temperatures than had previously been possible.

A later dual lip air ring design streamlined the baffles within the housing and reduced the vertical distance between primary and secondary stream introduction (22). Moreover, special attention was paid to the angle at which air streams left the deflector lips. A mostly parallel application of cooling air maintained bubble stability at high flow rates. Comparisons between dual and single lip air rings showed that greater throughputs were achieved using the former apparatus. Another configuration of this invention pictured a second dual lip air ring downstream from the die, so that the issuing air streams contacted the bubble just below the frostline. A solid tubular chamber joined the two dual lip air rings. No comparative tests

were made with this arrangement.

A more recent patent also proposed a stacked air ring configuration (1). In one arrangement, two conventional or classical rings are stacked loosely one on top of the other, very similar to Saint Eve's (12) earlier design, while a second configuration used a dual lip air ring located at the base of the film bubble and a raised conventional air ring. In contrast to Saint Eve's emphasis on improved film property balance, Jones et. al. (1) stressed the large total cooling flows possible with a stable bubble and the corresponding output increases over conventional cooling rings. Comparative tests between the two types of stacked air rings, a conventional air ring, and a dual lip air ring, indicated that the maximum output* was greatest for the dual and single lip air ring combination and smallest for a fan spray conventional air ring. The outputs for the dual lip ring and for the stacked conventional rings lie between these extremes, the former being closer to the single lip conventional air ring and the latter closer to the other stacked ring configuration. These rankings were achieved in processing both LDPE and LLDPE. The difference between maximum outputs was more pronounced for the linear polyethylene.

* On a cooling limited blown film production line, maximum output is realized with the largest cooling flow that maintains bubble stability and cools the film bubble below its blocking temperature.

2.3 State of the Art Cooling System

Over the past ten years, cooling systems have changed greatly and this evolution has led directly to increased outputs. The classic fan-type spray air ring has been almost universally replaced by a dual lip air ring, capable of applying a high volume of air along the film bubble. Air ring manufacturers have marketed services or sold kits to convert classical air rings to dual lip rings by replacing the deflector plates and baffles within the housing (17). New baffle designs are able to redirect tangental air flow towards the bubble with low static pressures. For example, a dual lip air ring typically operates between 3 and 10 inches of static pressure, as measured on a water column gauge, at 150 cfm per inch of die diameter (7). Conversely, a classical air ring with an intricate set of baffles usually operates in the 15 to 30 inch guage range, with much lower flow rates applied along the bubble than in the case of dual lip air rings. Thus, blower horsepower requirements can be reduced with the conversion of a conventional single lip air ring to a dual lip cooling device. Furthermore, the use of dual lip air rings has lead to a plurality of air ring accessories to cover most processing situations encountered. Deflector plates are available in different sizes, so that one air ring housing may be used with several

different dies or, if the ring is raised, accommodate different blow up ratios (20). Forming cones come in various sizes and shapes, to be used for a particular resin or blend (18). Specially machined deflector plate adjustment screws are marketed with claims to decrease the amount of turbulence in the exiting air streams, thereby allowing even higher velocity cooling air flows (17).

Production increases in LLDPE and HDPE resins, which form more 'fragile' bubbles than LDPE, have lead to the development of bubble stabilizing devices. The most recent development is the bubble sizing cage. One model is shown in Figure 2.5. The cage replaces aluminum or cardboard guide bars, which had not been modified since being used in conjunction with the first air rings. These cages are usually located just above the frostline but are equipped to be raised or lowered. A sizing cage contacts the bubble and provides greater control over bubble diameter and more stability by damping oscillations, keeps the bubble centered over the die, and increases heat transfer. The use of sizing cages on LLDPE and HDPE production lines is common.

The term 'cooling system' has taken hold in the industry with more elaborate arrangements of cooling equipment. A schematic of a state of the art blown film cooling system is shown in Figure 2.6. It includes two dual lip air rings, one raised to contact the solid portion of

FIGURE 2.5. Photograph of Bubble Sizing Cage

ELEVATING MECHANISM
FOR SIZING CAGE

SIZING AND STABILIZING CAGE

MOUNTING BRACKETS FOR
SECONDARY AIR RING

PRIMARY AIR RING
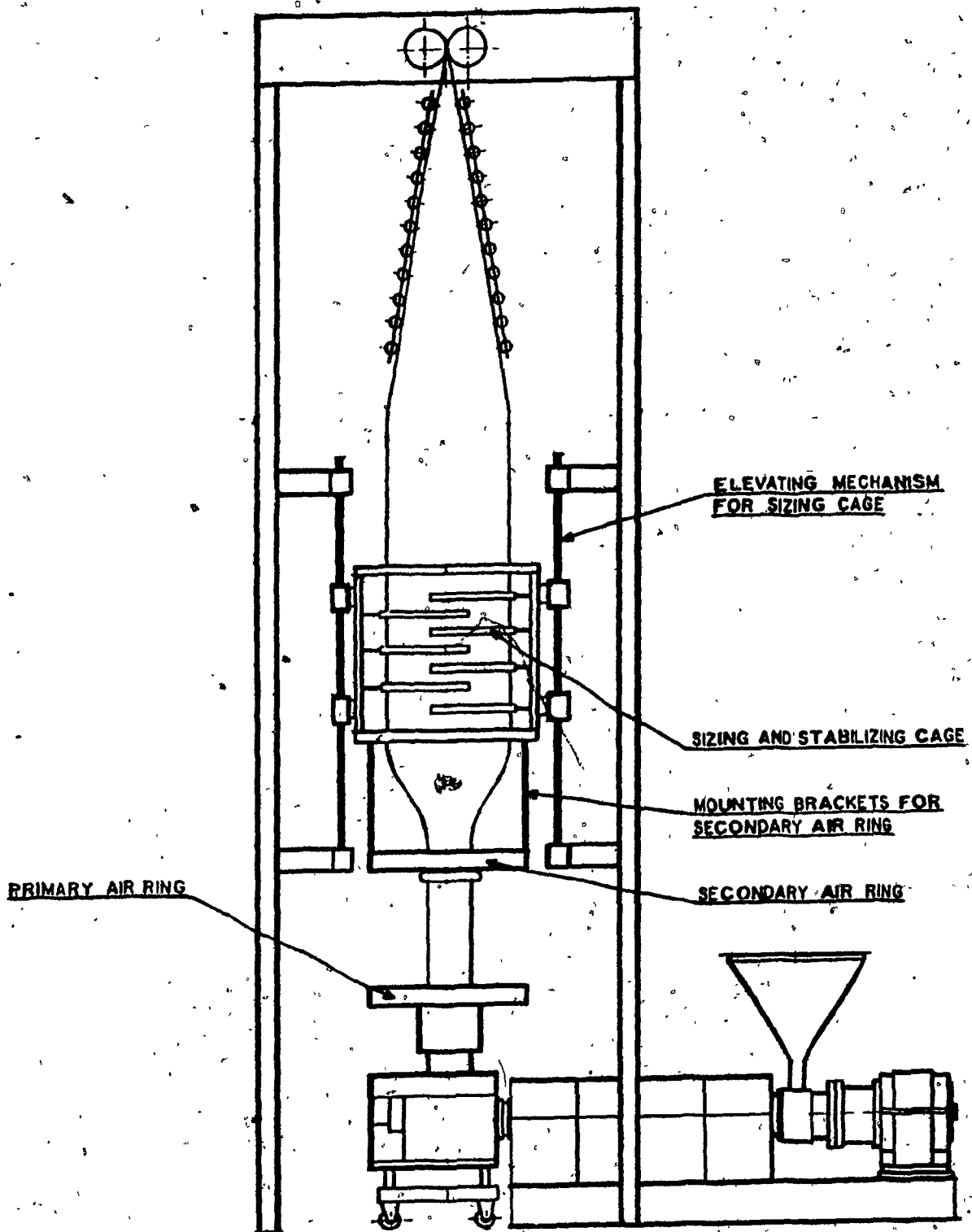
SECONDARY AIR RING

FIGURE 2.6   State of the Art Blown Film Cooling System

film bubble with a flow rate three to four times that applied at the base of the film bubble, and, downstream from this second air ring, a bubble sizing cage is located.

Internal bubble cooling(IBC) devices have tremendous potential, as the possibilty of heat transfer from the bubble interior had previously been neglected. The cooling systems discussed thus far require no fundamental change in extrusion system but IBC does. A new die, an internal air ring and a complex monitoring and control system are all required for an IBC device. Consequently, the cost of these systems are high. Only the newest LLDPE and HDPE blown film extrusion lines incorporate IBC. IBC has been mentioned here only for completeness, a broader discussion can be found in references 9 and 23.

The goal of any type of cooling innovation is to increase the rate of film cooling as indicated by a lower frostline height or film surface temperatures, while maintaining bubble stability. Once this is accomplished increased throughput is possible.

Chapter 3

Scope and Objectives

In commercial blown film extrusion processes the output is limited by the cooling capacity. An increase in cooling can yield a corresponding increase in throughput. However, simply increasing the flow of cooling air directed at the bubble may not be practical if bubble instabilities arise. Bubble instabilities lead to nonuniform dimensions and an unacceptable product.

The purpose of this work was to investigate the feasibility of using stronger cooling conditions while retaining a stable bubble. In a new approach to generate stronger cooling conditions, air was drawn down, countercurrently, along the bubble. Cooling air applied countercurrently may result in greater cooling than under normal cocurrent cooling conditions. Furthermore, the warmed air drawn down the bubble is collected. Collection of the heated air eliminates its localized accumulation in the operating area and presents the possibility of using the heat in the air for space heating of office areas or for preheating in film embossing.

3.1 Statement of Objectives

An experimental strategy to examine the possibilty of countercurrent blown film cooling is outlined in the following list of objectives:

1) Design a countercurrent cooling system and determine whether a stable bubble may be blown under countercurrent cooling conditions.

2) If a film bubble is stable under countercurrent cooling, determine a specific set of operating conditions for this process. All evaluations of cooling systems would then be carried out under these processing conditions. The operating conditions should be similar to those used under standard cocurrent cooling.

3) Evaluate the countercurrent cooling system by measuring dependent variables affected by changes in cooling conditions and compare them to variable measurements under cocurrent cooling conditions. For example, is the film surface temperature lower under the countercurrent cooling conditions than in standard cocurrent operation?

4)   Measure film properties under each cooling condition to determine whether the 'same' film is being produced. Furthermore, qualitatively determine the overall orientation of the film.

3.2 Evaluation Criteria

Prior to designing a countercurrent cooling apparatus, the existing blown film process was studied. The reason was two-fold; to familiarize the researcher with the technique of operating a blown film extruder, and secondly, to establish evaluation criteria, since the project objectives include a comparison of one cooling system with another.

Insufficient cooling will cause the polymer film to exceed its blocking temperature at the nip rolls and stick to itself. On the other extreme, large air flow rates used to maximize cooling are limited by bubble stability. Thus blocking temperature and bubble stability provide general guidelines for film production. Within these guidelines specific operating conditions, i.e. variables in Table I, Parts II and III, must be established. This requires holding the majority of variables within this group constant so that changes in cooling conditions can be directly measured.

In this work, the extruder could operate at maximum screw speed over a wide range of blow up ratios and nip roll speeds, with moderate cooling conditions without exceeding the blocking temperature. With throughput limited by extruder speed rather than by blocking temperature, an output was specified. The value decided upon was considered typical by those familiar with the extruder. By holding output, a dependent variable, constant independent variables screw speed and extruder and die temperatures also were fixed. The screen pack was not changed as it was considered standard for the resin used, which when coupled with constant extrusion temperature and screw speed, kept back pressure constant. Furthermore, with these variables constant, melt temperature was also fixed.

Film product dimensions were set under cocurrent cooling conditions and were expected to remain constant throughout. Product dimensions are determined directly from blow up ratio (or layflat width) and film thickness. By making these dependent variables constant, both nip roll speed and internal bubble air pressure become fixed. This is not entirely true as the cooling air flow rate slightly affects the shape of the neck region and subsequently bubble dimensions.

Cooling conditions were varied for each cooling system. The cooling apparatus design, which dictates the

manner in which cooling air is applied to the bubble and the quantity of cooling air, determines a cooling condition. Stronger conditions are limited by bubble stability. The maximum cooling condition is realized by a film bubble on the verge of instability. For each cooling condition, measurement of position dependent variables revealed the extent of cooling and provided a basis for comparisons between the cocurrent and countercurrent cooling systems.

The independent and dependent variables that were constant in this study are summarized in Table 3.1.

Table 3.1: Constant Independent and Dependent Variables

Screw Speed

Film Output

Screen Pack

Extruder Back Pressure

Extruder and Die Temperatures

Melt Temperature

Dimensions (BUR and film gauge)

Nip Roll Speed

Internal Bubble Pressure

Cooling Air Temperature

The remaining five chapters of this thesis attempt to meet the objectives outlined in this chapter. In Chapter 4, a countercurrent cooling apparatus is described and operating conditions established under which comparisons with standard cocurrent cooling were made. Dependent variables measurements are discussed under different cooling conditions in Chapter 5 and 6. Furthermore, heat transfer coefficients along the length of the bubble were calculated from the measured dependent variables and correlated with position above the die and air velocity. In Chapter 7, film property measurements are discussed, with particular reference to differences between film cooled under cocurrent and countercurrent cooling conditions. A discussion of film property measurements in terms of orientation follows in Chapter 8. Chapter 9 contains the conclusions of this study.

Chapter 4

Initial Experiences with Countercurrent Cooling

All of the current methods used to cool blown film blow
cooling air in the same direction as the film is travelling,
that is, in a cocurrent direction. This work looks at the
possibility of applying cooling air in an opposite or
countercurrent direction to the moving film. In this
research, several countercurrent air flow schemes were
proposed to cool film. However, before any comparative
tests could be made between the conventional cocurrent and
proposed countercurrent cooling modes, it was necessary to
establish a stable film bubble under countercurrent cooling
conditions. Once a stable bubble was achieved and operating
conditions specified, measurement of dependent variables
would reveal the method of greater cooling.

4.1 Material

A commercial high pressure low density polyethylene was
used throughout this study. The resin, DFDY 3312, was
supplied by Union Carbide Canada Ltd. It is an unmodified

resin, free of the additives commonly used to enhance film properties. This polyethylene is highly branched, has a broad molecular weight distribution and produces a high clarity film. The following specifications were provided by the manufacturer; melt index 1.7 g/10 min, melt flow ratio 65, and resin density 0.9235 g/cc. Melting and crystallization points of 110°C and 96°C, were determined by a Perkin-Elmer differential scanning calorimeter, model 2C, following ASTM D3418. A thermogram of the melting curve is shown in Appendix D3 and the crystallization point determination in Section 6.6.2, Figure 6.25.

4.2 Equipment

All blown film processing was carried out at the Technical Centre of Union Carbide Canada Ltd. in Pointe-aux-Trembles, Quebec. A one-inch, Wilmot extruder (Wilmot Flemming Engineering Co., Huntingdon Valley, Pa.) was used to process the low density polyethylene. The extruder contained a 24:1 length to diameter ratio standard screw, which fed molten polymer through a two and one half inch spider die (Union Carbide Corp., Bound Brook, N.J.). A conventional, high-cone, single lip air ring (Union Carbide Canada Ltd., Pointe-Aux-Trembles, Que.) redirected cooling

air, supplied by a central blower, along the bubble. This air ring was eventually replaced by a small-cone, single-lip air ring, which had been used in earlier research by Farber (24). Photographs of the extruder with each air ring in place are shown in Figures 4.1a and 4.2a. A cutaway sketch of each air ring, with major components labled, is presented in Figures 4.1b and 4.2b. The small cone of the air ring was designed to fit around the die, that is with cone point downwards. However, the deflector plates were positioned to redirect air cocurrently along the bubble. This 'inverted' air ring exposed more of the bubble to measuring techniques, which required a clear path perpendicular to the bubble surface. A second blower was necessary for the eventual countercurrent system used. It was a Powerland-Baley 10 bp blower (Powerland Engineering Ltd., Woodbridge, Ont.)

4.3 Operating Ranges Under Cocurrent Cooling

A discussion in Section 3.2 determined variables which would be held constant in this work. These operating conditions included independent and dependent variables listed in Table 1, Parts II and III. Cooling conditions were, of course, exceptions to this statement and necessarily varied.
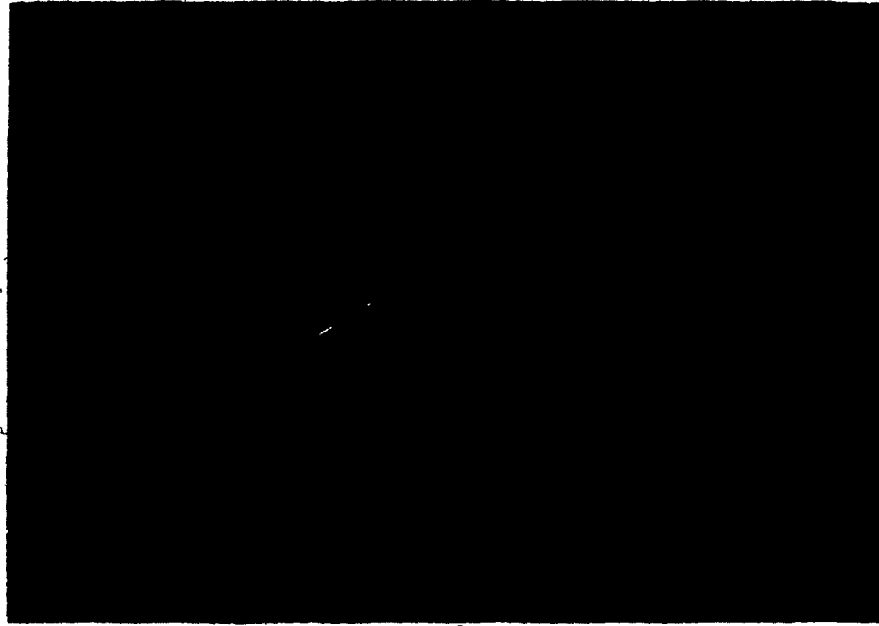
FIGURE 4.1a   Photograph of a Conventional High
Cone Air Ring Mounted Above a Die

High Cone

Air →

← Air

Baffles

Deflector
Plates
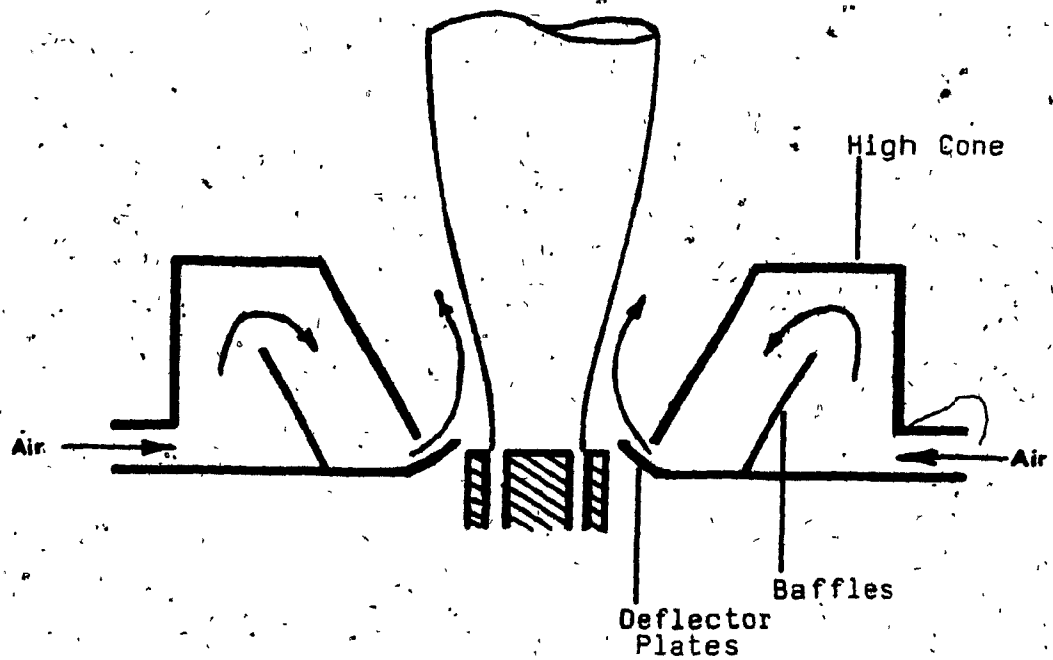
FIGURE 4.1b Cutaway View of a High Cone Air Ring
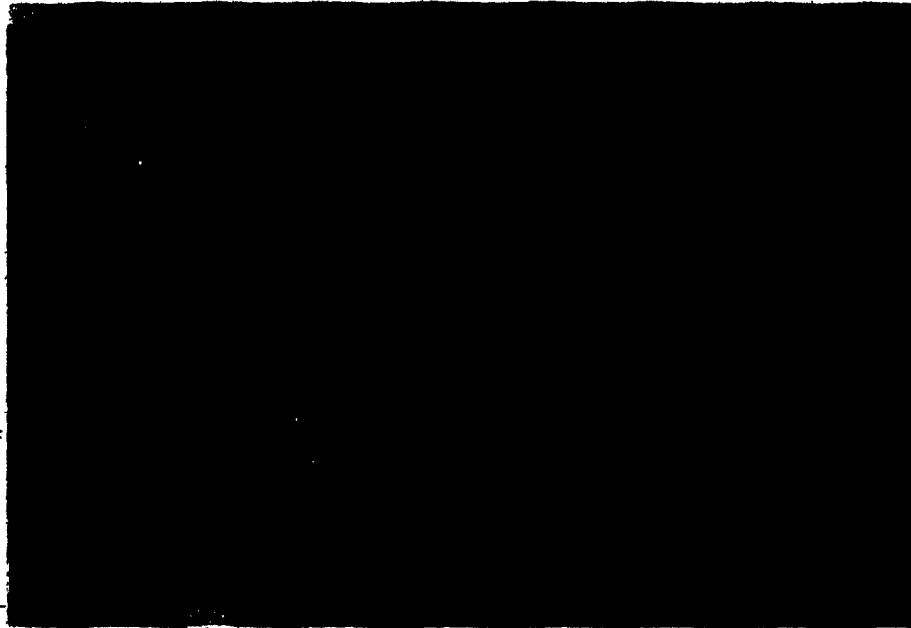
FIGURE 4.2a   Photograph of a Modified Low Cone
Air Ring Mounted Above a Die

Air →   ← Air

Low Cone   Deflector   Baffles
Plates
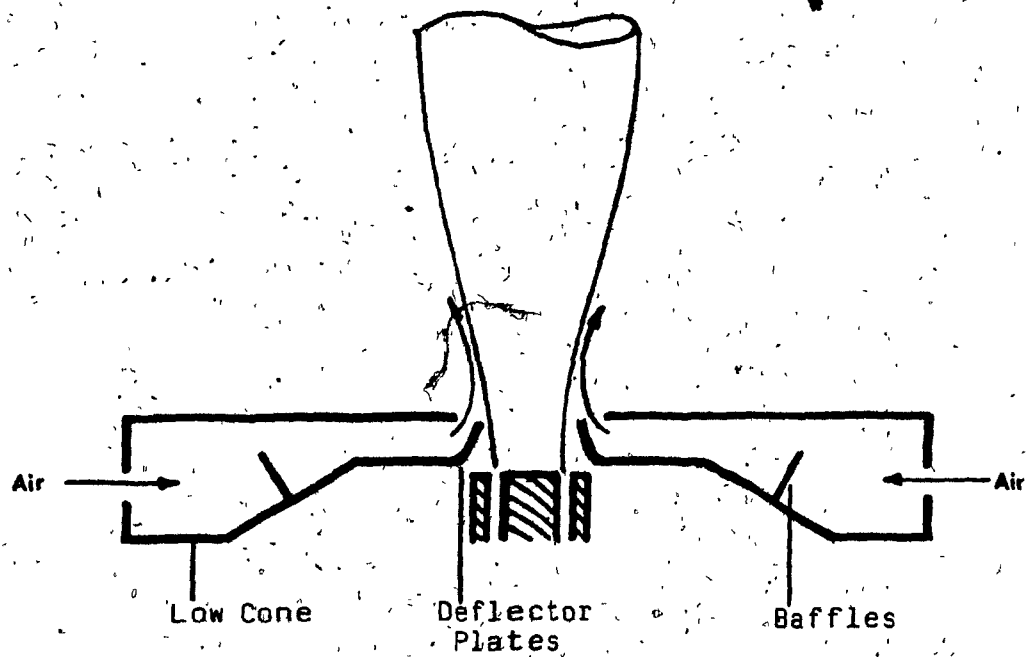
FIGURE 4.2b   Cutaway View of a Modified Low Cone
Air Ring

The high pressure resin used in this study was processed under a range of operating conditions, considered standard by those technicians familiar with this blown film extrusion system. The operating ranges were used as guidelines for countercurrent trials. It was important to obtain a stable film bubble under countercurrent cooling conditions, within these normal processing ranges. The cocurrent operating condition guidelines are presented in Table 4.1. The die and extruder temperatures were set independently in four zones. These temperatures were considered standard for this high pressure resin and were not changed. Also, a screen pack of 40-80-80-40 mesh was used throughout this study, although it was replaced periodically. The remaining variables were varied within these guidelines in each countercurrent cooling trial.

4.4 Countercurrent Cooling with Suction

The first attempt to apply countercurrent cooling air to the film bubble was nothing more than reversing the flow through the present air ring. This was the easiest approach to take, (as it only required connecting the air inlet ducts of the present ring to the air intake side of the Powerland blower. The cooling air drawn into the air ring by the

Table 4.1: Operating Ranges under Cocurrent Cooling

Variable	Range
Screen Pack	40-80-80-40 mesh
Die and Extruder Temperatures	163, 168, 177, 182 °C
Melt Temperature	190 - 215 °C
Screw Speed	45 - 65 RPM
Film Output	10 - 24 lb/hr (4.5 - 10.8 kg/hr)
Extruder Back Pressure	2500 - 3500 psi (17 - 24 MPa)
Nip Roll Speed	20 - 40 ft/min (6 - 12 m/min)
Film Thicknss	0.5 - 3.0 mils (0.01 - 0.08 mm)
Blow Up Ratio	1.75 - 4.0
Frostline Height	8 - 20 inches (0.2 - 0.5

blower was controlled by a butterfly valve located at the blower exit.

Film bubble start-up was not possible under these operating conditions. The punched molten film collapsed over the annular opening in the air ring through which air was being pulled. To circumvent this problem, a bubble was formed under cocurrent cooling conditions, and once the bubble was established the air flow was reversed. Immediately, the frostline increased and the bubble oscillated back and forth in a 'flapping' or 'fluttering' manner. In less than a minute the deformations became too severe and the film bubble broke, the lower portion of film being sucked into the air ring. This outcome was repeated for each set of processing conditions used. These conditions are listed in Appendix B1. With large drawing air flows, blow-up ratios and nip roll speeds, bubble breakage occurred virtually instantaneously. Under these same operating conditions however, decreasing the suction rate prolonged the life of the bubble marginally, but raised the frostline even more.

These observations indicated that suction through the air ring orifice greatly destabilized the bubble. Air withdrawn near the weakest section of bubble caused great deformations and ultimate breakage there. If suction was decreased, bubble stability improved, but cooling was

insufficient, as not enough air was drawn along the bubble. The temperature of withdrawn air was only slightly higher than the ambiant air (27.5 °C vs. 27.0°C) thus, a large portion of air flow entered the air ring without cooling the bubble. A sketch illustrating these occurrances is shown in Figure 4.3.

In order to force more air closer to the film tube, a cylindrical shroud was placed around the bubble. Thus, cooling air would be required to enter an annular gap between the bubble and the cylinder and flow down the length of the cylinder, near the bubble. It was hoped that more cooling would occur under a less than maximum countercurrent flow. By not using maximum suction, the destabilizing force would not be as great as in the previous trial. This configuration still relied solely of drawing cooling air countercurrently. A detailed drawing of the cylinder is shown in Appendix C. The cylinder extends above the highest frostline obtained with any combination of cocurrent operating variables (Table 4.1) and the diameter can accomodate blow-up ratios slightly greater than three.

The operating conditions used in the ensuing trial were at the lower operating ranges given in Table 4.1. In the previous trial, bubbles with small blow up ratios, formed with slower nip roll and screw speeds, proved longer lasting than bubbles blown with higher values of the processing
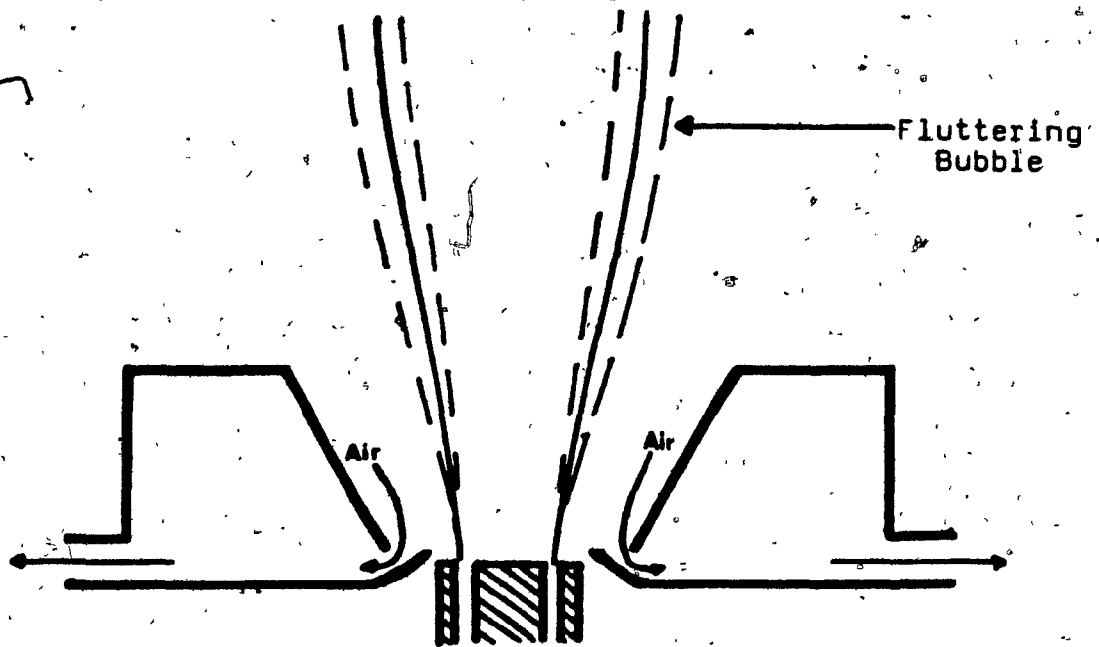
FIGURE 4.3 Countercurrent Cooling Using Existing
            Air Ring and Showing Bubble Instabilities

parameters. This same behavior was expected here. Specific operating conditions for each attempt to blow a stable bubble are listed in Appendix B2. Film bubble start-up was again not possible under the drawing flow. Thus, a bubble was first established under cocurrent flow. Once the flow along the established bubble was reversed, initiating less than maximum countercurrent air flow, bubble instabilities resulted. The neck region changed shape dramatically, first expanding until contacting the cylindrical wall and then contracting into a narrow tube. These deformations solidified at a frostline well above the cylinder and thus remained in the product. At some point, the oscillating bubble was pulled over against one side of the cylinder. In this position, the bubble soon stuck to the cylinder wall and broke, as the film was still molten within the cylinder. Maximum countercurrent air flow was then applied to provide more cooling and lower the frostline. With this change, the frostline was reduced but still remained above the cylinder, and the expansion-contraction oscillating pattern was dampened by extreme 'fluttering' at the base of the film bubble. This bubble was short-lived, lasting no more than a few minutes. Further attempts using a larger blow up ratio or faster screw speed were futile, as the bubble broke immediately. A sketch of the deformations is shown in Figure 4.4a and b.
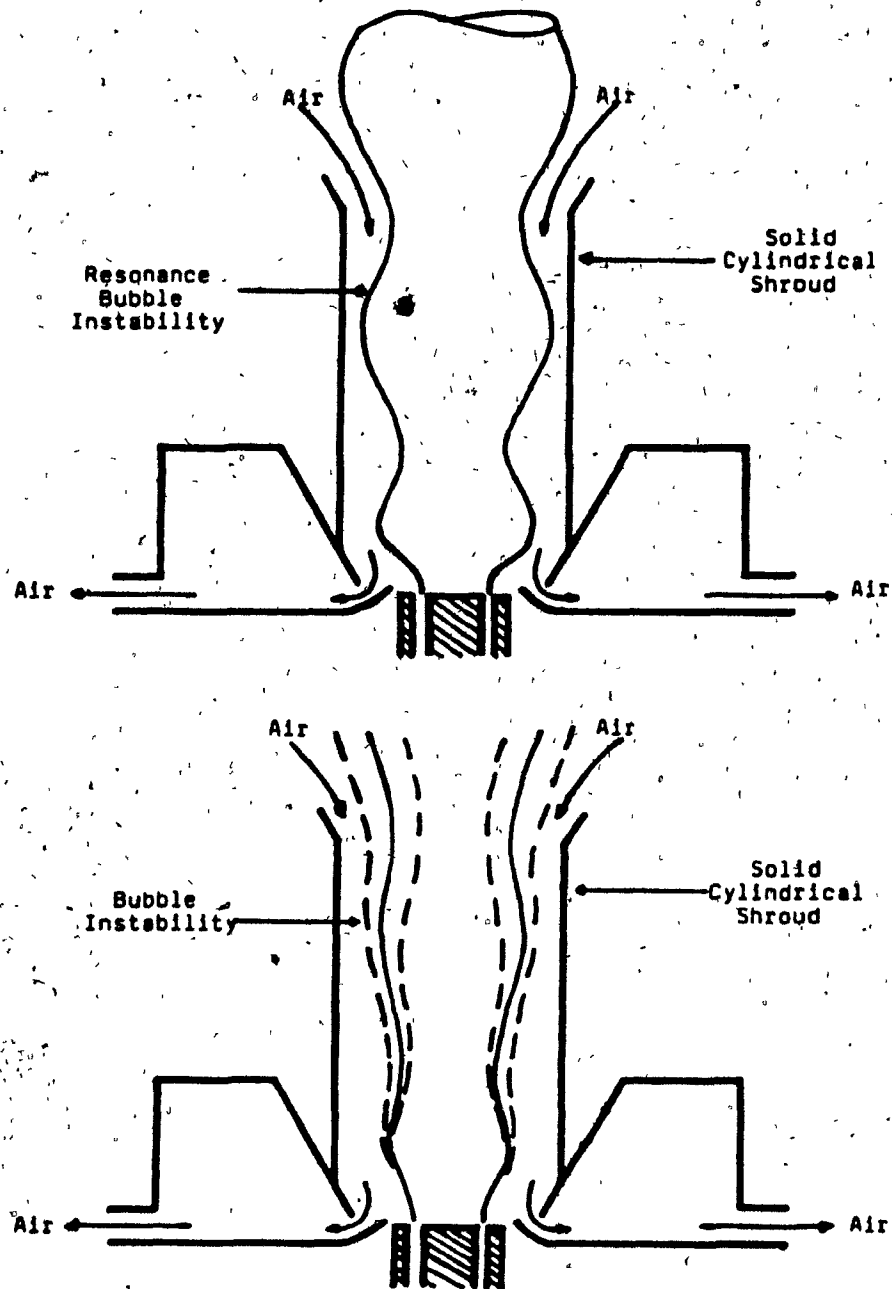
FIGURE 4.4   Countercurrent Cooling Incorporating a
            Solid Cylindrical Shroud and the Existing
            Air Ring   (a) Resonance Bubble Instability
            Under Moderate Countercurrent Air Flow
            (b) Fluttering Bubble Deformations with
            Maximum Countercurrent Cooling

Under 'less than maximum' countercurrent cooling, the film bubble remained too hot and was susceptible to an oscillating type deformation. Little cooling air contacted the lower section of film bubble, where the polymer was hottest and most fragile. This may be attributed to cooling air channeling near the cylinder wall rather than contacting the bubble. At maximum countercurrent air flow, cooling increased as the frostline was lowered. However, the large negative pressure applied near the molten bubble was destabilizing and caused the bubble to break there.

If a countercurrent suction flow was to be pursued, substantial changes would be required in apparatus design. The major problems were the destabilizing force felt by the bubble at the region of air withdrawl and insufficient cooling. An increased cooling air flow or better application of air along the bubble neck region would lead to greater film cooling. Partial or 'precooling' in the neck region would stiffen the bubble making it less susceptible to deformations. In order to direct more air to the fragile neck region, rows of circular holes were cut in the cylindrical shroud. If air entered through all the rows of holes, the limiting case of flow reversal through an air ring would be approached. However, rows of holes could easily be sealed off with tape or plastic film, thus

permitting the cooling air flow to be directed at a desired area. Still, there was no assurance that the fresh cooling air would contact the bubble rather than flowing directly into the air ring withdrawl orifice. In order to assure some contact between countercurrent cooling air and film surface, disc- or plate-like obstructions were fitted in the cylinder. This arrangement required the air to flow through a small annular gap between the inner plate edge and the film bubble surface. Thus, cooling air could be forced to flow along the hottest section of film bubble.

Plates within the cylinder provided an obstruction which the countercurrently drawn air had to flow around. This increased the pressure drop at the withdrawl orifice over the case where no obstructions were present. In this countercurrent cooling scheme there appeared to be a trade off between a destabilizing force at the air withdrawl point and potential increases in cooling, particularly in the neck region. However, both problems might be satisfied if the bubble neck was cooled somewhat, thus stiffening and possibly withstanding the applied negative pressure near the die. A sketch of this modified cylinder is shown in Figure 4.5.

The sketch in Figure 4.5 shows circumferential rows of circular holes arranged in an offset pattern along the cylinder length. Circular holes were chosen over long slots
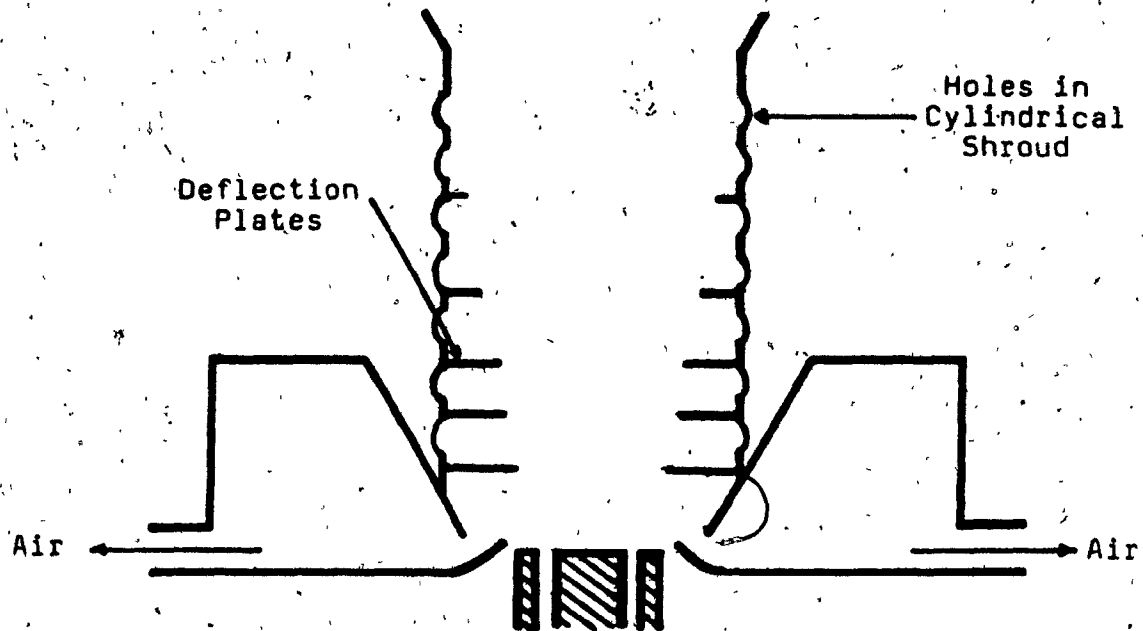
FIGURE 4.5 Countercurrent Cylindrical Shroud
Apparatus with Deflection Plates and
Cooling Air Entry Holes

as the opening geometry simply because they could be easily made using existing machine shop equipment. Although seven rows of holes were cut in the cylinder, any number could be blocked off, so that air could be directed at a particular portion of the bubble. The straight plate with square end geometry was primarily the result of machine shop restrictions. The outer plate diameter was constrained by the cylinder, while the inner plate diameter was designed for a small gap (0.38 to 0.5 inch) between plate and cocurrently cooled film bubble. The plate width increased, moving down the cylinder, from being able to accomodate a fully expanded bubble at the cylinder opening to fitting around a narrow film tube in the neck region at the base of the cylinder. After the previous trials, a stable bubble in countercurrent flow was not expected to have a blow up ratio greater than three. A blow up ratio of 2.75 was arbitrarily chosen as a model for plate width design. Five plates were fitted in the cylinder. Spacing between plates was smallest near the die and increased towards the frostline region. The close spacing of the plates in the neck region was another attempt to direct cooling air near the bubble. Detailed drawings of this apparatus are in Appendix C .

An attempt to form a bubble, surrounded by the cylindrical shroud of Figure 4.5, was made under countercurrent cooling conditions. A summary of the

processing conditions used are given in Appendix B3. For each set of conditions, attempts to form a stable bubble were made with different rows of cylinder holes blocked off. Bubble start-up was again only possible under cocurrent cooling conditions. Once a film bubble was formed with cocurrent cooling and moderate processing conditions, the cooling air was reversed. Bubble instabilities occurred immediately and fluttering at the base of the bubble soon caused breakage there. Under this air flow the bubble existed for such a short time, that the frostline height could not be measured, as it was still rising. The negative pressure necessary to draw air along the bubble was too great or was applied too close to the molten tube to allow a stable bubble to form and yet not great enough to provide adequate cooling. In an effort to distance this destabilizing force from the immediate vicinity of the bubble, the upper base plate of the air ring was removed. (Refer to Figure 4.1b.) The countercurrent flow now escaped through a larger annular opening between the lower deflector plate and the air ring housing. A film bubble was established under cocurrent flow and with the same operating conditions as the prior trial. (Refer to Appendix B3.) When the air stream was switched to a countercurrent flow, expanding - contracting oscillations occurred. Photographs of this instability are shown in Figure 4.6. These
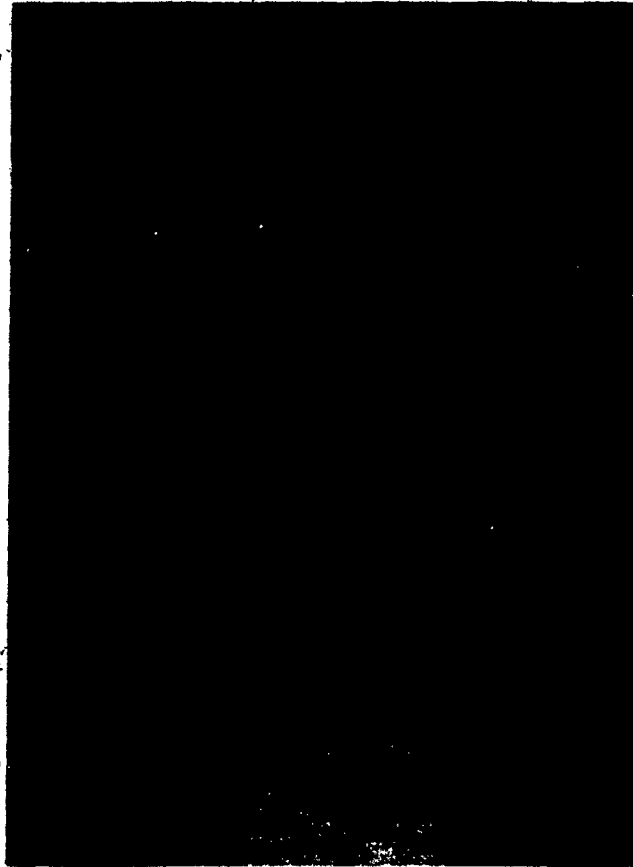
FIGURE 4.6 Photographs of Bubble Instabilities Under Countercurrent Cooling

oscillations were not steady, as their size increased with time. Within several minutes the expansions were so large that they contacted plates within the cylinder and, above the plates, the cylinder wall itself. Shortly afterwards, the hot bubble stuck to one of the plates and was torn.

In a last attempt to obtain a stable bubble under solely drawing flow, the upper base plate, which had just been removed, was placed on top of the cylinder. Film was blown with a 2.5 blow-up ratio, which allowed only a small amount of air to enter through the top of the cylinder. To concentrate the cooling air on the most fragile section of film bubble, all but the bottom two rows were blocked off with plastic film. A sketch of this scheme is shown in Figure 4.7.

A countercurrent flow was applied to the film bubble and a stable bubble was observed. A three to four foot high frostline indicated the bubble was hot, although the film did not exceed the blocking temperature at the nip rolls. When either the upper base plate located on top of the cylinder was raised, or the plastic wrap readjusted to uncover a third row of holes, the bubble began to oscillate. Stability was only restored by replacing the base plate or plastic wrap.

In each attempt to form a stable bubble, the drawing

Raised Air Ring
Base Plate

Plastic Wrap

Air

Air

Large Gap for
Cooling Air
Withdrawl
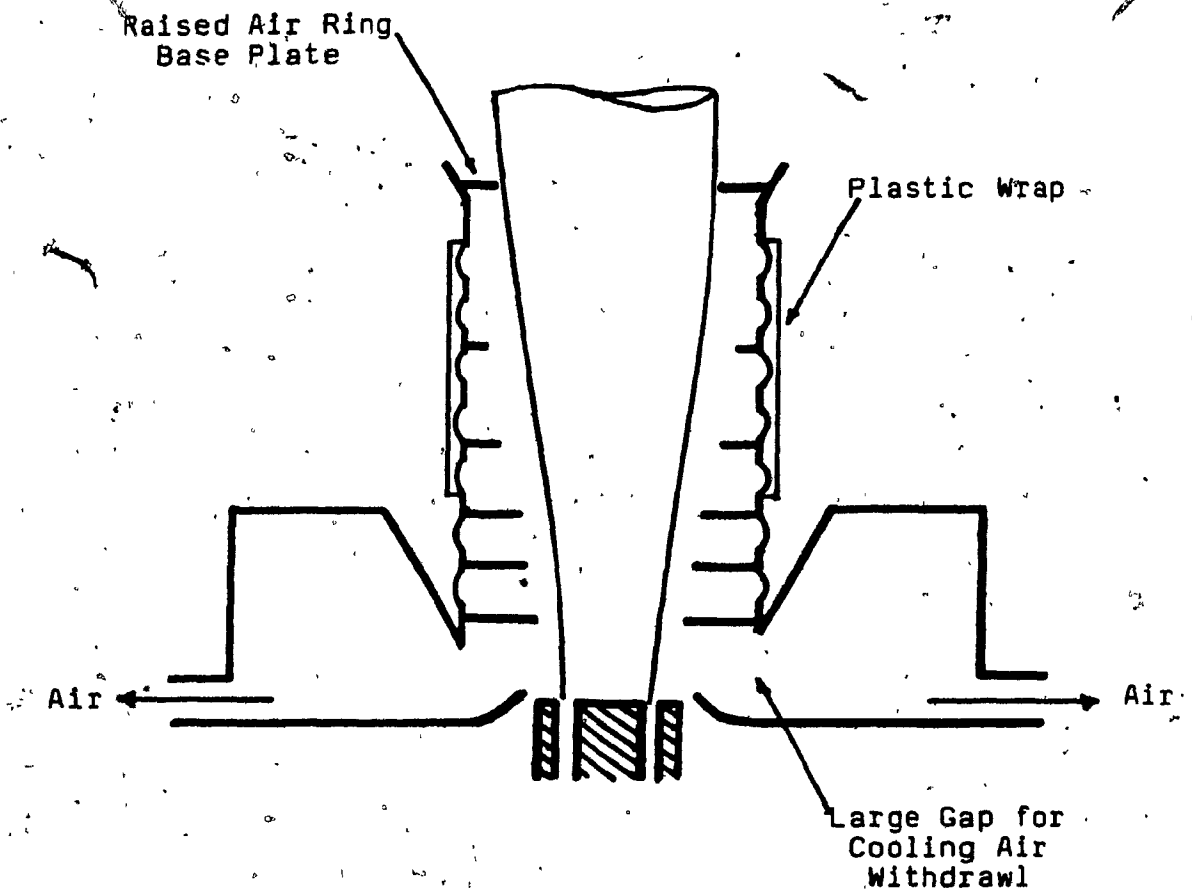
FIGURE 4.7   Countercurrent Cooling Apparatus
with Stable Film Bubble

-64-

flows applied to the base of the bubble were destabilizing
and did not provide enough cooling. Under the maximum
countercurrent flow the film bubble was literally torn apart
in the neck region. When countercurrent flow was reduced,
in an attempt to obtain a stable bubble, the frostline
height increased substantially and oscillations occurred due
to insufficient cooling. In the last trial, a stable bubble
was achieved under narrow processing conditions. The bubble
was only weakly cooled and on the verge of instability.
From these trials, it was concluded that no cooling
advantages would arise solely from drawing air through the
existing air ring.

4.5 Cocurrent - Countercurrent Combination Cooling

A new approach incorporating blowing air, rather than
solely drawing air, was thought necessary to establish a
stable, well cooled film bubble and allow comparisons with
conventional cocurrent cooling. Two approaches were
considered to the problem of applying more cooling air along
the bubble without destabilizing the bubble. Both methods
required a raised cooling device, which limits blow-up
ratios or requires a set of replaceable deflector plates to
operate over a range of blow up ratios. Also, they required

a second air blower.

In one proposed arrangement, an air ring was positioned near the frostline and directed air downwards toward the die. The air stream would first contact the bubble after the film had mostly solidified. By applying air to a mostly solid bubble, greater flow rates were thought possible than in conventional cooling where air contacts molten film. Commercial cooling systems with a raised cocurent air ring have an upper air flow rate three to four times greater than the flow applied at the base of the film bubble (25). It was not expected that such a larger flow rate would be possible with a raised air ring blowing countercurrently, since the air would soon contact a partially molten bubble and be a destabilizing force.

A problem arises in blowing air towards the die. The cooling air would warm from contact with film and collect around the die and molten tube. This collection of air would reduce heat transfer in the neck region. Therefore, a means of collecting the air near the die is required. An insulated air ring deflector plate could be mounted over the die and a slight negative pressure applied at the outer edge of the plate to remove the air. The suction required would be somewhat removed from the film bubble, but this would be a destabilizing force.

If a stable bubble could be formed with this cooling

scheme, the industrial concern of increased film cooling could, of course, be tested. Moreover, the academic interest in the efficiency of cocurrent versus countercurrent cooling could also be examined. The same amount of cooling air could be supplied in each case, the amount of entrained air assumed equal and the film surface temperature measured between die and frostline to give an indication of cooling ability, much like an investigation with a shell and tube heat exchanger.

In the other proposed arrangement a standard air ring would blow cooling air cocurrently along the neck region. The conventional cooling method would cool the most fragile section of bubble and help support and stabilize it. A raised collecting shroud or plenum located near the frostline region would then remove the cocurrently blown air and in addition, draw air down the solid portion of bubble. To collect the cooling air, a negative pressure would be applied by the plenum to a mostly solidified bubble. A solid bubble was expected to withstand the drawing forces, but some destabilizing effects on the molten region below the frostline were expected. Once a stable bubble was formed, a comparison between conventional cooling and this cocurrent and countercurrent combination system would test the industrial concern of increased film cooling.

The latter proposed arrangement was fabricated and a
sketch is shown in Figure 4.8. The previous trials had
emphasized the importance of cooling and stability in the
neck region. With this in mind, the stabilizing ability of
cocurrent cooling in this area was chosen over the unknown
film stability in countercurrnet air blowing and collecting.
Furthermore, the cocurrent and countercurrent combination
arrangement was expected to provide adequate bubble cooling
under moderate processing conditions, even in the limiting
case where only cocurrent air flow is applied along the
bubble.

The cocurrent and countercurrent cooling system shown
in Figure 4.8 incorporates a conventional air ring, the
cylindrical shroud with rows of holes and obstructing plates
from the previous trial, and a raised plenum with two outlet
ducts to withdraw the cooling air. The plenum was designed
to fit around the cylinder and can be raised or lowered to a
particular height above the die. Different plenum heights
change the section of bubble subjected to countercurrent
flow. Thus a new independent variable is introduced into
the problem. The plenum covered two rows of holes on the
cylinder, through which air was drawn. In order to create
an evenly distributed flow rate, portions of the circular
holes on the cylinder were blocked. Those holes nearest the
outlet ducts were blocked off to a greater extent than holes
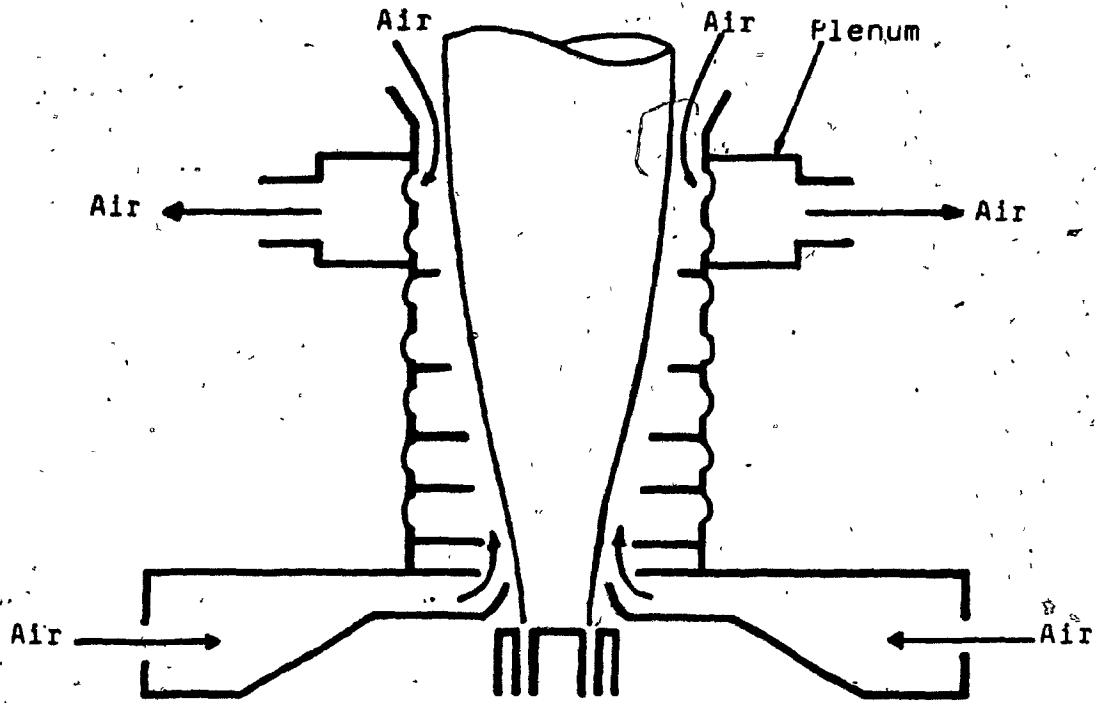
FIGURE 4.8 Cocurrent and Countercurrent Combination
Cooling System with Stable Film Bubbble
(pictured with low cone air ring)

furthest away from the exits. Prior to forming a film bubble the drawing air velocity was measured using a hot wire annemometer (Flow Corp., Cambridge, Ma.) at twelve equidistant positions. The measured velocities, at each position, differed from each other by a maximum of five percent.

A summary of the moderate processing conditions used in this trial are given in Appendix B4. The plenum was raised to its highest position on the cylinder. Thus, the negative pressure caused by drawing air was applied to a partially cooled portion of the bubble. In this position the plenum was expected to be least destabilizing. Initially, the holes in the cylindrical shroud were left open to allow the cocurrent air to flow over the neck region and to entrain surrounding air. Bubble start-up was carried out under cocurrent cooling conditions and countercurrent air flow was gradually added. A stable bubble was obtained over the countercurrent flow rates applied by the Powerland blower. The cylinder was then wrapped in clear plastic sheeting, which blocked the holes but allowed bubble behavior in the neck region to be observed. Again, a stable bubble resulted for the countercurrent air flows. Photographs of a stable bubble achieved under countercurrent flow are shown in Figure 4.9.

At high blow up ratios, screw speeds, or nip roll
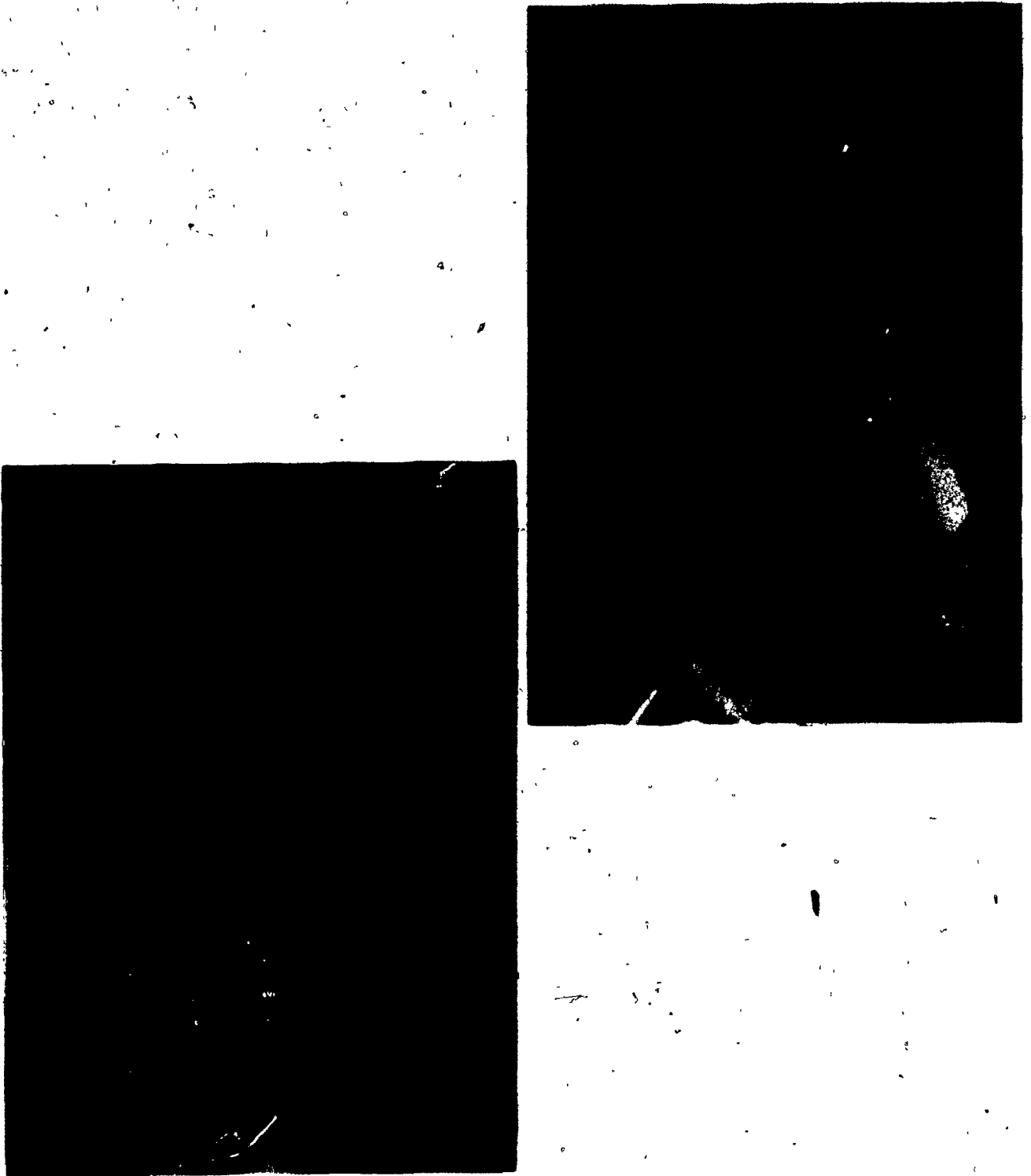
FIGURE 4.9 Photographs of a Stable Film Bubble
Under Cocurrent and Countercurrent
Combination Cooling Flow

speeds, bubble instabilities resulted when maximum countercurrent air flow was applied. In some cases a stable bubble, under mild countercurrent flow, gave way to fluttering-type deformations as suction was increased. In an extreme case, the film bubble was pulled over against one side of the cylinder and soon broke. Photographs of this situation are shown in Figure 4.10. Operating conditions are listed in Appendix B4. The instabilities resulted whether the cylinder was shielded with plastic wrap, partially shielded, or open to the surroundings. They are reflected in an observed poor quality film and dimensional variations outside the standard tolerances applied to film produced with this extruder. Film dimensions for most processing conditions are listed in Appendix B4.

The plenum was lowered to different positions above the die and attempts were made to obtain a stable bubble in countercurrent flow. Even under the smallest drawing flow (butterfly valve closed) severe fluttering in the neck region developed. In the lowest two plenum positions, covering rows one and two, and rows two and three above the die, the bubble was immediately torn apart. In light of this outcome, the plenum was repositioned near the top of the cylinder. Comparisons between cooling systems were made with the plenum fully raised. In the highest position, a stable bubble had been formed under moderate processing

FIGURE.4.10   Photographs of Film Bubble Instabilities
Under Cocurrent and Countercurrent
Combination Cooling Flow

conditions and a wide range of countercurrent flows. These moderate operating conditions are listed in Table 4.2, they are all within the standard processing ranges of cocurrently cooled film which were given in Table 4.1.

In each case where a stable bubble was formed in countercurrent flow, the frostline was within the cylindrical shroud and located just below the plenum. The frostline is a broad line or region, approximately horizontal. Small changes in cooling conditions cannot be detected by observing changes in frostline height. In fact, over the range of countercurrent air flows applied to the bubble, regardless of whether the cylinder was shielded, there was no apparent change in frostline height. In order to get an idea of the cooling occurring along the bubble, the film surface temperature was measured at points above and below the plenum, for each processing condition. Measurements were made with an infrared thermometer and the results are contained in Appendix B4. (The principles of operation and the experimental procedure used are given in Section 5.2.) In the case of a shielded cylinder, a small window was cut in the plastic wrap so that the bubble surface could be viewed without obstruction.

The film surface temperature measured below the plenum was marginally higher with a shielded cylinder around the bubble than with a cylinder open to the surroundings. This

Table 4.2: Operating Conditions

Variable	Value
Screen Pack	40-80-80-40 mesh
Die and Extruder Temperatures	163, 168, 177, 182 C
Melt Temperature	205 C
Screw Speed	50 RPM
Film Output	16.8 lb/hr (7.6 kg/hr)
Extruder Back Pressure	3100 psi (12 MPa)
Nip Roll Speed	25 ft/min (7.6 m/min)
Film Thickness	1.6 mils (0.025 mm)
Blow Up Ratio	2.25
Cooling Air Temperature	27.0 C
Height of Countercurrent Plenum	16 - 22 inches (0.4 - 0.6 m)
Area of Openings Along Countercurrent Cylinder	0 (holes blocked)
Cocurrent Flow Rate	123 cfm (0.058 m3/min)
Countercurrent Air Flow Rate	126 - 590 cfm (0.059 - 0.28 m3/min
Frostline Height	11 - 12 inches (0.28 - 0.31 m)

was attributed to the entrainment of ambiant air by the cocurrent air stream in the latter case. However, for both the shielded or open cylinder arrangements, the amount of countercurrent air flow did not affect the surface temperature. Above the plenum, the surface temperature varied depending on whether the cylinder holes were open or blocked and on the countercurrent air flow. With an open cylinder, which allowed the surrounding air to be entrained, the temperature above the plenum was independent of countercurrent air flow. However, with the cylinder wrapped in plastic film, the surface temperature varied markedly with countercurrent air flow. Larger cooling air flows reduced the surface temperature to a greater extent than little or no countercurrent flow. In the limiting case of solely cocurrent flow through a shielded cylinder, the surface temperature above the plenum was higher than if countercurrent cooling flow had been added but nearly equal to the open cylinder case for all countercurrent flows. Apparently with the cylinder holes opened, the drawing flow entered from outside the cylinder, both from above and below the plenum. The air flow entering just below the plenum was probably channeled towards the exiting duct without contacting the film bubble, as there was no obstruction plate between the first entrance points below the plenum and the plenum itself. Since air was entering below the plenum,

in the open cylinder arrangement, less cooling air was forced down along the upper or solid portion of bubble and little if any additional heat transfer occurred there with the application of countercurrent cooling air. From these surface temperature measurements the largest differences occurred between solely cocurrent cooling and cocurrent and countercurrent combination cooling with a shielded cylinder surrounding the film bubble. Therefore, further trials with the combination cooling system used a cylinder wrapped with plastic film.

In most of the experiments described above both high and low cone conventional air rings were used. Both have similar deflection plates that redirect the air in a fan-type spray toward the bubble. The cooling air redirected by the low cone air ring had a substantial tangential component, although this was only apparent in bubble start-up. No differences in product dimensions or film appearance were found in film cooled by each ring. Measurement of dependent variables along the bubble, such as surface temperature, air velocity and neck region shape, all required a clear path perpendicular to the bubble. This lead to selecting the small cone air ring for further cooling system measurements.

4.5.1 Summary of Stable Operating Conditions under Cocurrent – Countercurrent Combination Cooling

A summary of the processing conditions for the cocurrent and countercurrent combination cooling system is given in Table 4.2. Under these conditions, a stable bubble was established over a range of countercurrent air flow rates. All further tests with the combination cooling system were to be carried out using the operating conditions of Table 4.2. Furthermore, the extrusion system with solely cocurrent cooling, which was to be compared with the combination cooling system, was known to operate under these same conditions. Extruder and die zone temperatures were maintained at 163 °C, 168 °C, 177 °C, and 182 °C by millivolt-type analog controllers on the Wilmod extruder. A rheostat variable screw speed control was set at 50 RPM. Film speed above the frostline or nip roll speed was measured with a hand held tachometer (Doyle Electronic Products co., Grand Rapids, Mi.) Several film speed measurements were made and an average taken, although the difference was never greater than one percent.

Once machine control settings were specified, single-value dependent variables were measured. Constant screw speed and extruder and die temperatures limited throughputs to 16.8 lb/hr (7.6 kg/hr). Output was measured

by collecting flattened film for a minute and weighing it on a top pan scale (Mettler Corp., Zurich, Switzerland). A 40-80-80-40 screen pack, coupled with constant extrusion temperature and screw speed, fixed back pressure at 3100 psi (1.21×10^{7} N/m2) and melt temperature at 205 °C as measured by a bourdon tube pressure gauge on the extruder and a hand-held platinum resistance thermometer (Omega Engineering Inc., Stamford, Cn.) The blow-up ratio was not measured directly, rather the film layflat width was first determined on line with a ruler and again later on a film sample. Division of layflat width by $\Pi/2$ yielded a 2.25 blow-up ratio. Internal bubble pressure was not measured in this study. A constant blow-up ratio and nip roll speed led to an average film thickness of 1.6 mils (0.025 mm). This value was obtained by measuring film thickness at half inch intervals around the circumference of a film sample and averaging them. Thickness measurements were made with a micrometer (Mitutoyo Mfg. Co., Tokyo, Japan). Ambient air was the fluid used to cool the film bubble. The temperature of the air issuing from an air ring orifice was measured with a type J thermocouple connected to a digital thermometer (Fluke Mfg. Co., Seattle, Wa.). Air temperatures varied somewhat, with 24 °C being the most common reading.

The cocurrent flow rate listed with the operating conditions of Table 4.2, was determined to be the largest

cooling flow possible with the small cone air ring and without the cylindrical shroud present. Attempts to increase the cocurrent flow rate resulted in an unstable bubble and unacceptable dimensional variations. This same cocurrent flow rate was used in the combination cooling system. The countercurrent flow rates given in Table 4.2 correspond to a closed and open butterfly valve at the blower exit. Both countercurrent and cocurrent cooling flows were manipulated by varying a different butterfly valve. Once the valve position was determined, the flow rate was calculated from pitot tube measurements. The measurement procedure and calculation method are given in Section 5.1

Bubble stability is clearly an important consideration in forming a bubble in countercurrent flow. The lack of stability precluded the sole use of drawing air to cool a film bubble. Instabilities also dictated the plenum position on the cylinder. The high plenum position allowed negative pressure to be applied to a mostly solid bubble, but the destabilizing force was still felt in the molten neck region and limited the operating conditions under which a stable bubble could be formed. Furthermore, with the expected greater use of LLDPE and HDPE resins in film blowing, bubble stability becomes even more important and

cannot be overemphasized.

4.6 Suggestions for Future Designs of Countercurrent Cooling Systems

An extension of this project should concentrate on applying more countercurrent air to a larger portion of the film bubble surface than occurs at present. To accomplish this with a cocurrent and countercurrent combination cooling device, the cylindrical shroud should be extended upwards towards the collapsing frame and equipped with centering rings chosen for a particular blow up ratio. With these changes, cooling air would be forced countercurrently over a long section of the film bubble. In order to form the bubble, the entire cylinder would have to be raised about a foot and then lowered with some kind of lever device, so that the melt emerging from the die could be bunched together and drawn upwards.

Cooling blown film by strictly countercurrent air flow resulted in a stable bubble only under narrow operating conditions. A compromise was made to achieve stability over typical operating conditions, by incorporating both cocrrent and countercurrent air flow. It would be interesting to use only countercurrent flow to cool the film. From this study,

it is evident that simply drawing air along the film, creates a destabilizing force on the bubble. An alternative approach, which was mentioned in the previous section, incorporates a raised air ring which directs air in a direction opposite to that of film motion. A cylindrical or conical shroud around the bubble would keep the air near the film surface. If the raised air ring were positioned near the frostline, where the film is resistant to bubble deformations, cooling air flows larger than those isuing from a cocurrent air ring might be possible. Additionally a small negative pressure applied just below the die, i.e. outside the immediate vicinity of the neck region, would serve to collect and remove some of the warmed air, while possibly not destabilizing the bubble.

The previous suggestions are concerned with design of a mainly countercurrent cooling system. However attention can also be paid to comparisons between cooling systems. The majority of cooling innovation proposals, along with this project, compare a newly fabricated device with the standard fan spray air ring. An interesting comparison, with regard to this research, is between two stacked conventional air rings and the proposed cocurrent - countercurrent cooling device. These systems are similar in that both have a conventional air ring located over the die, which cools the

neck region with a cocurrent flow. However, the raised devices redirect air differently over the upper portions of the bubble. A comparison made at maximum cooling air flow rates would indicate qualitatively which type of flow is more suited for blown film cooling.

Chapter 5

Cocurrent - Countercurrent Combination Cooling System:
Measurement Techniques

Independent and single-value dependent variable measurements were briefly discussed in Section 4.5.1. The measurements were made by standard industrial methods. The exception in this group is air flow rate. Cooling flow rates are not normally measured in industry or in research, rather a frostline height is reported (26,27,28). This gives a gross indication of air flow, as frostline height depends on the cooling rate between the die and the frostline. Greater air flows cause greater film cooling and thus a lower frostline. This section discusses air flow rate determination and the techniques used to measure the dependent variables listed in Table 1, Part IV; surface temperature, film thickness, bubble shape, air temperature and air velocity. These are all distribution variables, that is they vary with position along the film bubble or radially outward from the bubble surface.

The distributions of heat transfer coefficient and fraction of crystallinity are included as dependent variables in Table 1, Part IV, but they are determined using

the results of dependent variable measurements and a thermal analysis, by use of a heat balance around an element of film bubble.

5.1 Air Flow Rates

To determine the amount of air used to cool a film bubble, the air flow rate was calculated. In the cocurrent - countercurrent combination cooling system, each of the two air flows was determined. The air flow rate gives an indication of cooling occurring along the bubble for a given air ring. Increasing the cocurrent flow rate leads to a lower frostline and greater cooling. Similarly, with a constant cocurrent cooling flow, increases in the countercurrent air flow rate indicate greater bubble cooling.

A compact pitot tube (29) was used to measure a point pressure difference. With the assumption of incompressible flow (constant density), the differential pressure measured at each point was converted into the local velocity by a simplified form of the Bernoulli equation. From the point velocities a 'log-linear' method was used to obtain the overall mean velocity.

The 'log-linear' method used to calculate volumetric

flow rate was devised by Winternitz and Fischl (30). It assumes that the velocity distribution along a diameter can be represented by the equation;

$$U(y) = A + B \log(y/D) + C (y/D) \qquad (1)$$

where $U(y)$ is the point velocity at a distance y from the wall of the pipe of diameter D, and A,B and C are constants having dimensions of velocity. The pipe is divided into a number of annular zones and one central circular zone, all of equal area. The measuring points are positions at which the exact mean zone velocities occur, if the velocity distribution can be adequately represented by Equation 1. Winternitz and Fischl quote supporting evidence for this log-linear velocity distribution in a variety of flows, including asymmetric velocity profiles in pipes. With the mean velocity of a given zone calculated from differential pressure measurements, summation over all zones yields the mean air velocity in the pipe and, subsequently, volumetric flow rate. A sketch illustrating this method of flow rate determination is shown in Figure 5.1.

The flow rate through the cocurrent air duct was measured before the duct split into three flexible hoses that fed the air ring. The only available point of measurement on the main air duct was between a band of

Air Supply
From Blower

Air Duct Diameter = 5.5in.

Flow Rate
Measured Here

Measurement
Points

Butterfly
Valve

Differential pressure measurements were taken at
0.10, 0.42, 0.84, 1.19, 3.51, 4.31, 4.76, 5.08,
and 5.40 inches from the wall according to the
method described in reference 30.

Air Used to Cocurrently
Cool Film Bubble
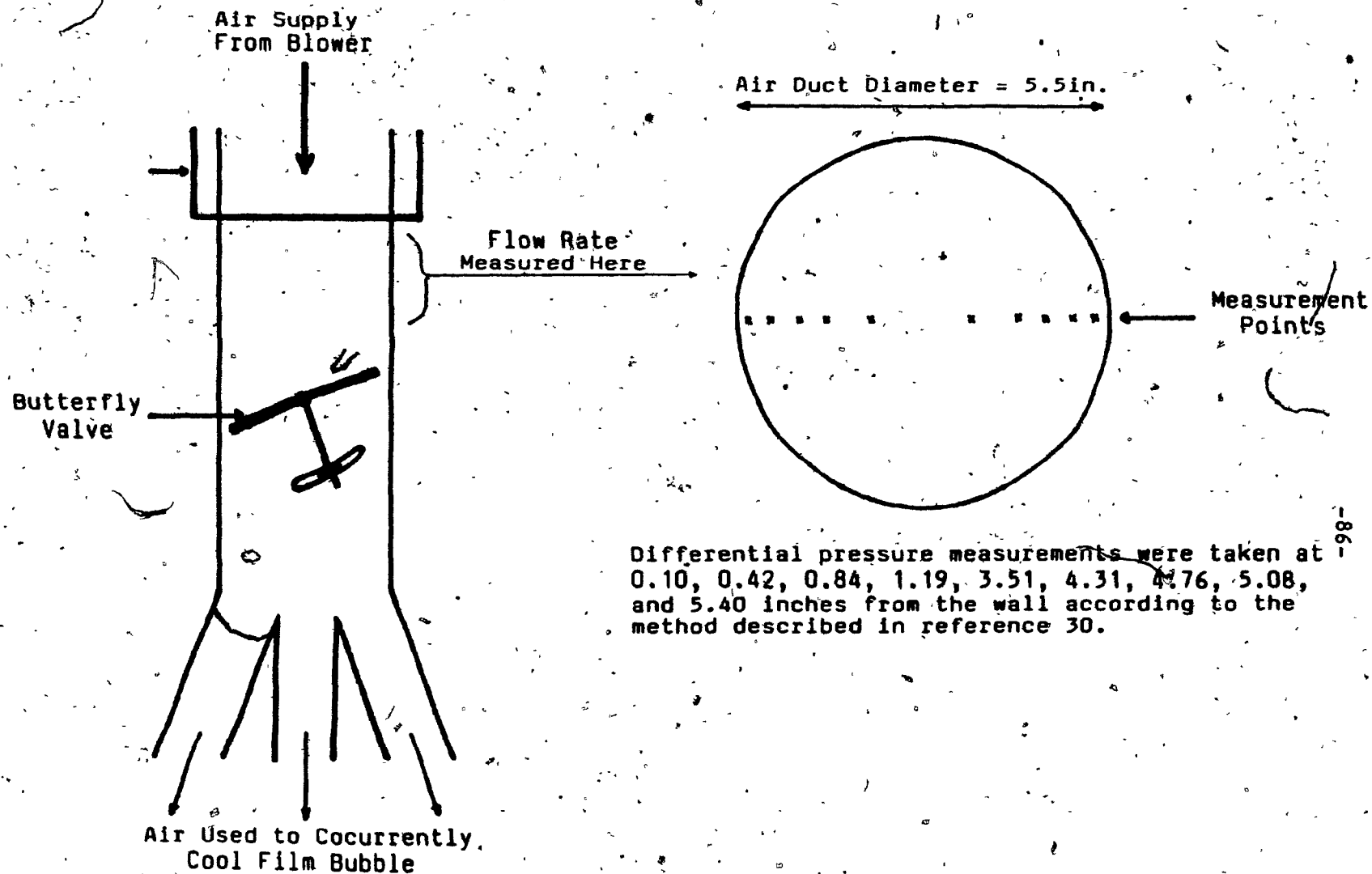
FIGURE 5.1   Sketch Illustrating Method of
Cooling Air Flow Rate Determination

insulation wrapped around the pipe and a butterfly valve
used to regulate the flow. The presence of the butterfly
valve immediately downstream from the point of measurement
suggested that the velocity profile might be asymmetric. In
countercurrent air flow, the air withdrawn through the
plenum travelled in one of two ducts to the blower. The
flexible hose ducts were joined just prior to entering the
blower intake. Measurements were made across a short
section of circular pipe where the ducts joined.
Disturbances on both sides of the measurement location
suggested that this flow would require a large number of
local pressure measurements to obtain a good approximation
of the velocity profile and enable volumetric flow rates to
be calculated.

In practice, a ten point pitot tube diameter traverse
was used to measure the differential pressure distribution
for each flow. Furthermore, under countercurrent flow it
was not sufficient to take readings along one diameter. In
this flow, the mean velocity for each zone was obtained from
four readings along diameters at 45 degree intervals.

5.1.1 Procedure

A compact pitot tube connected to a slanted arm manometer (Wilhelm Lambrecht Co., Goettingen, West Germany), containing a fluid of specific gravity 1.0, was used to measure the differential pressure. The pitot tube was mounted on a traverse mechanism (United Sensor and Control Corp., Watertown, Ma.) that allowed precise positioning within the circular air duct. A sketch of the apparatus is given in Figure 5.2.

(1) The location of each measuring point, in any circular duct, for the log-linear method is given in reference (30). The inner diameter of the air duct was measured and used to calculate the measuring point position of the compact pitot tube. (These positions are given in Appendix D1, along with the measurements.)

(2) One diameter traverse was made for each cocurrent flow rate, and four diameter traverses were made for each butterfly valve setting in countercurrent flow.

(3) The traverse mechanism was used to position the pitot tube for each measurement. A level mounted on the staging device ensured even movement of the pitot tube.

(4) In each measuring positon, the differential pressure was indicated by the distance the colored manometer fluid rose in the slanted arm manometer.

(5) Local velocities were calculated with the following equation (32):

$$U(Y) = F \left[2 \, (\Delta l \, \sin\phi) \, \rho_m \, g \, / \, \rho_{air} \right]^{\frac{1}{2}} \qquad (2)$$
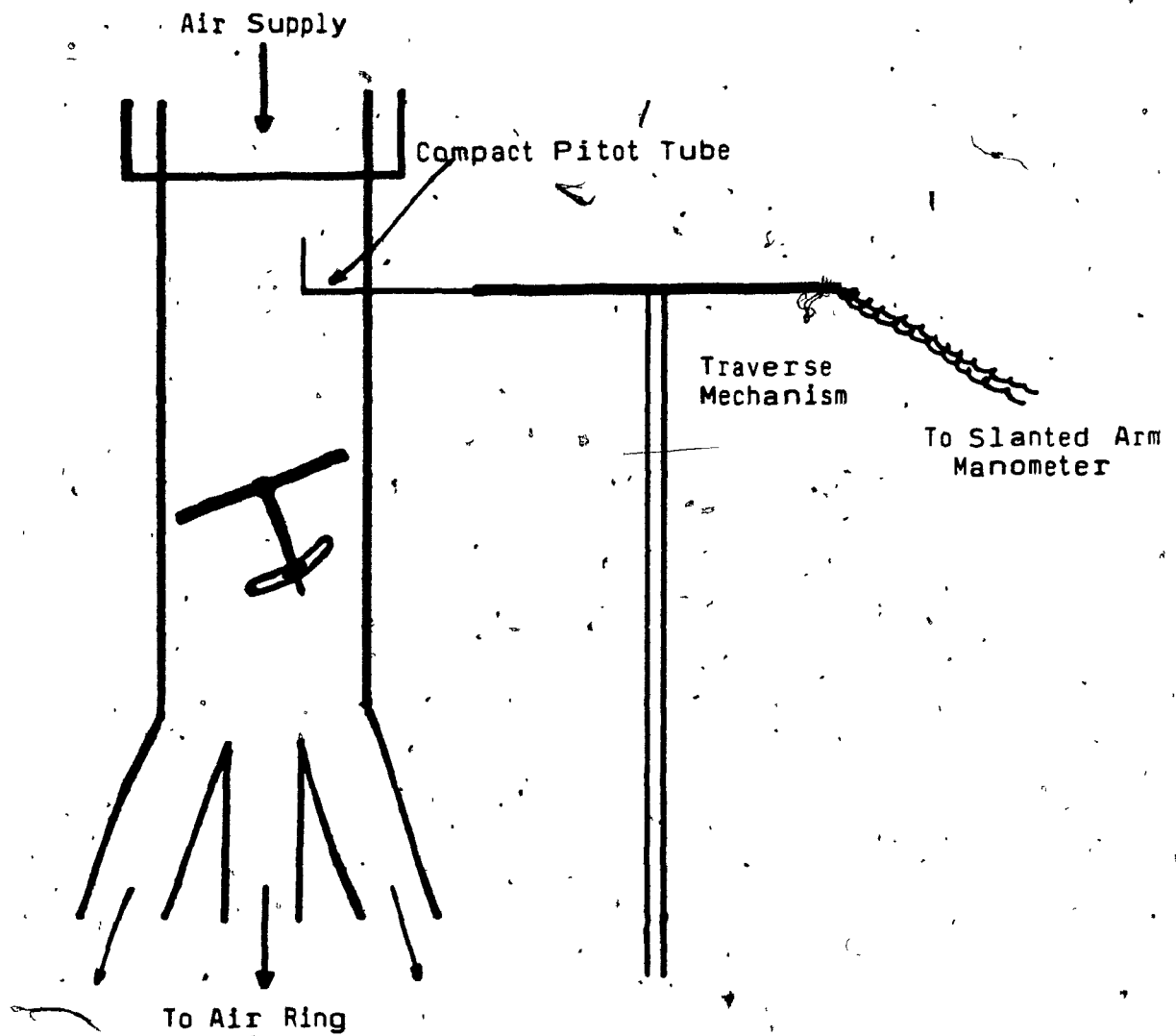
FIGURE 5.2 Sketch of Experimental Set Up for
Cooling Air Flow Rate Determination

where:

U(y) = point velocity a distance y from the
wall of the pipe and the mean velocity for
a given zone.

F = empirical constant taken to be 0.98

Δl = distance the manometer fluid has risen
in the slanted arm.

Φ = angle the slanted arm makes with the
horizontal.

ρ_m = density of manometer fluid

ρ_{air} = density of air

g = acceleration due to gravity

(6) Summation of the mean zone velocities gave a total mean
velocity. The volumetric flow rate was obtained by
multiplying the total mean velocity by the pipe
cross-sectional area.

An error anaylsis of this measurement is given in Appendix E.

5.2 Surface Temperature

Surface temperature varies along the film bubble with
distance above die. It is a position dependent variable and
is influenced by changes in any of the independent variables
in Table 1, Part II. Since all independent variables were
held constant except cooling air flow rate and the manner in
which air flow was applied to the bubble, surface
temperatures provided a quantitative indication of cooling

conditions along the entire bubble. In the regions above the frostline, for combination cooling flows, these measurements revealed the extent of countercurrent cooling. A simple estimate of the frostline height would not reveal greater cooling along these solid portions of the bubble, as frostline height only gives an indication of cooling in the molten neck region. Furthermore, surface temperature was used directly and as a derivative with respect to distance from the die, in an energy balance over an element of film, to calculate the heat transfer coefficient.

An infrared thermometer was used to measure surface temperature. This technique involves no contact with the film bubble, which is molten in the neck region. Plastic film, like all other materials, emits thermal radiation from its surface. The distribution and intensity of this thermal radiation are governed by the film chemical composition and temperature. This latter relationship allows temperature to be measured by a radiation thermometer that can quantitatively detect radiation intensity.

Plastic film is a 'gray body', in that it emits less thermal radiation than a 'black body'; the ideal or strongest emitter. The ratio of the radiance at wavelength w, of the film, to that of a black body at the same temperature is the spectral emittance, e. Values of é can range from 0 to 1, and this value varies with wavelength.

The emittance of a film sheet depends on its interacton with incident radiation. There are three possibilites for a stream of radiation incident on the film surface. A portion may be reflected, another portion transmitted through the film, and the remainder absorbed and degraded into heat. The sum of the fraction reflected, re, transmitted, tr, and absorbed, a, equals the total amount incident on the surface. Furthermore, the emittance of a substance is identical to the fraction absorbed.

$$e = a = 1.0 - tr - re \quad (2)$$

For a black body the transmitted and reflected fractions are zero and the emittance is unity. The reflected fraction r, was assumed to be 0.04 for polyethylene film and independent of thickness (31). The infrared thermometer used was sensitive to the 3.4 micron spectral band. In this region LDPE has zero transmission as shown in Figure 5.3. The solution of Equation 2 yields an emissivity of 0.96. With the emissivity of the film known, the infrared thermometer can be used directly to measure surface temperature.

The surface temperature measurement experimental set-up for the cocurrent and countercurrent combination cooling system is shown in Figure 5.4. With no cylindrical shroud
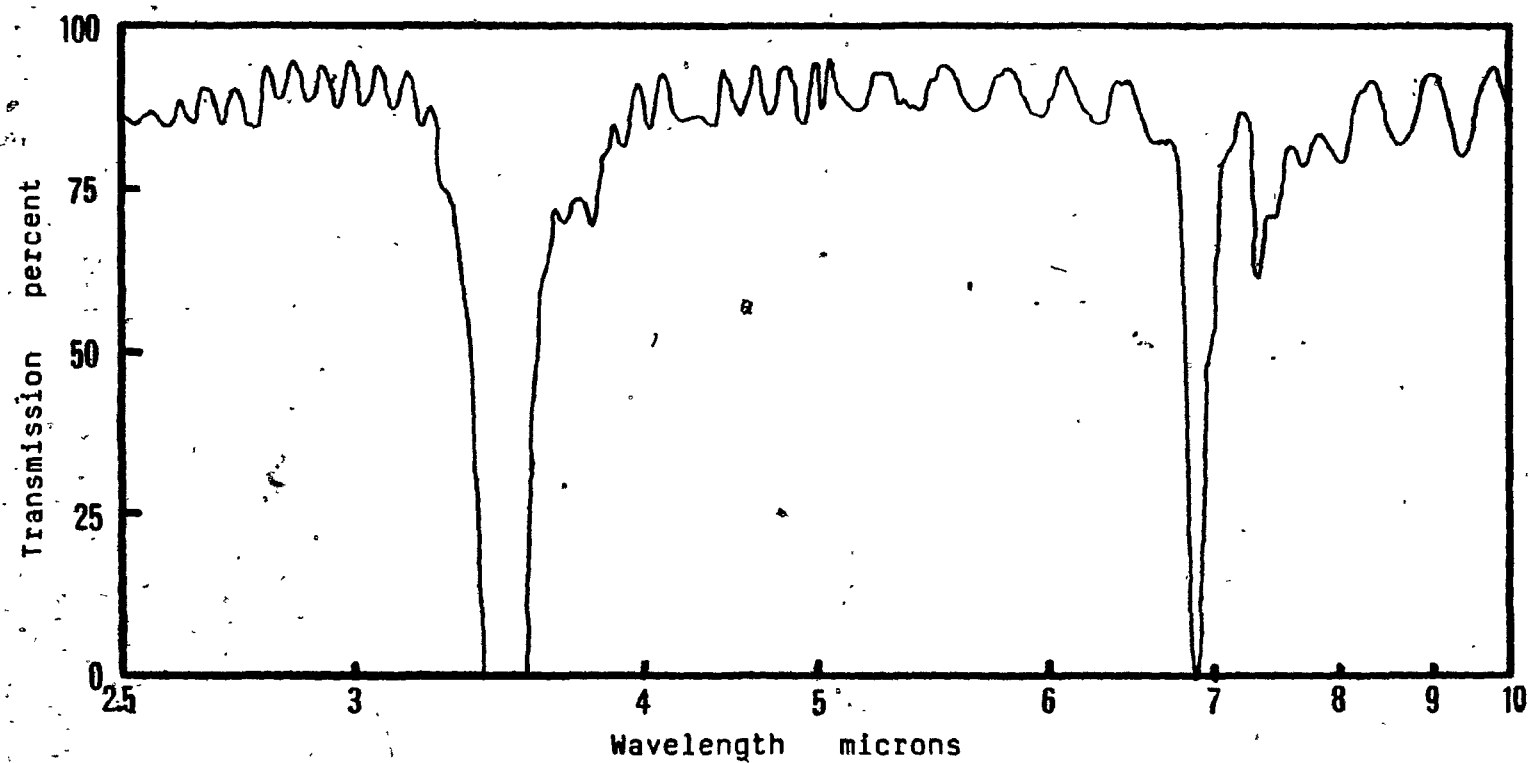
FIGURE 5.3   Infrared Spectrum of Union Carbide
Low Density Polyethylene DFDY 3312
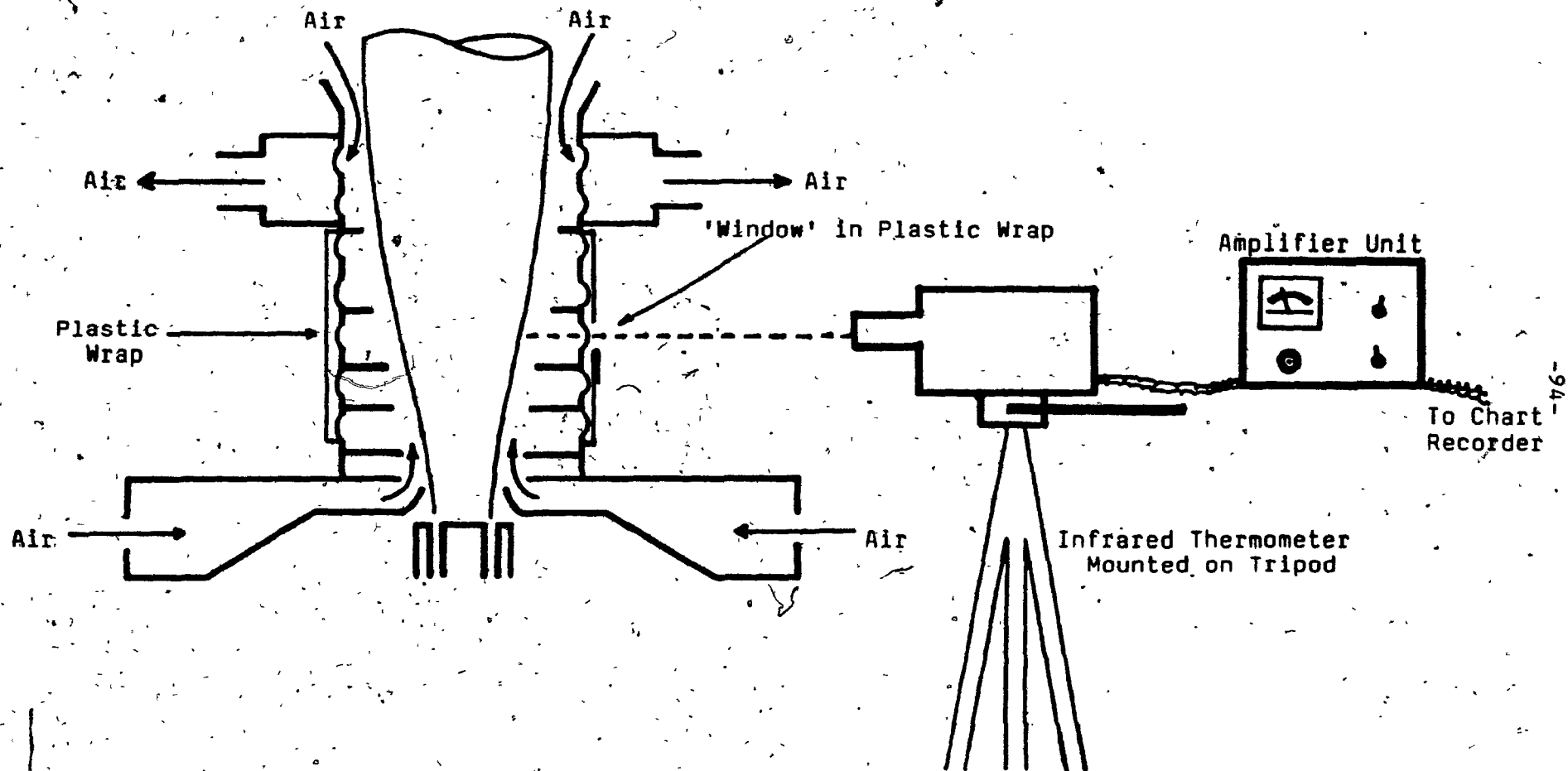
FIGURE 5.4   Sketch of Experimental Set Up for
Surface Temperature Measurements

present, the film temperature at any point above the die can be measured, as long as the bubble is within view of a radiation sensor of the instrument. This is not a severe limitation, as the thermometer can be 6 feet away from the bubble and still require only a one inch diameter viewing surface (32). The presence of a cylindrical shroud wrapped in plastic film complicates measurements, as the view of the bubble neck region is obstructed. To circumvent this problem several small one inch windows were cut in the plastic wrap, where holes (1.4 inch diameter) in the metal cylinder were present. Each time a measurement was made, a plastic 'window' was peeled back to allow an unobstructed view of the bubble. The requirement of a hole in the cylinder through which the film bubble could be 'seen' limited distances from the die at which measurements could be made. No film temperatures were obtained in the first several inches above the die, nor in the area blocked by the raised plenum.

5.2.1 Procedure

For each flow rate or combination of flow rates (14 cases in all) surface temperature was measured along the film bubble. An Ircon CH34 infrared thermometer (Skokie, Il.) was mounted on a tripod and raised a known distance

above the die to measure the film temperatures. The signal output was connected to a chart recorder (Hewlett Packard Inc., Pasadena, California) and · the millivolt reading converted to temperature (33). . . A description of the measurement procedure follows.

(1) The amplifier unit was calibrated by adjusting a deflection needle on an analog temperature scale to be within a fixed range.

(2) The 400°F temperature scale was selected. The first few measurements were made with this setting, and then the 300°F scale was used. .

(3) Emissivity was set at 0.96 on the amplifier unit.

(4) The optical head was focussed on the bubble surface at a known distance from the die. , The temperature was read off an analog scale and a millivolt reading was obtained from a chart recorder.

(5) In cocurrent flow the optical head was raised in one inch intervals, from an initial 3 inches above the die to 27 inches, and film temperatures were recorded.

(6) For the cocurrent and countercurrent combination cooling system, surface temperatures were measured at 5.1, 7.3, 9.8, 13.9, 22.0, 23.0, 26.0, and 27.0 inches from the die.

An error analysis of this measurement is given in Appendix E.

5.3 Bubble Shape

To determine the shape of the film bubble, the diameter of the extruded tube was measured. The diameter varied from 2.5 inches at the die to 5.8 inches at the frostline and was constant thereafter. The diameter in the upper region of the film bubble was calculated from the measured layflat width. Layflat width, and moreso bubble shape, give a gross indication of cooling along the bubble. This is a secondary effect of changing cooling conditions while trying to hold all other operating variables constant. Stronger cocurrent cooling conditions cause a marginally smaller blow up ratio or layflat width and thus provide a relative measure of cooling strength (5). This point will be discussed further in Secion 6.3, where bubble shape measurements are presented. Film bubble shape is also used in the heat balance over an element of film in Section 5.6, Equation 6, to calculate the heat transfer coefficient and fraction of crystallinity. It appears directly as a diameter term and indirectly in an angle term. The angle, Θ, between a tangent to the film surface and the axis of the bubble, was determined from diameter measurements symmetrically arranged around this axis at various distances from the die. The resulting plot has the appearance of an actual film bubble. This type of graph is shown in Figure 5.12. Above the

frostline, θ necessarily becomes 0.

Photographs at intervals along the neck region were used to measure the bubble diameter. With the diameter above the frostline region known, a photograph of the solid bubble allows a relationship between actual and measured bubble diameter to be found. Once this proportionality relationship is known, diameters in the neck region can be determined.

With cocurrent cooling and with no cylindrical shroud present, the bubble diameter could be determined from photographs at any height above the die. However, with the cocurrent and countercurrent combination cooling system present, the view of the bubble neck region was obstructed by the cylinder. Photographs of the neck region were limited to those distances from the die where the edges of the bubble were visible through the cylinder holes. The visible edges of the bubble were centered in the photograph to minimize distortion.

In order to distinguish the film bubble photographed through the cylindrical shroud wrapped in plastic, a colorant was added to the resin. Cadmium red was added to the feed hopper to form a roughly 2 per cent by weight composition. A photograph of the red bubble within the cylinder is shown in Figure 5.5.

FIGURE 5.5 Photograph of Film Bubble with
              Red Colorant

5.3.1 Procedure

A Nikon FM 6 camera (Tokyo, Japan) mounted on a tripod was used to photograph the bubble at various heights above the die. The camera was positioned the same distance from the bubble in each photograph with the camera lens perpendicular to the bubble surface. A sketch of the experimental setup is shown in Figure 5.6.

(1) Photographs of the bubble under both cocurrent and cocurrent and countercurrent combination cooling flows were taken at 4.8, 7.1, 12.1, and 14.4 inches above the die.

An additional photograph was made at 26 inches above the die under the combination cooling system. At this height the solid film bubble was above the cylindrical shroud.

(2) A proportionality relationship was determined between a bubble diameter measured from a photograph of the bubble above the frostline region, and the diameter calculated from layflat width. This relationship was used to calculate bubble diameters in the neck region, using diameters measured from photographs.

5.4 Air Temperatures

In cocurrent cooling, the cooling air is applied to the hottest portion of the film bubble and warms as it travels upward along the bubble surface. The velocity of cooling air is much greater than the film speed along most of the

Air   Air

Air   Air

Camera Mounted
on Tripod

Air   Air
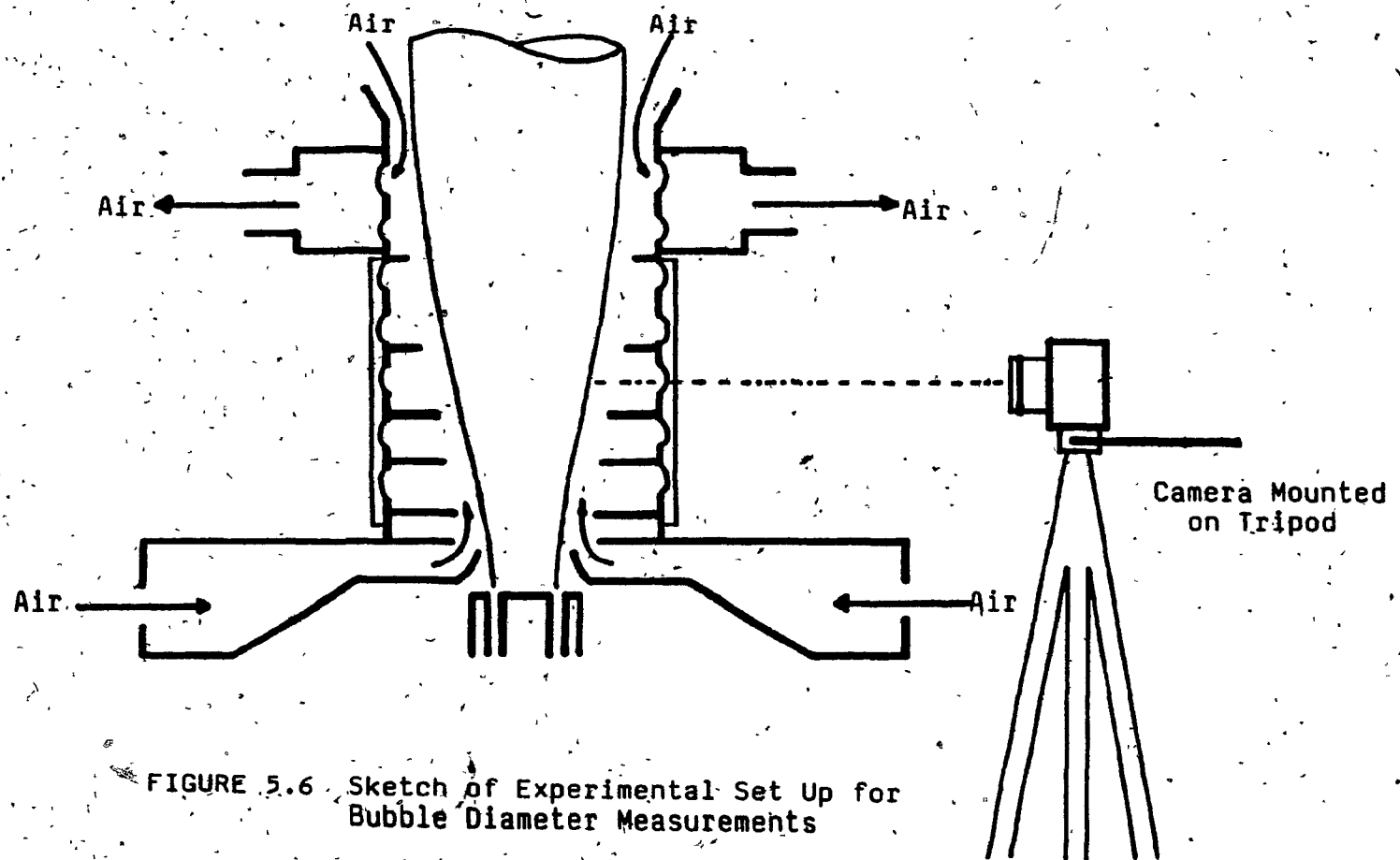
FIGURE 5.6   Sketch of Experimental Set Up for
Bubble Diameter Measurements

bubble surface, but near the nip rolls, where the film bubble is clamped together, the air velocity is reduced. Consequently, the warmed air collects around the nip rolls or uppermost portion of the film bubble. This stagnant heated air can be a problem for a film line operating under maximum cooling conditions and limited by blocking temperature. In some cases a production line has been slowed because of this phenomenon. Under countercurrent flow, the cooling air was drawn down the bubble and collected by a plenum so that there would be no accumulation of heated air. Collected air temperatures were measured by a thermocouple inserted in an air duct shortly after leaving the plenum.

It was also desirable to measure the air temperature near the bubble surface at various distances from the die and the air temperature distribution radially outward from the bubble, as this gives an indication of the cooling occurring along the bubble surface. The air temperature at the same location above the die and near the film surface was expected to be lower when larger cooling flows were applied to the bubble. Also, the shape of the radial air temperature distribution gives an indication of the thickness of the air stream participating in heat transfer.

The air temperature distributions along the film bubble and radially outward from the surface were measured with a

thermocouple mounted on a traverse mechanism. However, with the cylindrical shroud of the combination cooling system surrounding the film bubble, the possible measurement positions above the die were limited. As in the surface temperature measurements, small windows were cut in the plastic wrap where holes in the cylinder were present and the thermocouple was manipulated through these openings to any radial distance from the film bubble.

5.4.1 Procedure

An iron-constantan thermocouple equipped with an electronic cold junction (Omega Engineering Inc., Stamford, Ct.) was connected to a chart recorder to give a millivolt output, which was converted to temperature using standard tables (33). The thermocouple was moved to different positions with a traverse mechanism. A sketch of the experimental set-up is given in Figure 5.7.

(1) Under cocurrent cooling ,with no cylinder present, air temperatures were measured at 2.4, 5.3, 7.5, 9.8, 12.8, 22.4,and 27.1 inches above the die.

(2) Distances from the die were determined that coincided with the opennings or 'windows' in the cylindrical shroud under combination cooling. These distances were 4.5, 7.0, 12.4, 22.0, and 27.0 inches.

(3) At each position above the die, air temperatures were measured radially outward from the bubble. Under the combination cooling system, the radial measurement

Air   Air

Air

Air

Thermocouple

'Window' in Plastic Wrap

Plastic
Wrap

To Chart
Recorder

Air

Air

Traverse
Mechanism
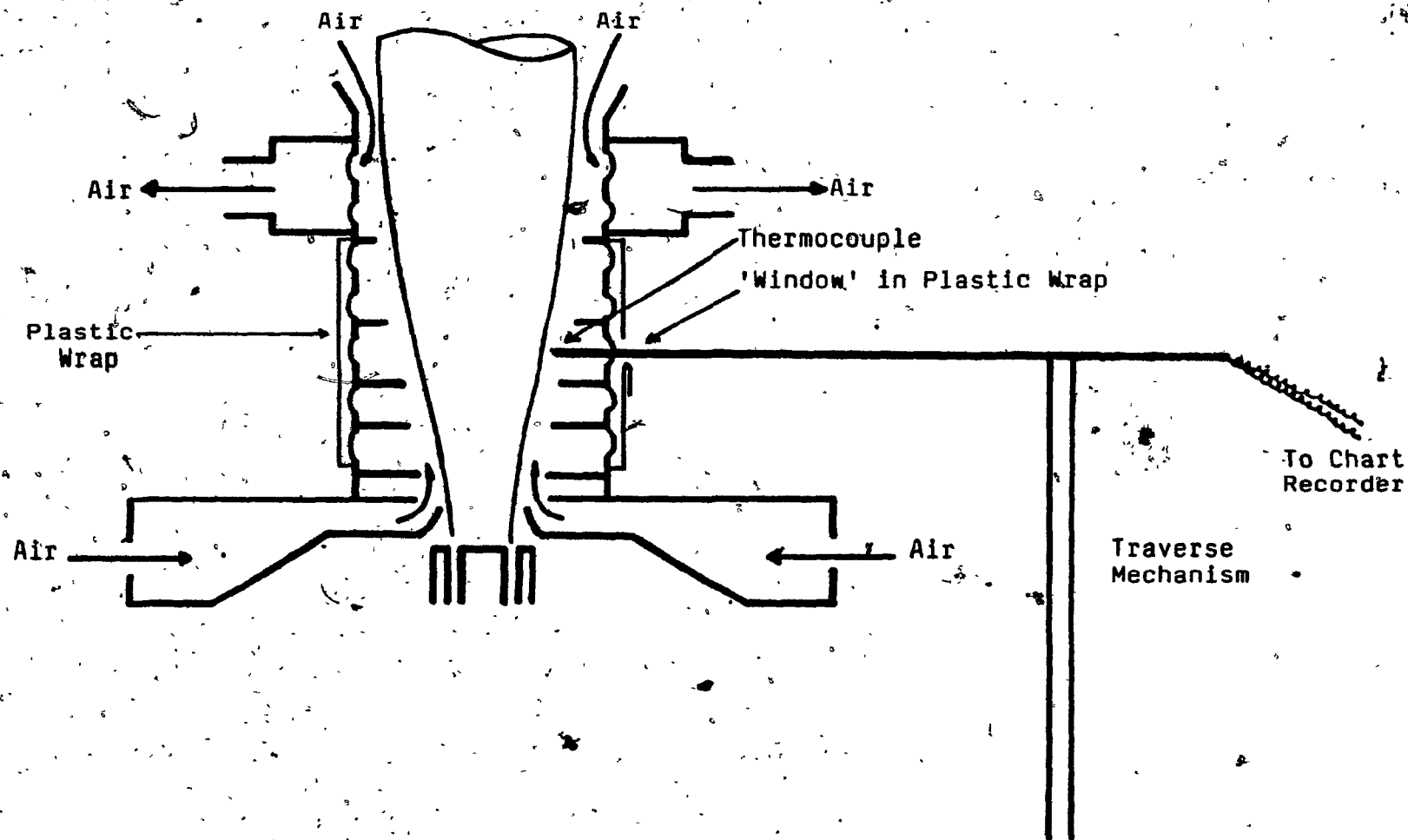
FIGURE 5.7 Sketch of Experimental Set Up for
Air Temperature Measurements

positions were constrained by the cylinder wall. These distances were approximately 0.5, 1.0, 1.5, 2.5, and 3.0 inches from the film bubble. Without the cylinder present, that is, in cocurrent cooling, air temperatures were also measured at these positions, and additionally at 6.0 inches from the bubble.

Once the traverse mechanism was raised to a given position, the thermocouple was moved laterally by the mechanism to a specified radial location from the bubble.

(4) Measurements were recorded in millivolts on a strip chart recorder and converted to temperature.

5.5 Air Velooities

Cooling air velocites vary along the bubble and radially outward from the film surface. They are listed in Table 1, Part III as a position dependent variable. For a particular cooling system, air velocities give an indication of the cooling occurring along the bubble surface. Greater air velocities near the surface correspond to a lower frostline and film temperatures (5). Furthermore, under countercurrent flow, velocity measurements reveal the thickness and magnitude of the drawn air stream and whether it is applied next to the film surface.

Mean air velocities were measured with a hot wire anemometer. An electrically heated wire was exposed to a

flowing medium. An increase in fluid speed increased the rate of heat flow from the wire and consequently cooled the wire. Cooling the wire, however, altered its resistence, so that a measurable effect was produced in the electrical heating circuit. In the anemometer used, a constant temperature was maintained across the hot wire by adjusting the current flowing through a bridge circuit (34). The current was determined by measuring the voltage drop across a standard resistance.

The output voltage of a constant-temperature anemometer is a non-linear function of the flow velocity. The relation between flow velocity (U) and anemometer output voltage (Va) can be expressed by this equation:

$$Va^2 = A + B \ (U)^{1/n} \tag{3}$$

where A and B are constants whose values depend on the hot wire probe used, and n is an empirically determined exponent. A voltage-velocity calibration curve is shown in Figure 5.8. Here, the change in voltage over a wide range of velocities is small and could lead to errors in velocities read from this graph. For this reason, the output voltage was linearized. A linearizer is basically an electronic analog computer which linearizes the anemometer output voltage with a transfer function, in this case:

$$Vlin = J \ (Va^2 - A)^n \tag{4}$$
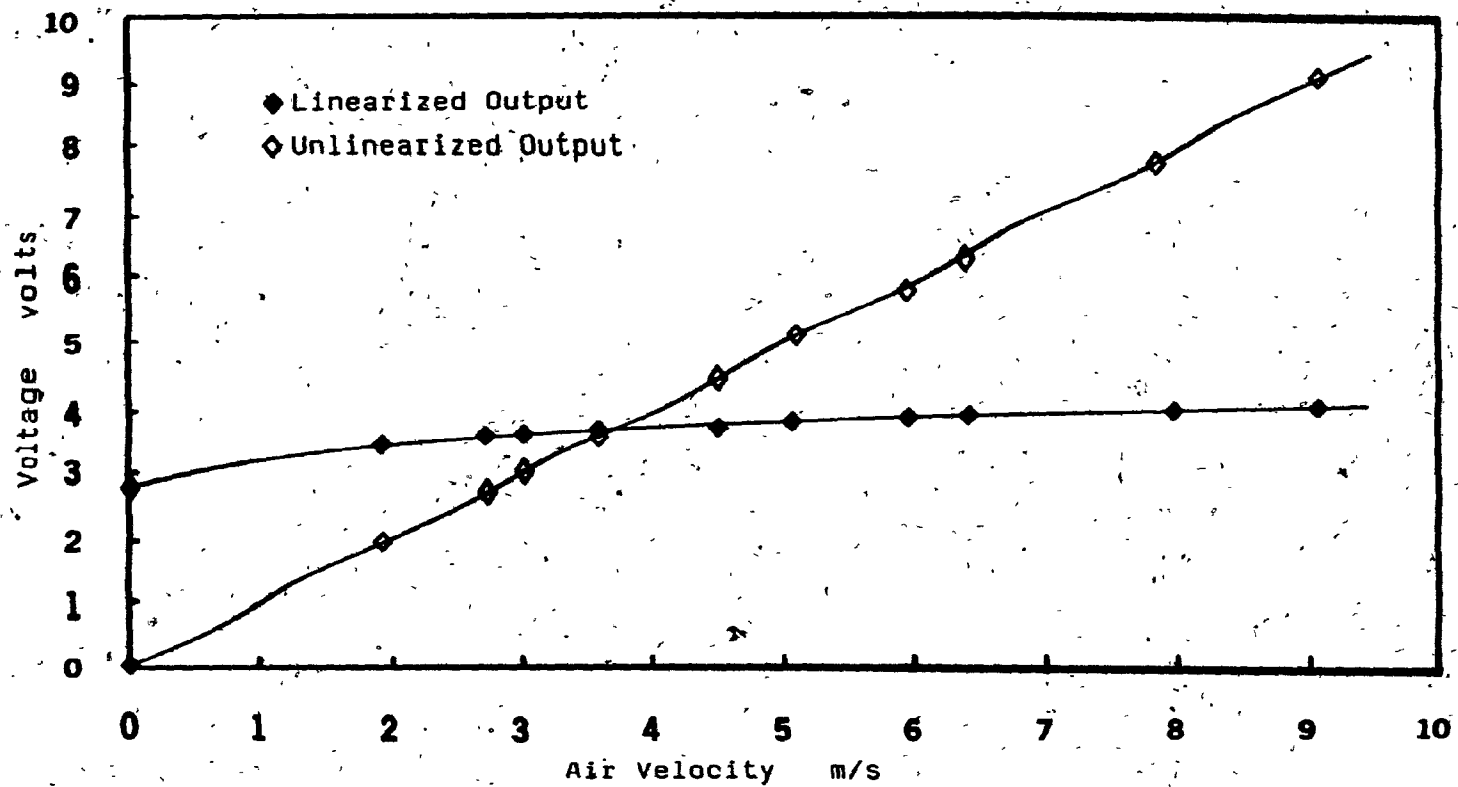
FIGURE 5.8 Hot Wire Anemometer Voltage Versus
Air Velocity Relationships

where Vlin is the linearized output voltage and J' is a constant depending on the conditions of measurement. Substituting Equation 3 into 4 and collecting all the constants into one term yields:

$$Vlin = J' (A + B U^{1/n} - A)^n = J U \qquad (5)$$

where J is a collection of constants. The linearizer output voltage is therefore proportional to the flow velocity U. A linearized calibration curve is also shown in Figure 5.8.

The cooling air flow along the film bubble, whose velocity was to be measured, varies in temperature. Without some kind of compensation, the constant-temperature hot wire probe would be influenced by this temperature fluctuation across the medium as well as by the flow velocity. A dual sensor probe containing a velocity sensor and a thermistor, which acts as a temperature sensor, was used to compensate for temperature changes in the medium.

Under the combination cooling system, the cylindrical shroud surrounding the neck region made manipulation of the probe very difficult. As in film surface and air temperature measurements, small windows cut in the plastic wrap provided openings to the air flow in this region. However, the probe was bent at a right angle in order to sition the hot wires perpendicular to the cooling stream.

It was this 'bent' section of the probe, 2.8 inches long, that was difficult to manipulate through the 1.4 inch window in the cylinder. Once in the cylinder, extreme care was required to position the probe in the small gap between the film bubble and the obstruction plate. A sketch of the experimental setup is shown in Figure 5.9.

5.5.1 Procedure

A modular hot wire anemometer system made by Disa Electronics (presently Dantec Electronics, Skoulunde, Denmark) was used to measure air velocities. The anemometer system consisted of a main unit anemometer with symmetrical bridge (Disa models 55M01 and 55M12), a linearizer(55D10), and a digital voltmeter(55D31). To the main unit anemometer was connected two coaxial probe cables 2.5 meters in length, followed by a probe guide tube(55H139), a right angle probe support(55H26), and a dual-sensor, temperature-compensating probe(55P81). The probe, support and guide tube were mounted on the traverse mechanism. Refer to the experimental _set-up sketch shown in Figure 5.9. A description of the procedure follows:

(1) The main unit anemometer controls were set to the following initial values:
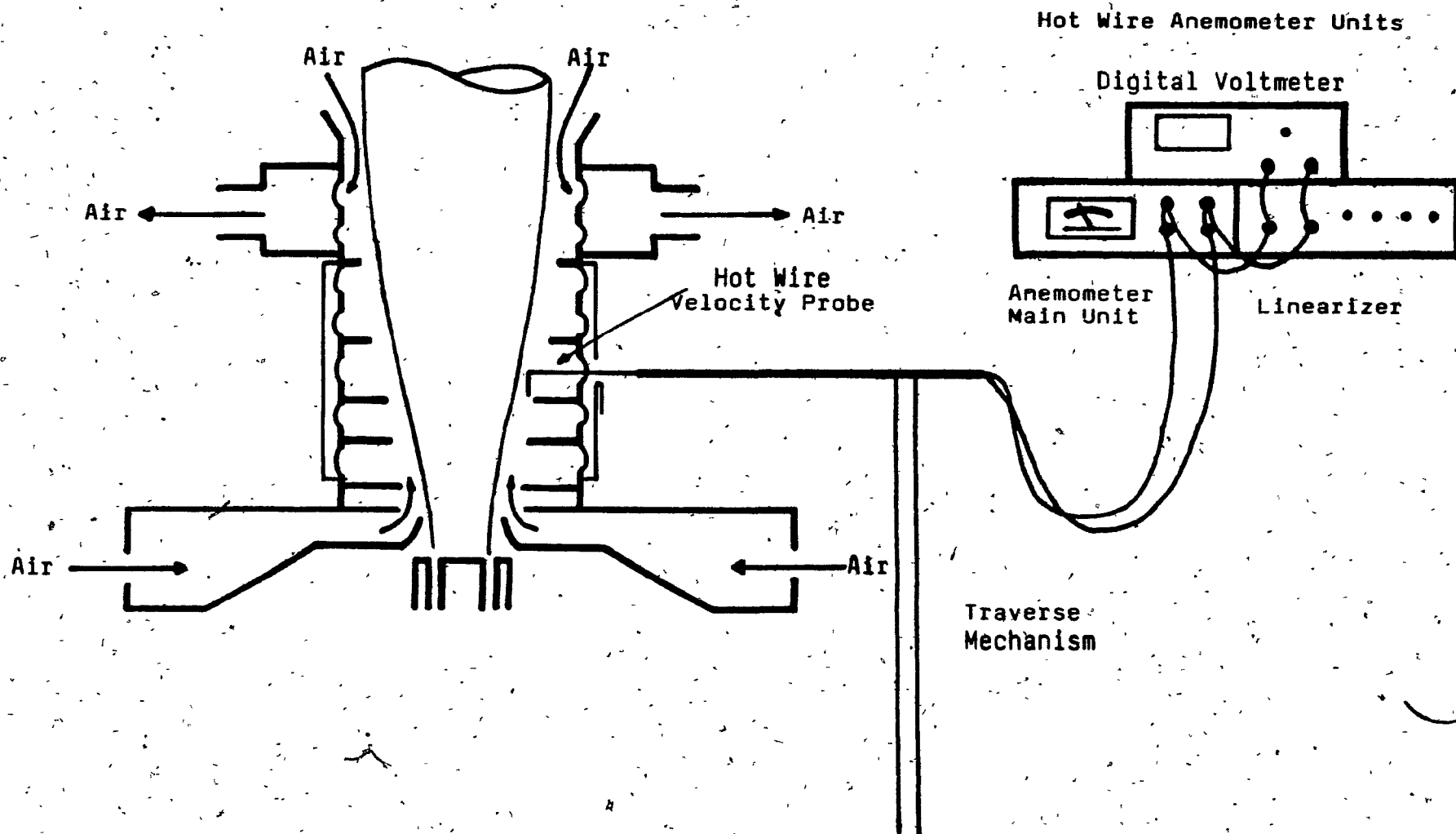
FIGURE 5.9   Sketch of Experimental Set Up for
            Air Velocity Measurements

SQUARE WAVE:	OFF
HF FILTER:	1.0
VOLTS:	1.0
FUNCTION:	STB. BY
PROBE TYPE:	WIRE
GAIN:	1.0
DECADE RESISTENCE:	00.00

(2) The dual sensor/probe was connected to the probe support.

(3) One of the two coaxial cables (one for each sensor) was plugged into the BNC receptor marked PROBE. The other end of this cable was connected to a probe short(55H32).

(4) The ZERO OHMS potentiometer was used to center a deflection needle to a red mark, midway on the anemometer unit output scale.

(5) The probe short was removed from the coaxial cable, and the cable was connected to the probe support from (2).

(6) The FUNCTION switch of the main unit was turned to RES. MES.(resistance measurement). The decade resistance setting was altered, so that the meter needle again covered the red scale mark.

The best way to do this is first to increase the left decade stepwise from zero until the meter needle suddenly goes to the opposite scale end. Then turn the decade one step backwards and repeat the procedure with the next decade, etc.

(7) Steps (5) and (6) were repeated with the other probe support cable.

(8) The probe support cable with the lower operating resistance was connected to the socket marked PROBE on the anemometer unit. The probe operating resistance was 4.58 ohms.

(9) The other support cable was connected to the EXTERNAL BRIDGE ARM also on the main unit.

(10) The probe sensor was covered with a protective plastic tube, so that stagnant air surrounded the sensor.

(11) A coaxial cable was used to connect an output socket on the main unit to the input receptor on the digital voltmeter.

(12) The RANGE of the voltmeter was set to 10 Volts and the TIME CONSTANT to 1 second. The FUNCTION switch on the main unit was turned to OPERATE. The anemometer output voltage at zero flow was 2.77 volts.

(13) In order to balance the bridge, an oscilloscope (Type 564, Tekronix, Portland, Or.) was hooked up to an OUT socket on the anemometer main unit. The oscilloscope was set to a sensitivity of 0.1 volts/division with a time sweep of 50 usec or 20 usec.

(14) The SQUARE WAVE generator on the main unit was set to 3. The waveform shown in Figure 5.10 was obtained after adjusting GAIN, HF FILTER and HF BALANCE. This waveform was similar to one given in the Disa operating guide (34).

First GAIN and HF FILTER were adjusted, and then HF BALANCE on the symmetrical bridge was 'fiddled' with by first moving the control knob left then right to eliminate tail oscillations and broaden the peak of the waveform. This procedure was repeated several times until the waveform in Figure 5.10 was obtained.

(15) The oscilloscope was disconnected and the SQUARE WAVE generator turned off. The probe was now ready to be calibrated.

(16) Calibration was carried out in the Mechanical Engineering Department, Aerodynamics Laboratory at McGill University. A sketch of the probe calibration setup is shown in Figure 5.11. A slanted arm manometer was used to measure the pressure difference between points 1 and 2. The velocity at point 2 was calculated from the equation:

$$U_2 = [2 (\Delta l \sin\phi) \rho_m g / \rho_{air}]^{\frac{1}{2}}$$

An explanation of this equation is given in Appendix D5.

At each calibration velocity, the output voltage of the anemometer was read from the digital voltmeter and
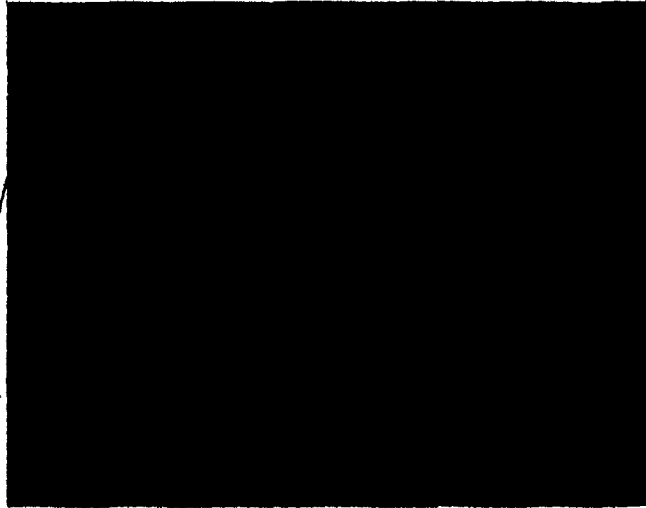
FIGURE 5.10   Waveform of Hot Wire Anemometer
              Wave Generator
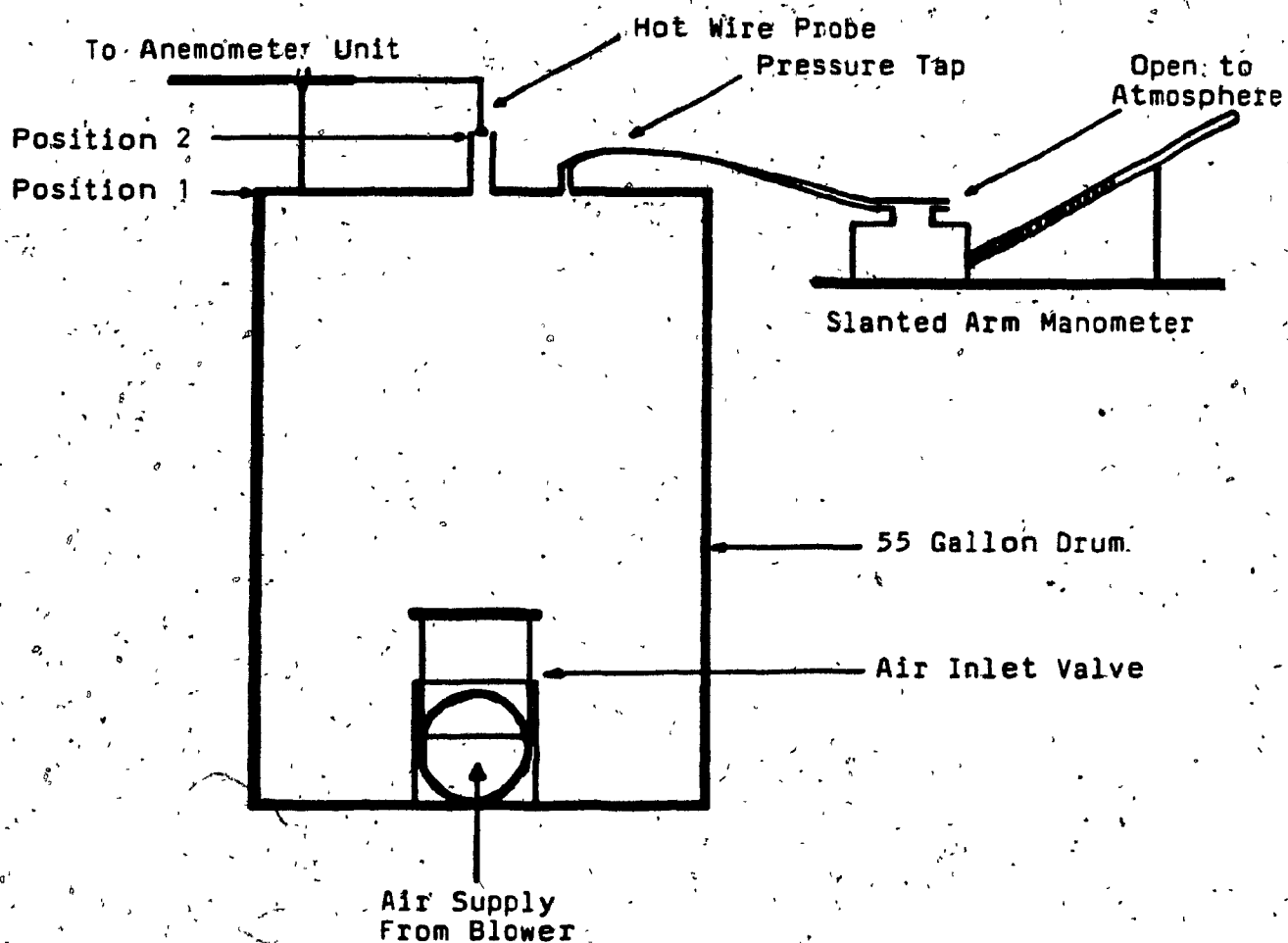
FIGURE 5.11   Sketch of Hot Wire Anemometer
Calibration Set Up

recorded. Calibration data are contained in Appendix D5.

(17) The exponent n of the transfer function (Equation 4) was determined:

From the calibration data, a log-log plot of $(Va/Vo*)^2 -1$ versus U meters/sec yielded a straight line, in which the inverse of the slope equaled the exponent n. The term Vo* is a corrected voltage at zero velocity; Vo* = Vo (s), where s is an empirical constant less than one.

A value of 0.925 was used for s and provided a linear calibration curve. The inverse of the slope, n, was equal to 2.14. Refer to Appendix D5 for the determination of s.

(18) The linearizer was connected to the anemometer main unit and digital voltmeter as shown in Figure 5.9.

Steps (19) through (22) refer to the linearizer module unit.

(19) Two controls marked EXPONENT were used to select the value n.

(21) The ZERO pushbutton was depressed and held. Two ZERO ADJ. (zero adjustment) controls were adjusted for zero linearizer output voltage. The pushbutton was then released.

(22) GAIN ADJ. controls were set, so that a one to one relationship existed between the linearizer output voltage and the velocity (1 volt to 1 m/sec).

(23) A 'calibration' test was carried out to confirm that the output voltage had actually been linearized, the results of which are listed in Appendix D5. A graph of the linearized output voltage is shown in Figure 5.8.

The hot wire anemometer was now ready to measure air velocities.

(24) The TIME CONSTANT on the digital voltmeter was set to 30 seconds.

(25) Under cocurrent cooling, the hot wire probe was positioned at 2.0, 4.3, 7.7, 11.8, 14.3, 20.0, and 25.0

inches above the die. In each position air velocities
were measured radially outward from the bubble at 0.3,
0.4, 0.6, 0.7, 0.8, 1.0, 1.2, 1.5, 2.0, 2.5, 3.0, 3.5,
4.5, 5.5, and 6.5 inches.

(26) Under the combination cooling system, the hot
wire probe was positioned at 1.0, 9.8, 23.1, 29.6,
33.3, and 38.8 inches above the die. In the first two
positions, 1.0 and 9.8 inches from the die, air
velocities were measured radially outward from the
bubble only at 0.5, 0.6, 0.7, 0.8, and 1.0 inches, due
to the constraint of the obstruction plates within the
cylindrical shroud. At 23.1 inches above the die,
which is within the cylinder but above the obstruction
plates, velocities were measured at 0.3, 0.4, 0.6, 0.8,
1.0, 1.2, 1.4, 1.7, 2.0, and 2.3 inches from the film
bubble. In the uppermost three positions, air
velocities were measured at 0.3, 0.5, 0.7, 1.0, 1.5,
2.0, 2.5, 3.0, 3.5, and 4.0 inches radially outward
from the bubble.

5.6 Heat Transfer Coefficient

The primary mechanisms of heat transfer along the
bubble are forced convection of cooling air and radiation to
the surroundings. Heat transfer coefficients and fraction
of crystallinity were determined from a heat balance over an
element of film bubble that incorporates these modes of heat
transfer. A sketch of a film element and the coordinate
system used is shown in Figure 5.12.

A differential heat balance over a vertical segment dz
leads to the equation:
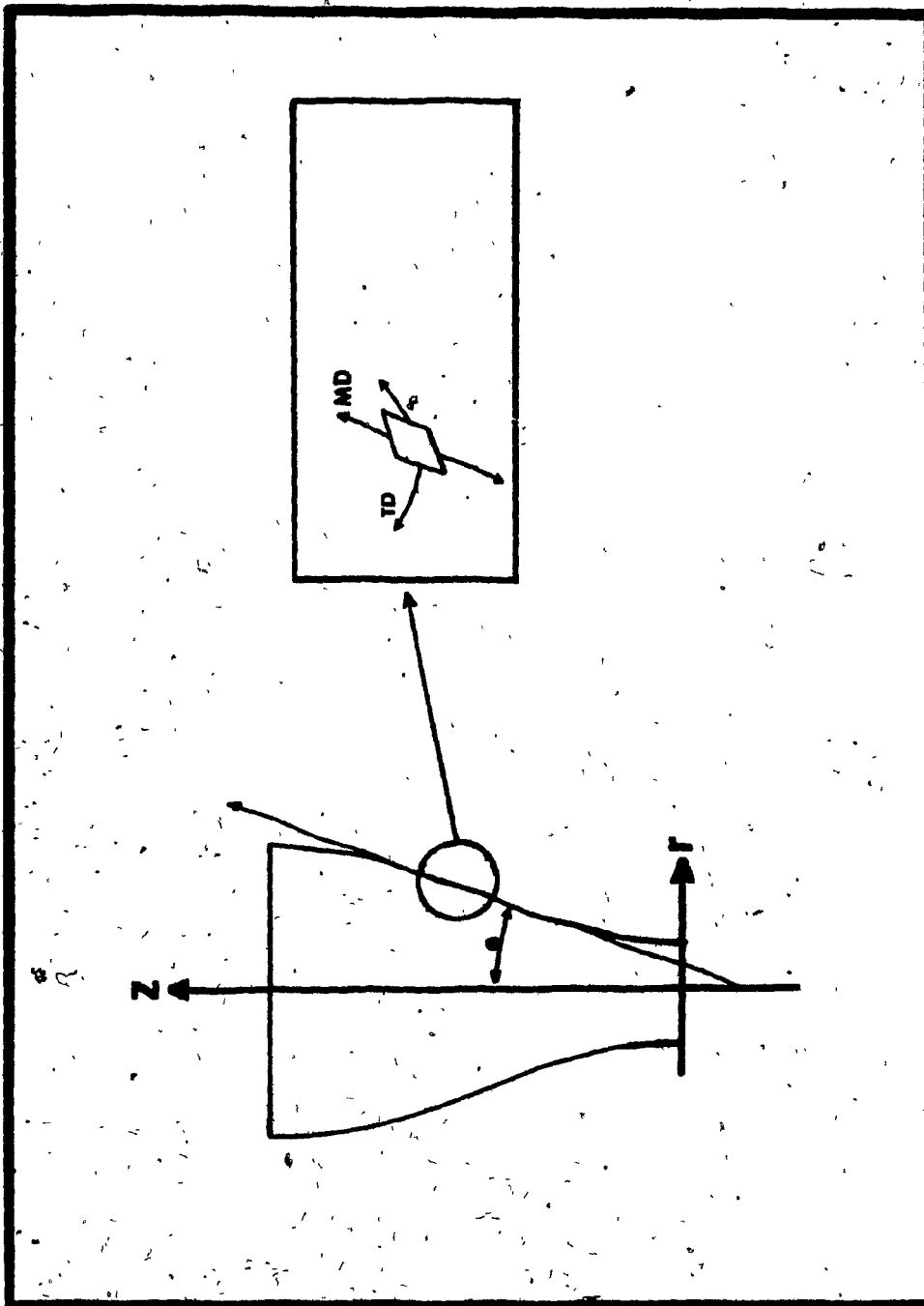
FIGURE 5.12 Film Bubble Element and Coordiante System

$$\dot{m} C_p \cos\theta \, dT_s/dz + m \, H_c \cos\theta \, dX_c/dz =$$

$$\pi D [h (T_s - T_c) + e K (T_s^4 - T_a^4)] \quad (6)$$

where:

   m = polymer mass flow rate

   Cp = specific heat

   θ = angle between a tangent to the film surface
        and the axis of the bubble (z-axis)

   Ts = film surface temperature

   Ta = temperature of the surroundings

   Tc = cooling air temperature (equal to Ta)

   z = distance from the die

   D = bubble diameter

   h = local heat transfer coefficient

   e = emissivity

   K = Stefan-Boltzman constant

   Hc = heat of crystallization

   Xc = fraction of crystallinity

The polymer mass flow rate and cooling temperatures were constant. These single-valued variables were determined as indicated in Section 4.5.1. Angle and diameter terms were calculated from bubble shape measurements. Similarly, cooling curve gradiants were obtained from surface temperature measurements. Emissivity

has been reported to depend on film thickness (35). Menges (27) has presented plots of low density polyethylene film thickness versus emissivity. These reported emissivity values were related to distance from the die through thickness measurements. The following section (Section 5.6.1) reveals the method used to obtain the film thickness distribution. Heat of crystallization and specific heat could not be determined by direct measurements in the film blowing process; rather a differential scanning calorimeter (DSC) and differential thermal analyzer (DTA) were used. The thermal analysis is discussed in Section 5.6.2.

A derivation of Equation 6 is given in Appendix Al. A similar heat balance has been given by White (26), and several balances without the heat of crystallization term are discussed in the literature (28)(36)(40). The term on the left hand side of Equation 6 represents the surface temperature variance with position along the length of the bubble and also the geometric deviation of the film bubble from a right cylinder. The first term on the right hand side is attributed to convective cooling and believed to be the major component of heat transfer from the bubble. The second bracketed term is the radiative contribution. Radiative cooling has been estimated at 10 to 20 per cent of the total heat transferred (27). The final term accounts for heat absorbed in the liquid-solid transition occurring

mostly in the frostline region.

Heat transfer coefficients were calculated directly
from the heat balance outside the frostline region. In
these areas, the term in Equation 6 containing the fraction
of crystallinity was assumed small and was neglected. A
plot of heat transfer coefficient versus distance from the
die was thus discontinuous in the heighborhood of the
frostline. However, heat transfer coefficients could be
estimated over this area and used in the heat balance to
obtain crystallinity fractions in the frostline region.

5.6.1 Thickness Distribution

Film thickness changes significantly from die to
frostline. Melt emerged from a 23 mil die gap, was
stretched and expanded until reaching the frostline, and was
all the time continuously cooled. At the frostline, the
melt solidified and film thickness remained constant
thereafter at 1.6 mils. This was not a monotonic decrease
in thickness from die gap to frostline, however, as the melt
swelled immediately after flowing from the die. The die
swell is not large by other process standards, since the
melt is being rapidly drawn by the nip rolls and thus does
not remain in an expanded state very long. Die swell does,

however, allow the melt to relax and 'forget' most of the orientation imparted to it during flow through the die. This last point will be discussed further in Chapter 8 in terms of film orientation.

Film thickness is used indirectly in the heat balance (Equation 6), to calculate the heat transfer coefficient and fraction of crystallinity. In order to make these calculations, the emissivity must be known as a function of distance from the die. Predoehl (35) has measured emissivity at various thicknesses for LDPE. Thus a thickness distribution between die and frostline could be used to relate emissivity to height above die.

The thickness of a film sample was measured with a micrometer and was found to be 1.6 mils under the processing conditions used. The film thickness distribution also needed to be measured with this micrometer, but the bubble is molten in the region where thickness changes. A technique was used to obtain a solid neck region, which was only possible with an unobstructed film bubble, that is, without a cylindrical shroud. Once a stable bubble was established, the nip rolls were stopped. Two rectangular wooden boards were used to clamp the base of the bubble together, holding the neck region in position as it quickly cooled. Thus, a 'solid' neck region was produced, whose thickness could be measured.

A sketch of this technique is shown in Figure 5.13. As the molten regions cool, clamped in place, the polymer undergoes some shrinkage. Cooling an amorphous melt causes denser crystalline regions to form and an accompanying volume reduction. Also, some deformations were likely to occur in the stationary film, due to gravity. Therefore, thickness measurements of the solid neck region probably deviated from those of the actual molten bubble. Nevertheless, this method was used and thickness distribution obtained from five solid neck region measurements, under standard cocurrent cooling conditions, was reproduced within 5 percent. Han (39) has alluded to a similar method to obtain bubble shape and thus diameter and θ values (angle between tangent to film surface and bubble axis) as a function of distance from the die.

5.6.1.1 Procedure

A micrometer was used to measure an average film thickness at various distances from the die.

(1) A solid neck region was formed by the technique discussed in the previous section and illustrated in Figure 5.13.

(2) The portion of film that was clamped together, 2 to 3 inches above the die, was separated from the rest of the sample and a double film thickness measured. Measurements were made at half inch intervals across
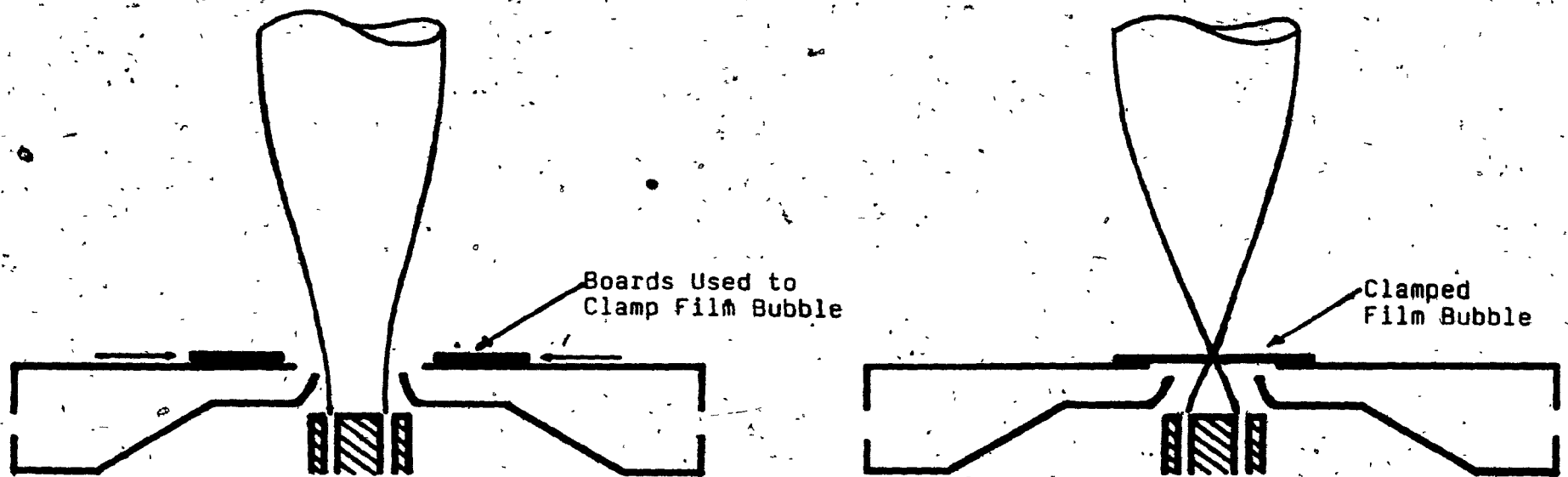
FIGURE 5.13   Sketch of Experimental Technique Used
to Obtain Thickness Measurements

the film tube (transverse direction). Values were averaged and divided by two to yield an average film thickness very close to the die.

(3) The thickness of the remaining neck region sample was measured at half inch intervals along the circumference of the tubular film, at each measurement position above the die, and the average film thickness was calculated. The measurement positions were increased in one inch increments from 3 to 18 inches above the die.

5.6.2 Thermal Analysis

In order to calculate the local heat transfer coefficient and fraction of crystallinity from the heat balance given by Equation 6, heat of crystallization and specific heats must be known. Specific heat is a function of temperature and therefore varies with distance from the die. However, neither specific heat nor heat of crystallization can be measured directly in the film blowing process. A thermal analysis was carried out using a differential scanning calorimeter to determine the heat of crystallization and a differential thermal analyzer was used to measure specific heats. These methods were only intended to provide an estimate of the polymer thermal properties. Both specific heat and heat of crystallization depend on the rate of heating or cooling and the degree of polymer orientation and are thus dependent on the processing conditions encountered in blowing film. These conditions

are very different than those experienced in thermal analysis techniques. However, the alternative to these methods was to use a single literature value and apply it over the entire film temperature range.

Whenever a material undergoes a change in physical state, such as melting or freezing, heat is either absorbed or liberated. Thermal analysis instruments are designed to determine the enthalpy changes for these processes by measuring the differential heat flow required to maintain a sample of the material, as well as an inert reference material at the same temperature. The instrument is programmed to scan a temperature range by increasing or decreasing linearly at a predetermined rate. In DTA systems, both sample and reference are heated by a single heat source. Temperatures are measured by sensors attached to pans containing the materials. The magnitude of the temperature change at a given time is proportional to the enthalpy change. With a DSC the sample and reference have individual heaters. The temperature sensors act as two control loops; one is for average temperature control, so that the temperature of the sample and reference may be increased at a predetermined rate, and the other adjusts power input to remove any temperature difference that develops between sample and reference. The output signal, dH/dt, is proportional to the difference between the heat

input to the sample and that to the reference.

A Perkin-Elmer DSC, model 2C, (Norwalk, Ct.) equipped with a microcomputer was programmed to lower the temperature of a polyethylene sample linearly from the melt to the solid state. A thermogram was made, and the curve integrated by computer to yield heat of crystallization. The area under the curve was calculated by estimating a scanning baseline.

When a sample is subjected to a linear temperature increase, the rate of heat flow into the sample is proportional to its instantaneous specific heat. Procedures to determine specific heat have been described in detail in the literature (37,38,39). Briefly, empty aluminium pans are placed in the sample and reference holders. A base line is recorded, and the temperature is programmed to increase linearly over a range. The procedure is repeated with a known mass of sample in the sample pan and a trace of dH/dt versus time is recorded. The thermogram shows a displacement due to the absorption of heat by the sample. This can be described by the following equation:

$$dH/dt = m \, C_p \, dT/dt \qquad\qquad (7)$$

where m, is the sample mass, Cp, the specific heat and dT/dt, the programmed rate of temperature increase. This

equation was used directly to obtain values of specific heat. A DuPont Instruments DTA, model 990, (Wilmington, Dl.) was used to make the specific heat measurements. It has an ordinate scale larger than the DSC plot and was thus suitable for obtaining dH/dt values for specific heat calculations. Both DSC and DTA instruments were made available by Union Carbide Canada Ltd. and samples were analyzed at their Technical Research Centre.

5.6.2.1 Procedure

A description of both heat of crystallization and specific heat determinations follow. These procedures are similar to ASTM Standard Test Methods D3417 and D3418. All weighings were done on a H10T Mettler balance (Zurich, Switzerland).

Specific Heat

(1) The thermal analysis instruments were calibrated for temperatures within 0.5 °C and for power using indium by technicians at Union Carbide.

(2) Dry nitrogen gas was circulated at a rate of 100 cc/min through the sample holder assembly.

(3) Two blank aluminum pans and covers were scanned at 20 °C/min between 50 and 150 °C to establish a base line.

(4) A film sample of known mass was placed in one of the aluminum pans. The second aluminum pan remained empty, as it was the reference. The sample was heated to 150 °C, held at that temperature for fifteen minutes

and cooled at a rate of 20 °C/min to 50 °C. After the average temperature of the sample holders equilibrated at 50 °C, the sample was scanned at a rate of 20 °C/min between 50 and 150 °C and the trace of dH/dt versus temperature recorded.

(5) The specific heat of the sample, at any temperature between 50 and 150 °C, was found by measuring dH/dt values directly from the thermogram and substituting them in Equation 7 along with sample mass and rate of temperature increase and then solving the equation.

Heat of Crystallization

Steps (1) and (2) from the specific heat procedure were repeated.

(3) A sample of known mass was heated to 150 °C, held at that temperature for fifteen minutes, and scanned at -10 °C/min between 150 and 50 °C.

(4) The computer was instructed to subtract a baseline (contained in memory), plot the scan, 'draw-in' a scan baseline and integrate the cooling curve. The area under the cooling curve was the heat of crystallization.

Chapter 6

Evaluation of Cocurrent - Countercurrent Cooling System:
Results and Discussion

This chapter completes the detailed specification of operating conditions given in Table 4.2, by describing the determination of the countercurrent air flow rates. With a criterion for comparing cooling systems established, the results of each variable measurement are presented. An analysis of these variables reveals the cooling occurring along the film bubble surface.

The results of surface temperature, film thickness, bubble shape and thermal property measurements were used to calculate the heat transfer coefficient and fraction of crystallinity as functions of distance from the die. An examination of the heat transfer coefficient reinforced the conclusions drawn from the dependent variable measurements. Finally, the heat transfer coefficient in cocurrent cooling was correlated with position above the die and the maximum air velocity.

6.1 Air Flow Rates

The cocurrent cooling air flow rate used in establishing operating conditions for the combination cooling system was limited by bubble stability. Thus, the cooling flow was governed by the maximum cocurrent air flow rate (Section 4.5.1). A second cocurrent air flow rate was also chosen to test the cocurrent and combination cooling systems. This volumetric flow rate was controlled by adjusting the butterfly valve on the air duct supplying cocurrent air to a position that was considered standard by technicians familiar with the extruder under the operating conditions listed in Table 4.2. These two cocurrent flow rates were used as standard or 'control' cases in comparing cooling systems. Velocity profiles of the two cocurrent flow rates are given in Figure 6.1. Reynolds Numbers of four and five thousand were calculated under these cocurrent flows. The velocity profiles can be described as 'blunt parabolas', indicative of turbulent flow. Point velocities were determined from pitot tube pressure measurements across a ten point diameter traverse, as discussed in Section 5.1. The ten point diameter traverse effectively divided the circular duct into ten zones of equal area. Flow rates were calculated in each concentric ring zone and summed to yield the total volumetric flow rate. These are given in Table
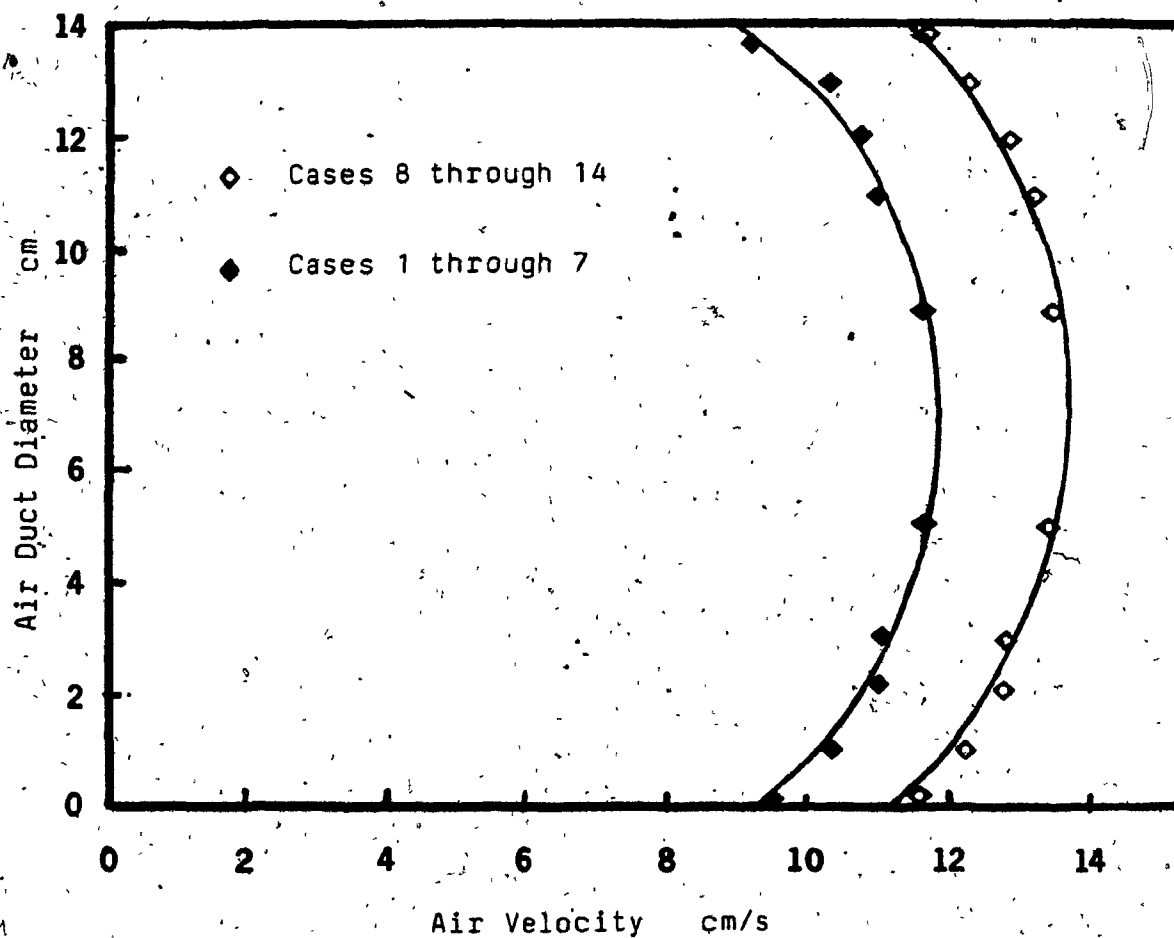
FIGURE 6.1   Velocity Profiles in Cooling Air
              Inlet Duct Used to Determine Flow
              Rates of Cocurrent Cooling Air

Table 6.1: Air Flow Rates

Cooling Condition	Cocurrent Air Flow Rate (cfm)	Countercurrent Air Flow Rate (cfm)
Case 1 (no cylinder)	103	---
Case 2	103	---
Case 3	103	126
Case 4	103	162
Case 5	103	200
Case 6	103	268
Case 7	103	272
Case 8 (no cylinder)	123	---
Case 9	123	---
Case 10	123	126
Case 11	123	162
Case 12	123	200
Case 13	123	268
Case 14	123	272

6.1.

These same cocurrent flow rates were used for the cocurrent and countercurrent combination cooling systems. Corresponding to each cocurrent flow rate, several countercurrent flow rates were used. The method of establishing a stable film bubble under maximum countercurrent drawing flow has been described in Section 4.5. Maximum countercurrent flow corresponded to a fully open butterfly valve at the outlet duct of a second blower. Additional countercurrent air flows were arbitrarily chosen by convenient settings of the blower butterfly valve. Local velocities were calculated from four, ten point pitot tube diameter traverses, as described in Section 5.1. The pressure measurements and velocity calculations of each measurement point are given in Appendix D1. An average velocity profile for two countercurrent flows is shown in Figure 6.2. Reynolds Numbers of 17,000 and 23,000 were determined under these countercurrent cooling flows. The turbulent and asymetric nature of the flow is indicated by the skewed velocity profiles. These velocities were used to determine the countercurrent flow rates, which are listed in Table 6.1 for each cooling condition. In all, fourteen different cooling flows were applied to the film bubble. Two solely cocurrent flows were used as standard or 'control' cooling conditions. The cocurrent flows were
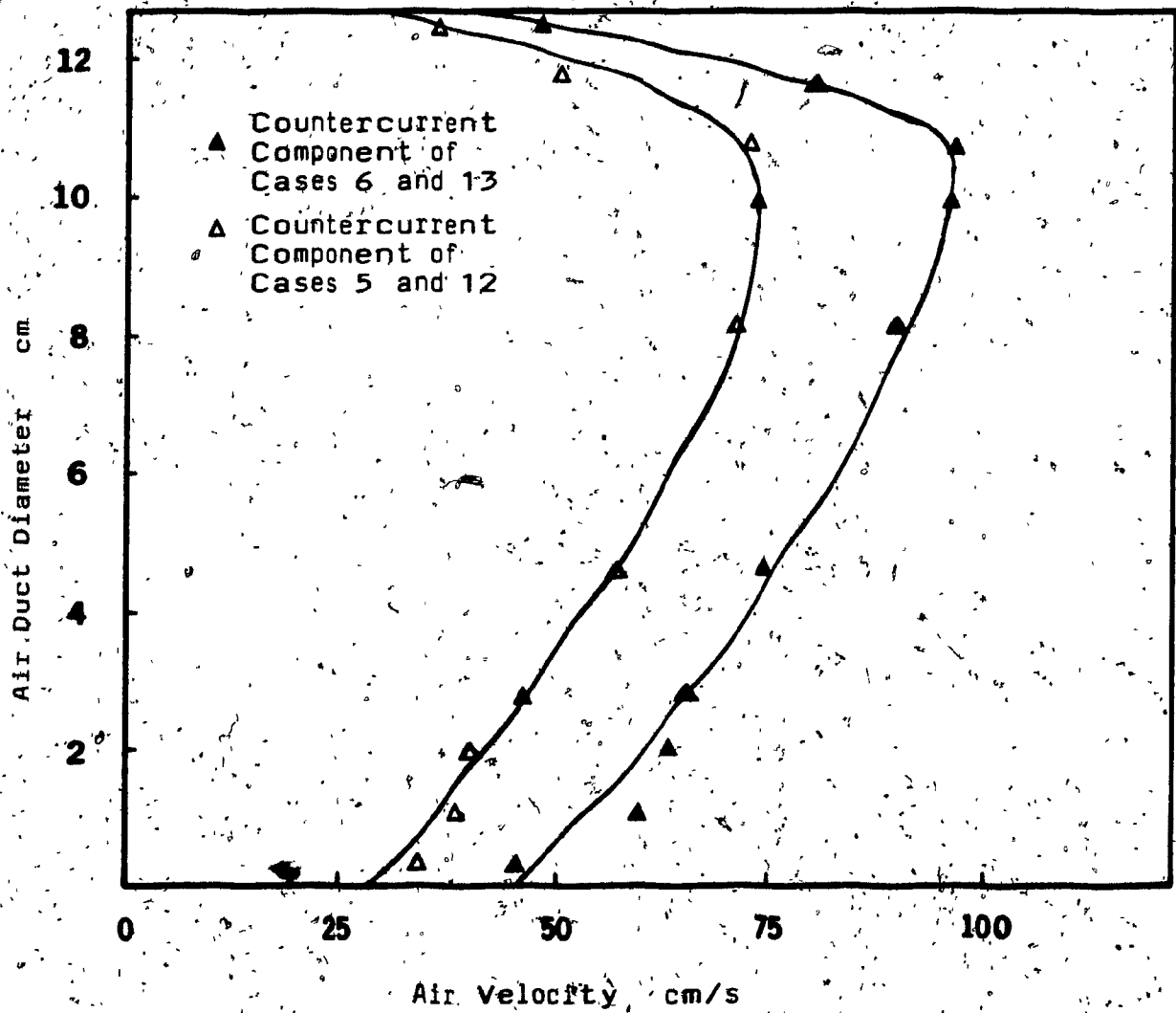
FIGURE 6.2   Velocity Profiles in Cooling Air
Outlet Duct Used to Determine Flow
Rates of Countercurrent Cooling Air

applied to the bubble with and without the cylindrical shroud present. In order to test the combination cooling system, five countercurrent flows were coupled with each cocurrent flow; thus ten cocurrent and countercurrent combination flows were studied.

6.2 Surface Temperature Measurements

Surface temperatures were measured along the film bubble under the operating conditions given in Table 4.2 and for each cooling condition outlined in the preceding section (Section 6.1). Thus, bubble surface temperatures were measured with fourteen different cooling flows. Appendix D2 gives measured temperatures tabulated with distance from the die for each case. Temperature gradiants are also included in this appendix. Both groups of values were used in a heat balance over an element of film to determine heat transfer coefficients (Equation 6, Section 5.6).

Surface temperature under standard cocurrent cooling conditions is plotted against distance from the die in Figure 6.3. These cooling conditions correspond to cases 1 and 8 in Table 6.1. In the immediate vicinity of the die, cooling was slow, as the cooling air first contacted the film bubble slightly above the die. Once beyond this
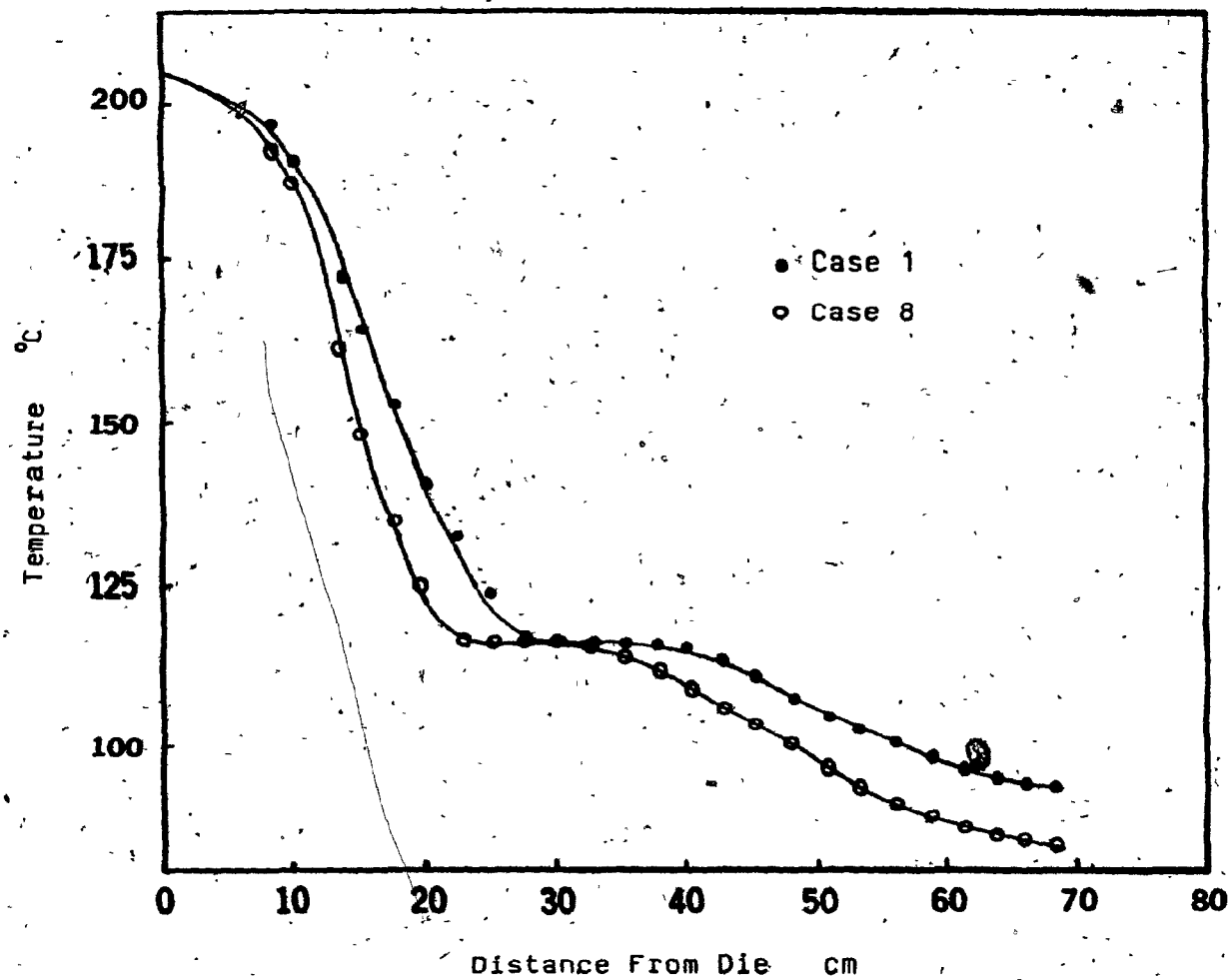
FIGURE 6.3   Surface Temperature Versus Distance
From Die Under Cooling Conditions of
Cases 1 and 8

initial section, the molten bubble was strongly cooled. In the neck region the temperature gradient was steepest, indicating that the greatest rate of cooling occurred there. The frostline was associated with a plateau in the cooling curve. From Figure 6.3, it was evident that the frostline is really not a true 'line', but rather a region in which solidification occurs. Beyond this region, the solid film bubble continued to cool, although at a slower rate than in the neck region.

In Figure 6.3, the cooling curve of case 8 lies below that of case 1 in all regions but the frostline, where the curves coincide. This trend was expected, since a greater cocurrent flow rate was applied in case 8. The length of the frostline region also gives an indication of cooling strength. A shorter plateau corresponds to more intensive cooling. In this comparison between two cocurrent cooling flows, case 8 had a solidification zone of five inches, while the plateau region was six inches long in case 1. Similar cooling curve characteristics have been reported for low density polyethylene over a wide range of cocurrent flow rates(5). It is interesting to note that the frostline occurs at the same temperature under different cooling conditions. In separate studies, Ast (5) and White (26) measured a frostline temperature between 115 and 117 °C, which coincide with the plateau temperature in Figure 6.3.

Cocurrent cooling conditions are compared with and without a cylindrical shroud surrounding the lower portion of the film bubble in Figure 6.4. The standard cocurrent cooling conditions correspond to cases 1 and 8 in Table 6.1 and those with the cylinder present, cases 2 and 9. The cylinder wrapped with plastic film extends two feet above the die, so that the film bubble emerges from the cylinder in the solid state.

· Near the die all four cases have similar surface temperatures, as the cooling air has only just contacted the film bubble. Farther from the die, in the lower neck region, the cooling curve splits in two. Cases 8 and 9, with the larger cooling air flow, had lower surface temperatures than cases 1 and 2. The steep decline in surface temperature continued for each two-case group through the neck region. However, at the last measurement point, just before the frostline, each group cooling curve separated. The standard cases, that is without the cylinder present, had lower surface temperatures than their counterparts with the cylinder. This trend was more pronounced beyond the frostline but within the cylinder. The lower surface temperatures measured without the cylinder were attributed to the entrainment of surrounding air by the cocurrent air stream. The entrained air serves to replenish the partially warmed cooling air. Thus, the 'effective'
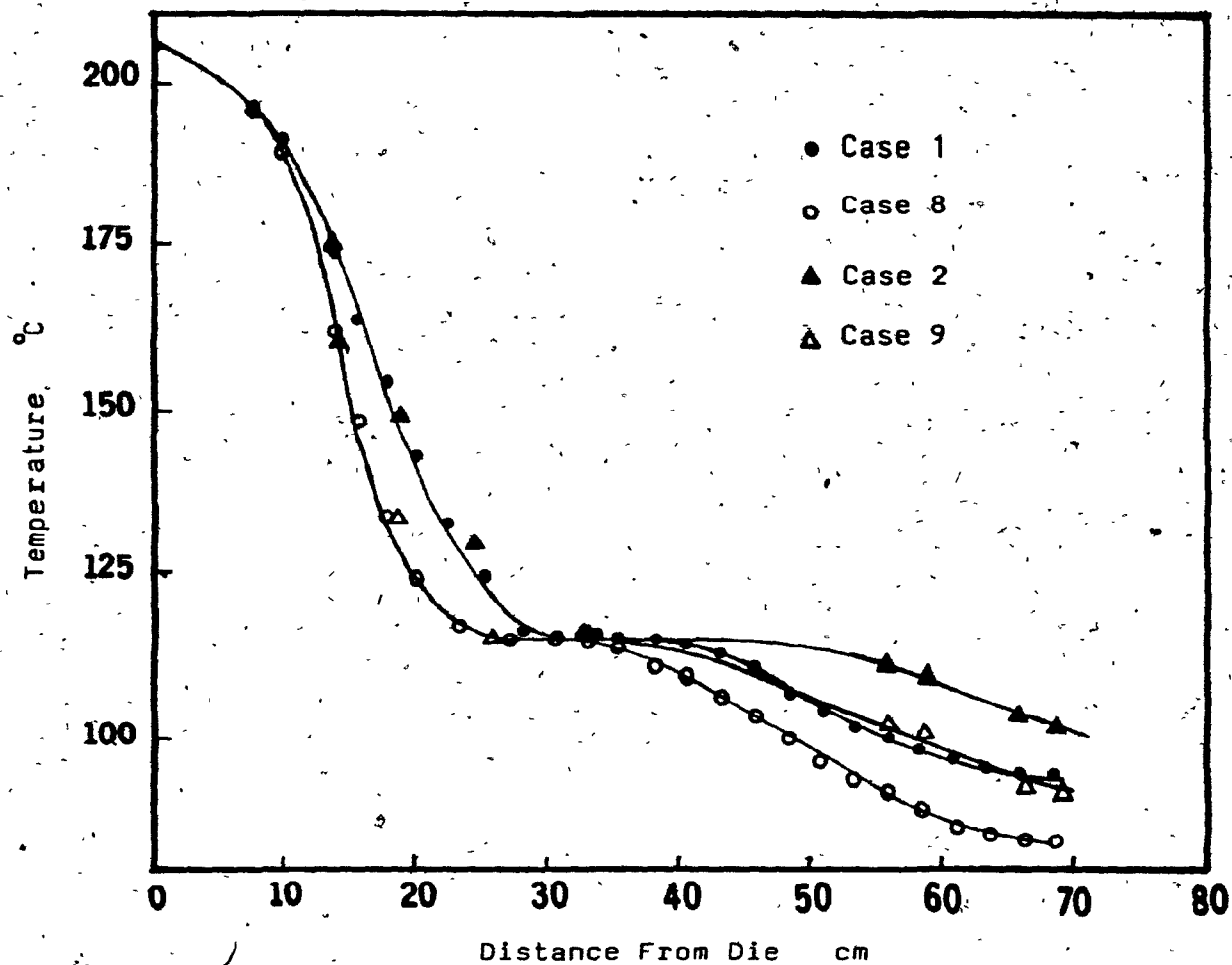
FIGURE 6.4   Surface Temperature Versus Distance
From Die Under Cooling Conditions of
Cases 1, 2, 8 and 9

cooling air flow, or the amount of air that actually participates in heat transfer, is greater in cases 1 and 8 than the air flow applied to the base of the film bubble. The cylindrical shroud around the bubble in cases 2 and 9 prevented entrainment of surrounding air and lead to higher surface temperatures than in cases 1 and 8.

In Figure 6.4, the frostline occurred at the same temperature in each case, about 115 °C. However, the length of the plateau region could not be determined with the cylindrical shroud present, as an unobstructed view of the bubble was not possible in all regions. Two surface temperature measurements were made downstream from the frostline and above the cylindrical shroud, and they showed that surface temperatures with the cylinder present were still higher than those without the cylinder, however the temperature difference between cases 2 and 9 and cases 1 and 8 had narrowed. This was attributed to the cocurrent cooling flows of cases 2 and 9 being able to entrain cooler surrounding air at positions above the cylindrical shroud. Within the cylindrical shroud the entrainment of ambient air was not possible.

It is interesting to note that the bubble formed under the maximum standard cocurrent cooling conditions of case 8 was perfectly stable, while the same cocurrent flow rate with the cylindrical shroud present caused small bubble

oscillations or instabilities. The bubble was weakened in case 9 by the presence of the cylinder and a marginally warmer neck region, so that the large cocurrent cooling flow was destabilizing. The expanding - contacting oscillations of case 9 were reflected in dimensional variations of the final film product, which are discussed in Section 6.3.

Surface temperature results for cases 2 through 7 were plotted as a function of distance from the die and are presented in Figure 6.5. In each case, the cylindrical shroud surrounded the lower portion of film bubble. Case 2 applied less than the maximum cocurrent cooling air to the base of the bubble and cases 3 through 7 used this same amount of cocurent air in conjuction with increased countercurrent air flows. In case 7, the maximum countercurrent air flow was withdrawn through the plenum. Additionally, case 9, which applied maximum cocurent cooling to the bubble, is also shown in Figure 6.5.

In the neck and frostline regions, that is, below the collecting plenum, cases 2 and 7 had nearly identical surface temperatures at a given distance from the die. The amount of countercurrent cooling air applied to the bubble had no apparent effect on surface temperature within these regions. However, an increase in the cocurrent air flow directed along the bubble, as in case 9, lowered surface
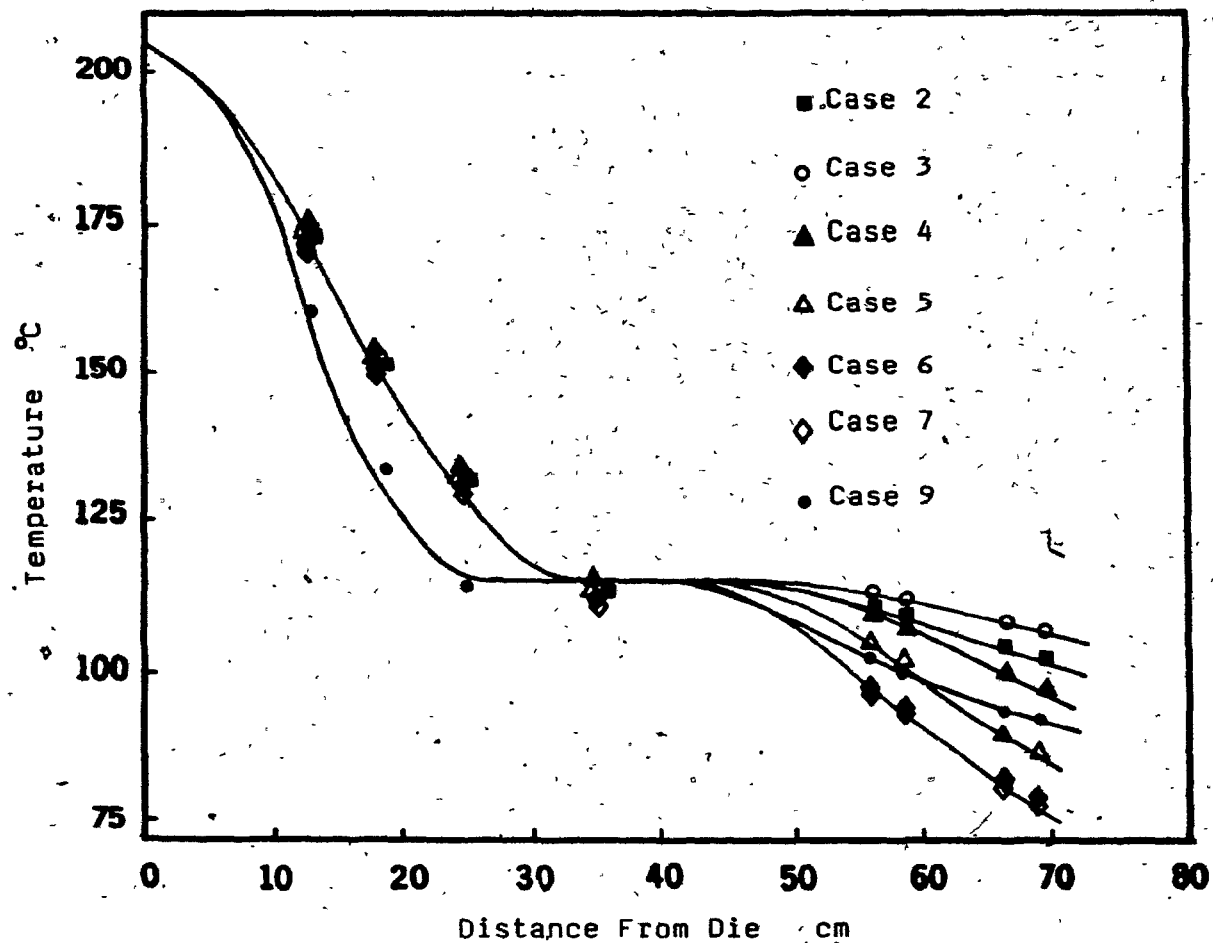
FIGURE 6.5   Surface Temperature Versus Distance
              From Die Under Cooling Conditions of
              Cases 2 through 7 and Case 9.

temperatures markedly. Thus, film cooling along the molten bubble was controlled by the amount of cocurrent air applied to the base of the bubble.

Above the frostline and the collecting plenum, surface temperatures along the solid bubble were affected by countercurrent cooling flow. The countercurrent and cocurrent cooling flows in case 3 were similar, that is, the amount of air withdrawn near the frostline was nearly equal to the air applied at the base of the bubble. As a result of this balanced cooling condition, little cooling occurred above the withdrawl plenum. This was reflected by the highest surface temperatures in this region of any of the cooling conditions. When the countercurrnet air flow was substantially greater than the cocurrent flow, as in cases 4 through 7, film surface temperatures were less than under the strictly cocurrent flow of case 2. As the amount of countercurrent air flow in the combination cooling system was increased, lower surface temperatures resulted. This trend occurred in cases 4 through 7. The small decrease in surface temperature between cases 6 and 7 reflected similar countercurrent flow rates. In Figure 6.5 the temperature difference was nearly $50°F$, between solely cocurrent bubble cooling and the combined cooling system with maximum countercurrent air flow (cases 2 and 7). A more realistic comparison was between cases 1 and 7, as case 1 cocurrently

cooled the bubble without the cylindrical shroud and was representative of classical blown film cooling. The temperature difference between cases 1 and 7 was roughly 35 °F at the highest measurement point above the die. Thus, the countercurrent drawing flow substantially reduced the film surface temperature over the solid portion of film bubble.

A similar explanation applies to the family of cooling flows that used maximum cocurrent air flow. Surface temperatures for cases 9 through 14 were plotted against distance from the die and are shown in Figure 6.6. Varying amounts of countercurrent flow are combined with the maximum cocurrent flow in cases 10 through 14. Case 14 includes maximum cocurrent and countercurrent cooling. Additionally, case 2 is included in Figure 6.6, to provide a cooling condition with a different cocurrent flow rate than the other cases compared in this graph. In each case the cylindrical shroud surrounded the lower portion of film bubble.

Below the solid bubble in the neck and frostline regions, cases 9 through 14 had similar surface temperatures at the same distance from the die. Case 2 surface temperatures were above this family of cooling flows incorporating maximum cocurrent air flow and thus reflected weaker cooling conditions. The frostline was at the same
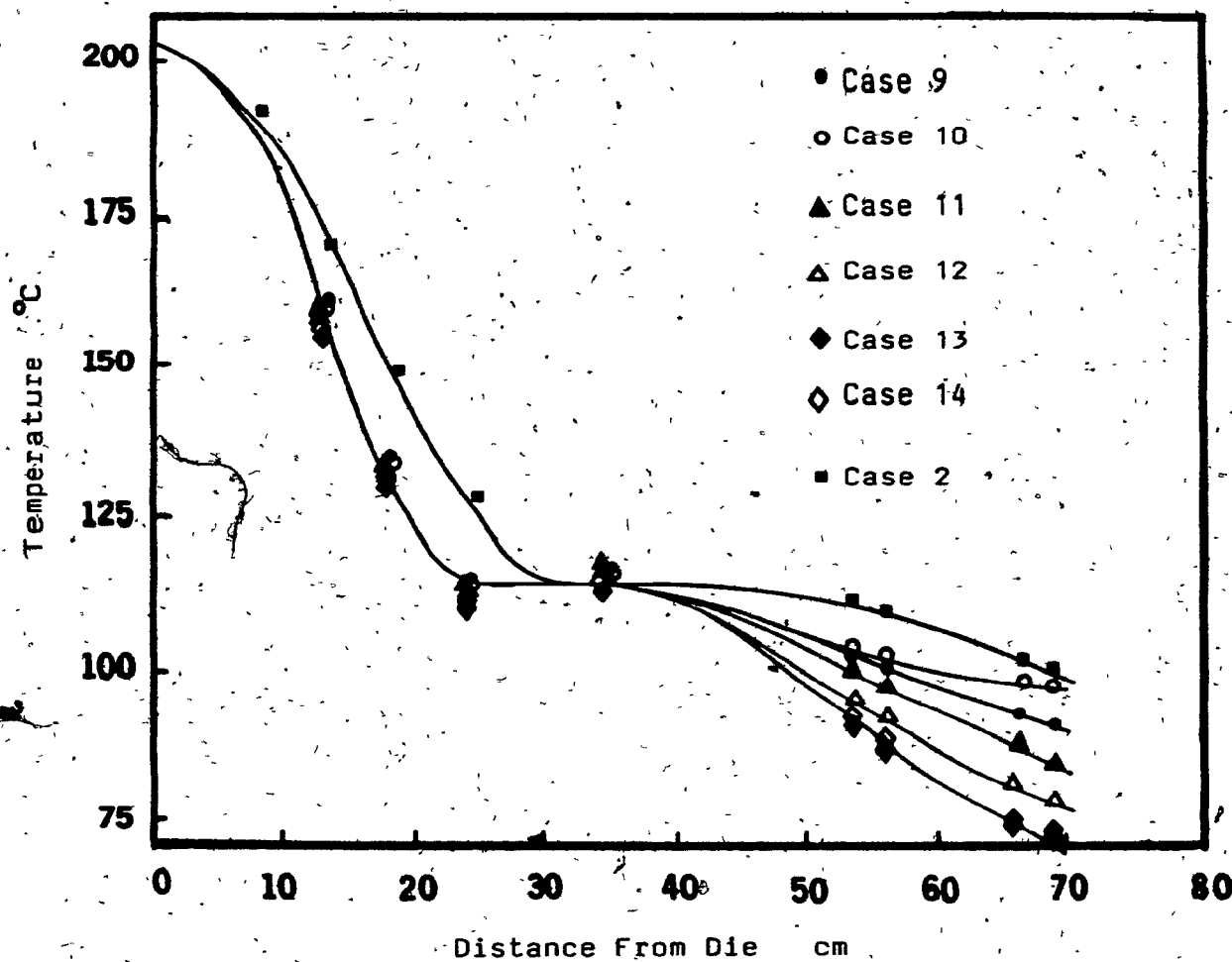
FIGURE 6.6 Surface Temperature Versus Distance
From Die Under Cooling Conditions of
Case 2 and Cases 9 through 14

temperature for all cooling flows, but the length of the
plateau region was again obscured by the cylinder and plenum
arrangement. Above the frostline, surface temperatures
spread out in order of increasing countercurrent flow.
Surface temperatures recorded under case 10 cooling
conditions were closer to those obtained for standard
cocurrent cooling than to surface temperatures measured
under maximum combination flow. From Figure 6.6 the surface
temperature difference between maximum cocurrent cooling
(case 9) and maximum combination cooling (case 14) was over
$40^{\circ}F$, at the highest position temperatures were measured. A
comparison between case 8, maximum cocurrent cooling without
the cylindrical shroud present, and case 14 yielded a $25^{\circ}F$
surface temperature difference at the same position on the
solid film bubble.

Surface temperature measurements along the film bubble,
for the cocurrent and countercurrent combination cooling
system, have shown that cooling in the neck region is
governed by cocurrent flow applied to the base of the film
bubble. Countercurrent cooling occurred above the frostline
and above the collecting plenum, over the solid portion of
film bubble. In this region, lower surface temperatures
were recorded under combination cooling flows than with
standard cocurrent cooling (no cylindrical shroud present).

Furthermore, surface temperatures decreased with increasing countercurrent flow. Comparisons between maximum countercurrent cooling and the standard cocurrent cases, yielded a maximum temperature difference of 35 °F at the highest position temperatures were measured.

6.3 Bubble Shape

Bubble shape is dependent on the stretching and expanding forces the polymer encounters while still in the molten state. Once in the solid state, film dimensions are constant. Diameters of film bubbles were measured from photographs, as described in Section 5.3. Diagrams intended to represent the actual film bubble were constructed from diameter measurements, symmetrically arranged around a central bubble axis, at various distances from the die. These plots were used to calculate the angle, θ, between a tangent to the film surface and the central axis of the bubble. Both diameter and angle values were used in a heat balance over an element of film surface to calculate the heat transfer coefficient and the fraction of crystallinty.

Diameters measured under the cooling conditions of cases 1 and 8 have been plotted to give the appearance of the actual film bubble in Figure 6.7. From this figure, the
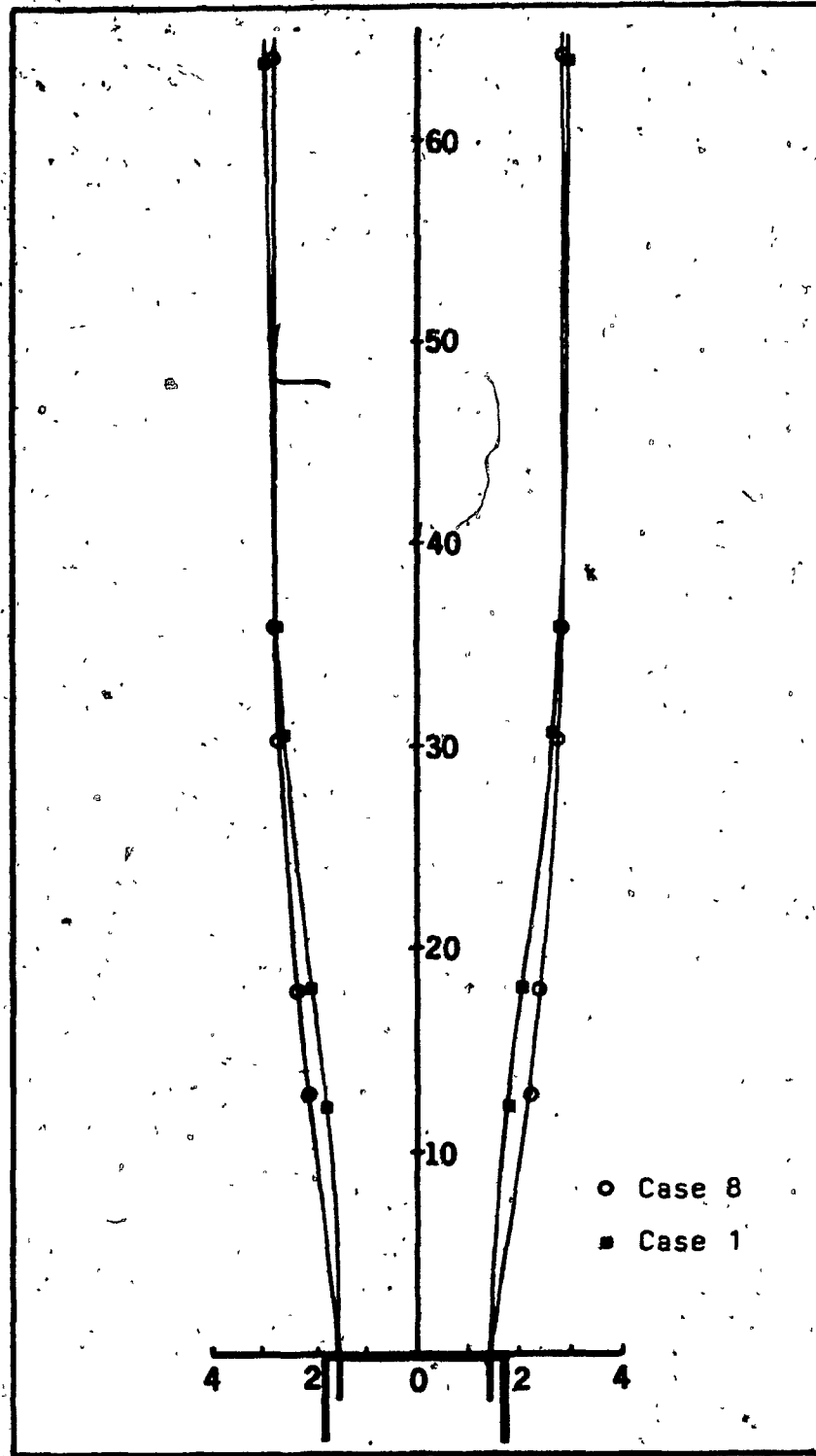
FIGURE 6.7   Film Bubble Diameters Symmetrically
Arranged Around Bubble Axis Under
Cooling Conditions of Cases 2 and 9

angle, θ was obtained at the same distances from the die at which diameters were measured. The small blow up ratios used in this study and the resulting moderate bubble expansion or 'pocket' shape in the neck region limited the range of θ. In case 2, θ varied from $9°$ at five inches above the die, to $0°$ at the frostline. Values of θ for each cooling condition were determined from similar diagrams and are listed along with position above die in Appendix D3.

Bubble shape is dependent not only on the stretching and expanding forces the polymer encounters in the molten regions but also on cooling conditions. The shape of the bubble gives an indication of the cooling occurring. Bubble diameters are plotted as a function of distance from die in Figures 6.8 and 6.9. Cases 2 through 7 along with case 9 are shown in Figure 6.8, and in Figure 6.9 case 2 and cases 9 through 14 are given. Bubble diameters are tabulated along with position above die in Appendix D3.

Under the strong cocurrent cooling conditins of cases 9 through 14, bubble diameters were larger near the die and smaller at the frostline than with the cooling flows of cases 2 through 7. In these latter cases, diameters expanded slowly in the molten region above the die and rapidly just below the frostline. Bubble expansion for cases 9 through 14 cooling conditions occurred more
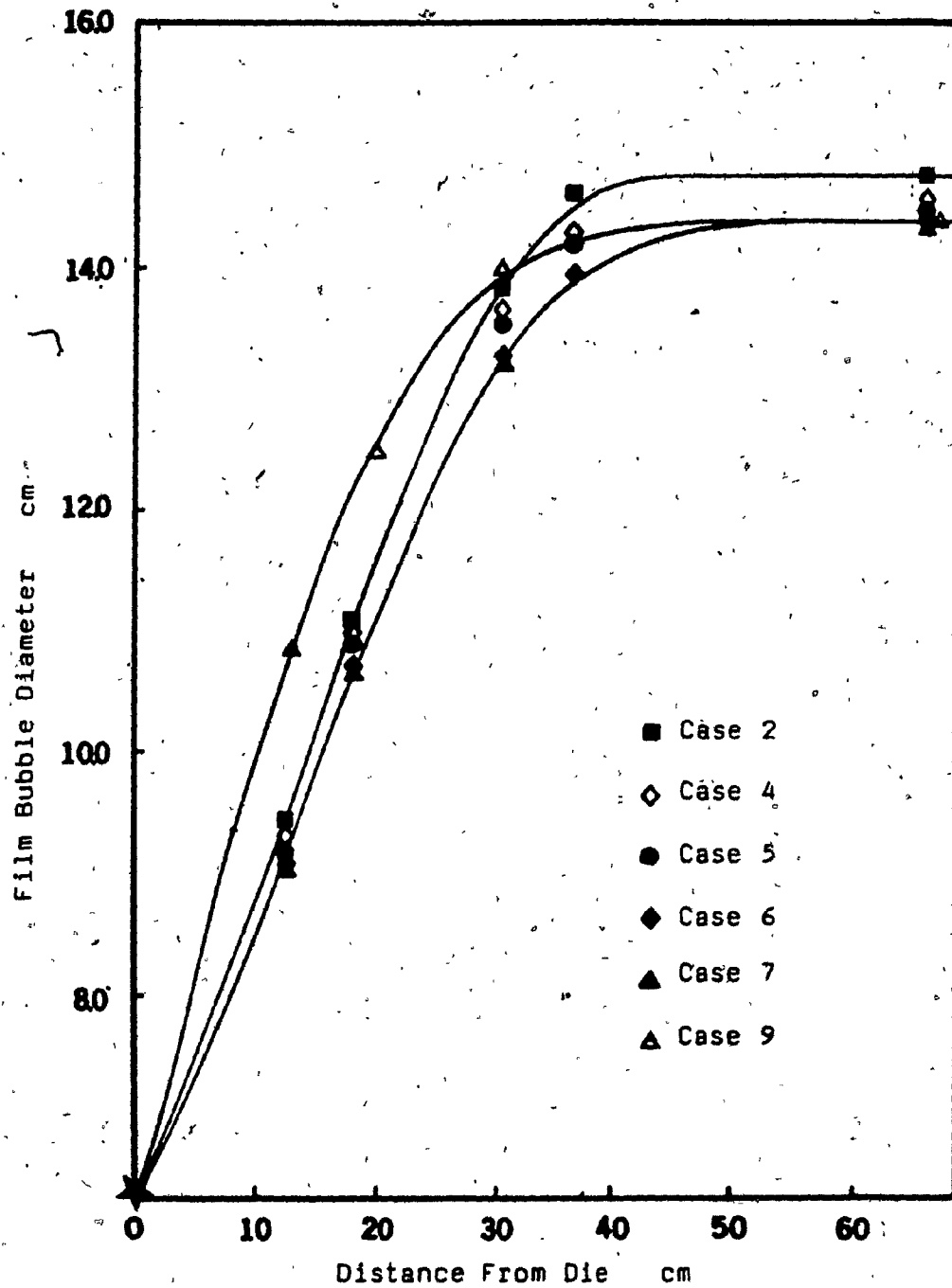
FIGURE 6.8   Film Bubble Diameters Versus Distance
From Die Under Cooling Conditions
of Cases 2 through 7 and Case 9
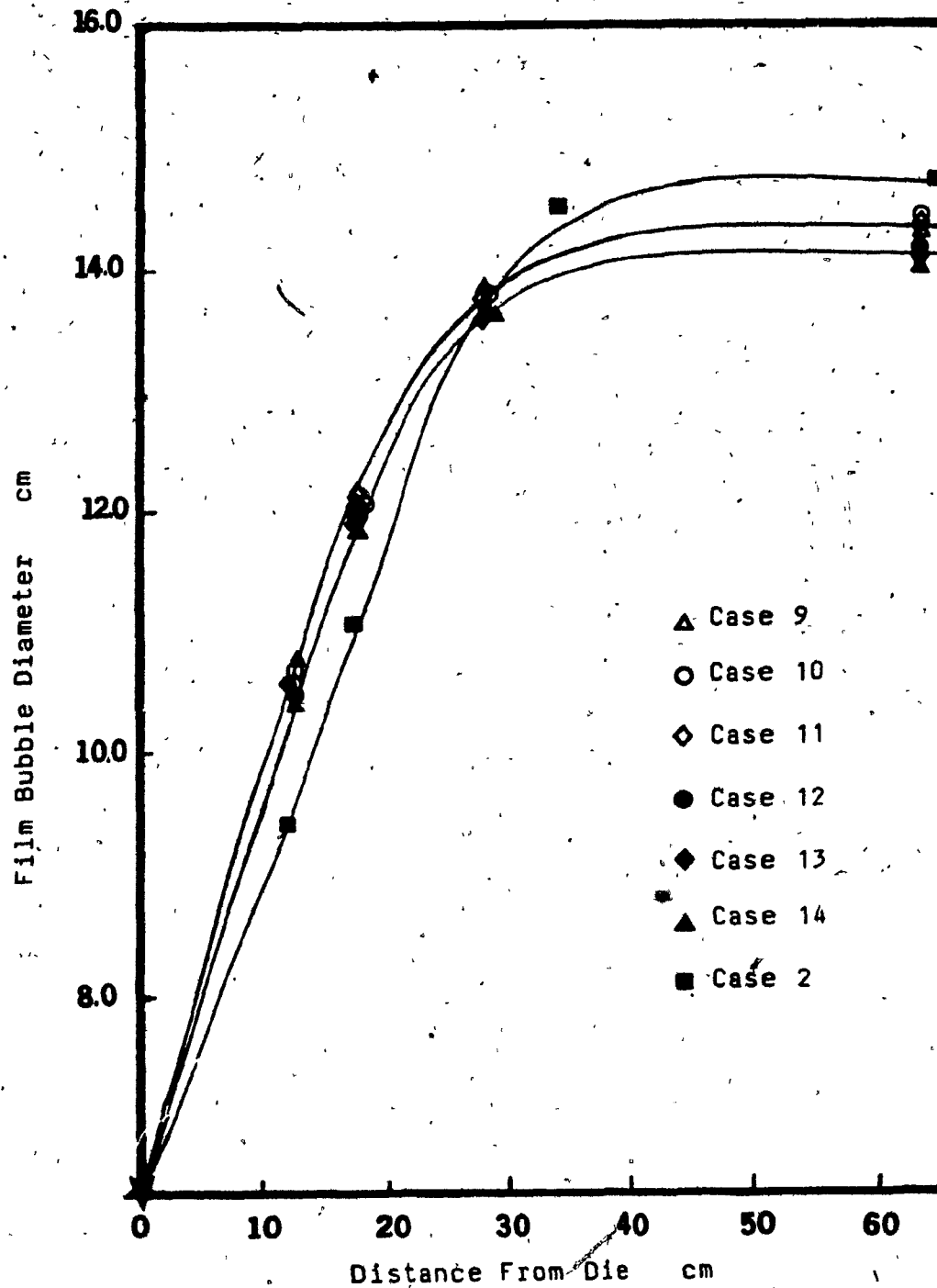
FIGURE 6.9   Film Bubble Diameters Versus Distance From Die Under Cooling Conditions of Case 2 and Cases 9 through 14

gradually between die and frostline.

The addition of countercurrent air flow decreased the bubble diameter marginally everywhere along the bubble. The trend towards smaller bubble diameters was more pronounced with larger contercurrent air flow rates. Changes in bubble shape occur because the fixed mass of air trapped within the bubble can be compressed to varying degrees altering the internal bubble pressure. In combination cooling, smaller diameters everywhere along the bubble suggest greater internal bubble air pressure than under only cocurrent cooling. From these observations it can be seen that the force to expand a polymer melt comes from a combination of the air pressure within a film bubble and the aerodynamic forces created by the cooling system. These aerodynamic forces depend on the volume and velocity of the cooling air streams as well as the manner in which they are applied to the bubble.

It was pointed out in Section 6.2 that the bubble formed under the maximum standard cocurrent cooling conditions of case 8 was perfectly stable while the same cocurrent flow rate with the cylindrical shroud present caused the bubble to oscillate somewhat in an expanding - contracting manner. These instabilities under the cooling conditions of case 9 were reflected in dimensional

variations of the final film product as shown in Table 6.2. Layflat width and thickness distributions were measured each time film was produced, and the values in Table 6.2 are representative of variations in film dimensions under the given cooling condition.

Cases 9 through 12 had a layflat standard deviation an order magnitude greater than cases 13 and 14. This suggests that the resonance oscillations were no longer present in the cases with large countercurrent flows. Somehow these large countercurrent flows provided the film bubble with more stability. It could be argued that the countercurrent flow reduced the bubble temperature somewhat, thus making the bubble 'tougher' so that it could withstand the destabilizing cocurrent air flow. However, surface temperatures in the neck region were very similar and within experimental error. A more probable explanation attributes bubble stability to the forces imposed by the large air flows in the countercurrent cooling system. These outward suction forces were observed to cause a small fluttering-type movement of the bubble in the neck region and did not allow the bubble to retreat in an oscillating pattern. As countercurrent flow was reduced from the maximum amount, fluttering-type deformations ceased and were quickly followed by resonance oscillations.

Table 6.2 also reveals a reduction in mean thickness

Table 8.2: Film Product Dimensions

Cooling Condition	Layflat Width		Blow Up Ratio	Film Thickness	
	Mean Value (cm)	Standard Deviation		Mean Value ($mm \times 10^2$)	Standard Deviation
Case 1	22.9	0.020	2.30	3.94	0.032
Case 2	23.1	0.035	2.32	3.89	0.052
Case 3	22.9	0.047	2.30	3.94	0.058
Case 4	22.8	0.041	2.28	3.96	0.041
Case 5	22.7	0.040	2.27	3.96	0.040
Case 6	22.5	0.047	2.26	3.99	0.042
Case 7	22.5	0.030	2.26	3.99	0.030
Case 8	22.5	0.035	2.25	4.01	0.055
Case 9	22.5	0.25	2.26	3.99	0.35
Case 10	22.6	0.19	2.27	3.99	0.30
Case 11	22.4	0.21	2.24	4.04	0.33
Case 12	22.2	0.21	2.22	4.06	0.27
Case 13	22.1	0.040	2.22	4.09	0.062
Case 14	22.1	0.063	2.21	4.09	0.069

standard deviation with larger countercurrent air flows. This trend was evident in each family of cocurrent flows; cases 2 through 7 and cases 9 through 14. Melt emerging from a die is generally not of uniform thickness. In the subsequent cooling process, the thinner sections cool first, while the thicker portions are still partially molten and susceptible to further stretching and expanding. Thus, the cooling process inherently smooths out gauge variations in the melt to some extent. The suction forces applied near the frostline further expanded any portions of film bubble still partially molten, that is, the thickest regions. Thus, countercurrent air flows from the combination cooling system created greater expanding forces and were able to reduce thickness variations to a greater extent than in standard cocurrent flows.

We have seen that cooling flow rates and the manner in which cooling air is applied to the bubble affect the geometry of tubular film. Cocurrent cooling flows influenced the general shape of the film bubble, while the application of countercurrent air flow slightly reduced diameters everywhere along the bubble. Therefore, under combination cooling flows, the shape of the bubble was similar to that for corresponding cocurrent flow, only somewhat smaller in all regions, depending on the magnitude

of countercurrent flow. Furthermore, the countercurrent air flow provided a stabilizing force on the film bubble after maximum cocurrent cooling flow had caused oscillations. Reductions in gauge variations were also attributed to countercurrent cooling.

An extreme case of different cooling conditions is illustrated in Figure 6.10. Weak cooling causes a 'stalk' or long neck bubble geometry, while a 'pocket-shaped' bubble is characteristic of strong cooling conditions.

Pocket Shaped   Long Necked
Bubble   Bubble
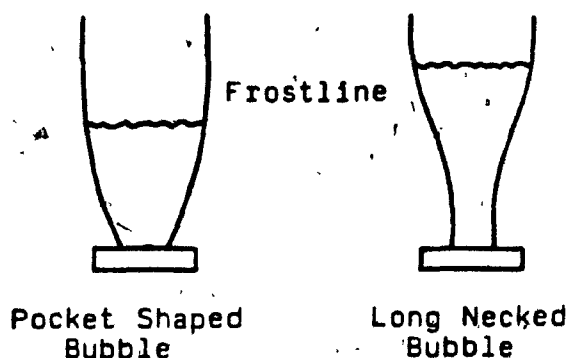
FIGURE 6.10   Film Bubble Shapes Under Different
                Cooling Conditions

The bubble shape in the neck region ultimately effects film properties. If cooling is intensive, the tube is stretched gradually in two directions from die to frostline, while for weak cooling the transverse stretching occurs

suddenly just below the frostline. Preferential molecular chain alignment or orientation imparted to the film by stretching and expansion forces as it cools becomes 'frozen-in' at the frostline. The deformations occurring near the frostline are thus more likely to cause 'frozen-in' orientation and to have a greater effect on film properties than deformations in the hotter, mostly amorphous regions near the die. This orientation gives plastic film a preferred direction for tearing and shrinkage. The effect of cooling on film properties is discussed in Chapters 7 and 8.

6.4 Air Temperature Measurements

Air temperatures near the bubble surface, at different heights above the die, give an indication of the cooling occurring along the bubble and the relative strength of various cooling conditions. Air temperature measurements made perpendicular to the film surface (outward from the film surface) suggest how thick a layer of air particpates in heat transfer. Air temperatures were measured at various distances above the die to obtain air temperature distributions both parallel and perpendicular to the film surface. Diagrams representative of these distributions are

presented in this section while air temperature data are
listed in Appendix D4.

The radial temperature distributions under the
cocurrent cooling conditions of cases 1 and 8 are given in
Figure 6.11 at two heights above the die. All curves showed
a maximum temperature near the film surface, which declined
to ambient temperature away from the bubble. Ambient
temperatures were not constant in these tests and varied
from 26.5 to 27.5 °C, as cool drafts periodically circulated
in the film blowing area. Under each cooling condition, the
shape of the temperature curve differed with distance from
die. At the lower position, the cooling curve decreased
steeply to ambient temperature, while temperatures at the
higher location underwent a more gradual decline. Thus, the
air stream broadened somewhat at greater distances from the
die. Nevertheless, the thickness of the warmed air stream
was roughly one inch several inches above the die and
expanded to only two inches at two feet above the die.
Similar air temperature variations have been reported by
Ast(5), who concluded that only layers of air in the direct
neighborhood of the film bubble participate in heat
transfer. Also in Figure 6.11, lower air temperatures were
recorded near the bubble under the stronger cocurrent air
flow at both positions above the die. This was expected, as
the larger volume cooling flows had similarly lowered the
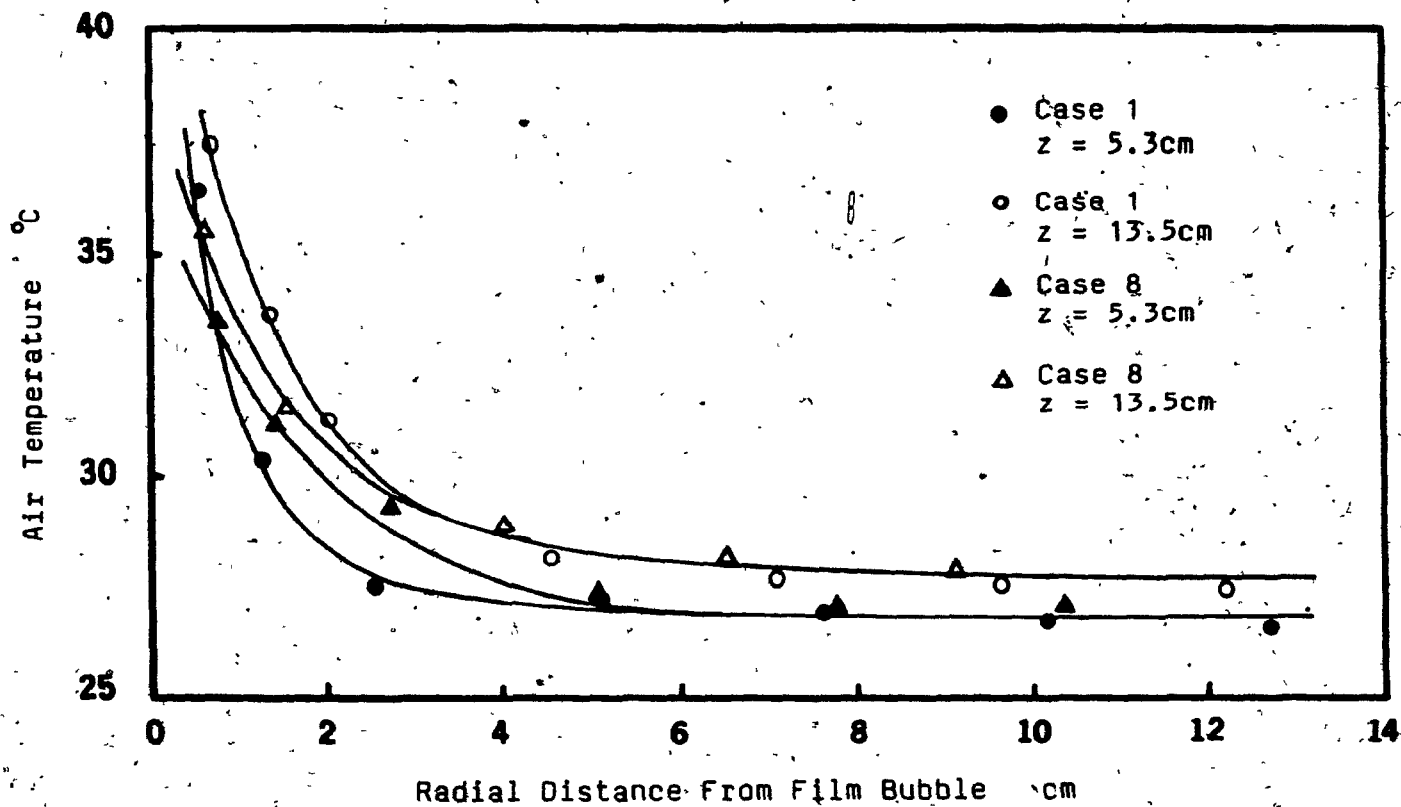
FIGURE 6.11   Air Temperature Measured Radially
From the Film bubble at 5.3 and
13.5 cm Above the Die Under Cocurrent
Cooling Conditions of Cases 1 and 8

surface temperature of the film bubble (Section 6.2).

Radial air temperature distributions for cocurrent and combination cooling systems are shown in Figure 6.12 for two positions above the die. Both positions are within the cylindrical shroud, one below the withdrawl plenum and the other above it. Measurements outward from the bubble were constrained by the cylindrical wall. Air temperatures under the cooling conditions of cases 9 and 11 coincided at the first measurement position above the die. Thus, at this position, the countercurrent cooling conditions had no effect on air stream temperatures. This result was similar to those of surface temperature measurements made below the plenum under cocurrent and combination cooling flows. Surface temperatures in this region depended only on cocurrent cooling, regardless of countercurrent air flow. At the measurement position above the withdrawl plenum, the air temperature curve for cocurrent cooling was broader than at the lower position. However, air temperatures for the combination cooling flow in case 11 showed a sharp decline from near the bubble surface to ambient conditions. Ambient temperatures were reached less than 1.5 inches from the bubble surface. Furthermore, with combination cooling, the final air temperature measured was less than the lowest temperature at this same position in case 9 and also less than the final temperatures reached in both cases at the
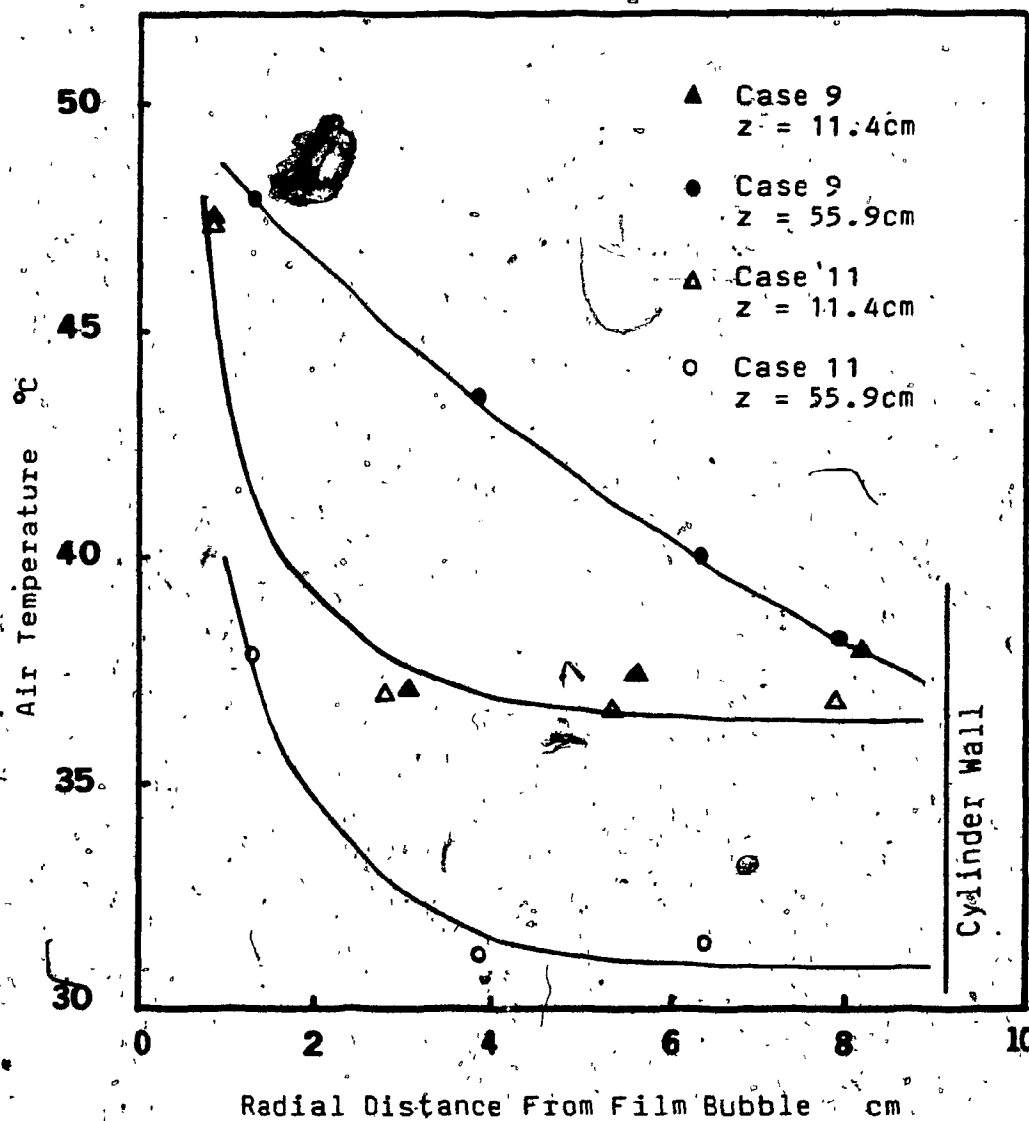
FIGURE 6.12   Air Temperature Measured Radially
From the Film Bubble at 11.4 and
55.9 cm Above the Die Under Cooling
Conditions of Cases 9 and 11

measurement position below the plenum. These results were attributed to the 'fresh' or 'new' cooling air drawn into the cylindrical shroud by the collecting plenum. This 'fresh' cooling air was drawn from the ambient surroundings of the solid bubble and probably had not been warmed by prolonged contact with the film bubble. Thus, this 'fresh' cooling air was drawn past the measurement point and into the plenum, resulting in a sharp drop in air temperature close to the bubble, while the warmed cocurrent cooling air of the combination flow was withdrawn before the measurement point.

Air temperatures at the same radial location near the bubble were plotted against distance from die in cocurrent and combination cooling systems and are shown in Figure 6.13. Under the cocurent cooling conditions of case 8, air temperature increased with distance from die. At greater distances, air temperatures approach an asymptotic value of 50 °C. Similar air temperature behavior was reported by Ast(5). Air temperatures measured with the combination cooling conditions of case 12, were similar to temperatures under solely cocurent cooling in regions below the collecting plenum. However, above the plenum ambient temperatures were recorded. The 'fresh' cooling air drawn from ambient surroundings of the upper bubble caused these lower temperatures. Ambient temperatures are found closer
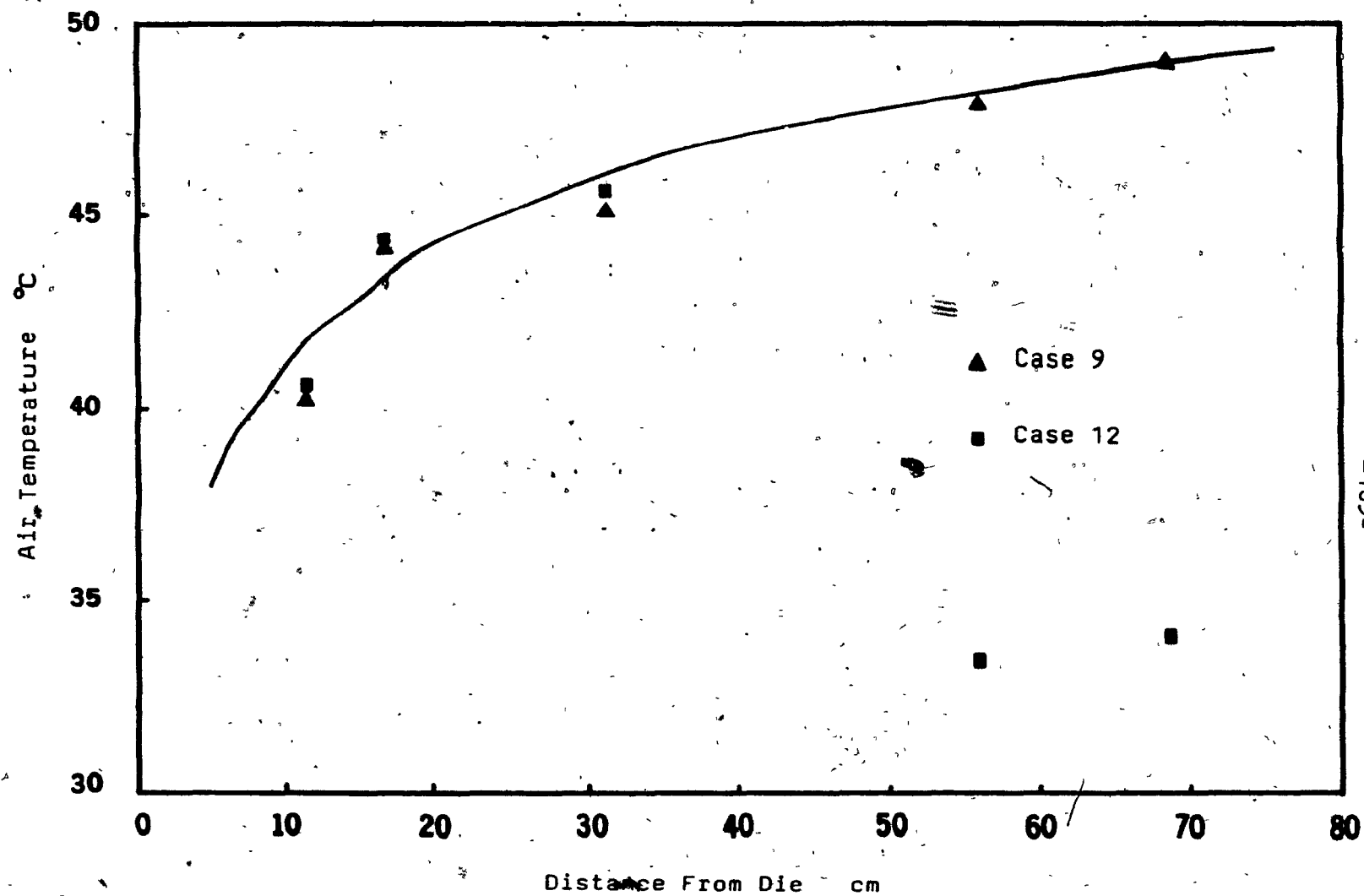
FIGURE 6.13   Air Temperature 1.3 cm From the
Film Surface Along the Length of
Film Bubble Under Cooling Conditions
of Cases 9 and 12

to the bubble in Figure 6.13 than in Figure 6.12, as the countercurent flow rate was greater in the former case. Low air temperatures close to the film bubble suggest that the air countercurrently drawn into the collecting plenum has had little contact with the film bubble and thus makes an uncertain contribution to heat transfer.

In each case where a countercurrent flow was applied to the bubble the air withdrawn was collected and exhausted away from the film blowing equipment. The temperature of the collected air was measured before entering the blower, and values are listed in Table 6.3. These values have been averaged from temperature measurements of collected air made concurrently with all dependent variable measurements. The highest air temperature was recorded for cases 3 and 10, where the amount of air withdrawn is nearly equal to that of the air flowing cocurrently. This cooling air had traveled along the hottest portion of film bubble before being withdrawn by the plenum. Under countercurrent air flows larger than in case 3 or 10, air flowing near the solid portion of the bubble mixed with air applied cocurrently, which served to reduce the bulk collected air temperature. With increased amounts of countercurrent air applied to the bubble, further reductions in collected air temperature occurred. Under maximum countercurrent cooling

Table 6.3: Air Temperatures of Countercurrently Drawn Collected Air

Cooling Condition	Collected Air Temperature (°C)
Case 3	37.0
Case 4	34.9
Case 5	32.2
Case 6	30.0
Case 7	29.8
Case 10	37.5
Case 11	33.8
Case 12	32.1
Case 13	30.4
Case 14	30.1

conditions, that is, cases 7 and 14, collected air temperatures were only 3 °C above the ambient temperature.

Air temperatures measured radially out from the film surface under all cooling conditions showed a sharp decline in moving from the surface to the surroundings. The temperature gradient was steeper at shorter distances from the die and moderated somewhat at larger distances. The thickness of the cocurrent air stream participating in heat transfer was about one third the bubble diameter. For the combination cooling system, countercurrent flow only affected air temperatures above the collecting plenum. There, the radial air temperature curves were very steep, and under large countercurrent flows, ambient temperatures were recorded within one half inch of the bubble surface. Furthermore, for these large flows, collected air temperatures were close to ambient. All this suggests that the countercurrent cooling air could have been applied much more efficiently along the bubble.

6.5 Air Velocity Measurements

Air velocities measured at the same location near the film, over the length of the bubble, give an indication of the cooling occurring along the film surface. If only cooling conditions are changed, Ast (5) has reported that greater air velocities near the bubble surface cause a lower frostline and lower surface temperatures. Air velocities measured radially outward from a film bubble indicate the thickness of the cooling air stream and its position, that is, whether the cooling air flow is near or removed from the bubble surface. Tables of radial velocity distributions at several positions above the die are given in Appendix D5.

Radial velocity distributions for the standard cocurrent cooling conditions of cases 1 and 8 were measured at several distances from the die and are shown in Figures 6.14 and 6.15. Maximum velocities were greatest near the air ring, where the air stream began, and declined at larger distances from the die. At a given position above the die the air velocities rose very rapidly near the bubble to a maximum and then, with increasing distance from the film bubble, declined to the ambient value. The decrease in air velocity from this maximum near the bubble to the surroundings was more gradual at larger distances from die, as the cooling air stream mixed with surrounding air slowed
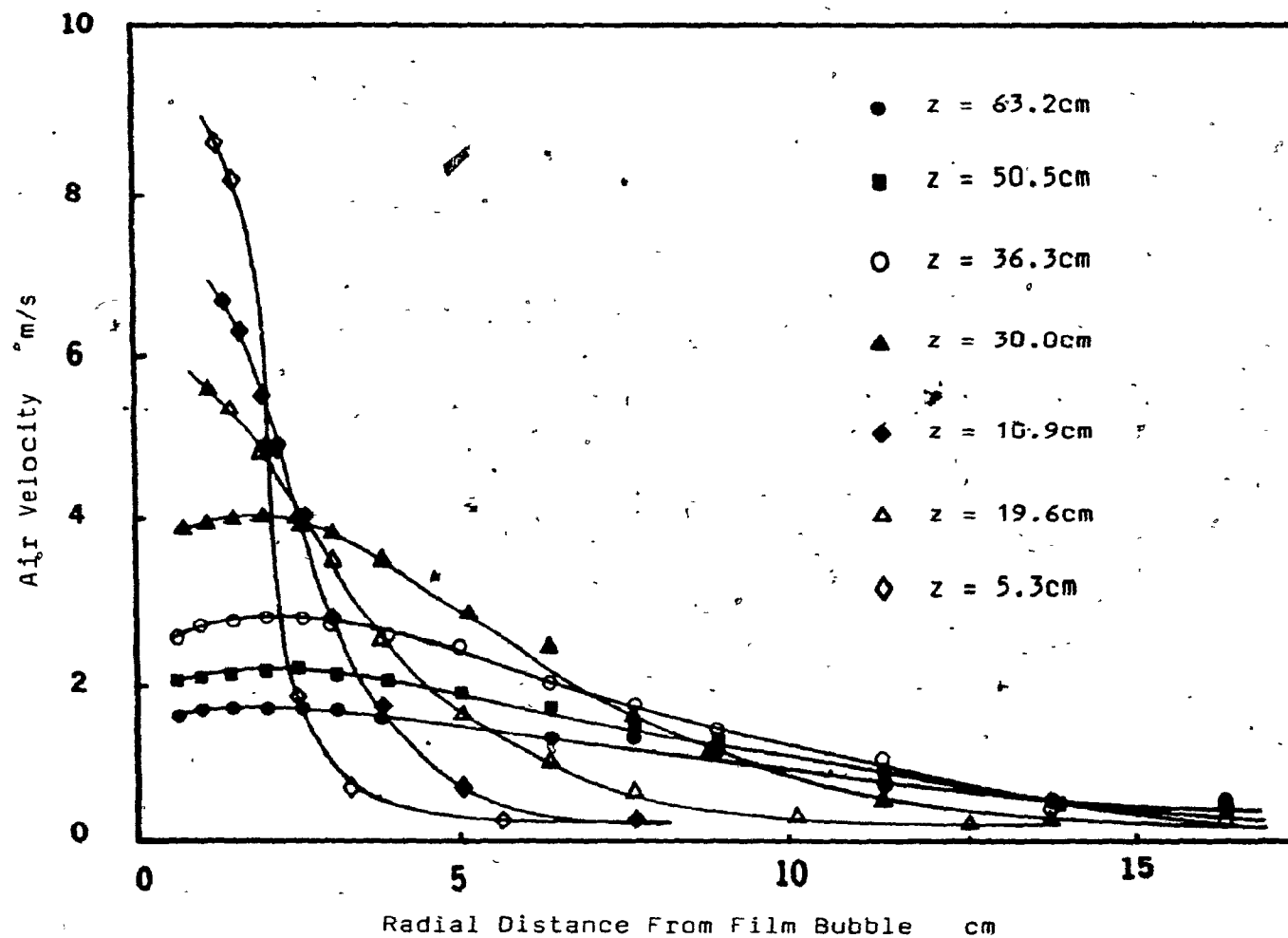
FIGURE 6.14   Air Velocity Measured Radially From
the Film Bubble at Different Positions
Above the Die Under Cooling Conditions
of Case 1
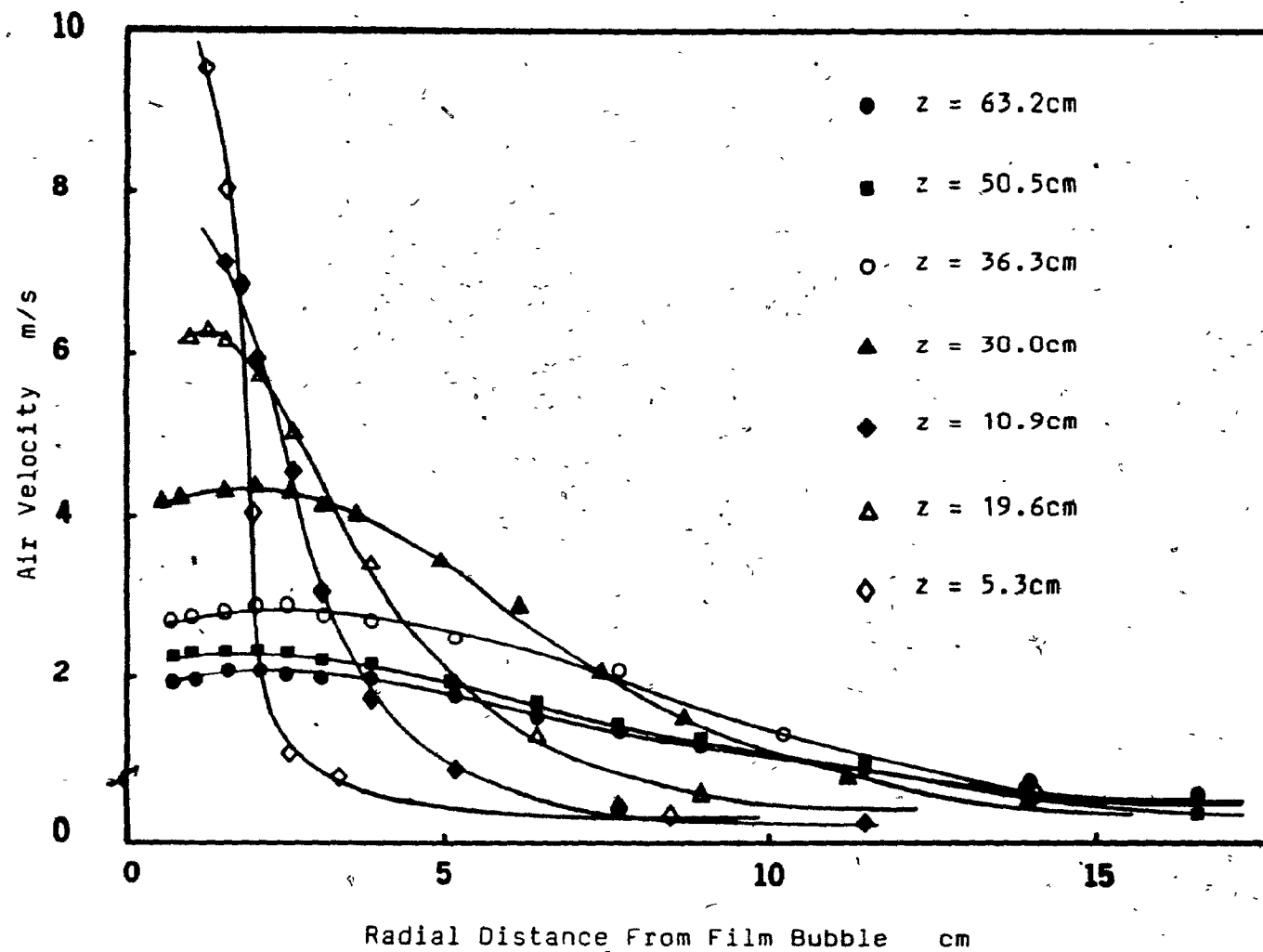
FIGURE 6.15   Air Velocity Measured Radially From
the Film Bubble at Different Positions
Above the Die Under Cooling Conditions
of Case 8

and broadened. Thus, the shape of the cooling stream changed markedly with position above die. Ast (5) obtained similar radial velocity distributions in a study of blown film cooling. Moreover, this trend of increasing air stream width at larger distances from die was previously observed in the air temperature measurements described in Section 6.4.

Figures 6.16 and 6.17 show the radial velocity distributions of cases 2 and 9, that is, cocurrent cooling with the cylindrical shroud present. The number of measurements within the cylinder was limited by either the cylinder wall or the obstruction plates mounted in the cylinder. The resulting radial velocity profiles were incomplete. Nevertheless, from the limited velocity measurements in Figures 6.16 and 6.17, trends can be observed that air similar to that of the standard cocurrent cases.

Air velocities one half inch from the bubble surface are plotted as a function of distance from die in Figure 6.18, for all cocurrent cooling conditions. Air velocities decreased with increasing distance from die. This was primarily attributed to the cooling stream mixing with surrounding air in cases 1 and 8, and with the cylindrical shroud positioned over the bubble in cases 2 and 9, decreases in velocity were attributed to obstruction or
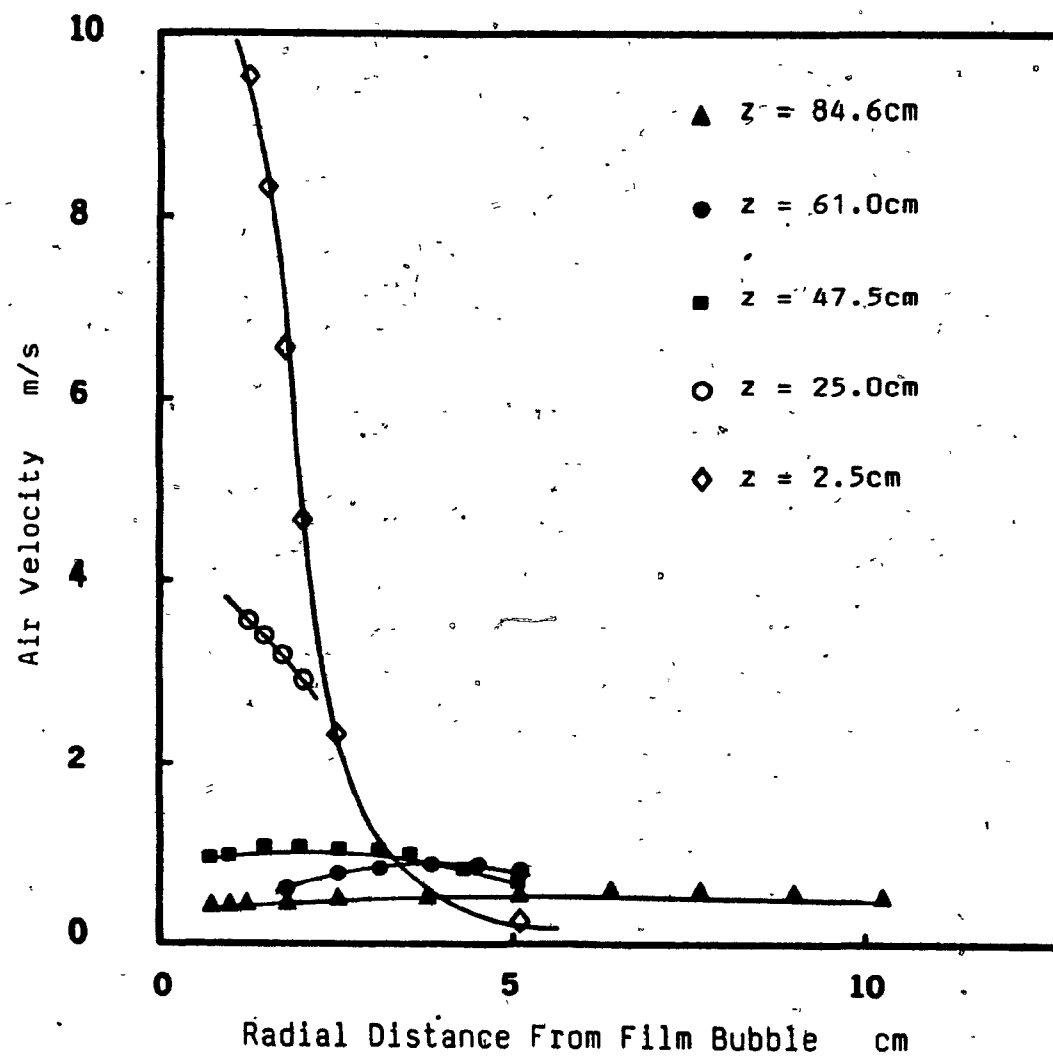
FIGURE 6.16   Air Velocity Measured Radially From
               the Film Bubble at Different Positions
               Above the Die Under Cooling Conditions
               of Case 2
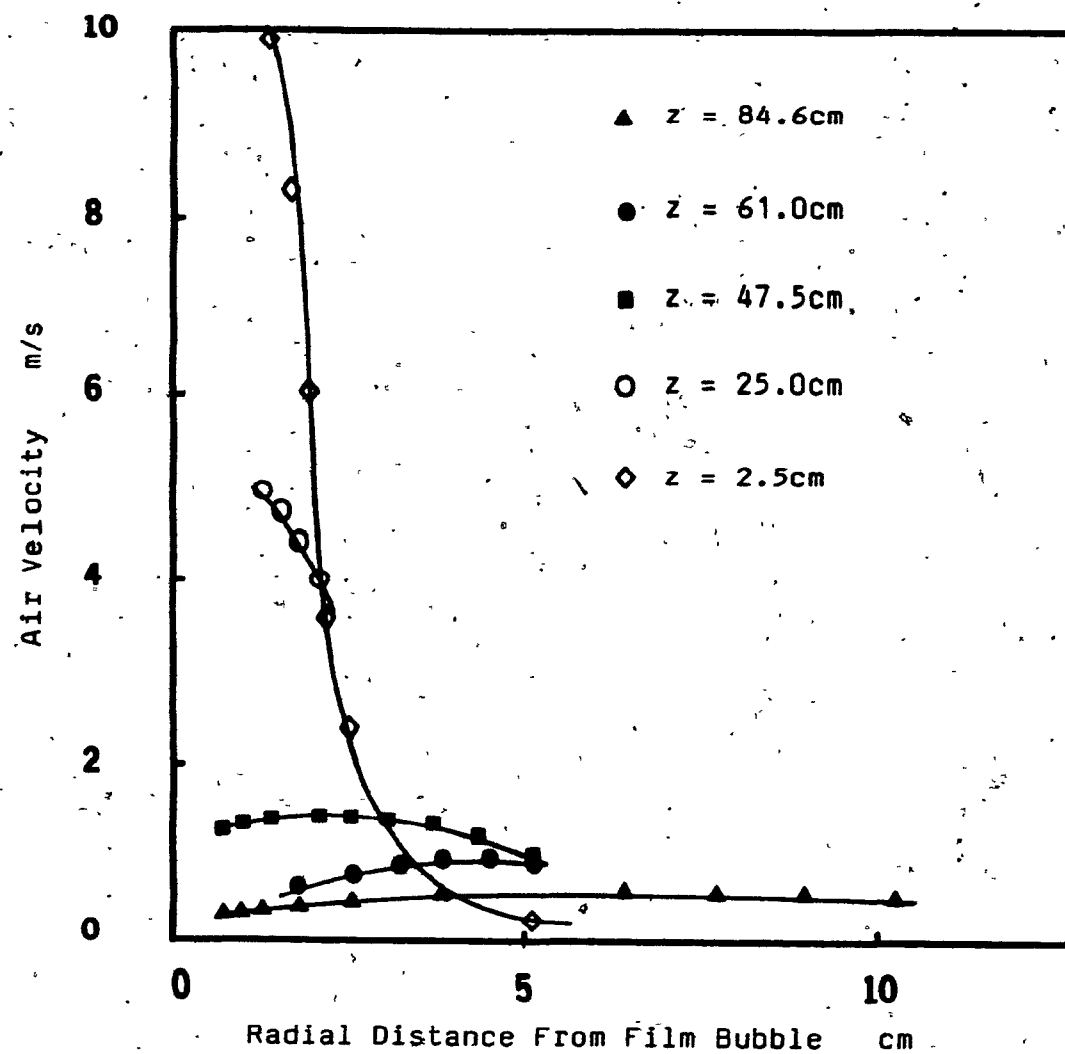
FIGURE 6.17   Air Velocity Measured Radially From
                the Film Bubble at Different Positions
                Above the Die Under Cooling Conditions
                of Case 9
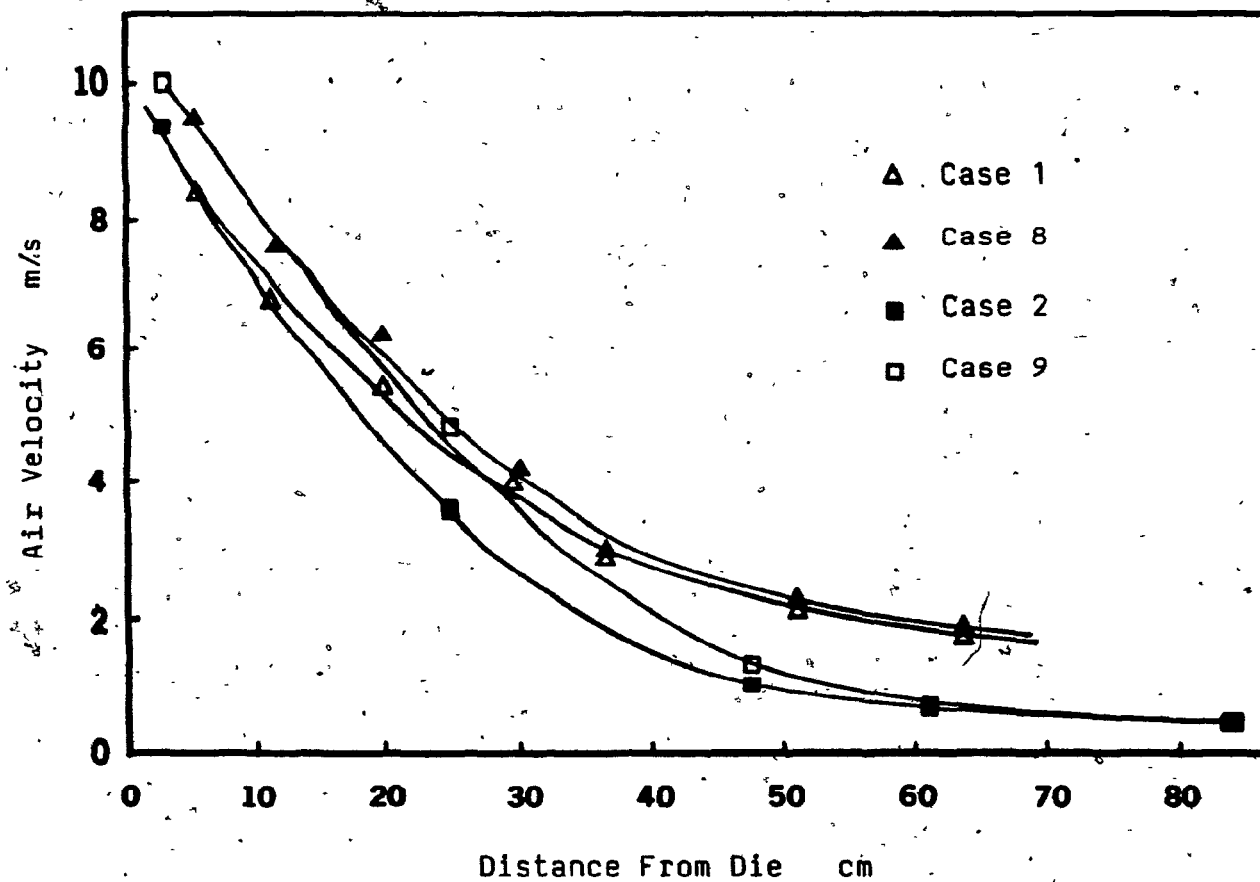
FIGURE 6.18   Air Velocity 1.3 cm From the Film
Surface Along the Length of Film
Bubble Under Cocurrent Cooling Conditions

-173-

deflector plates within the cylinder acting as 'brakes' against the onrushing cooling air. In all cases cooling air flowing over larger surface areas of an expanding bubble also contributed to smaller velocities at larger distances from die. In Figure 6.18, cases 1 and 8 have higher cooling velocities with increasing distances from the die than their counterparts in cases 2 and 9. This suggests that obstructions within the cylinder caused a greater reduction in air flow than the mixing with ambient air. Furthermore, this observation was reflected in surface temperature measurements for the same cooling conditions. In Figure 6.4, surface temperature differences between cases 1 and 2 and cases 8 and 9 similarly became larger with distance from the die.

Radial air velocity distributions for cocurrent cooling cases 2 and 9 and combination cooling cases 6 and 13 are shown in Figure 6.19 at two positions above the die. Measurement positions were within the cylindrical shroud and below the collecting plenum. At one inch above the die cocurrent and corresponding combination air velocities, that is cases 2 and 6 and cases 9 and 13, were nearly equal. However, at the higher position above the die, 9.8 inches, the velocities for these pairs of cases differed by as much as ten per cent. In each pair grouping, the combination
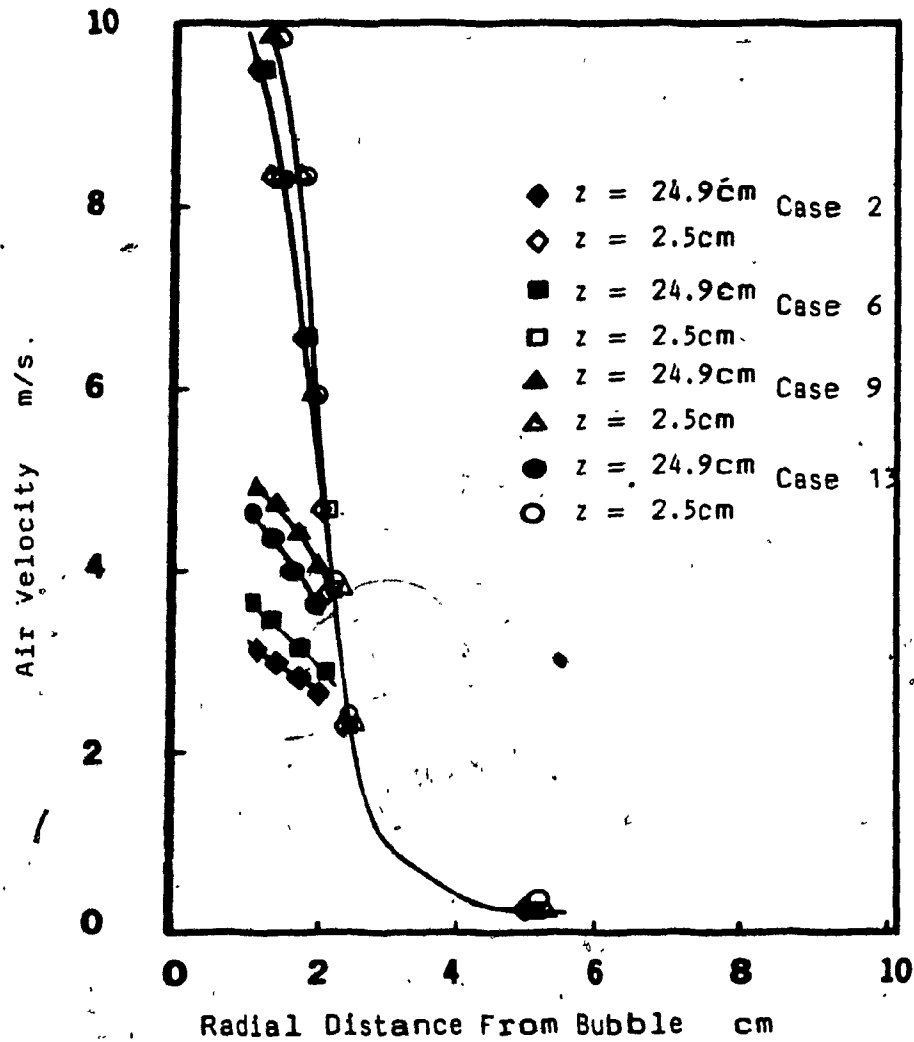
FIGURE 6.19   Air Velocity Measured Radially From
the Film Bubble at 2.5 and 24.9 cm
Above the Die Under Cooling Conditions
of Cases 2, 6, 9 and 13

cooling flow had somewhat lower velocities than the cocurrent flow. One possible explanation is that countercurrent flow drawn down the bubble and cocurrent air pushed upward in combination cooling compete with each other to be withdrawn by the collecting plenum. The result is that the countercurrent flow serves as a large 'brake' against the cocurrent stream, slowing its velocity and thus increasing the pressure on the outside of the tube, which in turn reduces the bubble size everywhere in the neck region. In cases 2 and 6 and cases 9 and 13, the velocity differences are accompanied by this compensating difference in bubble shape or cross-sectional annular gap area between bubble and deflector plate so that continuity of mass is satisfied. Calculations demonstrating the preservation of continuity are given in Appendix D5.

Radial air velocity distributions for the cooling conditions of Figure 6.19 and for additional combination cooling conditions are shown in Figure 6.20 for a higher position above the die than in Figure 6.19. In these combination cooling flows, the measurement point was above the plenum and yet within the cylindrical shroud. The probe was positioned parallel to the bubble with probe sensors pointed upwards anticipating air flow drawn countercurrently to the plenum. Under cocurrent cooling flow the probe sensors were orientated 180 degrees from this position and

10

Case 2
■ z = 47.5cm
□ Case 9

◆ Case 5
   z = 58.7cm
◇ Case 12

● Case 4
   z = 58.7cm
○ Case 11

▲ Case 6
   z = 58.7cm
△ Case 13

8

Air Velocity m/s

6

4

2

0

0   1   2   3   4   5   6   7

Radial Distance From Film Bubble   cm
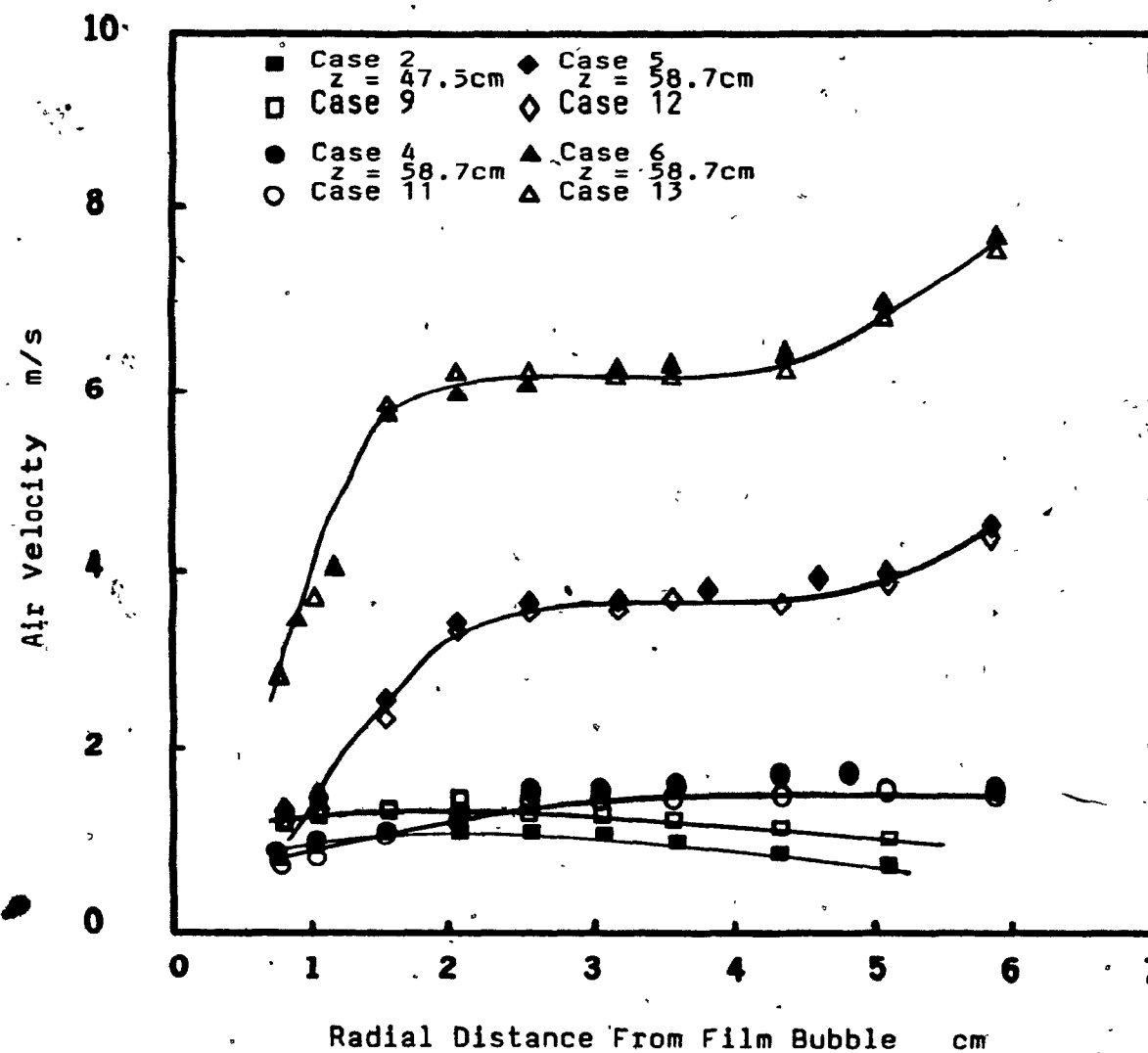
FIGURE 6.20   Air Velocity Measured Radially From
the Film Bubble at 47.5 cm Above the
Die Under Cooling Conditions of
Cases 2 and 9, and at 58.7 cm Above
the Die Under Cooling Conditions of
Cases 4, 5, 6, 11, 12 and 13

thus able to measure velocities upward, along the bubble.
The probe was bent at a right angle near the tip (Section
5.5), and the length of this bent section of probe accounts
for the difference in measurement position with cocurrent
and combination cooling flows, as the probe support was
inserted through the same cylinder 'window' in each case.
Air velocities for the cocurrent cooling conditions of cases
2 and 9 hovered around the 1 m/s mark from near the bubble
surface to the cylindrical wall, with case 9, having the
higher volume cocurrent flow and yielding somewhat higher
velocities than case 2. Under combination cooling flows,
different cocurrent components caused little or no change in
air velocities at this position above the plenum. Thus,
each pair of combination cooling conditions; cases 5 and 11,
6 and 12, and 7 and 13, could be treated as one cooling
condition. The dominant role of the countercurrent flow in
this region above the plenum had also been indicated by the
film surface temperature and air temperature measurements.
Countercurrent air velocities increased with increasing
countercurrent flow rates at each radial position. Under
the strong countercurrent cooling conditions of cases 7 and
13, the average velocity was roughly 6 m/s. However, the
radial velocity profile showed that the largest velocity (8m
/s) occurred near the edge of the cylinder and decreaesed
through a plateau or inflection point midway between bubble

and cylinder to smaller velocities near the bubble surface. This trend was opposite to the radial velocity distribution measured for cocurrent flow as shown in Figures 6.14 through 6.19. It indicated that most of the countercurrent air flow was channeled along the cylindrical wall. This observation when coupled with the air temperature measurements at a similar position above the die, shown in Figure 6.13, which showed essentially ambient temperatures within 0.5 inches of the film bubble, suggests that the bulk of the countercurrent air flow makes little contact with the film bubble.

Radial air velocity distributions are shown in Figures 6.21 and 6.22 for the same cooling conditions as in Figure 6.20 and at progressively greater distances from die. The countercurrent flows were measured at a position above the collecting plenum and also above the cylindrical shroud. These Figures reveal very low countercurrent air velocities along the entire radial traverse. These velocities were of the same magnitude as air simply circulating in the surroundings. In fact, the cocurrent air velocities roughly 33 inches above the die were two times greater than the largest countercurrent air flow measured only 10 inches above the collecting plenum. In Figure 6.22, countercurrent air velocities were measured with the probe pointed upwards to sense air drawn down the bubble, but the values were so
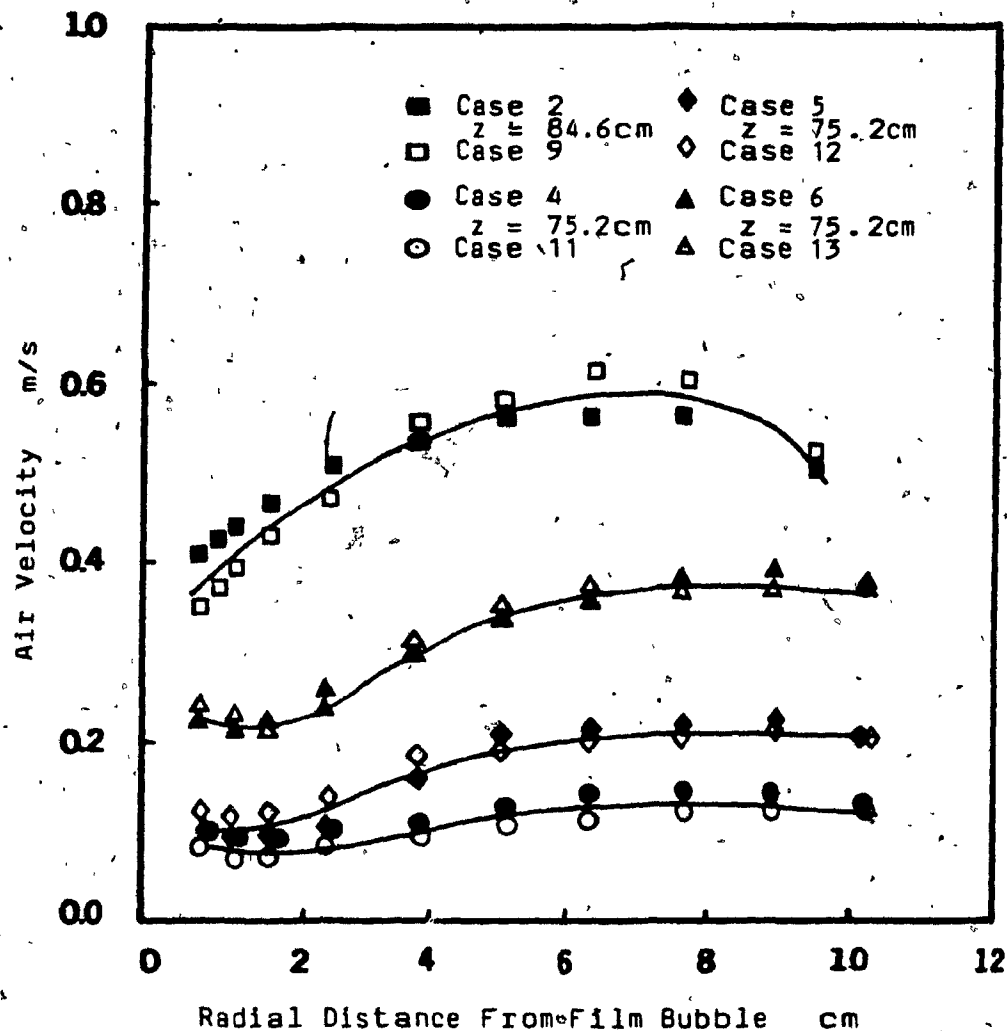
FIGURE 6.21   Air Velocity Measured Radially From the Film Bubble at 75.2 cm Above the Die Under Cooling Conditions of Cases 4, 5, 6, 11, 12 and 13, and at 84.6 cm Above the Die Under Cooling Conditions of Cases 2 and 9
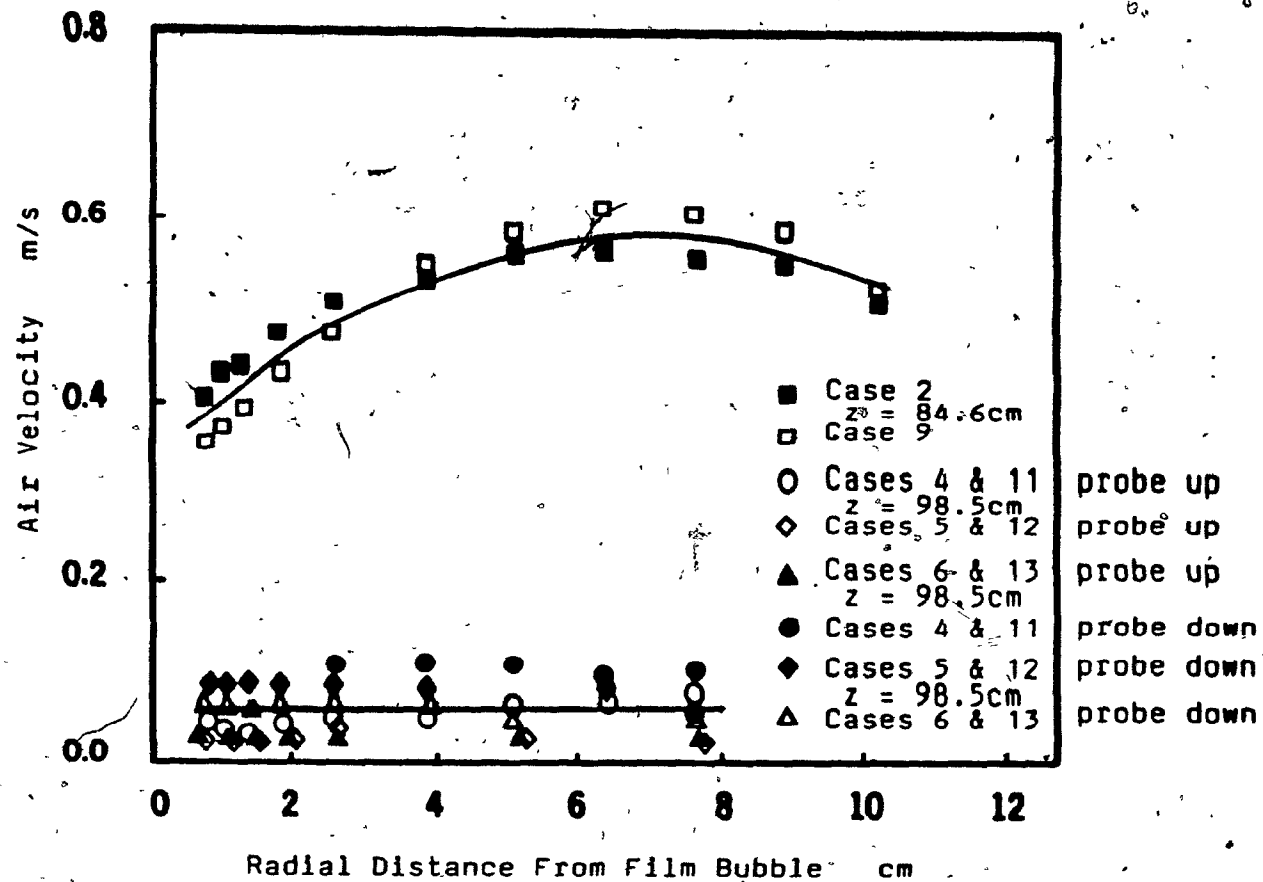
FIGURE 6.22   Air Velocity Measured Radially From the Film Bubble at 84.6 cm Above the Die Under Cooling Conditions of Cases 2 and 9, and at 98.6 cm Above the Die Under Cooling Conditions of Cases 4, 5, 6, 11, 12 and 13

small the probe was rotated 180°, as if the flow were cocurrent, and the velocities measured were again very small, although they were slightly above the previous measurements! These results indicated that virtually no cooling air was drawn down parallel to the bubble above the cylindrical shroud. Any cooling occurring in the upper reaches of the bubble was mostly attributed to bubble movement through quiescent surroundings.

The measurements of radial countercurrent air velocities in Figures 6.19 through 6.22 at several positions above the collecting plenum, show that velocities greater than 1.0 m/s measured parallel to the bubble are only present in the first eight inches above the plenum, and significant velocities near the bubble surface were found only within the cylindrical shroud. At a measurement point within the shroud the countercurrent velocities at the cylinder wall were roughly three to four times greater than those near the bubble, suggesting that the air flowed mainly from the surroundings, over the cylinder' lip, directly to the collecting shroud, without contacting the film bubble. Ambient air temperatures measured near the bubble at a similar position above the collecting plenum support this contention. A sketch of this situation is shown in Figure 6.23. Confirming the detailed air flow patterns in this sketch would be difficult from a standpoint of manipulating
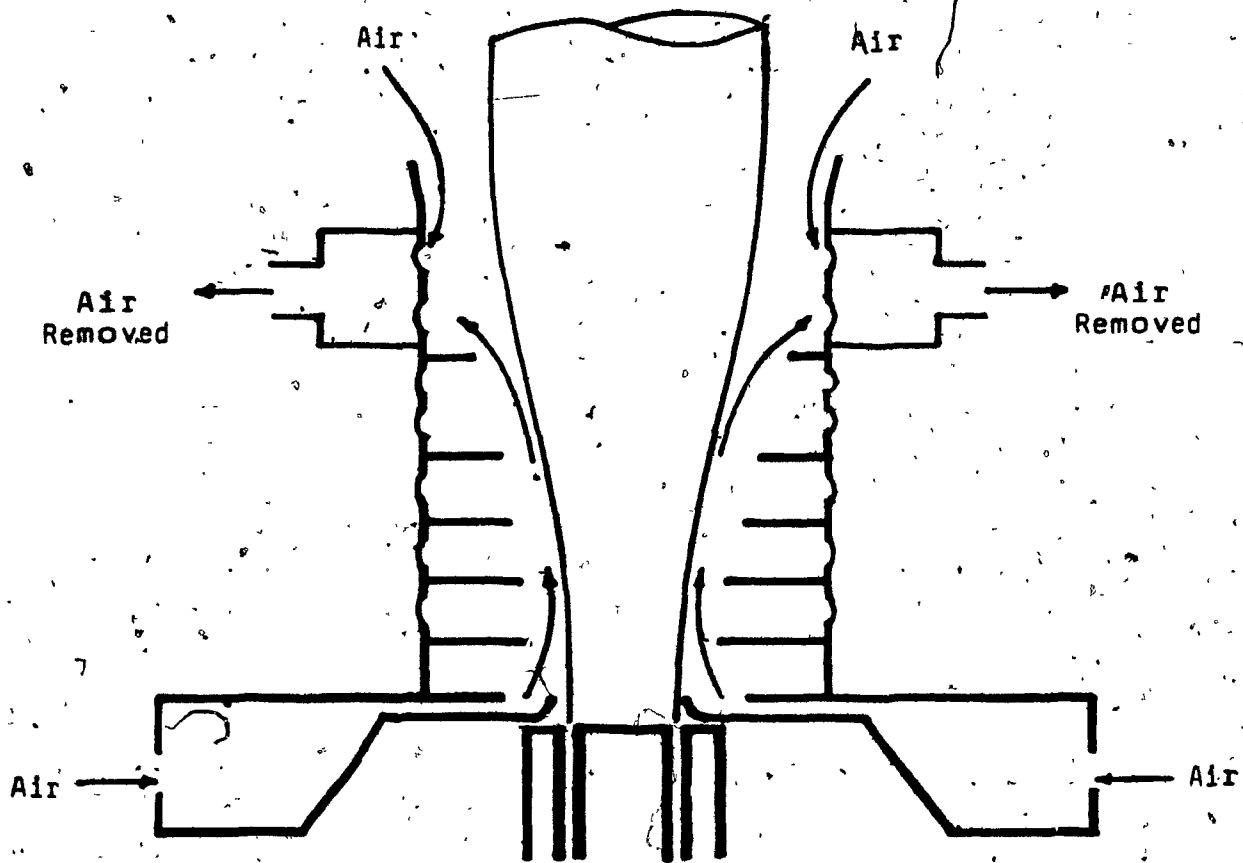
FIGURE 6.23   Sketch of Air Flows in Cocurrent-
Countercurrent Combination Cooling

a probe in this region and more importantly in measuring a flow which is three dimensional. A probe equipped with three velocity sensors and a sensor for temperature compensation would be required. Furthermore, the analysis technique for three simultaneous velocity signals is not well established (41).

6.6 Heat Transfer Coefficients

The heat transfer coefficient, h, can be calculated for regions where crystallization does not occur. This is carried out directly using Equation 6, which can be rearranged to yield:

$$\frac{\dot{m} \, C_p \, \cos\theta \, (dT/dz)}{\Pi \, D \, (T_s - T_c)} - \frac{e \, K \, (T_s^4 - T_a^4)}{(T_s - T_c)} = h$$

Data for the variables in Equation 6 were obtained from Sections 6.2, 6.3, 6.6.1, and 6.6.2. Surface temperature and temperature profile derivatives were determined as described in Section 6.2. In Section 6.3 it was explained how knowledge of bubble shape allowed the angle between a tangent to the bubble surface and the bubble axis to be determined. In the following sub-sections, 6.6.1 and 6.6.2,

methods of estimating emissivity and thermal properties of polyethylene are described.

6.6.1 Thickness Distribution

Film thickness was used to relate independent emissivity measurements to distance from the die, and this relationship was inserted into a heat balance for a film element (Equation 6) to obtain the local heat transfer coefficient. Predohl's (29) values of emissivity as a function of film thickness for low density polyethlene are plotted in Figure 6.24 along with thickness versus distance from the die measurements of this work. These relationships are listed in Appendix D6. In Figure 6.24, we see that the film thickness decreased from a maximum value of 22 mils at the die (ignoring die swell) to 1.6 mils near the frostline. The thickness of an element of film decreased in the molten region as a result of stretching by the nip rolls and bubble expansion. The amount of thickness reduction depends on these stretching forces and on the viscoelastic properties of the melt.

From Figure 6.24, a value of emissivity can be determined at any height above the die. Emissivity decreased with film thickness and thus with distance from
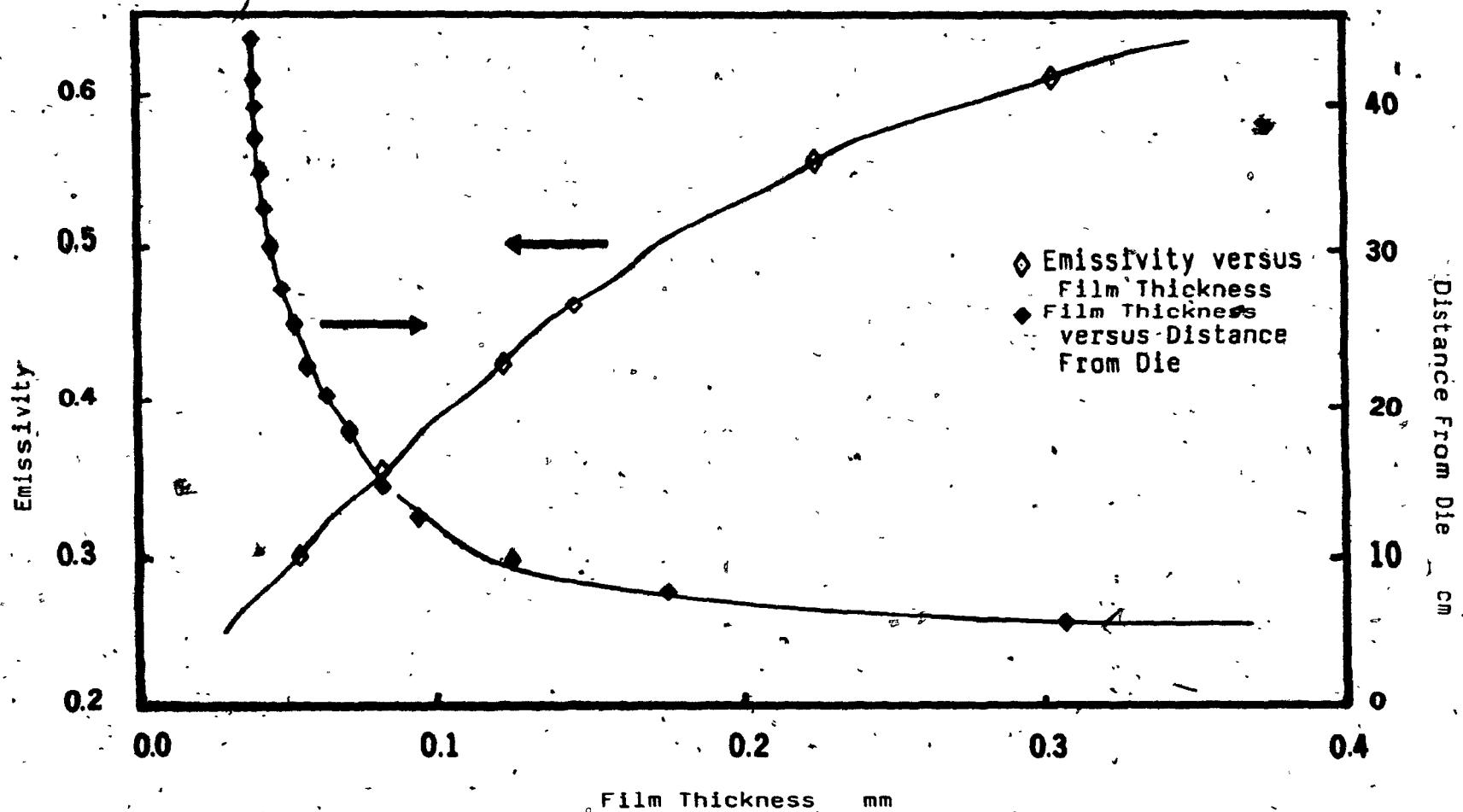
FIGURE 6.24   Plot of Emissivity (Reference 27) and
Distance From Die Versus Film Thickness
Under Standard Cocurrent Cooling Conditions

die. Through Kirchoff's law (42) emissivity was equated with absorbance, and the emissivity decline with thickness can be thought of as a lessoning ability of the material to absorb infrared radiation. This behavior is typical of plastics(43).

6.6.2 Thermal Analysis

Heat of crystallization and specific heat were estimated by a thermal analysis and used in a heat balance for an element of film (Equation 6) to calculate heat transfer coefficient and the fraction of crystallinity. The thermal analysis provided only an estimate of polymer thermal properties, as the cooling and stretching conditions the melt encountered in blown film cooling could not be duplicated. The results of the thermal analysis are shown graphically in Figures 6.25 and 6.26 and are listed in Appendix D6.

From Figure 6.25, the heat of crystallization was determined to be roughly 20 cal/gm-°C. Similar values for LDPE have been reported in the literature (43). The specific heat values, shown in Figure 6.26, were divided into amorphous and solid state regions. Everywhere below the frostline, that is, in the amorphous region, an average
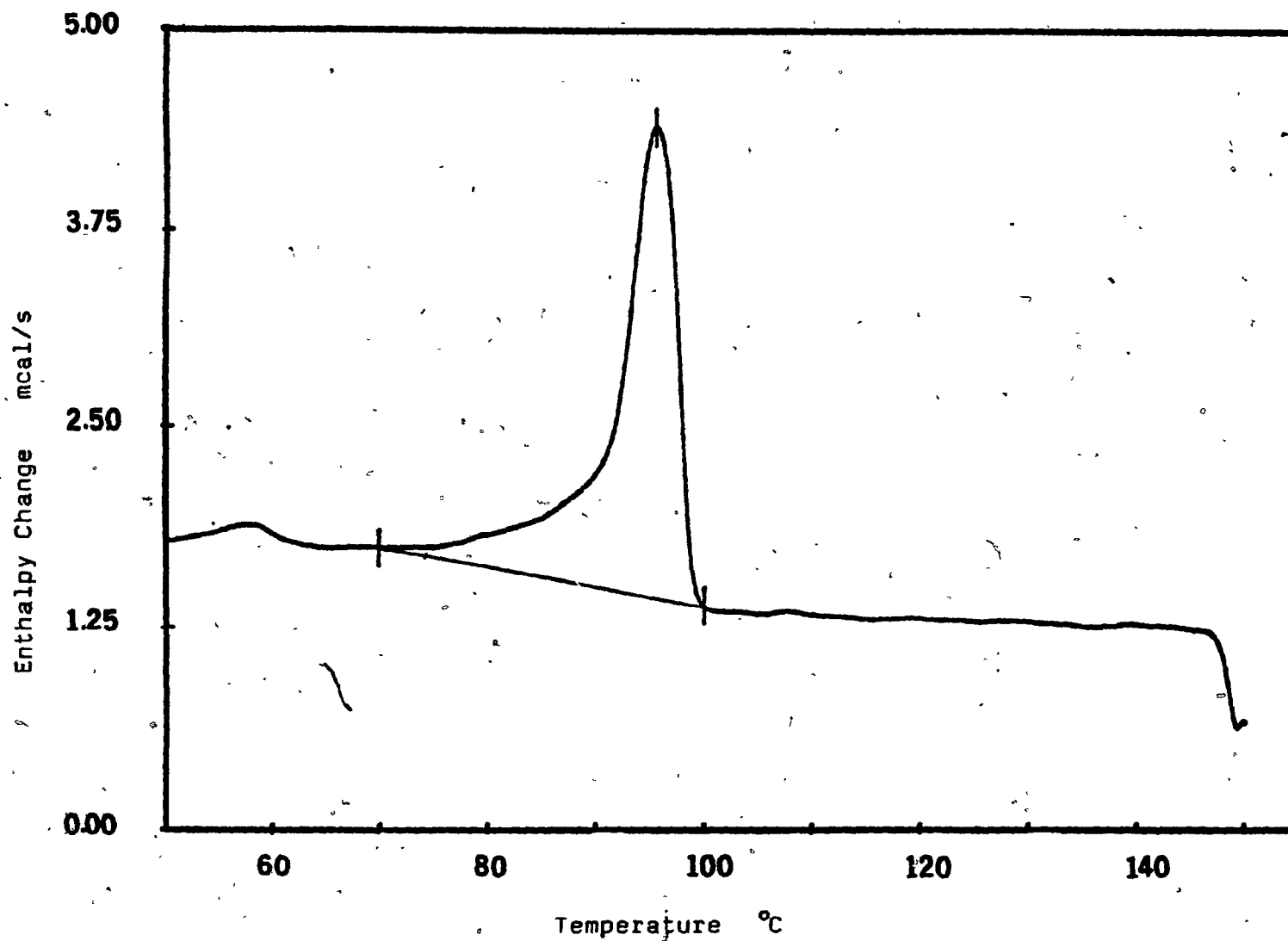
FIGURE 6.25. Heat of Crystallization Determination of Union Carbide Low Density Polyethylene DFDY 3312 by Differential Scanning Calorimetry
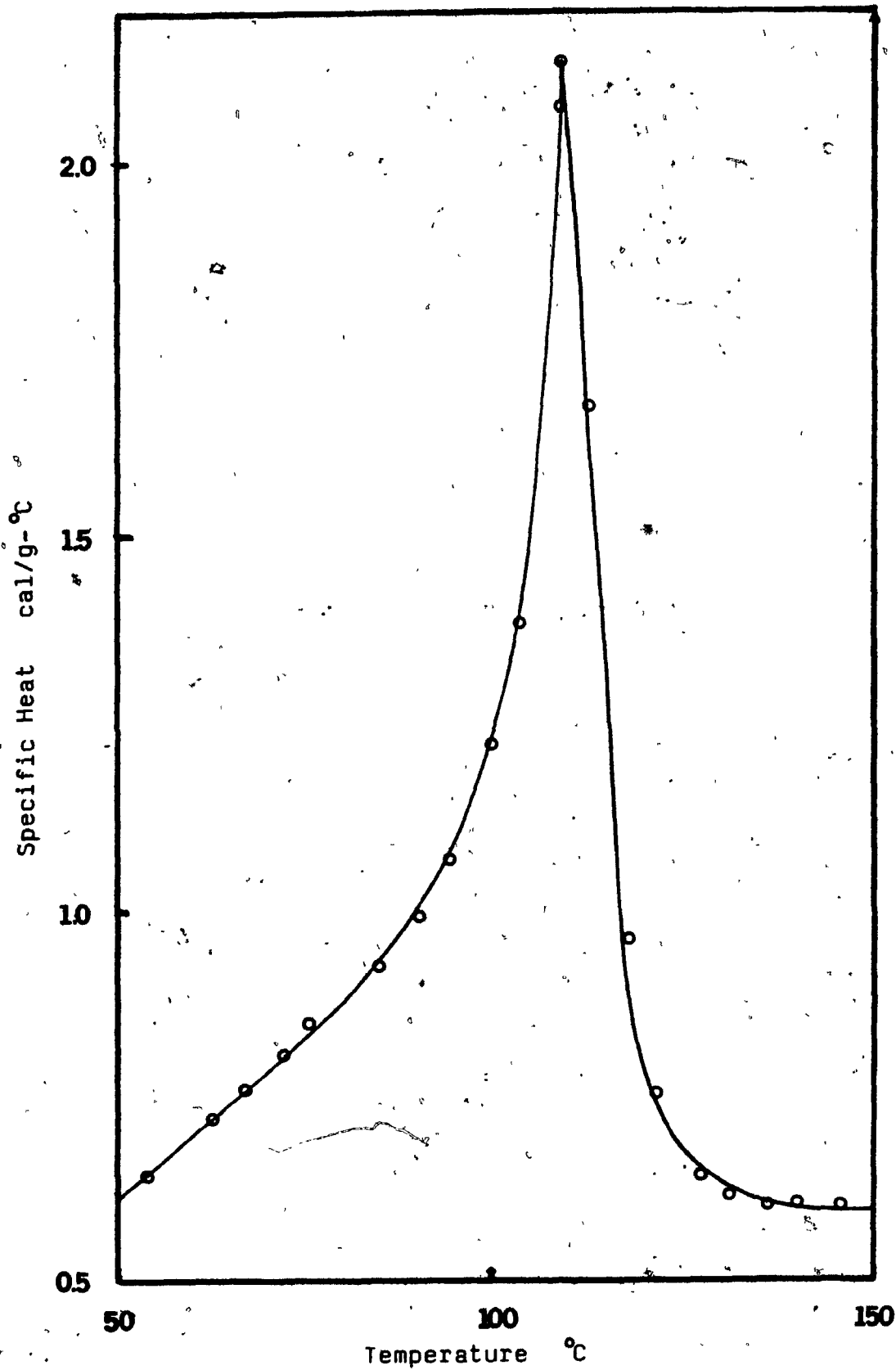
FIGURE 6.26   Plot of Specific Heat Versus Temperature
for Union Carbide Low Density
Polyethylene DFDY 3312

specific heat of 0.6 cal/gm-°C was used in the differential heat balance. However, just above the frostline the specific heat-temperature curve did not immediately drop to an equilibrium specific heat value. A moderate decline in specific heat with decreasing temperature was observed. Wynter (43) has reported similar results over this interval. Therefore, in the immediate region above the frostline, specific heats were variable. Over a small interval, 17 to 19 inches from the die, specific heats of 0.9 to 0.8 cal/gm-°C were inserted into Equation 6. Beyond this region the specific heat was estimated to be 0.6 cal/gm-°C. White (26) used a specific heat of 0.58 cal/gm-°C over the entire bubble, while Wagner (28) favored an empirical realtionship: $Cp = 0.478 + 8.46 \times 10 - 4(T)$ to approximate this thermal property.

The thermal analysis was used only to estimate specific heat and heat of crystallization, as the analysis was carried out under quiescent cooling conditions that were unlike those conditions encountered in the film blowing process. For example in determining the crystallization point, the DSC thermogram shown in Figure 6.25 gave a crystallization temperature of 96 °C. This thermogram was made for a cooling rate of 10 °C/min according to ASTM Standard Test Method D3418. Thermograms obtained with

stronger cooling conditions, up to 25 °C/min, revealed lower crystallization point temperatures. Under the film blowing cooling conditions in this research, a cooling rate of roughly 40 °C/s was encountered, which at first suggests a crystallization point temperature below the 96 °C value obtained with much slower cooling. However, in film blowing the area of crystallization roughly corresponds to the solidification region or frostline (26), and the frostline temperature was determined from Figure 6.3 to be 115 °C. The actual temperature is thus higher than the temperature predicted by differential scanning calorimetry. The temperature difference was attributed to the stretching and expanding forces the film experiences in the neck region. They serve to impart some orientation to the film as it cools and cause crystallization to occur at higher temperatures than if the melt was cooled quiescently. This discussion will be more fully developed in Chapter 8, where orientation in blown film is discussed.

6.6.3 Results and Discussion

The heat transfer coefficient, h, was calculated by use of a heat balance over an element of film (Equation 6) and is plotted versus distance from the die in Figure 6.27 for standard cocurrent cooling conditions. A sample
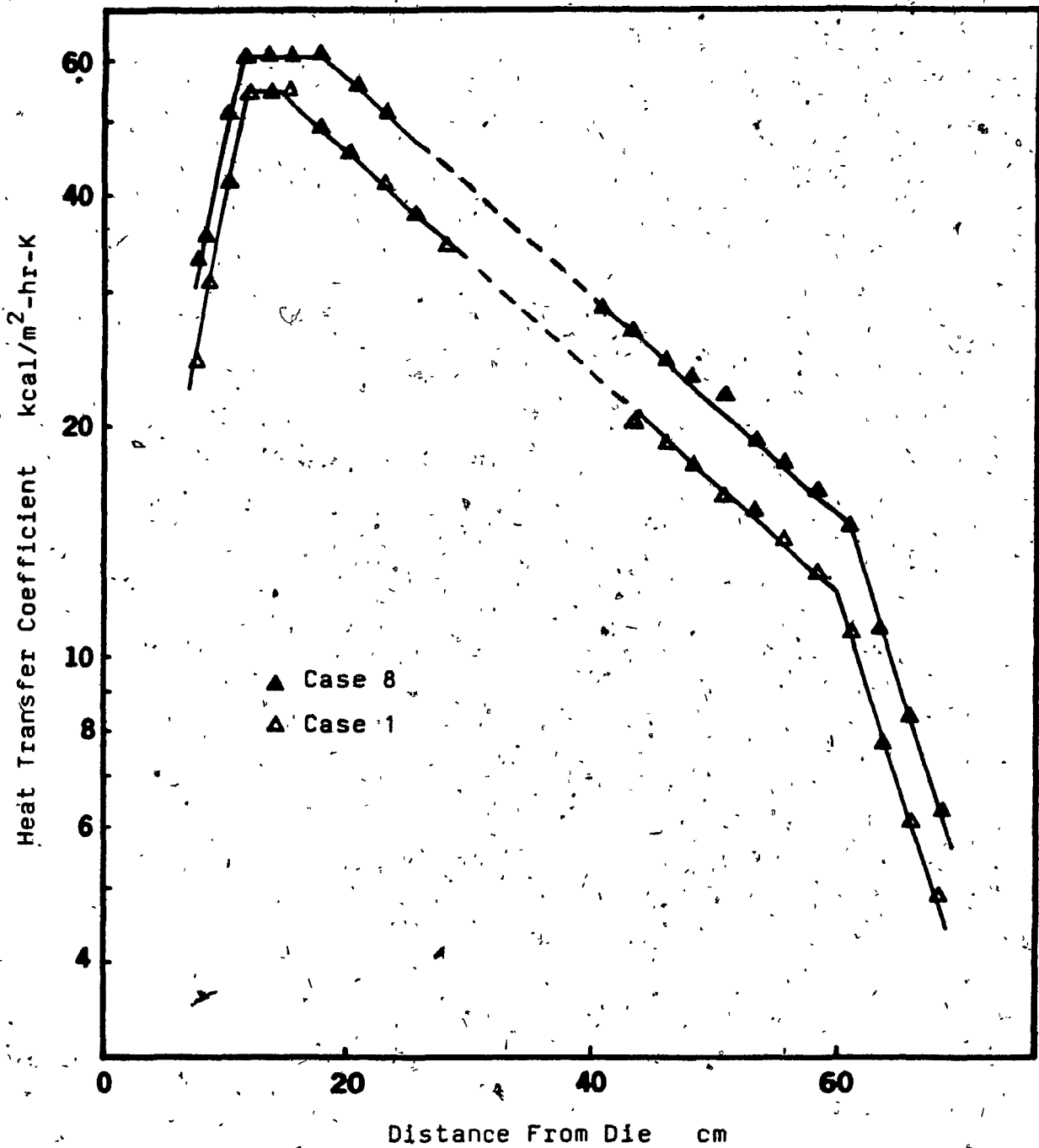
FIGURE 6.27   Plot of Heat Transfer Coefficient
Versus Distance From Die Under Standard
Cocurrent Cooling Conditions of
Cases 1 and 8

calculation of h at its maximum value is given in Appendix D7. Tables of heat transfer coefficient at various distances above the die, for each cooling condition, are also given in this Appendix. In Figure 6.27, we see that h rises rapidly from near the die to a maximum below the frostline, and then declines with increasing distance from die. The frostline region is indicated by dashes.

The maximum heat transfer coefficient occurrs in the molten region, that is, below the frostline. Maximum heat transfer coefficient is primarily due to a large surface temperature gradient (dTs/dz) and secondly to bubble diameters smaller than those in the solid state. These two terms in Equation 6 were only partially offset by the large temperature differences between film and ambient air. Specific heat was constant and estimated to be 0.6 cal/g-°C over this molten region and the angle term, $\cos\theta$, varied by only 1.8% and thus did not substantially affect the heat transfer coefficient. This analysis neglects the radiative term in Equation 6, as it accounted for only 5% of the local heat transfer coefficient in this region where the maximum heat transfer coefficient occurrs. The radiative term was largest near the die where the film and ambient air temperature difference was greatest. However its contribution to the heat transfer coefficient or overall heat transfer from the bubble was never greater than 17% of

the total. Menges (27) has estimated a 10 to 20% radiative contribution to total heat transfer.

Heat transfer coefficients were smaller at points within five inches of the die. This was attributed to a decline in the film temperature gradient and an increased temperature difference between film and ambient air, even though the diameter was smallest and radiative contribution largest in this region. Cooling air first contacted the film bubble slightly above the die and thus only moderate cooling occurred there. A moderate temperature gradient reflects these cooling conditions and leads to less than maximum heat transfer coefficients. A decline in the rate of temperature change in the immediate vicinity of the die was also observed by Ast (5). Furthermore, a similar trend in heat transfer coefficients has been reported by White(26) for low density polyethylene very near the die. However, the steepness of heat transfer coefficient decline was less in this earlier work than that shown in Figure 6.27. This was due to White's (26) steep temperature profile, and thus large temperature gradient, at positions close to the die.

Heat transfer coefficients declined from maximum values as the cooling curve gradient moderated somewhat below the frostline. This change in temperature gradient was again the largest contributor to smaller heat transfer coefficients, although its effect was partiallly offset by

the decline in film and ambient air temperature difference along the length of the bubble.

Above the broad frostline region, heat transfer coefficients continued to decline. The temperature gradient over this region was significantly less than in the areas prior to the frostline and the gradient declined somewhat with increasing distance from the die. Along this solid portion of the film bubble, the diameter and angle term in Equation 6 were constant. However, the specific heat varied somewhat immediately following the crystallization region. Specific heats of 0.85, 0.80, and 0.70 cal/g-°C were used in Equation 6 at 17, 18 and 19 inches from the die. This corresponded to a roughly 30 °C increase in the specific heat versus temperature curve, which was obtained under quiescent cooling conditions using the differential scanning calorimeter (Figure 6.25, Section 6.6.2). At distances 20 inches from the die and greater, a specific heat of 0.6 cal/g-°C was again used. At distances beyond 24 inches from the die, the decline in heat transfer coefficient accelerated. This decline is emphasized by a semi-logarithmic scale plot of the heat transfer coefficient versus distance from die as shown in Figure 6.28. The greater decline in heat transfer coefficients at large distances from the die was attributed to a 'leveling off' or 'flattening out' of the cooling curve at these distances.
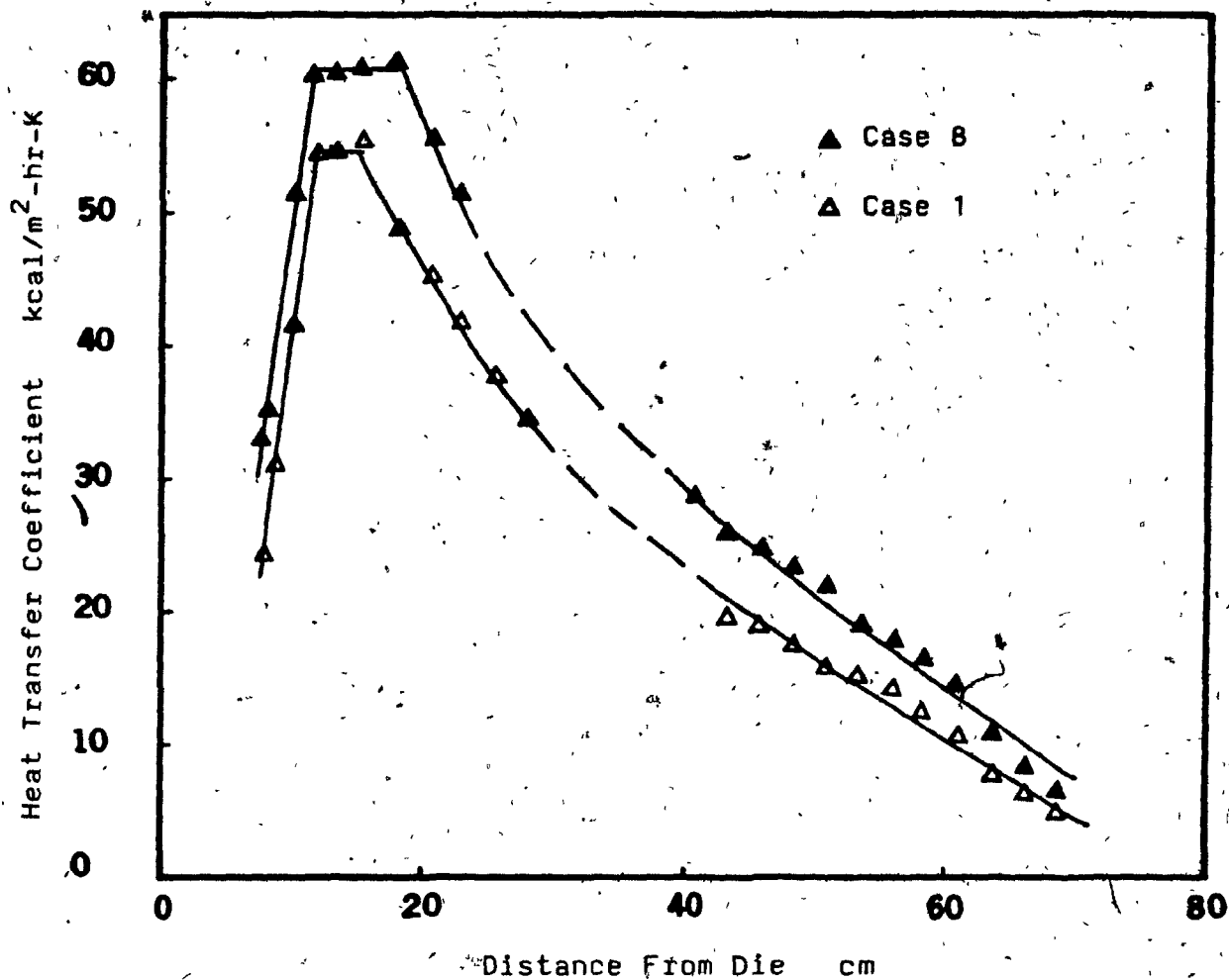
FIGURE 6.28   Semi-Logarithmic Scale Plot of Heat
Transfer Coefficient Versus Distance
From Die Under Standard Cocurrent
Cooling Conditions of Cases 1 and 8

Ast (5) also reported a similar 'leveling-off' of surface temperature decline with increasing distance from the die. However, when White's (26) heat transfer coefficients were plotted against distance from the die on a semi-logarithmic scale, no downturn in heat transfer coefficient at large distances from the die was evident. This could be anticipated from the reported surface temperature data, which did not decrease with increasing distance from die and may simply be the result of not measuring film temperatures at large enough distances to detect a 'leveling off' cooling curve.

Figure 6.27 also shows that heat transfer coefficients, under the cocurrent cooling conditions of case 8, are greater everywhere along the bubble than the coefficients calculated for case 1 cooling. This trend was expected, as the cooling conditions in case 8 are stronger than those in case 1. Stronger cooling conditions decreased surface temperatures and increased temperature gradients, which led to higher heat transfer coefficients. Similar results have been reported by White (26) for lower frostline heights, that is, stronger cooling conditions. Furthermore, heat transfer coefficients calculated with Ast's (5) data under different cooling conditions also showed this trend.

Heat transfer coefficients calculated for the cocurrent

cooling conditions of case 1 along the molten portion of
film bubble were almost identical to those of cases 2
through 7, for which the cocurrent cooling flow was the
same. A similar result was found for cases 8 through 14 in
this region. The maximum difference between heat transfer
coefficients calculated for standard cocurrent cooling and
for combination cooling systems was only 2 percent. Similar
heat transfer coefficients in the molten regions could have
been anticipated, as dependent variables for the same
cocurrent cooling flow yielded very similar values whether
or not a cylindrical shroud or countercurrent cooling flow
was present. For example, surface temperature differences
between the most extreme pairs of cooling conditions, that
is, cases 1 and 7 and cases 8 and 14, were largest just
below the frostline, with surface temperatures within the
cylindrical shroud being somewhat higher. The corresponding
differences in the term (T_s-T_a) in Equation 6, were 5.5 and
2.4 percent. Differences in bubble diameters at this same
position from the die, in cases 1 and 7 and cases 8 and 14,
varied by a maximum of 4.5 and 2.6 percent. Similar
diameters were measured for countercurrent cooling with the
cylindrical shroud present. These two effects were in
opposite directions and partially canceled each other.
Thus, the similarity in heat transfer coefficients for
cooling conditions with the same cocurrent flow was not

suprising.

Similarities between heat transfer coefficients below
the frostline for cocurrent and combination cooling flows,
were not expected to continue above this region, as film
temperatures varied markedly with cooling condition. At
large distances from the die, changes in surface temperature
accounted for all the difference in heat transfer
coefficients by affecting the (Ts-Ta) and (dTs/dz) terms in
Equation 6. The physical limitations imposed by the
collecting shroud, cooling tower supports, collapsing frame
and measurement positioning mechanism allowed measurements
at only four positions above the die. Specific values of
the temperature derivative are thus uncertain with only four
data points but increasing or decreasing cooling gradients
were discernable.

In Figure 6.29, heat transfer coefficients are plotted
against distance from the die for cocurrent cooling
conditions. Cases 2 and 9 are shown along with the standard
cocurrent cooling cases 1 and 8. Below the frostline
region, each pair of cooling conditions that have the same
cocurrent flow rate, that is cases 1 and 2 and cases 8 and
9, follow the same heat transfer coefficient curves.
However, above the frostline, at the first two positions,
where measurements with the cylindrical shroud present were
made, heat transfer coefficients calculated under cooling
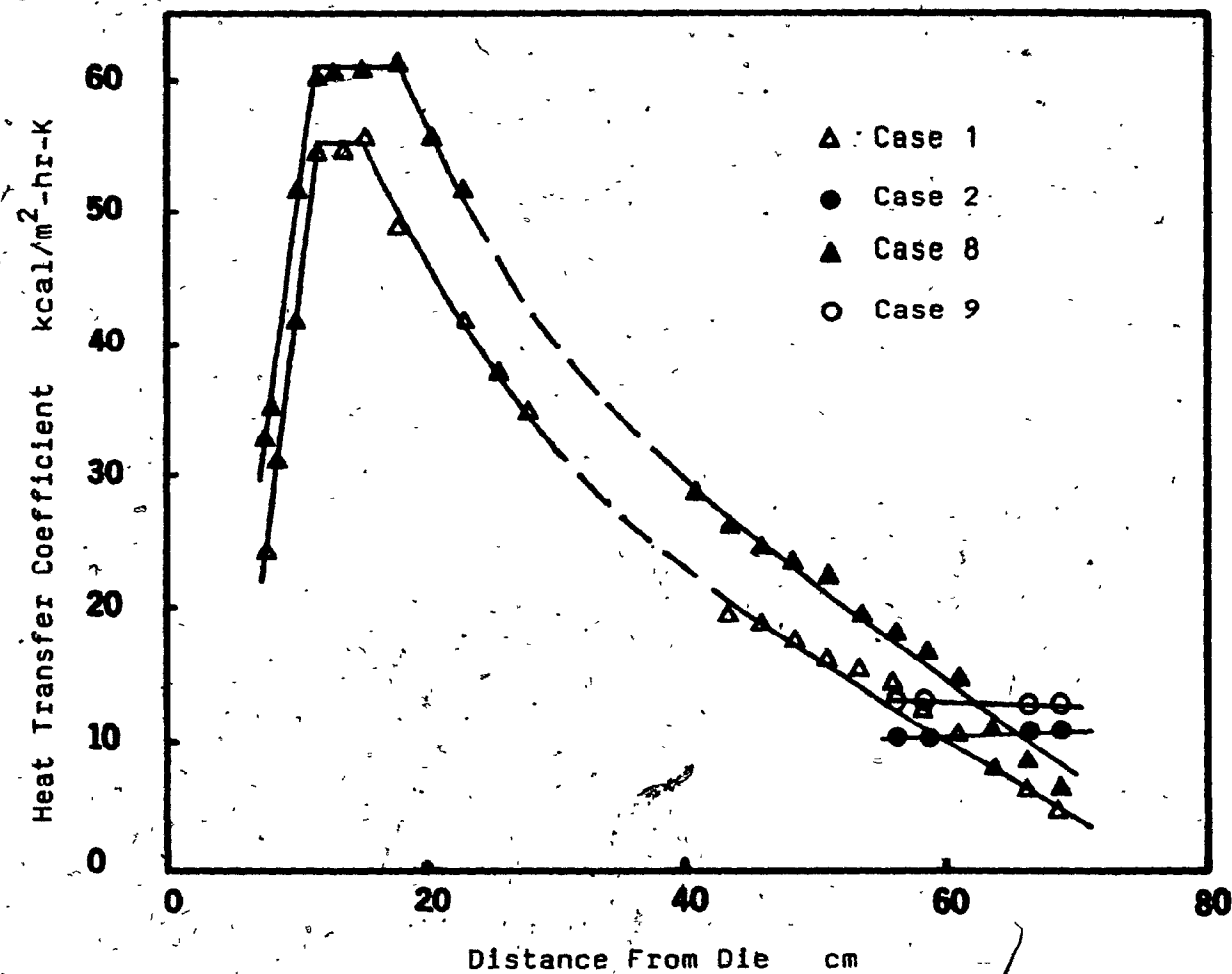
FIGURE 6.29   Plot of Heat Transfer Coefficient
Versus Distance From Die Under Cocurrent
Cooling Conditions of Cases 1, 2, 8 and 9

conditions of cases 2 and 9 were markedly lower than those of cases 1 and 8. At the highest positions above the die this trend was reversed, as heat transfer coefficients determined with the cylindrical shroud present were greater than those for standard cocurrent cooling conditions. The first two positions above the frostline were still within the cylinder, and surface temperatures (Figure 6.4, Section 6.2) were 11 $^\circ$C hotter in cases 2 and 9 than in the corresponding standard cocurrent cooling conditions of cases 1 and 8. In Section 6.2 this was attributed to the inability of cooling air to entrain ambient air from the surroundings with the cylinder, wrapped in plastic, present. Furthermore, the higher surface temperatures in cases 2 and 9 suggest that the cooling curves gradually slope downward from the frostline to these positions, 22 and 23 inches from the die. The gradual slopes, less than in corresponding cases 1 and 8, resulted in lower heat transfer coefficients in cases 2 and 9, even though the term (Ts-Ta) was slightly larger under the latter cooling conditions. Calculations of heat transfer coefficient are broken down into percentage changes of individual terms at positions 22 and 27 inches above the die, and are given in Appendix D7 for cases 1, 2, 8 and 9.

The measurement positions 26 and 27 inches from the die were above the frostline and also above the cylinder. The

surface temperatures at these positions were still greater for the cooling conditions of cases 2 and 9 than for cases 1 and 8, but the temperature difference had narrowed to $8 °C$, as the cocurrent air emerging from the cylinder was now able to entrain surrounding air. Between 22 and 27 inches above the die, the film temperature fell 5 and $6 °C$ in cases 1 and 8, while over this same interval in cases 2 and 9 the temperature declined 9 and $10 °C$. All this suggests that the cooling curve slopes are greater at these third and forth measurement positions above the frostline in cases 2 and 9 than in cases 1 and 8. Larger cooling curve gradients were reflected in larger heat transfer coefficients over this region.

Heat transfer coefficients over the regions where dependent variables were measured are plotted in Figure 6.30 for all cooling conditions. Below the frostline, heat transfer coefficient curves for the same cocurrent flow rate are similar. However, over the region of film bubble 22 to 27 inches from the die, where dependent variables were measured in countercurrent flow, heat transfer coefficients determined in cases 4 through 7 and cases 11 through 14 were larger than heat transfer coefficients calculated for standard cocurrent cooling cases 1 and 8. Furthermore, in all but one of the combination cooling flows shown in Figure 6.30, heat transfer coefficients increased or decreased only
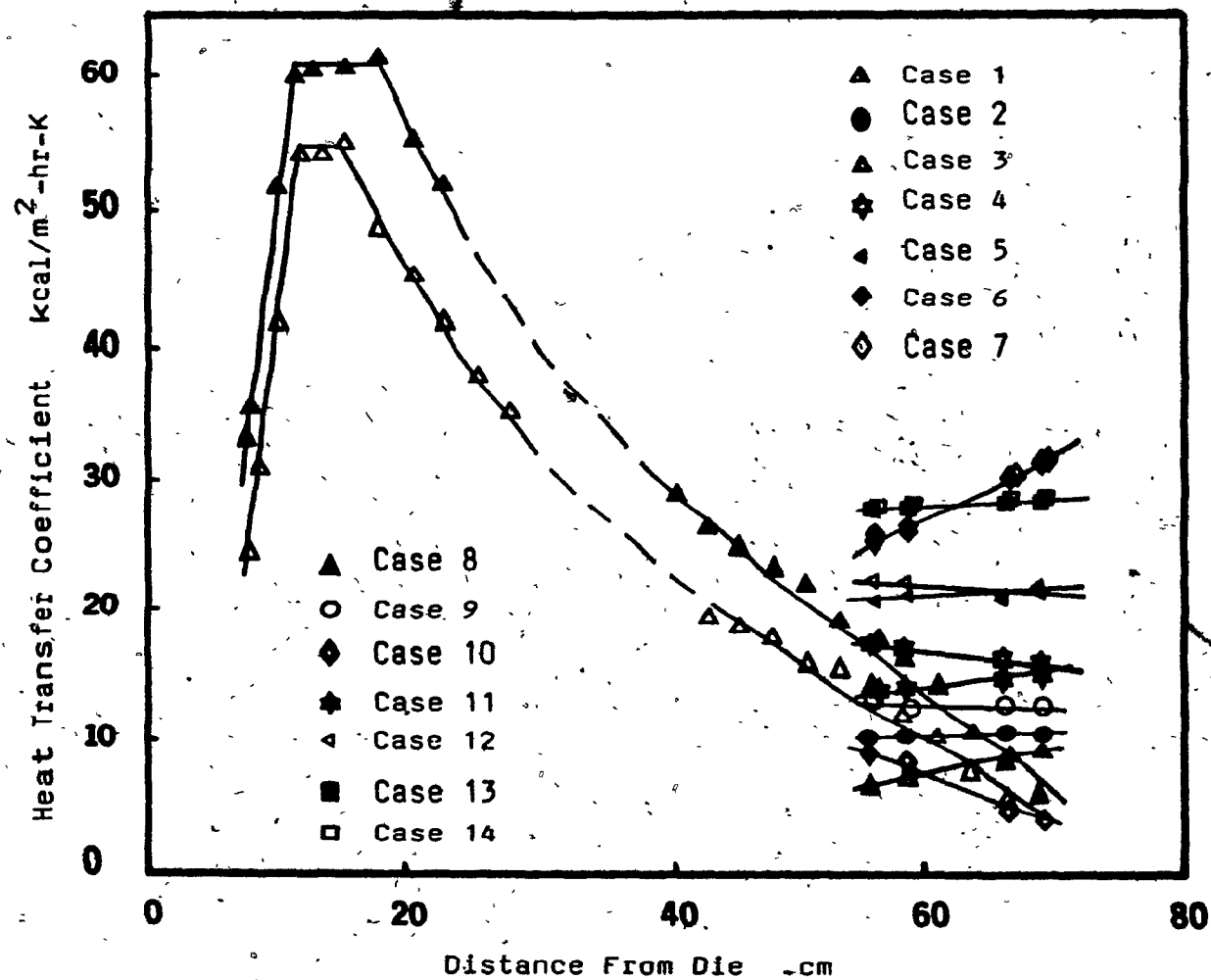
FIGURE 6.30   Plot of Heat Transfer Coefficient Versus
Distance From Die Under All Cooling Conditions
Conditions

-203-

marginally over this region, while heat transfer coefficients calculated for cocurrent cooling flows declined markedly in this same area. These observations were attributed to the low surface temperatures and moderate temperature gradients for countercurrent cooling conditions. Surface temperatures in cases 1 and 8 were generally higher and declined more slowly beyond 22 inches from the die than those in countercurrent cooling flows. The combination cooling of case 10 was an exception. For this cooling condition the same amount of air was applied cocurrently at the base of the film bubble as was withdrawn by the collecting plenum. Thus, above the plenum very little cooling occurred. This was reflected in high film temperatures and gradual decreases in temperature gradients. Consequently, heat transfer coefficients calculated for case 10 cooling conditions were smaller to those determined in cocurrent cooling cases 8 and 9 and decreased with increasing distance from die.

Heat transfer coefficients calculated for combination cooling conditions with the same countercurrent air flow but different cocurrent cooling flows, that is cases 3 and 10, 4 and 11, 5 and 12, 6 and 13, and 7 and 14, were somewhat larger for the stronger cocurrent cooling flows at 22 and 23 inches above the die than the coefficients calculated for the same countercurrent flow but with less cocurrent

cooling. This situation was reversed at positions 26 and 27 inches from the die. There, larger heat transfer coefficients were calculated for cooling conditions with smaller cocurrent flows. Surface temperatures measured at the first positions above the collecting plenum in cases 3 through 7, were substantially higher than in cases 10 through 14, which have the same countercurrent air flow but a larger cocurrent component. For example, under the weakest cooling conditions, cases 3 and 4, the film temperatures were within $5°C$ of the frostline, while their countercurrent counterparts, cases 10 and 11, were 10 to 15 $°C$ below this value. The combination of markedly higher surface temperatures and somewhat smaller temperature derivatives, in cases 3 through 7, leads to lower heat transfer coefficients than in corresponding cases 10 through 14. At 26 and 27 inches from the die, the drop in film temperature in cases 3 through 7 was greater than for the cooling conditions of cases 10 through 14, although the absolute surface temperature was still higher in the cases with the smaller cocurrent air flow. This suggests that the cooling curves for cases 3 through 7 are declining more rapidly than those in cases 10 through 14 and this leads to greater heat transfer coefficients in the former than in the latter cooling cases, at the furthest measurement positions from the die.

6.6.4 Correlations

Heat transfer coefficients and Nusselt Numbers can be calculated from established equations of heat transfer. The general equation is:

$$Nu = C' Re^O Pr^q Gr^s$$

which can be reduced for this problem to:

$$Nu = C Re^p$$

where Nu is local Nusselt Number, Re local Reynolds Number and C and p are constants. Menges (27) has shown that Nusselt Numbers and heat transfer coefficients calculated for flow along a cylinder, for plate flow, for pipe flow and for flow in a concentric ring slot are not the same as values calculated from a heat balance on a small area of film bubble. Similarly, heat transfer coefficients calculated from empirical correlations of cylindrical and planar wall jets (45, 46) were not found to be equivalent to heat transfer coefficients calculated directly from Equation 6. For this reason, heat transfer coefficients were correlated with position and air velocity, and a relationship was established between Nusselt and Reynolds

Numbers. In each correlation, no one relationship was found to be valid over the entire bubble length; rather several relationships were necessary.

From Figure 6.30 there was a linear relationship between the heat transfer coefficient and distance from the die below the point of maximum heat transfer coefficient, that is, below 4.5 inches from the die. Furthermore, heat transfer coefficients were mostly constant over a broad maximum peak, roughly 4.5 to 6 inches from the die in cases 1 through 7 and from 4.5 to 7 inches in cases 8 through 14. These relationships are summarized in Table 6.4. Beyond the point of maximum heat transfer coefficient in Figure 6.30 h declines nonlinearly with increasing distance from the die. However, when the heat transfer coefficient was plotted versus position on a semi-logarithmic scale, as in Figure 6.28, for cases 1 and 8 cooling conditions, h declined linearly from the plateau of maximum heat transfer coefficient to a position roughly 23 inches from the die, and then declined more steeply through the final measurement positions. The change in slope at 23 inches and the steeper decline thereafter correspond to the temperature profile 'flattening out' at large distances from the die. Relationships over these regions between heat transfer coefficient and position for standard cocurrent cooling

TABLE 6.4 Correlations of Heat Transfer Coefficient with Distance From Die
Under Cooling Conditions of Cases 1 and 8

Distance From Die (z = cm)	Heat Transfer Coefficient Correlations (h = kcal/hr-m^2-K)			
	Case 1		Case 8	
$z \leq 11.4$	$h = (19.1)z - 33.1$	(a)	$h = (19.1)z - 25.0$	(a)
$11.4 \leq z \leq 16.5$	$h = 54.8$	(a)	$h = 60.8$	(a)
$16.5 \leq z \leq 60.0$	$h = (86.2)10^{(0.036)z}$	(b)	$h = (108)10^{(0.036)z}$	(b)
$60.0 \leq z$	$h = (8000)10^{(-0.012)z}$	(b)	$h = (10900)10^{(-0.12)z}$	(b)

(a) - Determined from Figure 6.30

(b) - Determined from a semi-logarithmic scale plot of heat transfer coefficient
versus distance from die in Figure 6.28

conditions are listed in Table 6.4.

Under countercurrent cooling conditions, heat transfer coefficients were calculated only over the region 22 to 27 inches from the die. In Figure 6.30, these values were plotted against distance from die and straight lines were drawn through a set of four points for each cooling condition. The equations of these lines were determined and are listed in Table 6.5. In cases 3 through 7 the slope of heat transfer coefficient versus position from die was positive and increased with greater contercurrent flow, corresponding to a sharply decreasing cooling curve over this region. Under the cooling conditions of cases 10 through 14 this slope was initially negative and became less negative with increasing countercurrent cooling. In cases 13 and 14 a slightly positive slope was recorded. This behavior was attributed to only moderate surface temperature gradients over this region. Heat transfer coefficients for standard cocurrent cooling cases 1 and 8 declined sharply from 22 to 27 inches above the die as the temperature profile 'leveled or flattened out' with increasing distance from the die.

Air velocity is an indication of cooling conditions, and changes in cooling conditions dramatically affect the heat transfer coefficient. Correlations between cooling air

-210-

TABLE 6.5 Correlations of Heat Transfer Coefficient with
Position Over the 56 to 69 cm Interval From the
Die Under All Cooling Conditions

Cooling Condition	Heat Transfer Coefficient Correlation (kcal/m^2-hr-K)
Case 1	$h = -2.0z + 59.0$
Case 2	$h = 0.11z + 8.00$
Case 3	$h = 0.46z - 3.07$
Case 4	$h = 0.54z + 1.94$
Case 5	$h = 0.20z + 16.6$
Case 6	$h = 1.3z - 2.63$
Case 7	$h = 1.4z - 4.99$
Case 8	$h = -2.5z + 73.0$
Case 9	$h = -0.14z + 16.6$
Case 10	$h = -0.58z + 21.6$
Case 11	$h = -0.29z + 23.5$
Case 12	$h = -0.26z + 28.2$
Case 13	$h = 0.16z + 23.9$
Case 14	$h = 0.16z + 24.4$

velocity and heat transfer coefficient demonstrate this relationship. Local heat transfer coefficients are plotted against local air velocities in Figure 6.31, for the cooling conditions of cases 1 and 8. Air velocities measured at the closest radial position, that is 0.5 inches from the bubble surface, were used as reference velocities. Tables of heat transfer coefficient, air velocity and position above the die are given in Appendix D7. In Figure 6.31, heat transfer coefficients can be seen to reach maximum values over the 6 to 8 m/s range in case 8 and 6 to 7 m/s range in case 1. This broad peak corresponds to 4.5 to 7 inches and 4.5 to 6 inches above the die in cases 8 and 1. Closer to the die, heat transfer coefficients declined roughly linearly with increasing air velocities. Similarly, beyond the points of maximum value, heat transfer coefficients declined linearly with decreasing air velocities. At air velocities less than 2 m/s or more than 23 inches from the die, the decline of heat transfer coefficients was steepest. Over this final region, heat transfer coefficients fell along the same path for the two different cooling conditions. In Figure 6.31 as in Figure 6.28, four distinctive linear heat transfer coefficient regions were evident. Equations describing the relationship between air velocity and heat transfer coefficient are given in Table 6.6. Included in Table 6.6 are correlations of heat transfer coefficient and air
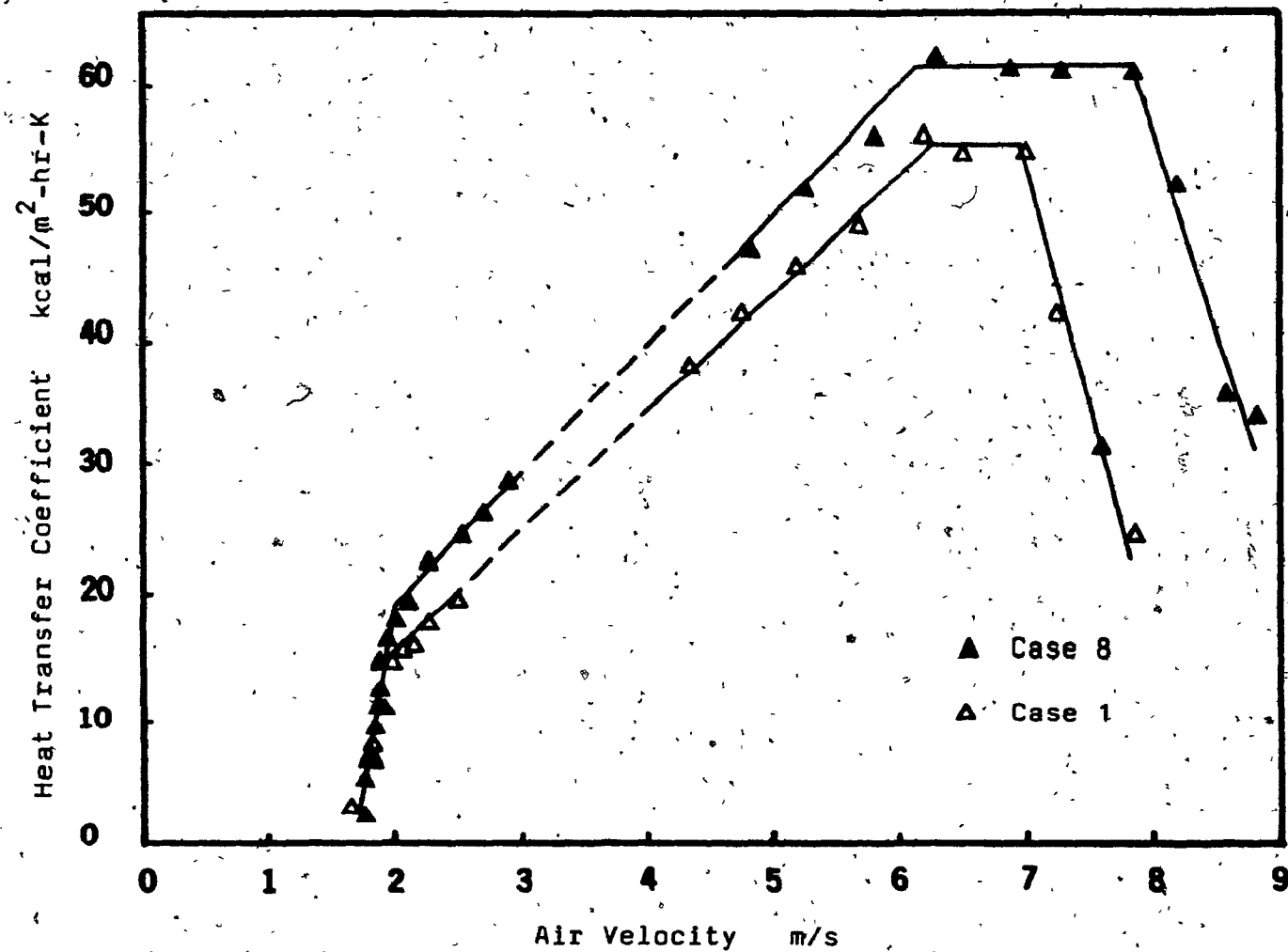
FIGURE 6.31   Plot of Heat Transfer Coefficient
Versus Air Velocity Measured 1.3 cm
From the Film Bubble Under Standard
Cocurrent Cooling Conditions of
Cases 1 and 8

TABLE 6.6 Correlations of Heat Transfer Coefficient with Cooling Air Velocity
Under Cooling Conditions of Cases 1 and 8

Velocity Range $(U = m/s)$	Heat Transfer Coefficient Correlations ($h = kcal/hr\text{-}m^2\text{-}K$)		
	Case 1	Case 8	Cases 1 and 8
$7.1 \leq U$	$h = (-37.7)U + 317$ (a)	$h = (-30.3)U + 298$ (a)	
	$h = (3.79 \times 10^7)U^{-6.94}$ (b)	$h = (2.52 \times 10^8)U^{-7.39}$ (b)	
$6.3 \leq U \leq 7.1$	$h = 54.6$ (a,b)	$h = 60.6$ (a,b)	
$2.0 \leq U \leq 6.3$	$h = (9.87)U - 5.86$ (a)	$h = (10.0)U - 0.5$ (a)	$h = (8.15)U^{1.09}$ (b)
	$h = (6.87)U^{1.15}$ (b)	$h = (8.51)U^{1.09}$ (b)	
$U \leq 2.0$	$h = (54.4)U - 89.81$ (a)	$h = (54.4)U - 89.81$ (a)	$h = (4.46 \times 10^{-3})U^{12.52}$ (b)
	$h = (4.46 \times 10^{-3})U^{12.52}$ (b)	$h = (4.46 \times 10^{-3})U^{12.52}$ (b)	

(a) - Determined from Figure 6.31

(b) - Determined from Figure 6.32

velocity determined from a double logarithmic plot of these two variables. This graph of heat transfer coefficient versus cooling air velocity, plotted on a double logarithmic scale, is shown in Figure 6.32. Over the velocity range 2 to 6.3 m/s or roughly from 6 to 22 inches from the die, one relationship was used to describe heat transfer coefficients for both cases 1 and 8 cooling conditions, although values differed by as much as ten percent from this extended correlation. At velocities less than 2 m/s one relationship satisfactorily described heat transfer coefficients calculated for both cooling conditions.

Both Menges (27) and White (26) have presented a single correlation of heat transfer coefficient above the frostline for maximum air velocities greater than 2 m/s, for several cooling conditions. Menges (27) reports correlations of :

$$h = 3.3 \ (U_{max})^{1.5}$$

and for a somewhat different set of operating conditions:

$$h = 3.04 \ (U_{max})^{1.3}$$

However in both cases, local heat transfer coefficients varied by as much as 18% from these multiple cooling condition correlations. White (26) reports a correlation
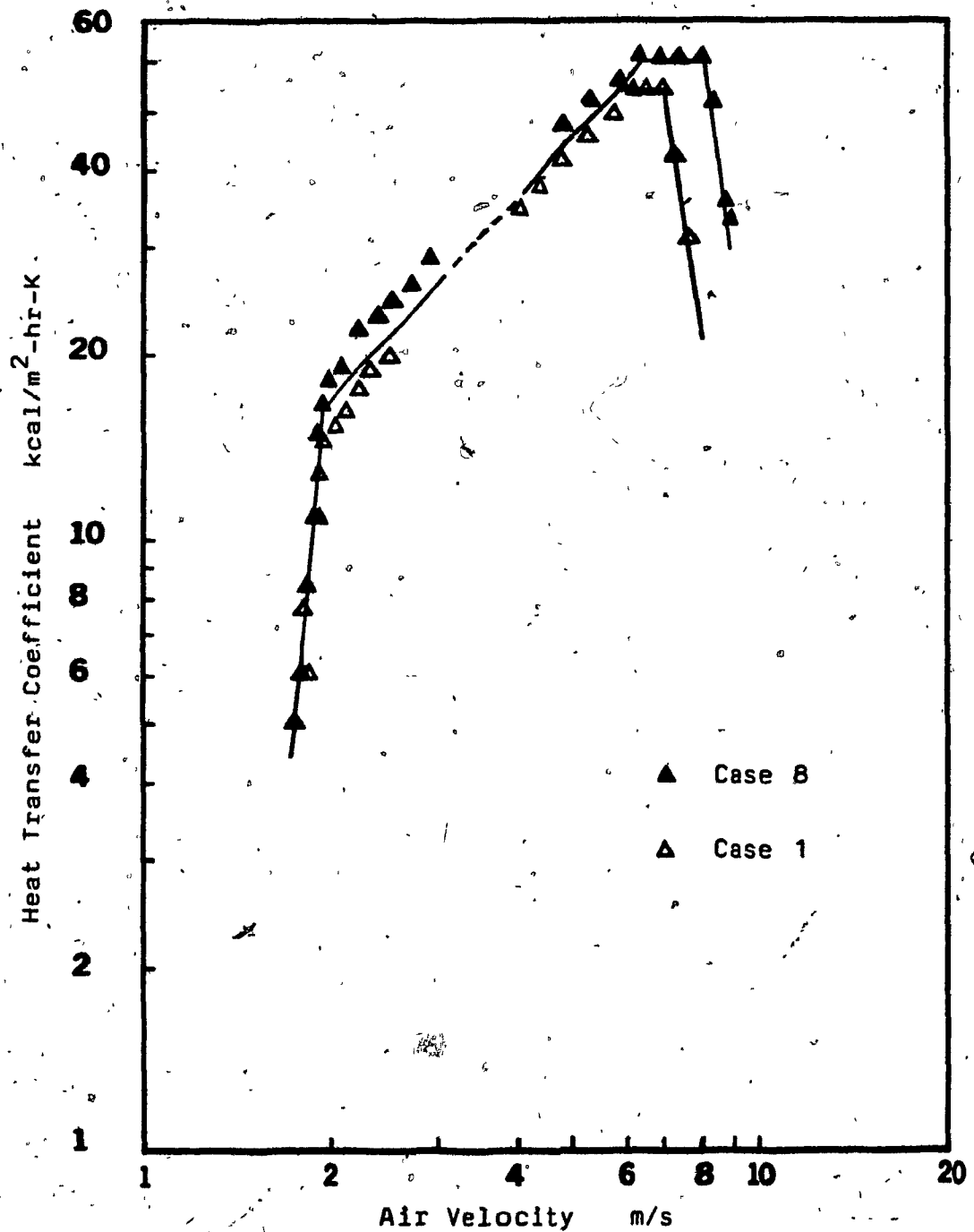
FIGURE 6.32 Double Logarithmic Scale Plot of Heat Transfer Coefficient Versus Air Velocity. Measured 1.3cm From the Film Bubble Under Cocurrent Cooling Conditions of Cases 1 and 8

applicable over the entire range of heat transfer coefficient from its maximum value to its mimimum, which corresponds to cooling velocities of roughly 6 to 2 m/s. However, in the region between the point of maximum heat transfer coefficient and the frostline, local heat transfer coefficients varied markedly with cooling conditions. All this suggests that several correlations are necessary to describe the relationship between heat transfer coefficient and air velocity along the length of the film bubble and that these correlations are valid only for a given set of operating conditions and only over a limited range of cooling conditions.

Heat transfer coefficients for countercurrent cooling conditions were not correlated with air velocity, becauase the cylindrical shroud blocked portions of the bubble from air velocity measurements. Above the collecting plenum but within the cylindrical shroud (roughly 23 inches from the die) the air speed was 5 m/s at 0.5 inches from the bubble surface. However, at 29 inches from the die, which is above the cylindrical shroud and was the next available measurement position, the air velocity parallel to the bubble was zero. The lack of measurements over this region made a good approximation of air velocity impossible. Furthermore, for cocurrent cooling, air velocities at radial

positions 0.5 inches from the bubble were used as reference
velocities and approximated the maximum local velocity.
However, at 23 inches from the die for countercurrent
cooling, the air speed one half inch from the bubble was the
lowest for any radial position. Thus, even when
countercurrent velocities can be measured, a problem arises
as to which air velocity is to be used in a correlation of
the heat transfer coefficient.

The local heat transfer coefficient can be incorporated
into the Nusselt Number, the local air velocity into the
Reynolds Number and a relationship between the two
dimensionless numbers determined. The Nusselt Number is
defined by:

$$Nu = \frac{h' L}{k_{air}}$$

and Reynolds Number is:

$$Re = \frac{L\, U_{r=\frac{1}{2}}}{\nu_{air}}$$

where k_{air} is the thermal conductivity of air, ν_{air}, the
kinematic viscosity of air, $U(r=1/2)$ refers to the local
cooling air velocity measured 0.5 inches from the bubble
surface, and L was taken as the distance from the maximum

local heat transfer coefficient to the position of measurement. Under the cooling conditions of case 1, the initial point, L=0, was 6 inches from the die, and in case 8 L=0 corresponded to a point 7 inches above the die. Local Nusselt and Reynolds Numbers are listed in Appendix D7 for the cooling conditions of cases 1 and 8. These values are plotted in Figure 6.33 and on a double logarithmic scale in Figure 6.34. Reynolds Number increased monotonically with increasing distance from position of maximum local heat transfer coefficient. Over the Reynolds Number range from 200 to 1200, Nusselt number increased linearly, as L increased more than h was decreasing. Above a Reynolds Number of 1200, or roughly 21 inches from the die, the Nusselt Number decreased linearly. The region of falling Nusselt Number corresponded to the temperature profile 'flattening out'. In Table 6.7 correlations between Nusselt and Reylnolds Numbers determined from both Figures 6.33 and 6.34 are given over the applicable Reynolds Number range. An 'average' or 'median' correlation is also given over the Reynolds Number range of 200 to 1200, which encompasses both cooling conditions. This latter correlation, obtained from a log-log plot of Nusselt versus Reynolds Number, is in the form typically used in the literature (26,27) for a given set of operating conditions.
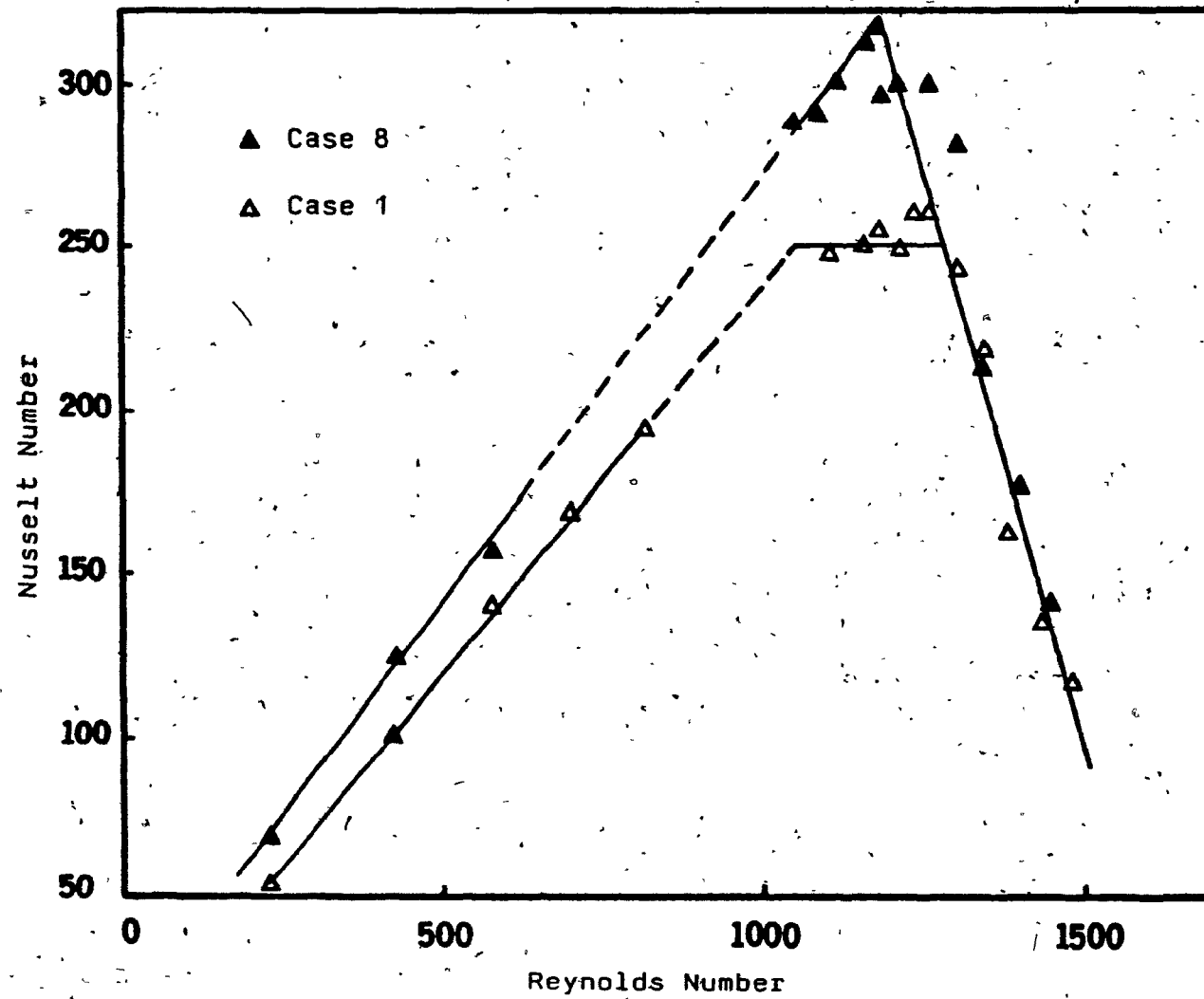
FIGURE 6.33 Plot of Local Nusselt Number Versus
Local Reynolds Number Under Standard
Cocurrent Cooling Conditions of
Cases 1 and 8
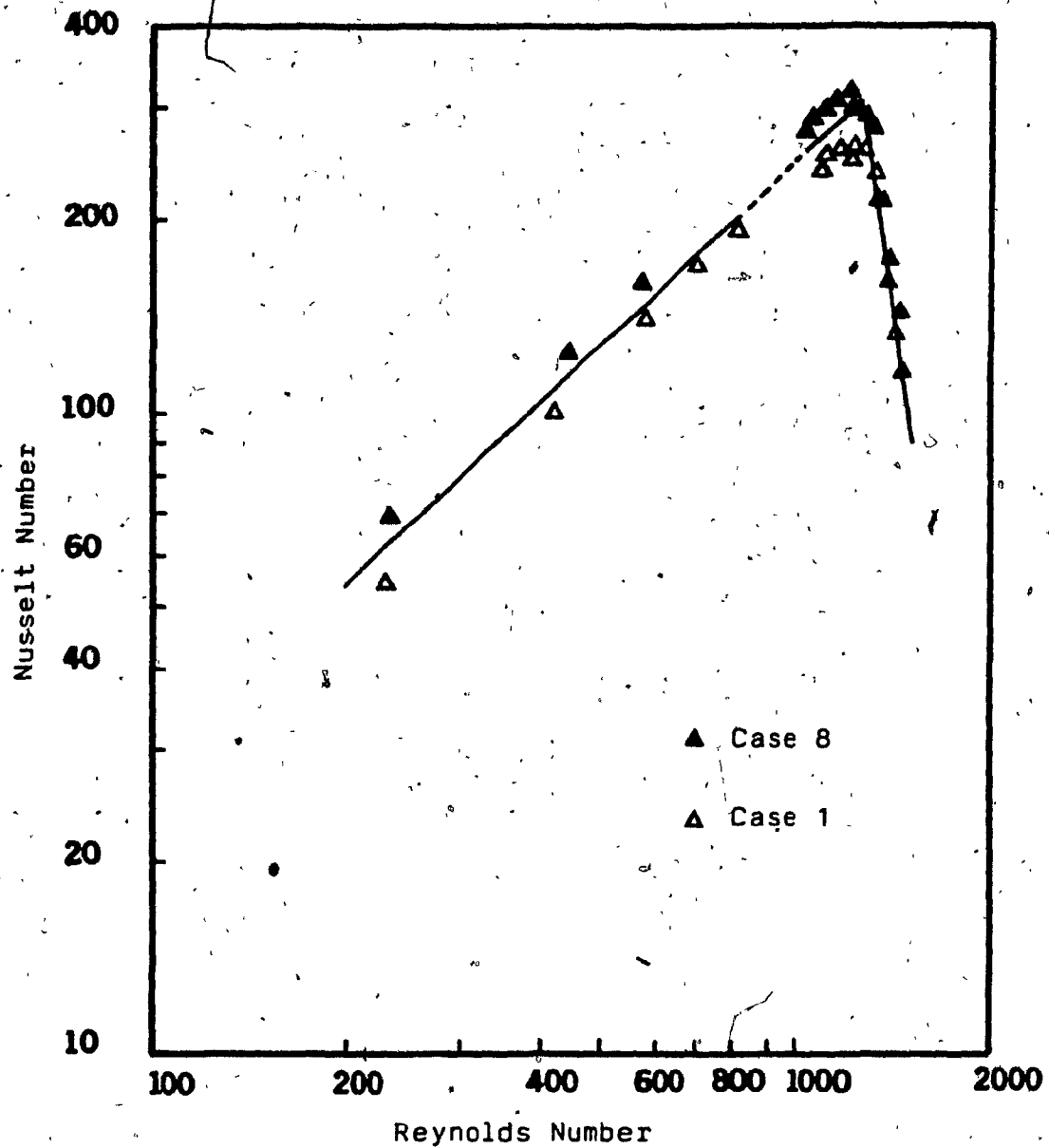
FIGURE 6.34   Double Logarithmic Scale Plot of Local
Nusselt Number Versus Local Reynolds
Number Under Standard Cocurrent Cooling
Conditions of Cases 1 and 8

TABLE 6.7 Correlations of Nusselt Number with Reynolds Number
Under Cooling Conditions of Cases 1 and 8

Cooling Condition	Reynolds Number Range $(RE = LU(r = 1/2)/\nu_{air}$	Nusselt Number Correlation $(Nu = Lh/k_{air})$
Case 1	$Re < 1025$	$Nu = (0.225)Re + 10.75$ (a)
		$Nu = (0.200)Re^{1.03}$ (b)
	$1025 < Re < 1250$	$Nu = 250.4$ (a,b)
	$1250 < Re$	$Nu = (-1.39)Re + 2070$ (a)
		$Nu = (3.4 \times 10^{-8})Re^{3.07}$ (b)
Case 8	$Re < 1200$	$Nu = (0.252)Re + 10.48$ (a)
		$Nu = (0.278)Re^{1.01}$ (b)
	$1200 < Re$	$Nu = (-1.39)Re + 2070$
		$Nu = (3.4 \times 10^{-8})Re^{3.07}$ (b)
Cases 1 and 8	$Re < 1200$	$Nu = (0.251)Re + 13.79$ (a)
		$Nu = (0.228)Re^{1.02}$ (b)
	$1200 < Re$	$Nu = (-1.39)Re + 2070$ (a)
		$Nu = (3.4 \times 10^{-8})Re^{3.07}$ (b)

(a) - Determined from Figure 6.33
(b) - Determined from Figure 6.34

6.6.5 Crystallinity

In film temperature measurements along the length of the bubble, a plateau corresponding to crystallization occurred. The variation of crystallinity with position in this region may be estimated using Equation 6 and heat transfer coefficients calculated as stated in Section 6.6.3. Over this plateau region Equation 6 can be rearranged to yield:

$$\frac{dX_c}{dz} = \frac{\Pi D [h (T_s - T_c) + e K (T_s^4 - T_a^4)]}{\dot{m} H_c}$$

where dX_c/dz is the change in fraction of crystallinity with respect to distance from the die. Heat transfer coefficients were obtained from Figure 6.27 (Section 6.6.3) over the frostline region and H_c, the heat of crystallization, was determined for a quiescently cooled, unoriented film sample by differential scanning calorimetry (Section 6.6.2). The remaining variables, surface temperature, T_s, diameter, D, and emissivity, e, were obtained from the dependent variable measurements of Sections 6.2, 6.3, and 6.6.1. Changes of crystallinity with position over the frostline region are listed at distances above the die in Appendix D7 for the cooling conditions of

cases 1 and 8. Crystallinity calculations for these standard cocurrent cooling conditions were assumed to approximate fractions of crystallinity determined in combination cooling systems using the same cocurrent flow. The presence of the cylindrical shroud in countercurrent cooling blocked portions of film bubble from dependent variable measurement and prevented determination of frostline length.

The local rate of crystallization as a function of distance from die and position of the frostline region in cases 1 and 8 allowed fractions of crystallinity to be graphically determined. In Figure 6.35 percent crystallinity is plotted versus distance from die over the frostline or plateau region. It was assumed that crystallization started at the frostline, that is, the molten portion of film bubble was predominantly amorphous. This corresponds to an assumption of zero percent crystallinity at the onset of the plateau region in Figure 6.35. At the end of this region, crystallinity was determined to be 24 and 28 percent for case 1 and case 8 cooling conditions. The crystallinity of the film product was 45 percent, as determined by density measurements taken two weeks after the film was blown*. Thus, the crystallinity at the end of the frostline region corresponded to roughly 60 percent of the crystallinity
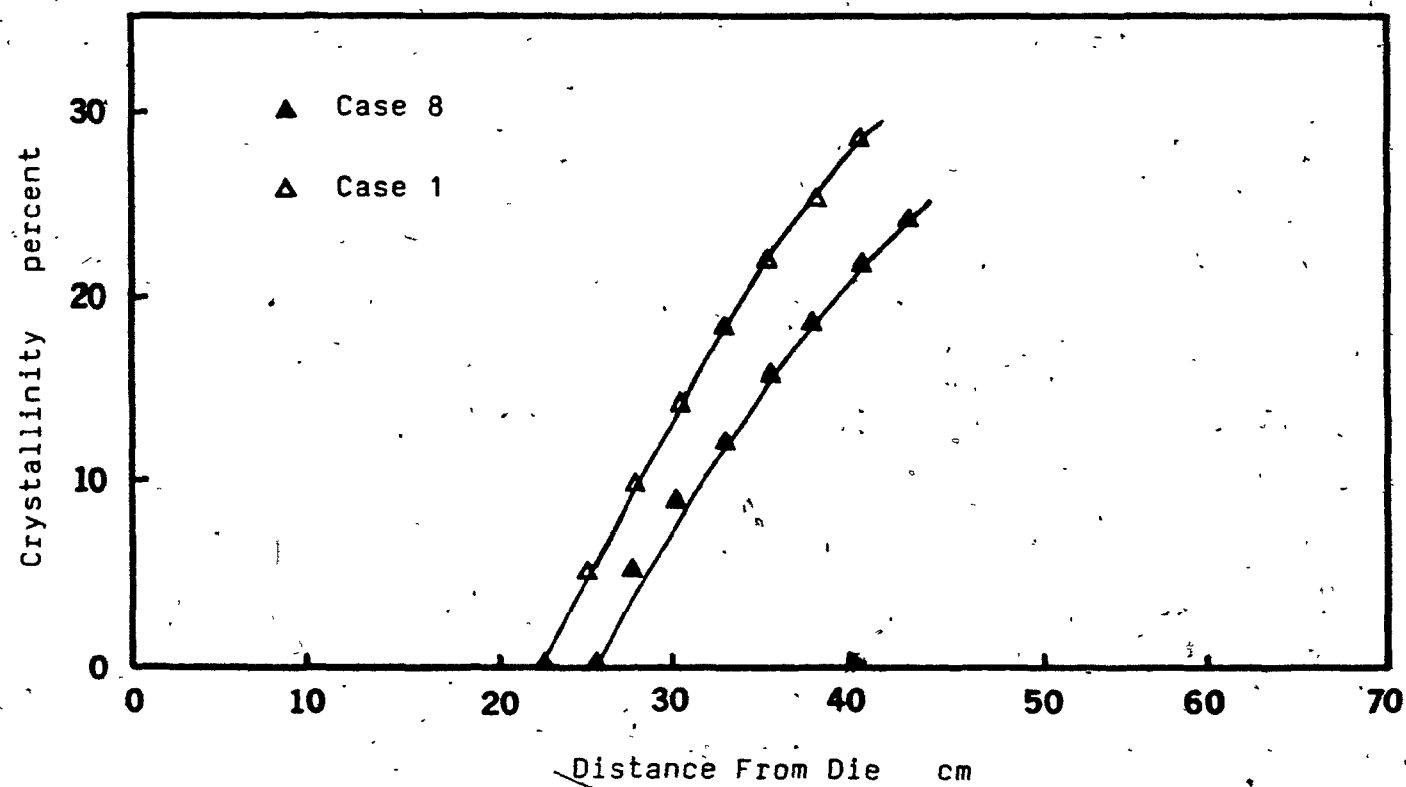
FIGURE 6.35   Plot of Percnet Crystallinity Versus
Distance From Die Over the Frostline Region

found in the final film.

In Figure 6.35, fractions of crystallinity were larger for the greater cooling flow. A similar trend of increasing fraction of crystallinity in the frostline region with decreasing frostline height or equivalently greater cooling flows was reported by White (26). Under the strong cocurrent cooling conditions of case 8, the heat transfer coefficient term in Equation 6 was larger than in case 1 cooling conditions and contributed to large changes in crystallinity with position and ultimately greater fractions of crystallinity. Small decreases in diameter with increasing cooling only partially offset this behavior.

Increases in crystallinity with increasing cooling would certainly not be expected under quiescent cooling conditions (2). However, in blown film the deformation and stress experienced by the melt and the degree of orientation of the cooling polymer greatly affect cyrstallization (2,48,49).

* To determine crystallinity (volume basis) from density measurements, the definition:

$$X_c = \frac{\rho_s - \rho_{am}}{\rho_c - \rho_{am}}$$

was used, where ρ_{am} is the density of the 'amorphous phase', taken to be 0.856 g/cc (47), ρ_c, the density of the 'crystalline phase', 1.001 g/cc (47) and ρ_s, the sample density determined from density column measurements (ASTM Standard Test Method D1505).

Deformations in the molten region have been hypothesized to cause some preferential molecular chain alignment there, which would in turn greatly increase orientation and crystallinity at the frostline (50). Under strong cooling conditions the film bubble expands rapidly near the die and continues to be deformed throughout the neck region. This may serve to impart some molecular alignment in the neck region and lead to large crystallinity values. On the other hand, in weak cooling the bubble expands only just below the frostline. Thus, little preferential chain alignment is possible in the amorphous regions, and perhaps this results in less crystallinity at the frostline. Further discussions regarding crystallizaton under stress are given in Chapter 8.

6.6.6 Summary

Heat transfer coefficients were calculated using dependent variable values and a heat balance over an element of film, and crystallinity was estimated over the frostline region from these heat transfer coefficient calculations. Crystallinity increased along the frostline and was greater with stronger cooling conditions. Heat transfer coefficients below the frostline were similar for the cooling conditions of cases 1 through 7 and cases 8 through

14. However, above the frostline heat transfer coefficients
for combination cooling were greater than those determined
in standard cocurrent cooling and over this region heat
transfer coefficients increased with increasing
countercurrent flow rate.

The heat transfer coefficient was correlated with
distance from die under cooling conditions of cases 1 and 8.
In each cooling flow, four relationships were required to
determine the heat transfer coefficient along the length of
the bubble. Correlations of heat transfer coefficient with
position were also determined for countercurrent cooling
conditions over the 22 to 27 inch interval from the die.
Each correlation was affected by the magnitude of the
countercurrent cooling flow.

Air velocities near the film bubble were correlated
with heat transfer coefficient under standard cocurrent
cooling conditions. Over a 2 to 6 m/s range, one
relationship was used to determine heat transfer coefficient
for cooling conditions of both cases 1 and 8. Similar
methods are used in the literature to express heat transfer
coefficients over a range of cooling conditions.
Furthermore, Nusselt Number was correlated with Reynolds
Number above the point of maximum heat transfer coefficient.
Two relationships were found to express Nusselt Number along
the length of the bubble beyond this point.

The heat transfer coefficient correlations determined were only valid over the range of operating and cooling conditions used in this study. Thus, differences in blown film equipment and conditions of operation limited direct comparisons with heat transfer coefficient correlations presented in the literature.

Variations of heat transfer coefficient with position in mathematical models of the blown film process are non-existent; rather these models employ constant heat transfer coefficients over the entire bubble (28,36). For example, Wagner (28) used a value of 30 kcal/(m)2-hr-C for an overall heat transfer coefficient between die and nip rolls. Heat transfer coefficients in this work and other research (26,27) varied from 60 to 6 kcal/(m)2-hr-C or less within two feet from the die. These absolute values are, of course, dependent on equipment and specific conditions, but the large variation with distance was considered typical.

The heat transfer coefficient, which enters into the heat balance around a small element of film bubble, must be known to obtain the film temperature. Furthermore, the film temperature is also required to evaluate the rheological properties of the melt. This interaction of the heat transfer between film and cooling medium with the temperature dependent rheological properties of the melt is

a major complication in developing a complete' model of the
blown film process.

Chapter 7

Film Property Measurement

Film produced from a given resin by the blown film process may have very different final properties depending on the processing conditions used (4,27,50,51). In this study, all parameters were held constant with the exception of the cooling conditions. Cooling air volumetric flow rates varied from 100 to 300 cfm (0.055 to 0.15 m^3/min) and the manner in which air was used to quench the bubble also differed. Because of these different processing conditions, it was necessary to examine the film product and determine whether film properties were the same. Any advantages that might be realized by increased cooling conditions could be negated by a significant deterioration in film properties. For example, some dual lip air rings, which cool film more intensely than standard fan-type air rings and thus allow production increases on cooling limited blown film lines, have produced film with poor property balance (4) and thus unsuitable for many applications.

In this Chapter, the film product corresponding to each cooling condition was subjected to four film tests. The tests were chosen on the basis of ease of testing and access to the test equipment. The results of shrinkage, Elmendorf

tear, birefringence, and sonic velocity measurements were compared. Differences in property values between film cooled cocurrently and under combination air flow would indicate dissimilar film quality. Film test results are interpeted in terms of overall molecular orientation in Chapter 8.

7.1 Shrinkage

As polyethylene is cooled between the die and the frostline, it experiences machine direction drawing and hoop expansion that orient the molecular chains. A rapid transition from molten to solid state at the frostline 'freezes-in' this molecular anistropy, thus orienting the film. When an oriented polymer film sample is annealed just below its melting temperature, these 'frozen-in' stresses are released. The polyethylene chains relax and assume a random configuration. An overall reduction in film surface area accompanies this relaxation, and the amount of reduction reflects the degree of orientation in the film.

Thin circular film samples immersed in a bath, for a sufficient time to allow the 'frozen-in' stresses to be released, assume an elliptical shape due to the imbalance of orientation in the machine and transverse directions. In

each principal direction an unrestrained linear shrinkage can be calculated:

$$\text{Percent Unrestrained Shrinkage} = (\frac{D_i - D_f}{D_f}) 100$$

where D_i is the initial length of film sample and D_f the length of film sample in a principal direction after shrinkage.

7.1.1 Procedure

The shrinkage apparatus was made available by Union Carbide Canada Ltd. A schematic diagram of thus instrument is shown in Figure 7.1. The shallow aluminum cup, filled with an oil, holds the sample. The oil bath was maintained at a prescribed temperature by a rheostated band heater and routinely checked with a thermocouple.

(1) Eight samples, 2 inches in diameter, were cut with a punch from a flattened sheet of tubular film for each cooling condition. Samples were equidistant from each other and cut at the same position on the film bubble.

(2) Samples were marked to show the machine direction.

(3) The aluminum cup was filled with silicon oil to a depth of approximately 0.1 inch and maintained at 107°C + or − 1°C by a band heater.

(4) Samples were immersed in the oil bath for two
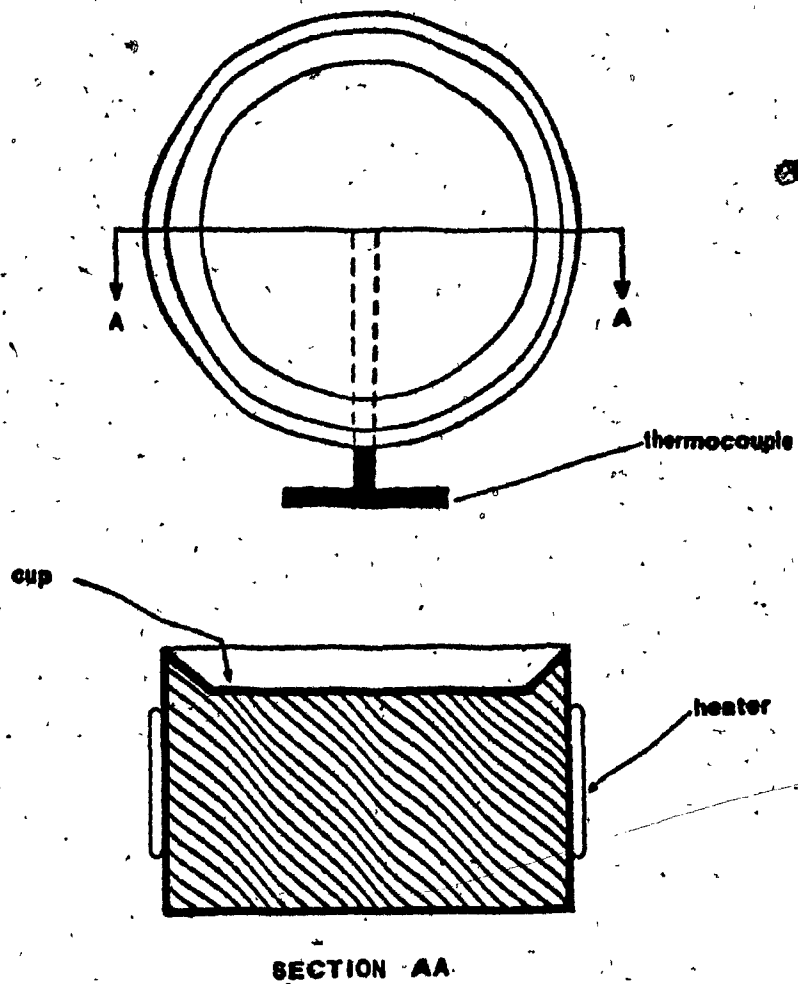
FIGURE 7.1 Schematic Diagram of Shrinkage Apparatus
(Reference 24)

minutes, then cooled in ambient air.

(5) The changes in linear dimensions in both machine and transverse directions were noted and the percent shrinkage calculated.

7.1.2 Results and Discussion

Average percent shrinkage in the machine and transverse directions is presented for each cooling conditon in Table 7.1. Shrinkage values for each sample are listed in Appendix G1. In Appendix E an error analysis is given.

Film shrinkage in the machine direction was similar under all cooling conditions and in the transverse direction under cooling conditions with the same cocurrent flow. However between the two 'families' or groups of results for cocurrent flow, shrinkage was somewhat greater in the transverse direction for cases 1 through 7 cooling conditions than for cases 8 through 14.

This trend in shrinkage measurements might be attributed to somewhat different bubble shapes in the neck region. Between die and frostline the film bubble under the larger cocurrent cooling flows of cases 8 through 14 expanded more gradually in the transverse direction than in cases 1 through 7 cooling conditions, where the transverse expansion was more abrupt and only occurred after substantial cooling (refer to Section 6.3). Deformations occurring just below the frostline region greatly influence

Table 7.1: Unrestrained Shrinkage.

Cooling Condition	Transverse Direction (%)	Machine Direction (%)	Transverse/Machine Ratio
Case 1	19	70	0.20
Case 2	20	66	0.30
Case 3	20	75	0.26
Case 4	18	73	0.25
Case 5	18	74	0.24
Case 6	19	71	0.27
Case 7	15	71	0.21
Case 8	11	71	0.15
Case 9	13	71	0.18
Case 10	14	75	0.19
Case 11	11	73	0.16
Case 12	15	72	0.19
Case 13	14	75	0.19
Case 14	13	73	0.18

final film orientation (52). Therefore, a pronounced bubble expansion near the frostline contributes to transverse orientation in the film. Furthermore, smaller blow up ratios were obtained for cases 8 through 14 than for cases 1 through 7. A smaller blow up ratio means less total stretching in the transverse direction. Thus, it seems reasonable that film cooled under the cooling conditions of cases 1 through 7 was slightly more oriented in the transverse direction than film produced with cases 8 through 14 cooling conditions, and this greater transverse orientation was reflected in a larger shrinkage.

7.2 Elmendorf Tear

The Elmendorf tear test determines the average force required to propagate tearing in a film sample. This force is measured by using a pendulum and deflecting pointer device. A photograph of this instrument is shown in Figure 7.2. Acted on by gravity, the pendulum swings through an arc, tearing the specimen starting from a precut slit. The specimen is held on one side by the pendulum and on the other side by a stationary clamp. The loss in energy of the pendulum is indicated by a pointer, the pointer scale reading being related to the force required to tear the

FIGURE 7.2 Photograph of Twing-Albert Elmendorf
Tearing Tester

specimen.

Due to orientation during processing, blown films usually show marked anistropy in their resistence to tear. Comparisons of this anistropy, by measurements of tear resistance in the machine and transverse directions, is used extensively in industry. Lindenmeyer and Lustig (51) have correlated tear strength with other mechanical properties and molecular orienation for high density polyethylene. However, ASTM Standard Test Method D1922 stresses caution in correlating film tearing data with other properties, as tear strength is not a well defined physical property and has little fundamental physical significance.

7.2.1 Procedure

Elmendorf tear tests were carried out at the Technical Center of Union Carbide Canada Ltd. A Thwing-Albert Elmendorf Tearing Tester (Thwing-Albert Instruments Co., Philadelphia, Pa.) was used. ASTM Standard Test Method D1922 was followed.

(1) Twelve samples, six in each principal direction, were cut with a punch from a flattened sheet of tubular film for each cooling condition. The geometry of the sample is shown in Figure 7.3. The six samples in the machine and transverse directions were equidistant from each other and cut at the same position on the bubble.

(2) The thickness of each sample was determined to the
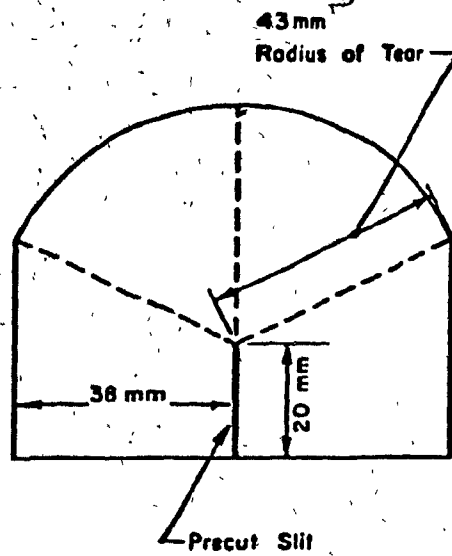
FIGURE 7.3 Constant Radius Test Specimen for
Elmendorf Tear Test

nearest 0.001 inch with a micrometer.

(3) With the pendulum at its raised station and the pointer at the zero mark of the scale, a pre-cut slit sample was placed between the clamps.

(4) The pendulum was rleased and the sample torn. As the pendulum completed its return swing it was caught without disturbing the pointer.

(5) The pointer value was noted and the tearing resistance, R, calculated:

$$R = S \, Cap \, / \, b$$

where S is the scale reading, Cap, the machine capacity and b, the sample thickness.

7.2.2 Results and Discussion

Average tear resistance measurements for each cooling condition are given in Table 7.2. Resistance to tear propagation values for each sample are listed in Appendix G2. An error analysis is given in Appendix E.

The ratio of the transverse to the machine machine direction tear resistance varies by as much as eleven percent depending on the cooling cases. However, there is no suggestion of a correlation between cooling air flow and resistance to tear over the range of cooling conditions used. Thus, each cooling case has similar tear resistance characteristics.

The maximum percent deviation of an individual sample from the average value was high, nearly fifteen percent in

Table 7.2: Elmendorf Tear Test

Cooling Condition	Transverse Direction (g/mil)	Machine Direction (g/mil)	Transverse/Machine Ratio
Case 1	224	161	1.39
Case 2	245	163	1.50
Case 3	231	157	1.48
Case 4	225	161	1.40
Case 5	219	149	1.47
Case 6	213	143	1.49
Case 7	210	152	1.37
Case 8	216	147	1.46
Case 9	226	167	1.35
Case 10	206	146	1.41
Case 11	220	152	1.45
Case 12	216	153	1.41
Case 13	235	169	1.39
Case 14	225	158	1.42

some cases. This may be attributed, in part, to samples not being cut from film parallel to a principal direction. It was observed that tears in a slightly different direction than the sample pre-cut slit (Figure 7.3) all resulted in higher values than those tears that followed the pre-cut slit.

7.3 Birefringence Measurements

Birefringence is an indication of the total molecular orientation in a sample. In uniaxially oriented samples, it is the difference between the principal refractive indices parallel and perpendicular to the direction of extension. The refractive index is a measure of the velocity of light in the medium and is a function of the polarizability of the molecular chains. As light enters an optically anisotropic sample, it splits along two mutually perpendicular paths and travels at different velocities. The two paths are recombined upon exiting the medium. Because of the different velocity along each path a phase difference occurs, which is measured. Division of the phase difference or retardation by the sample thickness yields the birefringence.

The velocity of light in a partially crystalline

material will depend on whether the light is travelling through an amorphous or crystalline region. Therefore, birefringence in polyethylene can be thought of as the sum of two distinct components. If all of the molecules are distributed randomly in a sample, the refractive index will be the same in all directions, and the difference between parallel and perpendicular components will be zero. Thus an unoriented sample has no birefringence. If the molecular chains are alligned perfectly parallel to the drawing direction, birefringence will be a combination of the ideal anistorpy of each region. Birefringence of samples stretched by processing lies between these extremes, depending on the extent of orientation imparted to the polymer by the process and the proportion of amorphous and crystalline phases present.

The assumption of a two phase model for semicrystalline polymers permits mathematical treatment of the contribution of each phase to the total orientation. A problem in applying this theory has been the difficulty in obtaining birefringence values of unoriented samples, which are required by the model and cannot be measured easily since the birefringnece of randomly oriented material is zero. In uniaxially extended isotatic polypropylene fibers, Samuels (53) has shown how sonic velocity, infrared dichroism and X-ray measurements can be used to calculate intrinsic

birefringences (birefringence of unoriented samples). These values were used in turn to determine contributions of crystalline and amorphous phases to total orientation. However, for biaxially stretched films, the theoretical treatment is considerably complicated by the additional deformation direction (54). In this work, birefringence measurements were interpreted qualitatively to give an indication of overall molecular orientation in blown film.

7.3.1 Procedure

A Reichert 'Zetopan-Pol' (West Germany) large polarization microscope was used with an Ehringhaus rotary quartz crystal compensator (Carl Zeiss Co., West Germany). A schematic of the principal components in this experimental setup are shown in Figure 7.4. Polarized light waves travel through the sample and then enter a compensator. After the compensator, the two retardation-free light waves pass through an analyzer to again produce plane polarized light.

(1) Ten samples, 1 x 2 cm, were cut out from a flattened sheet of tubular blown film for each cooling condition. Samples were equidistant from each other and cut at the same position on the film bubble.

(2) The thickness of each sample was measured with a micrometer to 0.0001 inch.

(3) The magnification on the Riechert microscope was
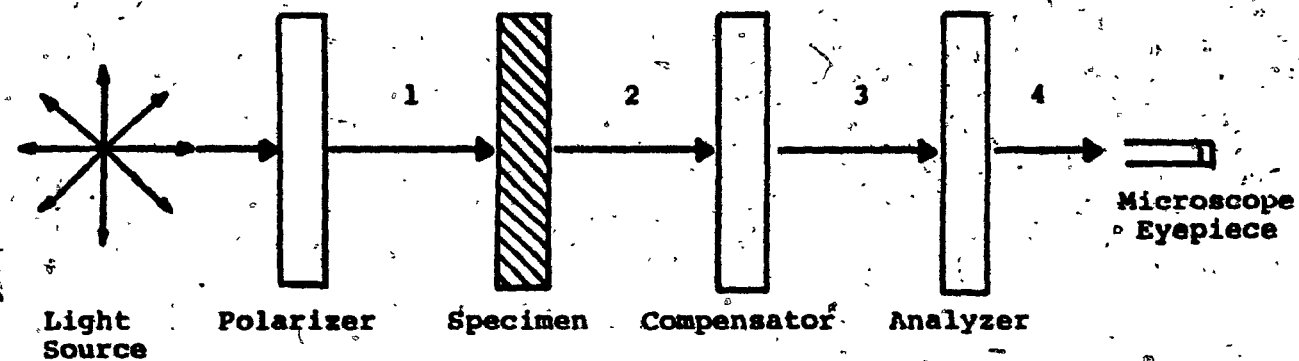
1. Plane-Polarized Light
2. Retardation Exhibiting Light
3. Retardation-Free Light
4. Plane-Polarized Light

FIGURE 7.4   Schematic Representation of the Set Up
Used for Measuring Birefringence

set at 10 x 5.6 = 56.

(4)   The polarizer and analyzer were set at right angles to each other

(5)   The sample was placed on the rotating stage of the microscope and viewed between cross polarizers.

(6)   The stage was rotated until maximum darkness was observed.

(7)   From a position of maximum darkness, the stage was rotated + or - 45 degrees, to maximum brightness.   The direction of rotation was determined by trial and error depending upon whether extinction (maximum darkness) was obtainable with the compensator.

(8)   The compensator was inserted in a SE - NW direction and adjusted to achieve extinction.   The angle of inclination between the quartz wedges in the compensator was measured in both clockwise and counterclockwise directions.

(9)   The measured angle was converted into a phase difference of light at the given inclination angle of the quartz wedge by use of a set of tables supplied by the manufacturer (55).

(10)   The total birefringence of the sample was obtained by dividing the phase difference by the thickness of the sample.

7.4 Sonic Velocity

Sonic velocity, like birefringence, is an indication of the total molecular orientation in a sample. Figure 7.5a is a schematic diagram of polymer chains oriented parallel to the stretch axis, while 7.5b shows the chains perpendicular to this axis. Simple physical considerations suggest that the sonic velocity in the stretch direction, z, will be
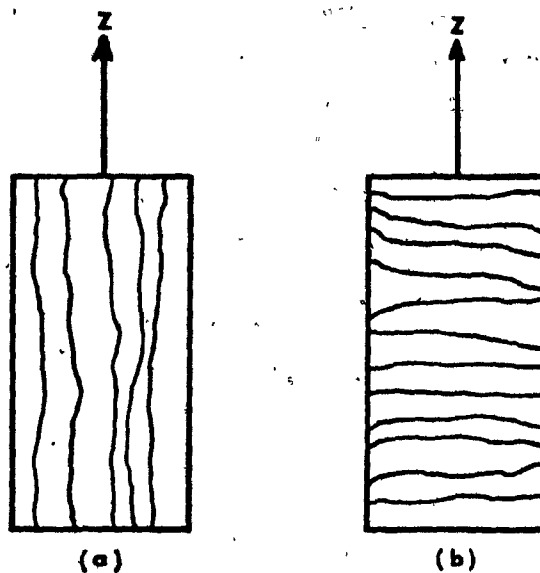
FIGURE 7.5   Schematic Representation of Molecular
              Chain Orientation in a Semi-Crystalline
              Polymer   (a) Perfect Parallel Orientaion
              (b) Perfect Perpendicular Orientation
              (Reference 56)

different for the two samples. In Figure 7.5a the mechanism of propagation occurs along the polymer chain (intramolecular bond stretching), while in Figure 7.5b the propagation occurs across the chains (intermolecular bond stretching). Based on these different mechanisms, theoretical calculations utilizing the force constants of bond stretching, have predicted that the rate of propagation will be greater when directed along the chain, that is, along the chemical bonds, than when directed perpendicular to the chain (57).

Mosely (58) attempted to quantify this prediction, by including intramolecular and intermolecular force constants and an average orientation parameter in his model of a semicrystalline polymer. Sameuls (53) has extended the earlier treatment of Mosely to consider uniaxially extended isotatic polypropylene. No extension of this model to biaxially oriented film samples has been found.

7.4.1 Procedure

The sonic velocity was measured using a Dynamic Modulus Tester, Model PPM-R5 (H.M. Morgan Co.Inc., Cambridge, Mass.). The Dynamic Modulus Tester is a complete system comprising the tester, strip chart recorder, sample mount and transducers. A block diagram of the Tester is shown in
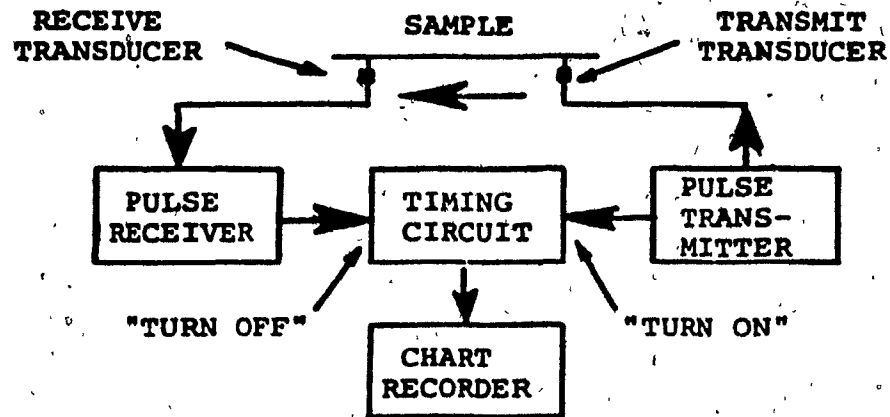
FIGURE 7.6   Block Diagram of Dynamic Modulus
Tester PPM-5R

Figure 7.6. The velocity of a longitudinal wave in the material was determined by measuring the transit time of a sonic pulse between the two transducers in contact with the sample.

(1) Ten samples, 1 x 15 cm, were cut out from a flattened sheet of blown film in the machine and transverse directions for each cooling condition. Samples were equidistant from each other and cut at the same position on the film bubble.

(2) The Dynamic Modulus Tester was set to the following operating conditions:

RANGE	400 usec
ZERO CONTROL	extreme right position
THRESHOLD CONTROL	response steady
CHART DRIVE	3/4 inches/min.

(3) A sample was positioned on the planar mount so that the transducer separation could be varied between zero and ten centimeters.

The tester was now ready to measure the transit time of the sonic pulse in the sample as a function of distance between the transducers.

(4) The transducers were initially set 10.0 cm. apart and then lowered to contact the sample. A pulse on the strip chart was recorded. This step was repeated in decreasing 1.0 cm. increments until the transducer separation was 5.0 cm. Thus, six pulses, representing the six transducer positions were recorded.

(5) The sonic velocity was obtained by plotting the transit times as a function of distance between the transducers, determining a best fit straight line, and taking the reciprocal of the slope.

7.4.2 Sonic Velocity and Birefringence Results and Discussion

Sonic velocity and birefringence results are given in Table 7.3. All average birefringence values were positive, but some samples under the same cooling conditions had negative birefringence. This is shown in Appendix G3 where the birefringence of samples is listed. Sonic velocities of each sample are also given in this Appendix. Appendix E contains an error analysis of these measurements.

Sonic velocity varied by as much as eleven percent between cooling conditions, and the ratio of the sonic velocities in the machine and transverse directions had a maximum difference of five percent. Birefringence showed greater variation than sonic velocity. Between cases 1 and 3 the difference was nearly 40 percent. Also, the maximum percent deviation of an individual sample from the average value in each cooling condition was high, in some cases it was 20 percent. Large differences in birefringence both between cooling conditions and within cooling conditions may, in part, be attributed to sample selection and the area of sample being viewed. The samples were small, 1 x 2 cm., and it was difficult to ensure that they came from the exact same position on the film bubble in each cooling condition, as blow up ratios changed somewhat with different amounts of cooling air. This problem was compounded by the even smaller

Table 7.3 Sonic Velocity and Birefringence

Cooling Condition	Sonic Velocity			Birefrigence
	Transverse Direction	Machine Direction	Transverse/Machine Ratio	
	(km/sec)	(km/sec)		(x10+4)
Case 1	1.72	1.66	1.04	3.25
Case 2	1.70	1.65	1.07	4.05
Case 3	1.81	1.69	1.06	3.85
Case 4	1.80	1.73	1.04	4.50
Case 5	1.79	1.70	1.05	3.22
Case 6	1.78	1.62	1.09	3.45
Case 7	1.72	1.66	1.05	3.82
Case 8	1.70	1.65	1.03	3.83
Case 9	1.73	1.66	1.04	4.49
Case 10	1.69	1.62	1.04	4.30
Case 11	1.76	1.68	1.05	3.72
Case 12	1.75	1.68	1.04	3.87
Case 13	1.68	1.58	1.06	4.06
Case 14	1.68	1.60	1.05	3.87

sample area viewed, from which birefringence was measured. Also, when repeating measurements, it was doubtful the exact same sample area was measured.

There appeared to be no correlation between cooling conditions and sonic velocity or birefringence. Thus each group of film samples produced over the range of cooling conditions studied showed similar amounts of anisotropy according to these two tests.

Blown film samples from each cooling condition were subjected to four film tests, and the measured properties were similar under all cooling flows. Thus, film produced under the strongest combination cooling conditions, and film made with no countercurrent flow at all, were basically the same.

In the neck and frostline regions, where the film stretches, expands and then solidifies, it undergoes a preferential alignment of molecules and becomes oriented. The distribution dependent variables measured in these regions under cooling flows of cases 1 through 7 were similar; as were dependent variables measured in the cooling conditions of cases 8 through 14. The countercurrent components of combination cooling flow were not a factor in these regions. Thus, cocurrent flows from a standard air

ring cooled the film bubble as it became oriented. Furthermore, these cocurrent cooling flows were not very different; they had flow rates of 100 vs. 120 cfm, and film bubbles formed under these cooling conditions yielded frostline heights of 12 vs. 11 inches and had similar overall bubble shapes. Therefore, with not too different cooling conditions in the neck region and with cooling in this area being crucial to film orientation, it was not suprising to obtain similar film properties. Moreover, with countercurrent air applied to the mostly solidified regions of the film bubble, these cooling flows had little if any effect on film properties and could be increased further without adversely affecting them.

Chapter 8

Interpretation of the Results of the Film Property Measurements

In blown film extrusion, the polymer encounters mostly shearing stresses within the die (59). Upon emerging from the die the molten polymer experiences a predominantly extensional stress field that deforms the melt while it is being cooled and shaped to its final dimensions (60). Quenching the melt leads to some crystallite formation and thus a semicrystalline product. It is this deformation history and crystallization process that determine the microstructure and orientation of the film and hence its final properties. This chapter describes film orientation theories and uses the measured film properties of Chapter 7 to infer the overall molecular orientation of the film.

8.1 Quiescent Crystallization

Single polymer crystals that have been formed from dilute solutions exhibit a folded chain structure (61). These folds are commonly referred to as chain-folded lamellae. Figure 8.1 shows the folded chain structure of a single polyethylene crystal. The crystal is orthorhombic in
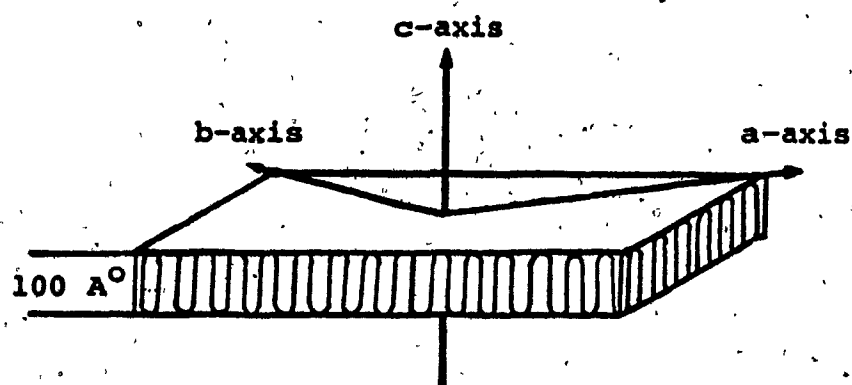
FIGURE 8.1   Schematic Representation of Polyethylene
             Single Crystals Showing Chain Folding
             and Orientation of Crystallographic Axes
             (Reference 63)

that it is specified by three mutually perpendicular axes of unequal lengths, a, b, and c (62). The chain axis lies along the crystallographic c-axis.

Dilute solution crystallization is not fundamentally different from crystallization from the polymer melt. The basic folded chain lamellae are still present (2), but now interchain entanglements and branching of the lamellae yield a complex three dimensional structure. Spherical polycrystalline regions form, made up of imperfect, yet distinct, folded chain lamellae. These regions are termed spherulites and are commonly observed in polymers crystallized from quiescent melts. When spherulites are viewed with a polarizing microscope they appear circular, with a Maltese cross superimposed (64). Figure 8.2 shows the specific symmetry of crystals within this characteristic birefringent pattern. The spherulites, composed of radial folded chain lamellae, grow outward along the lamellar 'spokes' or 'ribbons'. Thus, growth is parallel to the lamellar 'ribbon' axis or the crystallographic b-axis. The outward growth of a spherulite is halted when it has impinged upon the growing surface of another spherulite.
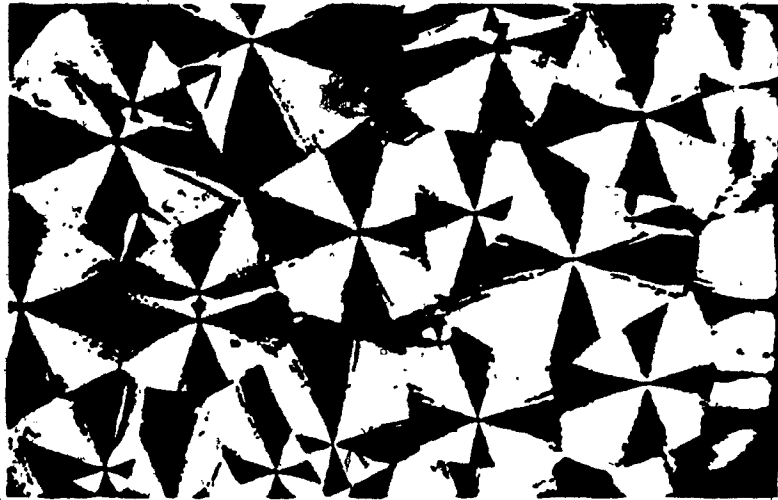
FIGURE 8.2   Optical Micrograph of Polyethylene
Spherulites (Reference 64)

8.2 Crystallization Under Stress

In polymer processing, the polymer melt infrequently has the opportunity to cool and partially crystallize in a quiescent manner. Crystallization typically occurs in a stress field under a thermal gradiant. Thus, it should be no surprise that the crystalline regions in polyethylene film produced by the blown film method are markedly different from the spherulitic geometry of quiescently crystallized polyethylene.

8.2.1 Microstructure and Orientation

A model for the crystallization of a polymer under stress has been proposed by Keller (65). A 'row' structure is formed by the pile-up of sliced spherulites, in which the b-axis of the polyethylene crystal orients radially, and the a- and c-axes are distrubted with cylindrical symmetry around the b-axis. The row structure model and the corresponding pole figure* are shown in Figure 8.3.

* A pole figure is the projection of the normals or 'poles' of crystal planes (51). In order to portray the orientation of all crystallites in a sample, one type of crystal plane is projected on each figure. Pole densities are indicated by contour lines. The technique for constructing pole figures is given by ASTM Standard Test Method E81-541.
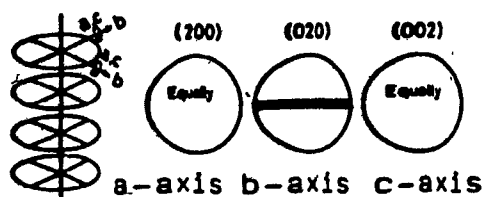
FIGURE 8.3   Keller's Row Structure Model and
             Calculated Pole Figures (Reference 65)

Stein (66) proposed a model in which the a-axis is
parallel to the direction of stress and the b- and c-axes
are cylindrically symmetric with respect to the a- axis.
Figure 8.4 shows Klein's a-axis orientation model.
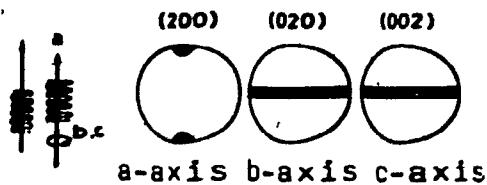
FIGURE 8.4   Stein's a-Axis Oriented Model and
               Pole Figure (Reference 66)

Lindenmeyer's (51) experimentally determined pole figures for high density polyethylene with a 2.1 blow up ratio are shown in Figure 8.5.
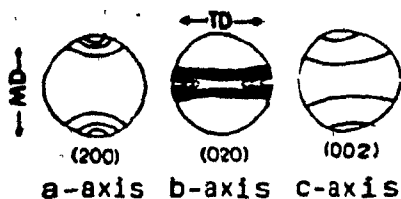
FIGURE 8.5. Pole Figures of Polyethylene Blown Film (Reference 51)

These figures show an a-axis and c-axis orientation in the machine direction, while the b-axis is oriented in the transverse direction. Consequently, neither Keller's row structure nor Stein's a-axis orientation model adequately describes crystallization of polyethylene in a stress field.

A more complex orientation model, proposed by Kobayashi (67) and Nagasawa (50) is based on electron microscopic studies of stress induced polyethylene crystallization in blown films. Initally, lamellar crystallites formed having a c-axis orientation which was parallel to the direction of principal stress. These crystallites along the c-axis

tended to stick together, allowing growth in a direction perpendicular to the stress, that is, along the crystallographic b-axis. The outward lamellar growth occurred in a twisting manner with the a- and c-axis rotating gradually with respect to the b-axis, as in a spherulite. The number of twisting lamellae was not very large as the growth of so many newly formed lamellae was limited by competition and entanglements. A screw-like rod structure developed as the thin lamellae were piled up on each other. Thus, the rods aligned predominantly in the extrusion direction. Figure 8.6 shows the formation and orientation of a screw-like rod structure. The specific shape and thickness of the crystalline regions ultimately depended on the amount of stress and the cooling conditions applied during crystallization.

A similar model has recently been proposed by Picot (66) to explain crystalline orientation in flat-film extrusion. Drawing promotes a slight alignment of the polymer chains in the molten state, and this provides sites for crystallization and forms chain folded lamellae at right angles to the machine direction. The lamellae are able to twist as they form under low extensional strain rates, while at higher strain rates they 'flatten-out'. Partial chain allignment as the polymer cools in the molten state influences the direction of crystal growth and determines
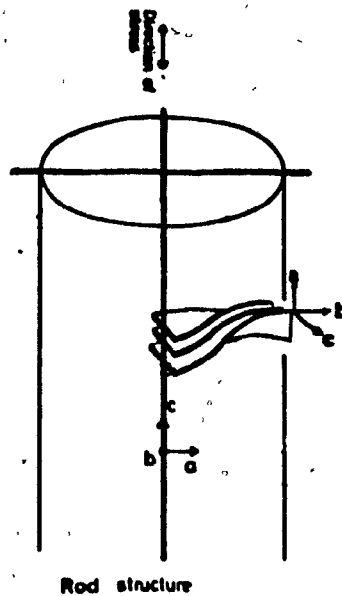
Rod structure

FIGURE 8.6   Rod Structure Model for Blown Film
             (Reference 50)

the amount of crystallization (50).

These models resemble the one presented by Keller (65) in Figure 8.3. However, the large number of twists present in Keller's model suggest that the a- and c-axes should be random. According to the Kobayashi (67), Nagasawa (50), and Picot (68) proposals the rod structure is thin, and this limits the number of twists and reasonably explains the a-axis and c-axis crystalline orientation found in blown polyethlene film.

Low density polyethylene is roughly half crystalline and half amorphous. Polymer chains in the amorphous phase can be thought of as filling the area between crystalline regions. They are by definition 'without specific shape' or simply non-crystalline. However, these chains can be preferentially oriented in one direction while still being unstructured or not compact enough to be considered crystalline. Because of this lack of definite shape they are more easily deformed than crystalline regions. Therefore, the amorphous areas are expected to reflect the predominant stress directions at the time of solidification and comprise a major portion of 'frozen-in' stress in blown film (50).

From this brief discussion of stress-induced crystallization in polyethylene blown films, the following

points have emerged:

1. The deformations and crystallization phenomena encountered in blown film greatly influence the microstructure and orientation of the film product.

2. Spherulitic crystalline regions, present in quiescent crystallization, do not form under the stresses encountered in blown film.

3. The stresses in blown film may slightly orient molecular chains in molten regions, and thus control the growth direction of crystallites (50). However, most orientation occurs during the crystallization process, that is in the upper neck and frostline regions of the film bubble.

4. Crystalline regions have a strong tendency to be oriented with the a-axis tilted a certain amount in the extrusion direction. Similarly, amorphous regions favor alignment in the direction of the greatest applied stress.

5. A definitive model of crystalline microstructure is not available. The model of Kobayashi (67) and

Nagasawa (50), which is based on an a-axis rod structure having a central core with c-axis orientation and twisted lamellae originating from the core along the b-axis, is probaly the most advanced proposal. Recently, Picot (68) has proposed a similar twisted lamellae model for flat film extrusion at low extensional strain rates. Little research has been reported on amorphous phase orientation in polyethylene blown film.

A last point to be made in this discussion of crystallization under stress is that the deformations that impart orientation to the film and that may actually begin in molten regions, greatly accelerate crystallization rates and are responsible for crystallization occurring at much higher temperatures than under quiescent conditions (50,69,70,71).

8.3   Orientation

Samples of blown film under each cooling condition were subjected to four film tests as desrcibed in Chapter 7. The results of the Elmendorf tear, shrinkage, birefringence and sonic velocity tests are summarized in Table 8.1. In the

Table 8.1: Summary of Film Property Tests

Property Test	Transverse Direction	Machine Direction	Transverse/Machine Ratio
Elmendorf Tear	222 (g/mil)	156 (g/mil)	1.42
Shrinkage	15 %	70 %	0.21
Sonic Velocity	1.73 (km/sec)	1.65 (km/sec)	1.04
Birefrigence	3.89 x 10-4		----

remaining sections of this Chapter, these results are discussed in terms of overall molecular orientation. It is shown that these property measurements can be interpreted in a way that is compatible with the Kobayashi (67) and Nagasawa (50) model.

8.3.1 Elmendorf Tear

Elmendorf tear tests indicate that it is easier to propagate a tear or rip in the machine direction than in the transverse direction. Lendenmeyer and Lustig (51) obtained similar tear strengths at comparable blow up ratios for low density polyethylene. This trend was more pronounced in their linear polyethylene results, where the ratio of transverse to machine tear propagation ratio was nearly three. Preferential ease of tear in the machine direction is termed 'splittiness'. Films produced with little or no splittiness are highly desirable and are said to have balanced properties.

Easier tear propagation in the machine direction suggests a greater overall orientation of polyethylene chains in this direction rather than in the transverse direction.

8.3.2 Shrinkage

The percent shrinkage in the machine direction is nearly five times greater than the shrinkage in the transverse direction. Similar results have been reported by Farber (24) under the same processing conditions. Furthermore, with blow up ratios greater than three, substantial increases in transverse direction shrinkage occurred (24,21).

These results suggest that the polyethylene chains are preferentially aligned in the machine direction at low blow-up ratios when the applied stress is mainly extensional and uniaxial. At larger blow up ratios the extensional stress is more biaxial, and thus the shrinkage in the transverse direction increases at the expense of some machine direction shrinkage. This brief analysis is consistent with the tear propagation results, indicating a preferred molecular orientation in the machine direction.

8.3.3 Sonic Velocity and Birefringence

Sonic velocity in the transverse direction was slightly greater than in the machine direction. Similar results have been reported in the literature for low density polyethylene films (72). Larger transverse direction sonic velocities

have been equated with a preferred orientation in that direction (49,72). However, the low sonic velocities and small transverse to machine direction velocity ratios for LDPE suggest this film is only slightly oriented. Comparisons of low density polyethylene with polypropylene and polyethylene terephthalate films have revealed velocities four to five times greater in these latter materials than in low density polyethylene (72). In fact based on these comparisons, Price (72) actually uses the LDPE blown film as an example of an unoriented material.

Birefringence values were small but positive, which implied an overall molecular orientation in the extrusion direction (73). Sammuels (53) stresses caution in using birefringent data to interpet orientation of a semicrystalline material. Two phases, crystalline and amorphous, can be imagined to contribute to orientation. However, as Sammuels points out, a positive total birefringence means that it is the sum of the two phase contributions that is positive, not necessarily each contribution. In Sammuels' study of isotatic polypropylene in fiber spinning, the total birefringence was always positive, but the smaller amorphous contribution was negative in the early stages of extension.

Stein (66) measured birefringence of uniaxially stretched low density polyethylene film samples and found

both phases contributed positively to the total birefringence. The crystalline contribution was twice as large as the amorphous contribution. It is interesting to note that in Stein's sample preparation, the film was annealed to remove any orientation incurred during film blowing. The birefringence of the 'unoriented' annealed film was 1×10^{-3}. However, this value was twice the highest birefringence measured in this study!

Sonic velocity and birefringence measurements were small and similar values have been interpreted by other researchers as a condition for unoriented film samples (66,72). These low values suggest that sonic velocity and birefringence are insensitive to the amount of molecular orientation in blown film. The deformations encountered in film blowing are much less than those present in fiber spinning, where crystalline deformations occur and large birefringence has been reported (71). In blown film the stretching in both machine and transverse directions probably occurs in the more easily deformed amorphous regions. In amorphous regions Kobayashi and Nagasawa (70) have reported very small birefringence for low density polyethylene even at high extension ratios. Furthermore, in an ongoing examination of LDPE films over a range of blow up ratios, sonic velocity and birefrigence showed little change (73).

The low density polyethylene film studied in this research was preferentially oriented in the machine direction according to tear propagation and shrinkage test results. Shrinkage was most sensitive to processing conditions. An overall molecular orientation in the extrusion direction was also favored by the Kobayashi (67) and Nagaava (50) model. Sonic velocity and birefringence measurements showed no preferred overall orientation, and this was attributed to the inability of these tests to detect non-crystalline or amorphous phase orientation in blown film.

Conclusions and Recommendations

9.1 General Conclusions

Many blown film production lines are limited by cooling. Any attempt to increase throughput without exceeding the film blocking temperature must be accompanied by an increase in the amount of cooling. However, higher cooling air flow rates decrease bubble stability, and this is reflected in bubble deformations, corresponding dimensional variations in the film and an unacceptable product. In this work, an attempt was made to generate stronger cooling by drawing air down along the film bubble in a countercurrent fashion, that is, in a direction opposite to that of film motion. From this investigation of countercurrent blown film cooling, the following general conclusions can be drawn.

1. Film bubble stability is an important consideration in applying countercurrent cooling air along a film bubble. Initial attempts to cool the film only by withdrawing air at the base of the film bubble were

unsuccessful. This resulted in a high frostline and large scale bubble deformations. These deformations caused the bubble to oscillate in an expanding and contracting manner or, in extreme cases, literally tore the bubble apart. Thus, both bubble instabilities and insufficient cooling prevented the formation of a stable film bubble with only countercurrent cooling air. These problems of cooling and stability are related; large cooling flows are required to reduce the film bubble temperature so that the film bubble is resistant to the deformations encountered in the process, but these large cooling flows are in themselves destabilizing.

2. A combination cooling system was designed that applied cocurrent air to the base of the film bubble and thus cooled and stabilized the hottest portion of the film, and at the same time countercurrent air was withdrawn just above the frostline thereby cooling the solidified portion of the film. In this cocurrent and countercurrent combination cooling system, a stable bubble was established over a wide range of cooling conditions. The destabilizing suction forces of the countercurrent flow were applied to a mostly solid region of the bubble that was more resistant to

deformations than the molten region.

The cooling ability of this type of operation was compared with that of a standard single lip air ring under maximum cooling conditions. Maximum cocurrent cooling flow corresponded to a film bubble on the verge of instability. In maximum combination cooling flows this same cocurrent air flow rate was used, along with the largest countercurrent flow rate possible with the available blower. Cooling methods were evaluated by comparing position dependent variables; surface temperature, air velocity, cooling air temperature and bubble shape. In addition, the properties of the film produced with the different cooling systems were compared.

3. Surface temperatures of the film bubble, for the combination cooling system, reveal that cooling in the neck region is governed by cocurrent air flow applied to the base of the film bubble. Countercurrent cooling occurs above the frostline and above the collecting plenum, over the solid portion of film bubble. Countercurrent cooling along the solid film bubble results in lower surface temperatures than in standard cocurrent cooling.

4. Film produced under cocurrent and combination cooling conditions was subjected to four film tests and the measurements of birefringence, sonic velocity, shrinkage and Elmendorf tear gave similar results, indicating that basically the same film was produced for each cooling system. This result was attributed to large countercurrent flow rates cooling the solid portion of the film bubble and thus not influencing the orientation of the film that occurred due to stretching and expanding forces in the cocurrently cooled molten region of the film bubble. Also, this outcome was in contrast to the performance of some dual lip air rings that cool film to a greater extent than single lip air rings but result in a film with less balanced properties.

5. The low surface temperatures and desirable balance of film properties achieved with the combination cooling system suggests the possibility of increasing polymer throughput by use of countercurrent cooling, without adversely affecting film properties.

6. Measurements of air velocity and cooling air temperature revealed that the collecting plenum and the cylindrical shroud apparatus used to control the flow

of countercurrent cooling air was a less' than optimal cooling system. This was, in part, attributed to uncertainty regarding the operating conditions under which a stable bubble in countercurrent cooling flow could be formed, and in particular the bubble dimensions that the cooling system had to be designed to accommodate.

7. Air velocity and cooling air temperature measurements showed that the countercurrent cooling air stream only contacted the film bubble above the collecting plenum and within the cylindrical shroud. Countercurrent air velocities were highest just above the collecting plenum and declined to zero above the cylindrical shroud. Furthermore, air velocities within the shroud were higher near the cylinder wall than next to the bubble. Ambient air temperatures measured near the film bubble above the collecting plenum also indicated that little countercurrently drawn cooling air contacted the film bubble above the cylindrical shroud. Furthermore, the bulk temperature of the collected air was only marginally warmer than the surrounding air and thus could have few, if any, secondary applications. These results suggest that the cooling air was drawn over the lip of the cylinder and

directly into the collecting plenum and thus made little contact with the film bubble.

8.   In order to design a countercurrent cooling apparatus that forces cooling air closer to the film bubble than occurs in the present countercurrent cooling system, it is necessary to have a good idea about the bubble shape to be expected for this type of air flow. The shape of the film bubble was shown, in this study, to be strongly affected by the cooling conditions.

9.   In maximum cocurrent air flow, the film bubble expanded gradually as it was stretched between die and frostline, forming what is generally referred to as a 'pocket' shaped bubble. With less than maximum cocurrent air flow, the largest bubble expansion occurred just below the frostline. In this weaker cooling flow, the frostline and surface temperatures were higher. Thus, the temperature of the film bubble appears to be an important factor in determining bubble shape.

10. Countercurrent cooling above the frostline reduced diameter somewhat all along the film bubble. Smaller

diameters were measured under increasing countercurrent cooling flows. Thus, the amount of countercurrent cooling air and the manner in which it was applied along the film bubble influence its shape.

11. Bubble shape in the cocurrent and countercurrent combination cooling system was affected by the heat transfer from the molten bubble to the surroundings, the stretching and expanding forces in the neck region, and the aerodynamic forces exerted by the cooling air on the film bubble.

9.2 Recommendations

Further development of a countercurrent cooling system should concentrate on forcing cooling air closer to the film bubble and causing it to flow over a larger portion of film than occurred in this study. To help accomplish this, the following suggestions are proposed.

1. Increase the height of the present cocurrent and countercurrent combination cooling apparatus to cause the cooling air to flow over a larger portion of the film bubble. The higher cylinder should fit closely

around the desired film bubble) or contain some type of obstruction device to prevent the cooling air from channeling along the cylinder wall.

2. Design a countercurrent cooling system incorporating a raised air ring that blows air down along the bubble toward the die. The raised air ring should be located above the frostline, so that the cooling flow first contacts a solid film that can more easily withstand the aerodynamic forces of the cooling stream than the molten region of the film. Cooling air withdrawal or collection should occur below the die so that the fragile molten regions are disturbed as little as possible. Furthermore, a raised air ring would allow the use of chilled cooling air.

In both of these suggestions, it is important to control the factors that determine bubble shape in countercurrent cooling in order to design a cooling system closely around the film bubble, and thus force cooling air next to the bubble over a large portion of its surface. However, controlling film bubble shape suggests a more fundamental approach to the problem of increasing film cooling rates. This requires knowing the effect of stretching, expansion and the aerodynamic forces experienced

by the melt as it cools to its semicrystalline solid state.

LIST OF SYMBOLS

a	Absorptivity.
b	Film Thickness
A,B,C,C',J J',o,p,q,s.	Constants
Cap	Elmendorf tear apparatus capacity
C_p	Specific heat
D	Diameter
D_i	Initial length of film sample
D_f	Final length of film sample
e	Emissivity
F	Empirical constant taken to be 0.98
g	Acceleration due to gravity
Gr	Grasshof number
h	Heat transfer coefficient
H	Enthalpy
ΔH_c	Heat of crystallization
K	Stefan-Boltzman constant
k_{air}	Thermal conductivity of air.
L	Distance from the maximum local heat transfer coefficient to the position of measurement
Δl	Distance manometer fluid has risen in a slanted arm manometer
m	Mass
$\dot{m}$	Polymer mass flow rate
n	Empirically determined exponent used to linearize hot wire anemometer output voltage
Nu	Nusselt number

Pr	Prandtl number
Q	Volumetric flow rate
r	Radius of film bubble
R	Tearing resistance
re	Reflectivity
Re	Reynolds number
S	Elmendorf tear apparatus scale reading
t	Time
tr	Transmissivity
T	Temperature
T_a	Ambient temperature
T_c	Cooling air temperature
T_s	Film surface temperature
U	Air velocity
U_{max}	Maximum air velocity
U_s	Velocity of film
$U_{(y)}$	Point velocity a distance y from the wall of a pipe
V_a	Hot wire anemometer output voltage
V_{lin}	Linearized hot wire anemometer output voltage
V_o	Hot wire anemometer voltage at zero velocity
V_o^*	Corrected hot wire anemometer voltage at zero velocity
w	Wavelength
X_c	Crystallinity fraction
z	Distance from the die along the bubble axis

ϕ Angle slanted arm manometer makes with the horizontal

ξ_1 Tangent to bubble surface

ξ_2 Normal to bubble surface

ρ_{air} Density of air

ρ_c Density of crystalline phase

ρ_m Density of manometer fluid

ρ_s Density of film sample

θ Angle between the tangent to the film bubble surface and the bubble axis

ν_{air} Kinematic viscosity of air

REFERENCES

1. D.N. Jones and S.J. Kurtz, U.S. Patent 4,330,501 (1982).

2. Z. Tadmor and C.G. Gogos, "Principles of Polymer Processing", John Wiley and Sons, New York (1979).

3. A. Griff, "Plastics Extrusion Technology", VanNostrand Reinhold, New York (1968).

4. L.E. Dowd, SPE ANTEC, 30, 40 (1984).

5. W. Ast, Kunstoffe, 64, 146 (1974).

6. J.M. McKelvey, "Polymer Processing", John Wiley and Sons, New York (1962).

7. R.D. Krycki, TAPPI Paper Synthetics Conference, Book 2, 335 (1983).

8. O.J. Sweeting, Ed., "Science and Technology of Polymer Films", Interscience, New York (1968).

9. W.D. Wright, Plastics Engineering, 37, 9, 30 (1981).

10. W.D. Wright, SPE ANTEC, 28 (1982).

11. A. Ebert and E. Pirot, U.S. Patent 3,544,667 (1970).

12. D.R. Saint Eve and A.K. Bose, U.S. Patent 3,888,609 (1975).

13. F.J. Herrington, U.S. Patent 3,959,425 (1976).

14. F.J. Herrington, U.S. Patent 4,022,558 (1977).

15. F.J. Herrington, U.S. Patent 4,118,453 (1978).

16. Polysystem Machinery Mfg., Private Communication.

17. Sterling Extruder Corp., Private Communication.

18. Gloucester Engineering Co. Inc., Private Communication.

19. Macro Engineering Co. Ltd., Private Communication.

20. A. Toporek, Sano Design and Machine Co. Inc. Newsletter, "A Systems Approach for the Extrusion of LLDPE" (1984).

21. D.R. Hinrichs, U.S. Patent 3,548,042.

22. K. Masuda, K. Hasegawa and A. Okamoto, U.S. Patent 3,568,252.

23. R.B. Alderfer and G.H. Scheibner, U.S. Patent 4,115,048.

24. R. Farber, "Measurement of Deformation Rates in the Film Blowing of Polyethylene", M.Eng. Thesis, McGill University, Montreal (1973).

25. Uni-Flo Design Inc., Private Communication.

26. T. Kanai and J.L. White, PATRA Report No. 203 (1983).

27. G. Menges and W.O. Predöhl, Polym. Eng. Sci., 15, 5, 394 (1975).

28. M.H. Wagner, Rheol. Acta, 15, 40 (1976).

29. R.H. Perry and C.H. Chilton, Eds., "The Chemical Engineers' Handbook", McGraw Hill, New York (1977).

30. F.A.L. Winternitz an C.F. Fischl, Water Power, 9, 225 (1957).

31. Ircon Inc. Technical Notes, "Plastic Film Measurement" (1982).

32. Ircon Inc., Radiation Thermometer Operations Manual, CH-34 Series (1968).

33. R.C. Weast and M.J. Astle, Eds., CRC Handbook of Chemistry and Physics, 63 ed. (1982).

34. Disa Electronics Inc., Hot Wire Anemometer Operations Manual, 55 Series (1972).

35. W. Predöhl, Kunstoffe, 61, 489 (1971).

36. C.D. Han and J.Y. Park, J. Appl. Polym. Sci., 19, 3277 (1975).

37. E.M. Barrall and J.F. Johnson, Tech. Methods Polymer Eval., 2, 1 (1970).

38. L.W. Ortiz and R.N. Rogers, Thermochim. Acta, 3, 383 (1972).

39. E.M. Barrall, Thermochim. Acta, 5, 377 (1973).

40. C.J.S. Petrie, Rheol. Acta, 12, 92 (1973).

41. Disa Electronics Inc., Technical Report, No. 16 (1976).

42. W.H. McAdams, "Heat Transmission", McGraw Hill, New York (1954).

43. S.S. Schwartz and S.H. Goodman, "Plastics Materials and Processes" VanNostrand Reinhold, New York (1982).

44. R.C. Wynter, "Measurement of the Thermal Conductivity and Diffusivity of Polymer Melts", M.Eng. Thesis, McGill University, Montreal (1978).

45. V.S. Manian, T.W. McDonald and R.W. Besant, Int. J. Heat and Mass Transfer, 12, 673 (1969).

46. R.A. Seban and L.H. Black, Int. J. Heat and Mass Transfer, 3, 255 (1961).

47. B. Wunderlich, "Macromolecular Physics", Vol. 2, Academic Press, New York (1976).

48. N.C. Shih and S. Middleman, Polym. Eng. Sci., 10, 1, 4, (1970).

49. F.H. Moi, "Microstructure and the Distribution of Tensile Properties in Injection Molded Polyethylene", Ph.D. Thesis, McGill University, Montreal (1980).

50. T. Nagasawa, T. Matsumura and S. Hoshino, Appl. Polym. Symb., 20, 275 (1973).

51. P.H. Lindenmeyer and S. Lustig, J. Appl. Polym. Sci., 9, 227 (1965).

52. R. Farber and J. Dealy, Polym. Eng. Sci., 14, 6, 435 (1974).

53. R.J. Samuels, "Structural Polymer Properties", John Wiley and Sons, New York (1973).

54. R.S. Stein and F.H. Norris, J. Polym. Sci., 21, 381 (1956).

55. American Optical Corp., "Michel-Lévy Birefringence Charts" New Jersey (1980).

56. R.S. Stein and G.L. Wilkes, "Structure and Properties of Oriented Polymers", I.M. Ward Ed., John Wiley and Sons, New York (1975).

57. W.J. Lyons, J. Appl. Phys., 29, 1429 (1958).

58. W.W. Moseley Jr., J. Appl. Polym. Sci., 3, 226 (1960).

59. H.H. Winter and P.R. Soskey, Presented at the Industrial Materials Research Institute of the National Research Council of Canada, 3rd minisymposium on "Mathematical Modelling of Plastics Processing Operations", Montreal (1984).

60. H.H. Winter, Pure and Appl. Chem., 55, 6, 943 (1983).

61. P.H. Geil, "Polymer Single Crystals", Wiley-Interscience, New York (1963).

62. C.W. Bunn, Trans. Faraday Soc., 35, 482 (1939).

63. T. Alfrey and E.F. Gurnee, "Organic Polymers", Prentice Hall Series in Material Science, Prentice Hall, New Jersey, (1967).

64. F.P. Price, J. Polym. Sci., 37, 71 (1954).

65. A. Keller, J. Polym. Sci., 15, 31 (1955).

66. J.T. Judge and R.S. Stein, J. Appl. Phys., 32, 2357 (1961).

67. K. Kobayashi and T. Nagasawa, J. Appl. Polymer Sci., C15, 163 (1966).

68. J.J.C. Picot, Polym. Eng. Sci., 24, 6, 415 (1984).

69. J.E. Spruiell and J.L. White, Polym. Eng. Sci., 15, 9, 660 (1975).

70. K. Kobayashi and T. Nagasawa, J. Macromol. Sci.-Phys., B4(2), 331 (1970).

71. K. Oda, J.L. White and E.S. Clark, Polym. Eng. Sci., 18, 1, 53 (1978).

72. H.L. Price, SPE Journal, 24, 54 (1968).

73. S.L. Aggarwal, G.P. Tilley and O.J. Sweeting, J. Appl. Polym. Sci., 1, 91 (1959).

74. A. Haber, McGill University, Private Communication.

APPENDIX A

Derivation of a Heat Balance
Over a Small Segment of Film Bubble

The following assumptions were made about heat transfer from the film bubble to the surroundings:

1) Heat transfer between the inner surface and the air trapped within the film bubble is negligible.

2) Heat conduction in the thin film is negligible.

3) The cooling of the bubble is controlled by radiative and convective heat transfer.

4) Heat generation due to the frictional force is negligible.

5) The effects of surface tension, air drag, and inertial force are negligible compared to the axial tension.

6) The film is thin so that variations in the flow field across it may be neglected.

The coordiante system used is shown in Figure A1 where:

r Film bubble radius

ξ_1 Tangent to film bubble surface

ξ_2 Normal to film bubble surface

z Distance from die measured along the axis of the bubble
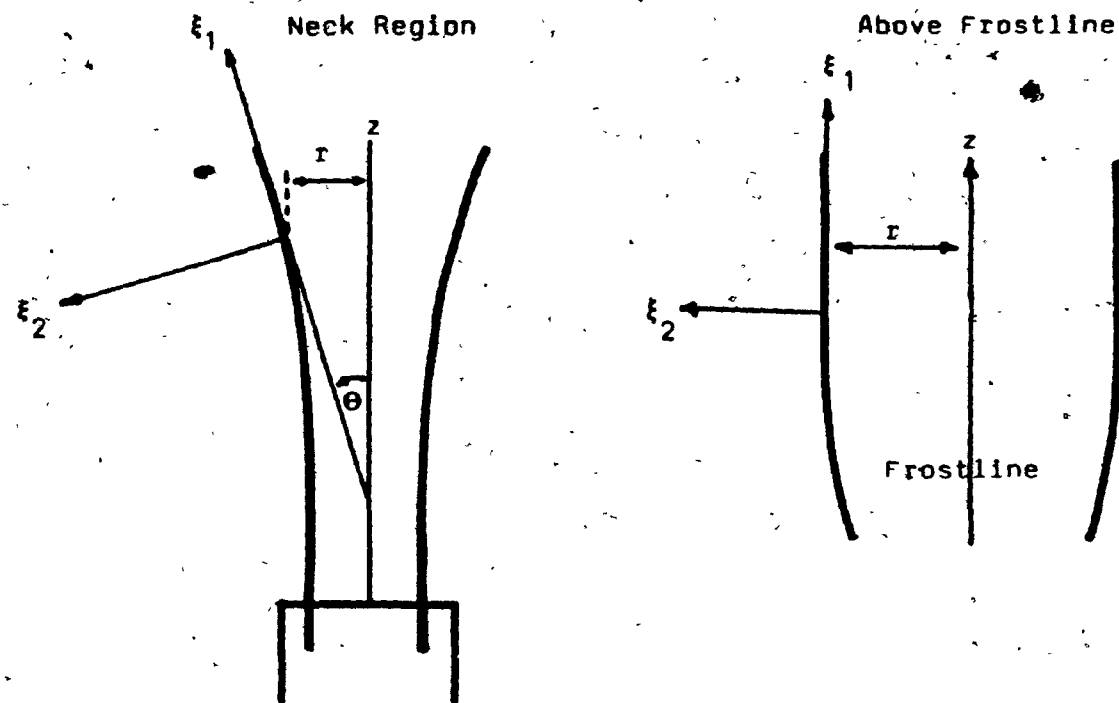
Figure A1: Coordinate for Differential Heat Balance Around an Element of Film Bubble.

θ Angle that the tangent to the film bubble surface makes with the centerline of the film bubble.

In Figure A2 a small element of film bubble is shown over which a differential heat balance is made:

$$\rho_s\, C_p\, U_s\,(T_s - T_o)\Big|_z\, 2\,\Pi\, r\, \Delta\xi_2 - \rho_s\, C_p\, U_s\,(T_s - T_o)\Big|_{z + \Delta z}\, 2\,\Pi\, r\, \Delta\xi_2 +$$

$$U_s\, \Delta H_c\, X\Big|_z\, 2\,\Pi\, r\, \Delta\xi_2 - U_s\, \Delta H_c\, X\Big|_{z + \Delta z}\, 2\,\Pi\, r\, \Delta\xi_2 - q_r\Big|_{r = r}\, 2\,\Pi\, r\, \Delta\xi_1 = 0$$

where: ρ_s Density of film element

C_p Specific heat of film element

U_s Velocity of film

T_s Film surface temperature

r Film bubble radius

ΔH_c Heat of crystallization

X Fraction of crystallinity

q_r Rate of heat transfer from film surface to the surroundings

Dividing the above equation by $\Delta\xi_1\Delta\xi_2 2\Pi r$ yields:

$$\frac{\rho_s\, C_p\, U_s\,(T_{s_{z + \Delta z}} - T_{s_z})}{\Delta\xi_1} + \frac{U_s\, \Delta H_c\,(X_{z + \Delta z} - X_z)}{\Delta\xi_1} = \frac{q_{r_{r = r}}}{\Delta\xi_2}$$

Thermal Energy Out
by Bulk Flow

Direction of
Film Travel

Heat Loss by
Crystallization

Convective and Radiative
Losses to the Surroundings

Δz

Δr

Thermal Energy in
by Bulk Flow
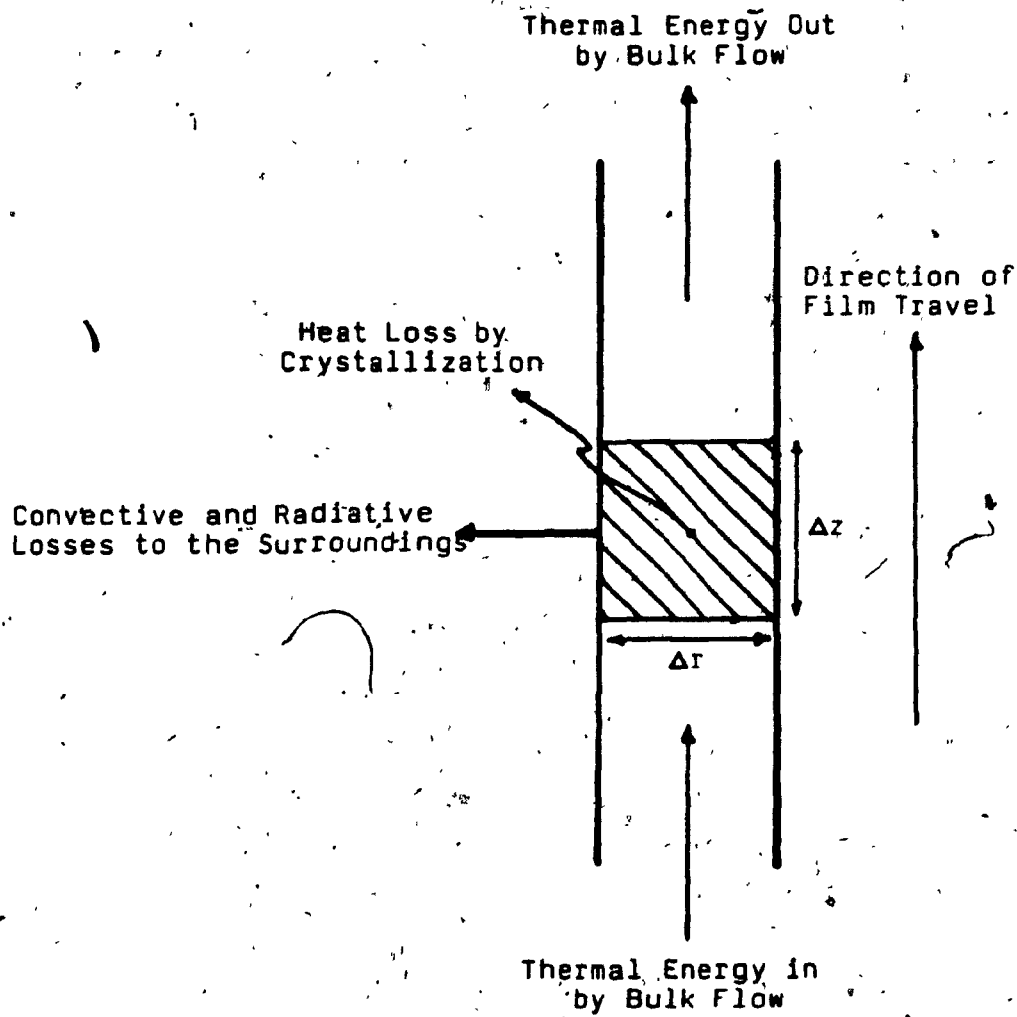
Figure A2:   Element of Film Bubble.
             (Cross-sectional View)

and taking the limit as $\Delta\xi_1\rightarrow 0$ and $\Delta\xi_2\rightarrow 0$ results in:

$$\rho_s\,C_p\,U_s\,dT/d\xi_1 + U_s\,\Delta H_c\,dX/d\xi_1 = dq/d\xi_2$$

Substitution of the geometric relationships;

$$dT_s/d\xi_1 = dT_s/dz\,\cos\theta \quad\text{and}\quad dX/d\xi_1 = dX/dz\,\cos\theta$$

obtained from Figure A1 yields:

$$\rho_s\,C_p\,U_s\,\cos\theta\,dT_s/dz + U_s\,\Delta H_c\,\cos\theta\,dX/dz = dq/d\xi_2$$

The boundary conditions are:

1) $\xi_2 = 0$ (surface on inside of film bubble)
   $q^2 = 0$

2) $\xi_2 = b$ (surface on outside of film bubble)
   $q^2 = h(T_s - T_c) + e K(T_s^4 - T_a^4)$

where: b Film thickness

h Local heat transfer coefficient

T_c Cooling air temperature

T_a Ambient air temperature

K Stefan-Boltzman constant

e Emissivity

Integrating the above equation and evaluating the boundary conditions yields:

$$\rho_s \, C_p \, U_s \, \cos\theta \, dT/dz \; + \; U_s \, \Delta H_c \, \cos\theta \, dX/dz \; = $$

$$h \, (T_s - T_c) \; + \; e \, K \, (T_s^4 - T_a^4)$$

Using the relationship $\dot{m} = U_s \, \rho_s \, (\Pi D)$ and $\dot{m}/\rho_s = Q$ in the above equation and rearranging results in:

$$\dot{m} \, C_p \, \cos\theta \, dT/dz \; + \; Q \, \Delta H_c \, \cos\theta \, dX/dz \; = $$

$$\Pi D \, [h \, (T_s - T_c) \; + \; e \, K \, (T_s^4 - T_a^4)] \qquad (6)$$

Above the frostline the majority of crystallization was assumed to have already occurred and thus Equation 6 can be simplified:

$$\dot{m} \, C_p \, \cos\theta \, dT/dz \; = \; \Pi D \, [h \, (T_s - T_c) \; + \; e \, K \, (T_s^4 - T_a^4)]$$

APPENDIX B

Extrusion Conditions

APPENDIX B1

Countercurrent Cooling Through Existing Air Ring

EXTRUSION CONDITIONS

Material	U.C. DFDY 3312 HP-LDPE
Extruder	1 Inch diameter, 24:1 L/D screw
Die	2.5 Inch spider
Die Gap	23 mils
Screen Pack	40-80-80-40 mesh

Extrusion Parameters	Set Conditions	Trial 1	Trial 2	Trial 3	Trial 4
Extruder Temperatures					
Zone 1	325°F (163°C)				
Zone 2	335°F (168°C)				
Die Temperatures					
Zone 1	350°F (177°C)				
Zone 2	360°F (182°C)				
Melt Temperature	401°F (205°C)				
Screw Speed	varied rpm	45	50	55	60
Back Pressure	psi	3000	3100	3200	3350
Output.	lb/hr	15.1	16.8	18.5	20.2
Film Speed	25 ft/min				
Blow Up Ratio	2.5				
Layflat	9.8 in				
Thickness	mil	1.3	1.45	1.6	1.75
Frostline Height	feet	2.0	2.5	Bubble	broke.
Cooling Air Temp.	75 °F				
Temp. of Withdrawn Air	Not measured				
Cocurrent Flow Rate	0 ft³/min				
Countercurrent Flow Rate	162 ft³/min				

EXTRUSION CONDITIONS

Material   U.C. DFDY 3312 HP-LDPE
Extruder   1 inch diameter, 24:1 L/D screw
Die   2.5 inch spider.
Die Gap   23 mils
Screen Pack   40-80-80-40 mesh

Extrusion Parameters	Set Conditions	Trial 1	Trial 2	Trial 3	Trial 4
Extruder Temperatures					
Zone 1	325°F (163°C)				
Zone 2	335°F (168°C)				
Die Temperatures					
Zone 1	350°F (177°C)				
Zone 2	360°F (182°C)				
Melt Temperature	401°F (205°C)				
Screw Speed	varied rpm	45	50	55	60
Back Pressure	psi	3000	3100	3200	3350
Output	lb/hr	15.1	16.8	18.5	20.2
Film Speed	25 ft/min				
Blow Up Ratio	2.5				
Layflat	9.8 in				
Thickness	mil	1.3	1.45	1.6	1.75
Frostline Height	feet	Bubble	broke.		
Cooling Air Temp.	75 °F				
Temp. of Withdrawn Air	Not measured				
Cocurrent Flow Rate	0 ft³/min				
Countercurrent Flow Rate	272 ft³/min				

EXTRUSION CONDITIONS

Material   U.C. DFDY 3312 HP-LDPE
Extruder   1 inch diameter, 24:1 L/D screw
Die   2.5 inch spider
Die Gap   23 mils
Screen Pack   40-80-80-40 mesh

Extrusion Parameters	Set Conditions	Trial 1	Trial 2	Trial 3	Trial 4
Extruder Temperatures					
Zone 1	325°F (163°C)				
Zone 2	335°F (168°C)				
Die Temperatures					
Zone 1	350°F (177°C)				
Zone 2	360°F (182°C)				
Melt Temperature	401°F (205°C)				
Screw Speed	50 rpm				
Back Pressure	3100 psi				
Output	16.8 lb/hr				
Film Speed	25 ft/min				
Blow Up Ratio	varied	2.0	2.5	3.0	3.5
Layflat	inches	7.9	9.8	11.8	13.7
Thickness	mil	1.8	1.5	1.3	1.1
Frostline Height	feet	<3	<3	Bubble	broke.
Cooling Air Temp.	75 °F				
Temp. of Withdrawn Air	Not measured.				
Cocurrent Flow Rate	0 ft³/min				
Countercurrent Flow Rate	162 ft³/min				

EXTRUSION CONDITIONS

Material   U.C. DFDY 3312 HP-LDPE
Extruder   1 inch diameter, 24:1 L/D screw
Die   2.5 inch spider
Die Gap   23 mils
Screen Pack   40-80-80-40 mesh

Extrusion Parameters	Set Conditions	Trial 1	Trial 2	Trial 3	Trial 4
Extruder Temperatures					
Zone 1	325°F (163°C)				
Zone 2	335°F (168°C)				
Die Temperatures					
Zone 1	350°F (177°C)				
Zone 2	360°F (182°C)				
Melt Temperature	401°F (205°C)				
Screw Speed	50 rpm				
Back Pressure	3100 psi				
Output	16.8 lb/hr				
Film Speed	25 ft/min				
Blow Up Ratio	varied	2.0	2.5	3.0	3.5
Layflat	inches	7.9	9.8	11.8	13.7
Thickness	mil	1.8	1.5	1.3	1.1
Frostline Height	feet	Bubble	broke.		
Cooling Air Temp.	75 °F				
Temp. of Withdrawn Air	Not measured				
Cocurrent Flow Rate	0 ft³/min				
Countercurrent Flow Rate	272 ft³/min				

EXTRUSION CONDITIONS

Material   U.C. DFDY 3312 HP-LDPE
Extruder   1 inch diameter, 24:1 L/D screw
Die   2.5 inch spider
Die Gap   23 mils
Screen Pack   40-80-80-40 mesh

Extrusion Parameters	Set Conditions	Trial 1	Trial 2	Trial 3	Trial 4
Extruder Temperatures					
Zone 1	325°F (163°C)				
Zone 2	335°F (168°C)				
Die Temperatures					
Zone 1	350°F (177°C)				
Zone 2	360°F (182°C)				
Melt Temperature	401°F (205°C)				
Screw Speed	50 rpm				
Back Pressure	3100 psi				
Output	16.8 lb/hr				
Film Speed	varied ft/min	20	25	30	40
Blow Up Ratio	2.5				
Layflat	9.8 in				
Thickness	mil	1.9	1.5	1.25	1.0
Frostline Height	feet	<3	<3	Bubble	broke.
Cooling Air Temp.	Not measured				
Temp. of Withdrawn Air	75 °F				
Cocurrent Flow Rate	0 ft³/min				
Countercurrent Flow Rate	162 ft³/min				

EXTRUSION CONDITIONS

Material   U.C. DFDY 3312 HP-LDPE
Extruder   1 inch diameter, 24:1 L/D screw
Die   2.5 inch spider
Die Gap   23 mils.
Screen Pack   40-80-80-40 mesh

Extrusion Parameters	Set Conditions	Trial 1	Trial 2	Trial 3	Trial 4
Extruder Temperatures					
Zone 1	325°F (163°C)				
Zone 2	335°F (168°C)				
Die Temperatures					
Zone 1	350°F (177°C)				
Zone 2	360°F (182°C)				
Melt Temperature	401°F (205°C)				
Screw Speed	50 rpm				
Back Pressure	3100 psi				
Output	16.8 lb/hr				
Film Speed	varied ft/min	20	25	30	40
Blow Up Ratio	2.5				
Layflat	9.8 in				
Thickness	mil	1.9	1.5	1.25	1.0
Frostline Height	feet	Bubble	broke.		
Cooling Air Temp.	75 °F				
Temp. of Withdrawn Air	Not measured				
Cocurrent Flow Rate	0 ft³/min		—		
Countercurrent Flow Rate	272 ft³/min				

APPENDIX B2

<u>Countercurrent Cooling Through the Existing Air Ring</u>

<u>Incorporating a Solid Shroud Around the Film Bubble</u>

EXTRUSION CONDITIONS

Material   U.C. DFDY 3312 HP-LDPE
Extruder   1 Inch diameter, 24:1 L/D screw
Die   2.5 Inch spider
Die Gap   23 mils
Screen Pack   40-80-80-40 mesh

Extrusion Parameters	Set Conditions	Trial 1	Trial 2	Trial 3	Trial 4
Extruder Temperatures					
Zone 1	325°F (163°C)				
Zone 2	335°F (168°C)				
Die Temperatures					
Zone 1	350°F (177°C)				
Zone 2	360°F (182°C)				
Melt Temperature	401°F (205°C)				
Screw Speed	varied rpm	45	50	45	45
Back Pressure	psi	3100	3150	3100	3100
Output	lb/hr	15.2	17.0	15.2	15.2
Film Speed	25 ft/min				
Blow Up Ratio		2.25	2.25	2.25	2.0
Layflat	inches	8.8	8.8	8.8	7.9
Thickness	mil	1.3	1.45	1.3	1.4
Frostline Height	feet	<3	<3	<3	Severe oscillations.
Cooling Air Temp.	75 °F				
Temp. of Withdrawn Air	Not measured as bubble broke in a short time.				
Cocurrent Flow Rate	.0 ft³/min				
Countercurrent Flow Rate	varied ft³/min	126	162	272	

EXTRUSION CONDITIONS

Material	U.C. DFDY 3312 HP-LDPE
Extruder	1 inch diameter, 24:1 L/D screw
Die	2.5 inch spider
Die Gap	23 mils
Screen Pack	40-80-80-40 mesh

Extrusion Parameters	Set Conditions	Trial 1	Trial 2	Trial 3	Trial 4
Extruder Temperatures					
Zone 1	325°F (163°C)				
Zone 2	335°F (168°C)				
Die Temperatures					
Zone 1	350°F (177°C)				
Zone 2	360°F (182°C)				
Melt Temperature	401°F (205°C)				
Screw Speed	50 rpm				
Back Pressure	3100 psi				
Output	17.0 lb/hr				
Film Speed	25 ft/min				
Blow Up Ratio	varied	2.5	3.0	2.0	2.5
Layflat	inches	9.8	11.8	7.9	9.8
Thickness	mil	1.45	1.2	1.8	1.45
Frostline Height	feet	<3	<3	<3	Severe oscillations.
Cooling Air Temp.	75 °F				
Temp. of Withdrawn Air	Not measured as stable bubble was unobtainable.				
Cocurrent Flow Rate	0 ft^3/min				
Countercurrent Flow Rate	varied ft^3/min	126	126	272	272

EXTRUSION CONDITIONS

Material   U.C. DFDY 3312 HP-LDPE
Extruder   1 inch diameter, 24:1 L/D screw
Die   2.5 inch spider
Die Gap   23 mils
Screen Pack   40-80-80-40 mesh

Extrusion Parameters	Set Conditions	Trial 1	Trial 2	Trial 3	Trial 4
Extruder Temperatures					
Zone 1	325°F (163°C)				
Zone 2	335°F (168°C)				
Die Temperatures					
Zone 1	350°F (177°C)				
Zone 2	360°F (182°C)				
Melt Temperature	401°F (205°C)				
Screw Speed	50 rpm				
Back Pressure	3100 psi				
Output	17.0 lb/hr				
Film Speed	varied	25	30	25	30
Blow Up Ratio	2.25				
Layflat	8.8 in				
Thickness	mil	1.45	1.2	1.45	1.2
Frostline Height	feet	<3	Severe	oscillations.	
Cooling Air Temp.	75 °F				
Temp. of Withdrawn Air	Not measured	as stable	bubble	was unobtainable.	
Cocurrent Flow Rate	0 ft^3/min				
Countercurrent Flow Rate	varied ft^3/min 126	126	272	272	

APPENDIX B3

Countercurrent Cooling Through the Existing Air Ring
Incorporating a Modified Cylindrical Shroud Around the Film Bubble

EXTRUSION CONDITIONS

Material	U.C. DFDY 3312 HP-LDPE
Extruder	1 Inch diameter, 24:1 L/D screw
Die	.2.5 inch spider
Die Gap	23 mils
Screen Pack	40-80-80-40 mesh

Extrusion Parameters	Set Conditions	Trial 1	Trial 2	Trial 3	Trial 4
Extruder Temperatures					
Zone 1	325°F (163°C)				
Zone 2	335°F (168°C)				
Die Temperatures					
Zone 1	350°F (177°C)				
Zone 2	360°F (182°C)				
Melt Temperature	401°F (205°C)				
Screw Speed	varied rpm	50	55	50	55
Back Pressure	psi	3100	3200	3100	3200
Output	lb/hr	16.8	18.5	16.8	18.5
Film Speed	25 ft/min				
Blow Up Ratio	2.5				
Layflat	9.8 in				
Thickness	mil	1.45	1.6	1.45	1.6
Frostline Height	Not measured	as bubble broke in a short time.			
Cooling Air Temp.	75 °F				
Temp. of Withdrawn Air	Not measured				
Cocurrent Flow Rate.	0 ft^3/min				
Countercurrent Flow Rate	162 ft^3/min 162 ft^3/min				
Rows of Openings on Shroud	varied	7 open 0 closed		5 open 2 closed	(uppermost)

EXTRUSION CONDITIONS

Material   U.C. DFDY 3312 HP-LDPE
Extruder   1 Inch diameter, 24:1 L/D screw
Die   2.5 Inch spider
Die Gap   23 mils
Screen Pack   40-80-80-40 mesh

Extrusion Parameters	Set Conditions	Trial 1	Trial 2	Trial 3	Trial 4
Extruder Temperatures					
Zone 1	325°F (163°C)				
Zone 2	335°F (168°C)				
Die Temperatures					
Zone 1	350°F (177°C)				
Zone 2	360°F (182°C)				
Melt Temperature	401°F (205°C)				
Screw Speed	varied rpm	50	60	50	55
Back Pressure	psi	3100	3300	3100	3200
Output	lb/hr	16.8	20.2	16.8	18.5
Film Speed	25 ft/min				
Blow Up Ratio	2.5				
Layflat	9.8 in				
Thickness	mil	1.45	1.75	1.45	1.6
Frostline Height	Not measured as bubble broke in a short time.				
Cooling Air Temp.	75 °F				
Temp. of Withdrawn Air	Not measured				
Cocurrent Flow Rate	0 ft³/min				
Countercurrent Flow Rate	162 ft³/min				
Rows of Openings on Shroud	varied	5 open(bottommost) 2 closed		2 open(uppermost) 5 closed	

EXTRUSION CONDITIONS

Material U.C. DFDY 3312 HP-LDPE
Extruder 1 inch diameter, 24:1 L/D screw
Die 2.5 inch spider
Die Gap 23 mils
Screen Pack 40-80-80-40 mesh

Extrusion Parameters	Set Conditions	Trial 1	Trial 2	Trial 3	Trial 4
Extruder Temperatures					
Zone 1	325°F (163°C)				
Zone 2	335°F (168°C)				
Die Temperatures					
Zone 1	350°F (177°C)				
Zone 2	360°F (182°C)				
Melt Temperature	401°F (205°C)				
Screw Speed	varied rpm	50	55	50	60
Back Pressure	psi	3100	3200	3100	3300
Output	lb/hr	16.8	18.5	16.8	20.2
Film Speed	25 ft/min				
Blow Up Ratio	2.5				
Layflat	9.8 in				
Thickness	mil	1.45	1.6	1.45	1.75
Frostline Height	Not measured as bubble broke in a short time.				
Cooling Air Temp.	75 °F				
Temp. of Withdrawn Air	Not measured				
Cocurrent Flow Rate	0 ft³/min				
Countercurrent Flow Rate	162 ft³/min				
Rows of Openings on Shroud	varied	3 open(middle) 4 closed		2 open(bottommost) 5 closed	

EXTRUSION CONDITIONS

Material   U.C. DFDY 3312 HP-LDPE
Extruder   .1 inch diameter, 24:1 L/D screw
Die   2.5 inch spider
Die Gap   23 mils
Screen Pack   40-80-80-40 mesh

Extrusion Parameters	Set Conditions	Trial 1	Trial 2	Trial 3	Trial 4
Extruder Temperatures					
Zone 1	325°F (163°C)				
Zone 2	335°F (168°C)				
Die Temperatures					
Zone 1	350°F (177°C)				
Zone 2	360°F (182°C)				
Melt Temperature	401°F (205°C)				
Screw Speed	varied rpm	50	55	50	55
Back Pressure	psi	3100	3200	3100	3200
Output	lb/hr	16.8	18.5	16.8	18.5
Film Speed	25 ft/min				
Blow Up Ratio	2.0				
Layflat	7.9 in				
Thickness	mil	1.8	2.0	1.8	2.0
Frostline Height	Not measured as bubble broke in a short time.				
Cooling Air Temp.	75 °F				
Temp. of Withdrawn Air	Not measured				
Cocurrent Flow Rate	0 ft³/min				
Countercurrent Flow Rate	162 ft³/min				
Rows of Openings on Shroud	varied	2 open (uppermost) 5 closed		3 open (middle) 4 closed	

EXTRUSION CONDITIONS

Material	U.C. DFDY 3312 HP-LDPE
Extruder	1 inch diameter, 24:1 L/D screw
Die	2.5 inch spider
Die Gap	23 mils
Screen Pack	40-80-80-40 mesh

Extrusion Parameters	Set Conditions	Trial 1	Trial 2	Trial 3	Trial 4
Extruder Temperatures					
Zone 1	325°F (163°C)				
Zone 2	335°F (168°C)				
Die Temperatures					
Zone 1	350°F (177°C)				
Zone 2	360°F (182°C)				
Melt Temperature	401°F (205°C)				
Screw Speed	varied rpm	50	60	50	55
Back Pressure	psi	3100	3300	3100	3100
Output	lb/hr	16.8	20.2	16.8	18.5
Film Speed	25 ft/min				
Blow Up Ratio	2.0				
Layflat	7.9 in				
Thickness	mil	1.8	2.2	1.8	2.0
Frostline Height	Not measured	as bubble broke in ashort time.			
Cooling Air Temp.	75 °F				
Temp. of Withdrawn Air	Not measured				
Cocurrent Flow Rate	0 ft³/min				
Countercurrent Flow Rate	varied	162	162	200	200
Rows of Openings on Shroud	varied	2 open(bottommost) 5 closed		2 open(uppermost) 5 closed	

EXTRUSION CONDITIONS

Material   U.C. DFDY 3312 HP-LDPE
Extruder   1 Inch diameter, 24:1 L/D screw
Die   2.5 inch spider
Die Gap   23 mils
Screen Pack 40-80-80-40 mesh

Extrusion Parameters	Set Conditions	Trial 1	Trial 2	Trial 3	Trial 4
Extruder Temperatures					
Zone 1	325°F (163°C)				
Zone 2	335°F (168°C)				
Die Temperatures					
Zone 1	350°F (177°C)				
Zone 2	360°F (182°C)				
Melt Temperature	401°F (205°C)				
Screw Speed	varied rpm	50	55	50	55
Back Pressure	psi	3100	3100	3100	3100
Output	lb/hr	16.8	18.5	16.8	18.5
Film Speed	25 ft/min				
Blow Up Ratio	2.0				
Layflat	7.9 in				
Thickness	mil	1.8	2.0	1.8	2.0
Frostline Height	Not measured	as bubble broke in a short time.			
Cooling Air Temp.	75 °F				
Temp. of Withdrawn Air	Not measured				
Cocurrent Flow Rate	0 ft³/min				
Countercurrent Flow Rate	200 ft³/min				
Rows of Openings on Shroud	varied	3 open(middle) 4 closed		2 open(bottommost) 5 closed	

EXTRUSION CONDITIONS

Material   U.C. DFDY 3312 HP-LDPE
Extruder   1 inch diameter, 24:1 L/D screw
Die   2.5 inch spider
Die Gap   23 mils
Screen Pack   40-80-80-40 mesh

Extrusion Parameters	Set Conditions	Trial 1	Trial 2	Trial 3	Trial 4
Extruder Temperatures					
Zone 1	325°F (163°C)				
Zone 2	335°F (168°C)				
Die Temperatures					
Zone 1	350°F (177°C)				
Zone 2	360°F (182°C)				
Melt Temperature	401°F (205°C)				
Screw Speed	varied rpm	50	60	50	55
Back Pressure	psi	3100	3300	3100	3200
Output	lb/hr	16.8	20.2	16.8	18.5
Film Speed	30 ft/min				
Blow Up Ratio	2.5				
Layflat	9.8 in				
Thickness	mil	1.25	1.5	1.25	1.4
Frostline Height	Not measured	as bubble broke in a short time.			
Cooling Air Temp.	75 °F				
Temp. of Withdrawn Air	Not measured				
Cocurrent Flow Rate	0 ft³/min				
Countercurrent Flow Rate	162 ft³/min				
Rows of Openings on Shroud	varied	2 open(uppermost) 5 closed		3 open(middle) 4 closed	

EXTRUSION CONDITIONS

		Note:	Upper base plate
Material	U.C. DFDY 3312-NP-LDPE		of air ring removed
Extruder	1 inch diameter, 24:1 L/D screw		to enlarge air
Die	2.5 inch spider		withdrawal orifice.
Die Gap	23 mils		
Screen Pack	40-80-80-40 mesh		

Extrusion Parameters	Set Conditions	Trial 1	Trial 2	Trial 3	Trial 4
Extruder Temperatures					
Zone 1	325°F (163°C)				
Zone 2	335°F (168°C)				
Die Temperatures					
Zone 1	350°F (177°C)				
Zone 2	360°F (182°C)				
Melt Temperature	401°F (205°C)				
Screw Speed	varied rpm	50	55	50	55
Back Pressure	psi	3100	3200	3100	3200
Output	lb/hr	16.8	18.5	16.8	18.5
Film Speed	25 ft/min				
Blow Up Ratio	2.0				
Layflat	7.9 in				
Thickness	mil	1.8	2.0	1.8	2.0
Frostline Height	Severe bubble oscillations.				
Cooling Air Temp.	75 °F				
Temp. of Withdrawn Air	Not measured.				
Cocurrent Flow Rate	0 ft³/min				
Countercurrent Flow Rate	162 ft³/min				
Rows of Openings on Shroud	varied	2 open(uppermost) 5 closed		3 open(middle) 4 closed	

EXTRUSION CONDITIONS

Material : U.C. DFDY 3312 HP-LDPE   Note: Upper base plate
Extruder   1 inch diameter, 24:1 L/D screw   of air ring removed
Die   2.5 inch spider   to enlarge air
Die Gap   23 mils   withdrawal orifice.
Screen Pack   40-80-80-40 mesh

Extrusion Parameters	Set Conditions	Trial 1	Trial 2	Trial 3	Trial 4
Extruder Temperatures					
Zone 1	325°F (163°C)				
Zone 2	335°F (168°C)				
Die Temperatures					
Zone 1	350°F (177°C)				
Zone 2	360°F (182°C)				
Melt Temperature	401°F (205°C)				
Screw Speed	varied rpm	50	55	50	55
Back Pressure	psi	3100	3200	3100	3200
Output	lb/hr	16.8	18.5	16.8	18.5
Film Speed	varied ft/min	25	25	30	30
Blow Up Ratio	2.0				
Layflat	7.9 in				
Thickness	mil	1.8	2.0	1.55	1.7
Frostline Height	Severe bubble oscillations.				
Cooling Air Temp.	75 °F				
Temp. of Withdrawn Air	Not measured				
Cocurrent Flow Rate	0 ft³/min				
Countercurrent Flow Rate	162 ft³/min				
Rows of Openings on Shroud	varied	2 open(bottommost) 5 closed		2 open(uppermost) 5 closed	

EXTRUSION CONDITIONS

Material | U.C. DFDY 3312 HP-LDPE
Extruder | 1 Inch diameter, 24:1 L/D screw
Die | 2.5 Inch spider
Die Gap | 23 mils
Screen Pack | 40-80-80-40 mesh

Note: Upper base plate of air ring removed to enlarge air withdrawal orifice.

Extrusion Parameters	Set Conditions	Trial 1	Trial 2	Trial 3	Trial 4
Extruder Temperatures					
Zone 1	325°F (163°C)				
Zone 2	335°F (168°C)				
Die Temperatures					
Zone 1	350°F (177°C)				
Zone 2	360°F (182°C)				
Melt Temperature	401°F (205°C)				
Screw Speed	varied rpm	50	55	50	55
Back Pressure	psi	3100	3200	3100	3200
Output	lb/hr	16.8	18.5	16.8	18.5
Film Speed	varied ft/min	30	30	25	25
Blow Up Ratio	varied	2.0	2.0	2.25	2.25
Layflat	inches	7.9	7.9	8.8	8.8
Thickness	mil	1.55	1.7	1.45	1.6
Frostline Height	Severe bubble oscillations.				
Cooling Air Temp.	75 °F				
Temp. of Withdrawn Air	Not measured.				
Cocurrent Flow Rate	0 ft^3/min				
Countercurrent Flow Rate	162 ft^3/min				
Rows of Openings on Shroud	varied	2 open(bottommost) 5 closed		2 open(uppermost) 5 closed	

EXTRUSION CONDITIONS

		Note:	Upper base plate
Material	U.C. DFDY 3312 HP-LDPE		of air ring removed
Extruder	1 inch diameter, 24:1 L/D screw		to enlarge air
Die	2.5 inch spider		withdrawal orifice.
Die Gap	23 mils		
Screen Pack	40-80-80-40 mesh		

Extrusion Parameters	Set Conditions	Trial 1	Trial 2	Trial 3	Trial 4
Extruder Temperatures					
Zone 1	325°F (163°C)				
Zone 2	335°F (168°C)				
Die Temperatures					
Zone 1	350°F (177°C)				
Zone 2	360°F (182°C)				
Melt Temperature	401°F (205°C)				
Screw Speed	varied rpm	50	55	50	55
Back Pressure	psi	3100	3200	3100	3200
Output	lb/hr	16.8	18.5	16.8	18.5
Film Speed	varied ft/min	25	25	30	30
Blow Up Ratio	2.25				
Layflat	8.8 in				
Thickness	mil	1.45	1.6	1.4	1.55
Frostline Height	Severe bubble oscillations.				
Cooling Air Temp.	75 °F				
Temp. of Withdrawn Air	Not measured				
Cocurrent Flow Rate	0 ft^3/min				
Countercurrent Flow Rate	162 ft^3/min				
Rows of Openings on Shroud	varied	2 open(bottommost) 5 closed		2 open(uppermost) 5 closed	

EXTRUSION CONDITIONS

Material	U.C. DFDY 3312 HP-LDPE	Note:	Upper base plate
Extruder	1 Inch diameter, 24:1 L/D screw		of air ring removed
Die.	2.5 inch spider		and repositioned
Die Gap	23 mils		on top of cylinder.
Screen Pack	40-80-80-40 mesh		

Extrusion Parameter	Set Conditions	Trial 1	Trial 2	Trial 3	Trial 4
Extruder Temperatures					
Zone 1	325°F (163°C)				
Zone 2	335°F (168°C)				
Die Temperatures					
Zone 1	350°F (177°C)				
Zone 2	360°F (182°C)				
Melt Temperature	401°F (205°C)				
Screw Speed	varied rpm	50	55	50	55
Back Pressure	psi	3100	3200	3100	3200
Output	lb/hr	16.8	18.5	16.8	18.5
Film Speed	25 ft/min				
Blow Up Ratio	2.5				
Layflat	9.8 in				
Thickness	mil	1.25	1.4	1.25	1.4
Frostline Height	Severe bubble oscillations.				
Cooling Air Temp.	75 °F				
Temp. of Withdrawn Air	Not measured.				
Cocurrent Flow Rate	0 ft³/min				
Countercurrent Flow Rate	162 ft³/min				
Rows of Openings on Shroud	varied	2 open(uppermost) 5 closed		3 open(middle) 4 closed	

EXTRUSION CONDITIONS

Material	U.C. DFDY 3312 HP-LDPE	Note:	Upper base plate
Extruder	1 inch diameter, 24:1 L/D screw		of air ring removed
Die	2.5 inch spider		and repositioned
Die Gap	23 mils		on top of cylinder.
Screen Pack	40-80-80-40 mesh		

Extrusion Parameters	Set Conditions	Trial 1	Trial 2	Trial 3	Trial 4
Extruder Temperatures					
Zone 1	325°F (163°C)				
Zone 2	335°F (168°C)				
Die Temperatures					
Zone 1	350°F (177°C)				
Zone 2	360°F (182°C)				
Melt Temperature	401°F (205°C)				
Screw Speed	varied rpm	50	55	50	55
Back Pressure	psi	3100	3200	3100	3200
Output	lb/hr	16.8	18.5	16.8	18.5
Film Speed	25 ft/min				
Blow Up Ratio	2.5				
Layflat	9.8 in				
Thickness	mil	1.25	1.4	1.25	1.4
Frostline Height	feet	<3	Bubble	oscilla	tions.
Cooling Air Temp.	75 °F				
Temp. of Withdrawn Air	Not measured.				
Cocurrent Flow Rate	0 ft³/min				
Countercurrent Flow Rate	varied ft³/min	162	162	200	200
Rows of Openings on Shroud	2 open (bottommost) 5 closed				

EXTRUSION CONDITIONS

Material	U.C. DFDY 3312 HP-LDPE	Note; Upper base plate
Extruder	1 Inch diameter, 24:1 L/D screw	of air ring removed
Die	2.5 inch spider	and repositioned
Die Gap	23 mils	on top of cylinder.
Screen Pack	40-80-80-40 mesh	

Extrusion Parameters	Set Conditions	Trial 1	Trial 2	Trial 3	Trial 4
Extruder Temperatures					
Zone 1	325°F (163°C)				
Zone 2	335°F (168°C)				
Die Temperatures					
Zone 1	350°F (177°C)				
Zone 2	360°F (182°C)				
Melt Temperature	401°F (205°C)				
Screw Speed	varied rpm	50	55	50	55
Back Pressure	psi	3100	3200	3100	3200
Output	lb/hr	16.8	18.5	16.8	18.5
Film Speed	30 ft/min				
Blow Up Ratio	2.5				
Layflat	9.8 in				
Thickness	mil	1.25	1.4	1.25	1.4
Frostline Height	Bubble oscillations prevented measurement.				
Cooling Air Temp.	75 °F				
Temp. of Withdrawn Air	Not measured.				
Cocurrent Flow Rate	0 ft^3/min				
Countercurrent Flow Rate	162 ft^3/min				
Rows of Openings on Shroud	varied	2 open(uppermost) 5 closed		2 open(bottommost) 5 closed	

APPENDIX B4

Cocurrent - 'Countercurrent Combination Cooling

EXTRUSION CONDITIONS

Material   U.C. DFDY 3312 HP-LDPE
Extruder   1 inch diameter, 24:1 L/D screw
Die   2.5 inch spider
Die Gap   23 mils
Screen Pack   40-80-80-40 mesh

Extrusion Parameters	Set Conditions	Trial 1	Trial 2	Trial 3	Trial 4
Extruder Temperatures					
Zone 1	325°F (163°C)				
Zone 2	335°F (168°C)				
Die Temperatures					
Zone 1	350°F (177°C)				
Zone 2	360°F (182°C)				
Melt Temperature	401°F (205°C)				
Screw Speed	varied rpm	50	60	50	60
Back Pressure	psi	3100	3300	3100	330
Output	lb/hr	16:8	20.2	16.8	20.2
Film Speed	25 ft/min				
Blow Up Ratio	2.25				
Layflat	8.8 in				
Thickness	mil	1.45	1.75	1.45	1.75
Frostline Height	inches	13	within plenum	13	within plenum
Cooling Air Temp.	75 °F				
Temp. of Withdrawn Air	Not measured				
Cocurrent Flow Rate	103 ft³/min				
Countercurrent Flow Rate	varied ft³/min	162	162	200	200
Rows of Openings on Shroud	varied	5 open and 0 closed	and 0 closed and	5 closed and 0 open	
Plenum Position	highest (covers two uppermost rows of openings)				

EXTRUSION CONDITIONS

Material   U.C. DFDY 3312 HP-LDPE
Extruder   1 inch diameter, 24:1 L/D screw
Die   2.5 inch spider
Die Gap   23 mils
Screen Pack   40-80-80-40 mesh

Extrusion Parameters	Set Conditions	Trial 1	Trial 2	Trial 3	Trial 4
Extruder Temperatures					
Zone 1	325°F (163°C)				
Zone 2	335°F (168°C)				
Die Temperatures					
Zone 1	350°F (177°C)				
Zone 2	360°F (182°C)				
Melt Temperature	401°F (205°C)				
Screw Speed	varied rpm	50	50	50	60
Back Pressure	psi	3100	3100	3100	3300
Output	lb/hr	16.8	16.8	16.8	20.2
Film Speed	25 ft/min				
Blow Up Ratio	2.25				
Layflat	8.8 in				
Thickness	mil	1.45	1.45	1.45	1.75
Frostline Height	inches	13	12	12	unstable
Cooling Air Temp.	75 °F				
Temp. of Withdrawn Air	Not measured				
Cocurrent Flow Rate	varied ft^3/min	103	123	123	123
Countercurrent Flow Rate	varied ft^3/min	272	162	272	272
Rows of Openings on Shroud	varied	5 open and 0 closed and 5 closed and 0 open			
Plenum Position	highest (covers two uppermost rows of openings)				

EXTRUSION CONDITIONS

Material   U.C. DFDY 3312 HP-LDPE
Extruder   1 Inch diameter, 24:1 L/D screw
Die   2.5 Inch spider
Die Gap   23 mils
Screen Pack   40-80-80-40 mesh

Extrusion Parameters	Set Conditions	Trial 1	Trial 2	Trial 3	Trial 4
Extruder Temperatures					
Zone 1	325°F (163°C)				
Zone 2	335°F (168°C)				
Die Temperatures					
Zone 1	350°F (177°C)				
Zone 2	360°F (182°C)				
Melt Temperature	401°F (205°C)				
Screw Speed	varied rpm	50	50	50	60
Back Pressure	psi	3100	3100	3100	3300
Output	lb/hr	16.8	16.8	16.8	20.2
Film Speed	30 ft/min				
Blow Up Ratio	2.25				
Layflat	8.8 in				
Thickness	mil	1.2	1.2	1.2	1.45
Frostline Height	inches	14	14	14	within plenum
Cooling Air Temp.	75 °F				
Temp. of Withdrawn Air	Not measured				
Cocurrent Flow Rate	103 ft³/min				
Countercurrent Flow Rate	varied ft³/min	162	200	272	272
Rows of Openings on Shroud	varied	5 open and 0 closed and 5 closed and 0 open			
Plenum Position	highest (covers two uppermost rows of openings)				

EXTRUSION CONDITIONS

Material   U.C. DFDY 3312 HP-LDPE
Extruder   1 inch diameter, 24:1 L/D screw
Die   2.5 inch spider
Die Gap   23 mils
Screen Pack   40-80-80-40 mesh

Extrusion Parameters	Set Conditions	Trial 1	Trial 2	Trial 3	Trial 4
Extruder Temperatures					
Zone 1	325°F (163°C)				
Zone 2	335°F (168°C)				
Die Temperatures					
Zone 1	350°F (177°C)				
Zone 2	360°F (182°C)				
Melt Temperature	401°F (205°C)				
Screw Speed	varied rpm	50	60	50	60
Back Pressure	psi	3100	3300	3100	3300
Output	lb/hr	16.8	20.2	16.8	20.2
Film Speed	30 ft/min				
Blow Up Ratio	2.25				
Layflat	8.8 in				
Thickness	mil	1.2	1.45	1.2	1.45
Frostline Height	inches	13	within plenum	13	within plenum
Cooling Air Temp.	75 °F				
Temp. of Withdrawn Air	Not measured				
Cocurrent Flow Rate	123 ft^3/min				
Countercurrent Flow Rate	varied ft^3/min	162	162	272	272
Rows of Openings on Shroud	varied	5 open and 0 closed and 5 closed and 0 open			
Plenum Position	highest (covers two uppermost rows of openings)				

EXTRUSION CONDITIONS

Material   U.C. DFDY 3312 HP-LDPE
Extruder   1 inch diameter, 24:1 L/D screw
Die   2.5 inch spider
Die Gap   23 mils
Screen Pack   40-80-80-40 mesh

Extrusion Parameters	Set Conditions	Trial 1	Trial 2	Trial 3	Trial 4
Extruder Temperatures					
Zone 1	$325^{\circ}F$ $(163^{\circ}C)$				
Zone 2	$335^{\circ}F$ $(168^{\circ}C)$				
Die Temperatures					
Zone 1	$350^{\circ}F$ $(177^{\circ}C)$				
Zone 2	$360^{\circ}F$ $(182^{\circ}C)$				
Melt Temperature	$401^{\circ}F$ $(205^{\circ}C)$				
Screw Speed	varied rpm	50	50	60	50
Back Pressure	psi	3100	3100	3300	3100
Output	lb/hr	16.8	16.8	20.2	16.8
Film Speed	35 ft/min				
Blow Up Ratio	2.25				
Layflat	8.8 in				
Thickness	mil	1.0	1.0	1.2	1.0
Frostline Height	inches	14	14	within plenum	14
Cooling Air Temp.	75 $^{\circ}F$				
Temp. of Withdrawn Air	Not measured				
Cocurrent Flow Rate	103 ft^3/min				
Countercurrent Flow Rate	varied ft^3/min	162	200	200	272
Rows of Openings on Shroud	varied	5 open and 0 closed and 5 closed and 0 open			
Plenum Position	highest (covers two uppermost rows of openings)				

EXTRUSION CONDITIONS

Material	U.C. DFDY 3312 HP-LDPE
Extruder	1 inch diameter, 24:1 L/D screw
Die	2.5 inch spider
Die Gap	23 mils
Screen Pack	40-80-80-40 mesh

Extrusion Parameters	Set Conditions	Trial 1	Trial 2	Trial 3	Trial 4
Extruder Temperatures					
Zone 1	325°F (163°C)				
Zone 2	335°F (168°C)				
Die Temperatures					
Zone 1	350°F (177°C)				
Zone 2	360°F (182°C)				
Melt Temperature	401°F (205°C)				
Screw Speed	varied rpm	50	60	50	60
Back Pressure	psi	3100	3300	3100	3300
Output	lb/hr	16.8	20.2	16.8	20.2
Film Speed	35 ft/min				
Blow Up Ratio	2.25				
Layflat	8.8 in				
Thickness	mil	1.0	1.2	1.0	1.2
Frostline Height	inches	13	within plenum	13	unstable
Cooling Air Temp.	75 °F				
Temp. of Withdrawn Air	Not measured				
Cocurrent Flow Rate	123 ft^3/min				
Countercurrent Flow Rate	varied ft^3/min	162	162	272	272
Rows of Openings on Shroud	varied	5 open and 5 closed	0 closed and 0 open		
Plenum Position	highest (covers two uppermost rows of openings)				

EXTRUSION CONDITIONS

Material	U.C. DFDY 3312 HP-LDPE
Extruder	1 inch diameter, 24:1 L/D screw
Die	2.5 inch spider
Die Gap	23 mils
Screen Pack	40-80-80-40 mesh

Extrusion Parameters	Set Conditions	Trial 1	Trial 2	Trial 3	Trial 4
Extruder Temperatures					
Zone 1	325°F (163°C)				
Zone 2	335°F (168°C)				
Die Temperatures					
Zone 1	350°F (177°C)				
Zone 2	360°F (182°C)				
Melt Temperature	401°F (205°C)				
Screw Speed	varied rpm	50	60	50	50
Back Pressure	psi	3100	3300	3100	3100
Output	lb/hr	16.8	20.2	16.8	16.8
Film Speed	25 ft/min				
Blow Up Ratio	2.5				
Layflat	9.8 in				
Thickness	mil	1.45	1.75	1.45	1.45
Frostline Height	inches	13	15	13	13
Cooling Air Temp.	75 °F				
Temp. of Withdrawn Air	Not measured				
Cocurrent Flow Rate	103 ft³/min				
Countercurrent Flow Rate	varied ft³/min	162	162	200	272
Rows of Openings on Shroud	varied	5 open and 0 closed and 5 closed and 0 open			
Plenum Position	highest (covers two uppermost rows of openings)				

EXTRUSION CONDITIONS

Material	U.C. DFDY 3312 HP-LDPE
Extruder	1 inch diameter, 24:1 L/D screw
Die	2.5 inch spider
Die Gap	23 mils
Screen Pack	40-80-80-40 mesh

Extrusion Parameters	Set Conditions	Trial 1	Trial 2	Trial 3	Trial 4
Extruder Temperatures					
Zone 1	325°F (163°C)				
Zone 2	335°F (168°C)				
Die Temperatures					
Zone 1	350°F (177°C)				
Zone 2	360°F (182°C)				
Melt Temperature	401°F (205°C)				
Screw Speed	varied	50	60	50	60
Back Pressure	psi	3100	3300	3100	3300
Output	lb/hr	16.8	20.2	16.8	20.2
Film Speed	25 ft/min				
Blow Up Ratio	2.5				
Layflat	9.8 in				
Thickness	mil	1.45	1.75	1.45	1.75
Frostline Height	inches	12	14	12	14
Cooling Air Temp.	75 °F				
Temp. of Withdrawn Air	Not measured				
Cocurrent Flow Rate	123 ft^3/min				
Countercurrent Flow Rate	varied ft^3/min	162	162	272	272
Rows of Openings on Shroud	varied	5 open and 5 closed	0 closed and 0 open		
Plenum Position	highest (covers two uppermost rows of openings)				

EXTRUSION CONDITIONS

Material   U.C. DFDY 3312 HP-LDPE
Extruder   1 inch diameter, 24:1 L/D screw
Die   2.5 inch spider
Die Gap   23 mils
Screen Pack   40-80-80-40 mesh

Extrusion Parameters	Set Conditions	Trial 1	Trial 2	Trial 3	Trial 4
Extruder Temperatures					
Zone 1	325°F (163°C)				
Zone 2	335°F (168°C)				
Die Temperatures					
Zone 1	350°F (177°C)				
Zone 2	360°F (182°C)				
Melt Temperature	401°F (205°C)				
Screw Speed	varied rpm	50	50	50	60
Back Pressure	psi	3100	3100	3100	3300
Output	lb/hr	16.8	16.8	16.8	20.0
Film Speed	30 ft/min				
Blow Up Ratio	2.5				
Layflat	9.8 in				
Thickness	mil	1.25	1.25	1.25	1.5
Frostline Height	inches	14	14	14	unstable
Cooling Air Temp.	75°F				
Temp. of Withdrawn Air	Not measured				
Cocurrent Flow Rate	103 ft³/min				
Countercurrent Flow Rate	varied ft³/min	162	200	272	272
Rows of Openings on Shroud	varied	5 open and 0 closed and 5 closed and 0 open			
Plenum Position	highest (covers two uppermost rows of openings)				

EXTRUSION CONDITIONS

Material   U.C. DFDY 3312 HP-LDPE
Extruder   1 inch diameter, 24:1 L/D screw
Die   2.5 inch spider
Die Gap   23 mils
Screen Pack   40-80-80-40 mesh

Extrusion Parameters	Set Conditions	Trial 1	Trial 2	Trial 3	Trial 4
Extruder Temperatures					
Zone 1	325°F (163°C)				
Zone 2	335°F (168°C)				
Die Temperatures					
Zone 1	350°F (177°C)				
Zone 2	360°F (182°C)				
Melt Temperature	401°F (205°C)				
Screw Speed	varied	50	60	50	60
Back Pressure	psi	3100	3300	3100	3300
Output	lb/hr	16.8	20.2	16.8	20.2
Film Speed	30 ft/min				
Blow Up Ratio	2.5				
Layflat	9.8 in				
Thickness	mil	1.25	1.5	1.25	1.5
Frostline Height	inches	13	within plenum	13	unstable
Cooling Air Temp.	75 °F				
Temp. of Withdrawn Air	Not measured				
Cocurrent Flow Rate	123 ft³/min				
Countercurrent Flow Rate	varied ft³/min	162	162	272	272
Rows of Openings on Shroud	varied	5 open and 0 closed	and 5 closed and 0 open		
Plenum Position	highest (covers two uppermost rows of openings)				

EXTRUSION CONDITIONS

Material   U.C. DFDY 3312 HP-LDPE
Extruder   1 inch diameter, 24:1 L/D screw
Die   2.5 inch spider
Die Gap   23 mils
Screen Pack   40-80-80-40 mesh

Extrusion Parameters	Set Conditions	Trial 1	Trial 2	Trial 3	Trial 4
Extruder Temperatures					
Zone 1	325°F (163°C)				
Zone 2	335°F (168°C)				
Die Temperatures					
Zone 1	350°F (177°C)				
Zone 2	360°F (182°C)				
Melt Temperature	401°F (205°C)				
Screw Speed	varied rpm	50	50	50	60
Back Pressure	psi	3100	3100	3100	3300
Output	lb/hr	16.8	16.8	16.8	20.2
Film Speed	25 ft/min				
Blow Up Ratio	3.0				
Layflat	11.8 in				
Thickness	mil	1.3	1.3	1.3	1.6
Frostline Height	inches	12	12	12	unstable
Cooling Air Temp.	75 °F				
Temp. of Withdrawn Air	Not measured				
Cocurrent Flow Rate	103 ft^3/min				
Countercurrent Flow Rate	varied ft^3/min	162	200	272	272
Rows of Openings on Shroud	varied	5 open and 5 closed	0 closed and 0 open		
Plenum Position	highest (covers two uppermost rows of openings)				

EXTRUSION CONDITIONS

Material U.C. DFDY 3312 HP-LDPE
Extruder 1 inch diameter, 24:1 L/D screw
Die 2.5 inch spider
Die Gap 23 mils
Screen Pack 40-80-80-40 mesh

Extrusion Parameters	Set Conditions	Trial 1	Trial 2	Trial 3	Trial 4
Extruder Temperatures					
Zone 1	325°F (163°C)				
Zone 2	335°F (168°C)				
Die Temperatures					
Zone 1	350°F (177°C)				
Zone 2	360°F (182°C)				
Melt Temperature	401°F (205°C)				
Screw Speed	varied rpm	50	60	50	60
Back Pressure	psi	3100	3300	3100	3300
Output	lb/hr	16.8	20.2	16.8	20.2
Film Speed	25 ft/min				
Blow Up Ratio	3.0				
Layflat	11.8 in				
Thickness	mil	1.3	1.6	1.3	1.6
Frostline Height	inches	11	13	11	unstable
Cooling Air Temp.	75 °F				
Temp. of Withdrawn Air	Not measured				
Cocurrent Flow Rate	123 ft^3/min				
Countercurrent Flow Rate	varied ft^3/min	162	162	272	272
Rows of Openings on Shroud	varied	5 open and 0 closed and 5 closed and 0 open			
Plenum Position	highest (covers two uppermost rows of openings)				

EXTRUSION CONDITIONS

Material   U.C. DFDY 3312 HP-LDPE
Extruder   1 inch diameter, 24:1 L/D screw
Die   2.5 inch spider
Die Gap   23 mils
Screen Pack   40-80-80-40 mesh

Extrusion Parameters	Set Conditions	Trial 1	Trial 2	Trial 3	Trial 4
Extruder Temperatures					
Zone 1	325°F (163°C)				
Zone 2	335°F (168°C)				
Die Temperatures					
Zone 1	350°F (177°C)				
Zone 2	360°F (182°C)				
Melt Temperature	401°F (205°C)				
Screw Speed	varied rpm	50	50	50	60
Back Pressure	psi	3100	3100	3100	3300
Output	lb/hr	16.8	16.8	16.8	20.2
Film Speed	30 ft/min				
Blow Up Ratio	3.0				
Layflat	11.8 in				
Thickness	mil	1.1	1.1	1.1	1.3
Frostline Height	inches	13	13	13	unstable
Cooling Air Temp.	75 °F				
Temp. of Withdrawn Air	Not measured				
Cocurrent Flow Rate	103 ft³/min				
Countercurrent Flow Rate	varied ft³/min	162	200	272	272
Rows of Openings on Shroud	varied	5 open and 0 closed and 5 closed and 0 open			
Plenum Position	highest (covers two uppermost rows of openings)				

EXTRUSION CONDITIONS

Material   U.C. DFDY 3312 HP-LDPE
Extruder   1 inch diameter, 24:1 L/D screw
Die   2.5 inch spider
Die Gap   23 mils
Screen Pack*   40-80-80-40 mesh

Extrusion Parameters	Set Conditions	Trial 1	Trial 2	Trial 3	Trial 4
Extruder Temperatures					
Zone 1	325°F (163°C)				
Zone 2	335°F (168°C)				
Die Temperatures					
Zone 1	350°F (177°C)				
Zone 2	360°F (182°C)				
Melt Temperature	401°F (205°C)				
Screw Speed	varied rpm	50	60	50	60
Back Pressure	psi	3100	3300	3100	3300
Output	lb/hr	16.8	20.2	16.8	20.2
Film Speed	30 ft/min				
Blow Up Ratio	3.0				
Layflat	11.8 in				
Thickness	mil	1.1	1.3	1.1	1.3
Frostline Height	inches	12	14	12	unstable
Cooling Air Temp.	75 °F				
Temp. of Withdrawn Air	Not measured				
Cocurrent Flow Rate	123 ft^3/min				
Countercurrent Flow Rate	varied ft^3/min 162	162	272	272	
Rows of Openings on Shroud	varied	5 open and 0 closed and 5 closed and 0 open			
Plenum Position	highest (covers two uppermost rows of openings)				

EXTRUSION CONDITIONS

Material   U.C. DFDY 3312 HP-LDPE
Extruder   1 inch diameter, 24:1 L/D screw
Die   2.5 inch spider
Die Gap   23 mils
Screen Pack   40-80-80-40 mesh

Extrusion Parameters	Set Conditions	Trial 1	Trial 2	Trial 3	Trial 4
Extruder Temperatures					
Zone 1	325°F (163°C)				
Zone 2	335°F (168°C)				
Die Temperatures					
Zone 1	350°F (177°C)				
Zone 2	360°F (182°C)				
Melt Temperature	401°F (205°C)				
Screw Speed	varied rpm	50	55	50	50
Back Pressure	psi	3100	3200	3100	3100
Output	lb/hr	16.8	18.5	16.8	16.8
Film Speed	25 ft/min				
Blow Up Ratio	2.25				
Layflat	8.8 in				
Thickness	Film bubble could not be formed.				
Frostline Height	Film bubble could not be formed.				
Cooling Air Temp.	75 °F				
Temp. of Withdrawn Air					
Cocurrent Flow Rate	103 ft³/min				
Countercurrent Flow Rate	varied ft³/min	126	126	126	162
Rows of Openings on Shroud	varied	0 open,	5 closed	5 open,	0 closed
Plenum Position	lowest (covers two lowermost rows of openings)				

EXTRUSION CONDITIONS

Material   U.C. DFDY 3312 HP-LDPE
Extruder   1 inch diameter, 24:1 L/D screw
Die   2.5 inch spider
Die Gap   23 mils
Screen Pack   40-80-80-40 mesh

Extrusion Parameters	Set Conditions	Trial 1	Trial 2	Trial 3	Trial 4
Extruder Temperatures					
Zone 1	325°F (163°C)				
Zone 2	335°F (168°C)				
Die Temperatures					
Zone 1	350°F (177°C)				
Zone 2	360°F (182°C)				
Melt Temperature	401°F (205°C)				
Screw Speed	varied rpm	50	55	50	55
Back Pressure	psi	3100	3200	3100	3200
Output	lb/hr	16.8	18.5	16.8	18.5
Film Speed	25 ft/min				
Blow Up Ratio	2.25				
Layflat	8.8 in				
Thickness	Film bubble could not be formed.				
Frostline Height	Film bubble could not be formed.				
Cooling Air Temp.	75 °F				
Temp. of Withdrawn Air					
Cocurrent Flow Rate	103 ft³/min				
Countercurrent Flow Rate	126 ft³/min				
Rows of Openings on Shroud	varied	5 open	0 closed	0 open	5 closed
Plenum Position	Rows 2 and 3 (above the die) covered by plenum				

EXTRUSION CONDITIONS

Material   U.C. DFDY 3312 HP-LDPE
Extruder   1 inch diameter, 24:1 L/D screw
Die   2.5 inch spider
Die Gap   23 mils
Screen Pack   40-80-80-40 mesh

Extrusion Parameters	Set Conditions	Trial 1	Trial 2	Trial 3	Trial 4
Extruder Temperatures					
Zone 1	325°F (163°C)				
Zone 2	335°F (168°C)				
Die Temperatures					
Zone 1	350°F (177°C)				
Zone 2	360°F (182°C)				
Melt Temperature	401°F (205°C)				
Screw Speed	50 rpm				
Back Pressure	3100 psi				
Output	16.8 lb/hr				
Film Speed	25 ft/min				
Blow Up Ratio	2.25				
Layflat	8.8 in				
Thickness	1.6 mil				
Frostline Height	inches	11	12		
Cooling Air Temp.	75 °F				
Temp. of Withdrawn Air					
Cocurrent Flow Rate	varied ft^3/min	103	123		
Countercurrent Flow Rate					
Film Temp. Above Plenum (22 in above die)	°F	227	211		
Film Temp. Below Plenum (12 in above die)	°F	240	240		
Rows of Openings on Shroud	5 open 0 closed				
Plenum Position	highest (covers two uppermost rows of openings) (16 - 22 in above die)				

EXTRUSION CONDITIONS

Material   U.C. DFDY 3312 HP-LDPE
Extruder   1 inch diameter, 24:1 L/D screw
Die   2.5 inch spider
Die Gap   23 mils
Screen Pack 40-80-80-40 mesh

Extrusion Parameters	Set Conditions	Trial 1	Trial 2	Trial 3	Trial 4
Extruder Temperatures					
Zone 1	325°F (163°C)				
Zone 2	335°F (168°C)				
Die Temperatures					
Zone 1	350°F (177°C)				
Zone 2	360°F (182°C)				
Melt Temperature	401°F (205°C)				
Screw Speed	50 rpm				
Back Pressure	3100 psi				
Output	16.8 lb/hr				
Film Speed	25 ft/min				
Blow Up Ratio	2.25				
Layflat	8.8 in				
Thickness	1.6 mil				
Frostline Height	inches	11	12	11	12
Cooling Air Temp.	75 °F				
Temp. of Withdrawn Air					
Cocurrent Flow Rate	varied ft^3/min	103	123	103	123
Countercurrent Flow Rate	0 ft^3/min				
Film Temp. Above Plenum (22 in above die) °F		227	211	232	215
Film Temp. Below Plenum (12 in above die) °F		240	240	240	240
Rows of Openings on Shroud	varied	5 open	0 closed	0 open	5 closed
Plenum Position	highest (covers two uppermost rows of openings) (16 - 22 in above die)				

EXTRUSION CONDITIONS

Material   U.C. DFDY 3312 HP-LDPE
Extruder   1 inch diameter, 24:1 L/D screw
Die   2.5 inch spider
Die Gap   23 mils
Screen Pack   40-80-80-40 mesh

Extrusion Parameters	Set Conditions	Trial 1	Trial 2	Trial 3	Trial 4
Extruder Temperatures					
Zone 1	325°F (163°C)				
Zone 2	335°F (168°C)				
Die Temperatures					
Zone 1	350°F (177°C)				
Zone 2	360°F (182°C)				
Melt Temperature	401°F (205°C)				
Screw Speed	50 rpm				
Back Pressure	3100 psi				
Output	16.8 lb/hr				
Film Speed	25 ft/min				
Blow Up Ratio	2.25				
Layflat	8.8 in				
Thickness	1.6 mil				
Frostline Height	inches	12	12	12	12
Cooling Air Temp.	75 °F				
Temp. of Withdrawn Air °F			93	Not measured.	
Cocurrent Flow Rate	103 ft³/min				
Countercurrent Flow Rate	varied ft³/min	0	162	0	162
Film Temp. Above Plenum (22 in above die) °F		227	225	225	225
Film Temp. Below Plenum (12 in above die) °F		240	240	240	240
Rows of Openings on Shroud	varied	5 open	0 closed	2 open (near plenum) 3 closed (near die)	
Plenum Position	highest (covers two uppermost rows of openings) (16 - 22 in above die)				

EXTRUSION CONDITIONS

Material   U.C. DFDY 3312 HP-LDPE
Extruder   1 inch diameter, 24:1 L/D screw
Die   2.5 inch spider
Die Gap   23 mils
Screen Pack   40-80-80-40 mesh

Extrusion Parameters	Set Conditions	Trial 1	Trial 2	Trial 3	Trial 4
Extruder Temperatures					
Zone 1	325°F (163°C)				
Zone 2	335°F (168°C)				
Die Temperatures					
Zone 1	350°F (177°C)				
Zone 2	360°F (182°C)				
Melt Temperature	401°F (205°C)				
Screw Speed	50 rpm				
Back Pressure	3100 psi				
Output	16.8 lb/hr				
Film Speed	25 ft/min				
Blow Up Ratio	2.25				
Layflat	8.8 in				
Thickness	1.6 mil				
Frostline Height	inches	12	12	12	12
Cooling Air Temp.	75 °F				
Temp. of Withdrawn Air °F		Not measured.		91	90
Cocurrent Flow Rate	103 ft^3/min				
Countercurrent Flow Rate	varied ft^3/min	0	162	200	272 ✝
Film Temp. Above Plenum (22 in above die) °F		226	227	225	226
Film Temp. Below Plenum (12 in above die) °F		240	240	240	240
Rows of Openings on Shroud	varied	2 open(near die) 3 closed(near plenum)		5 open 0 closed	
Plenum Position	highest (covers two uppermost rows of openings) (16 - 22 in above die)				

EXTRUSION CONDITIONS

Material   U.C. DFDY 3312 HP-LDPE
Extruder   1 Inch diameter, 24:1 L/D screw
Die   2.5 Inch spider
Die Gap   23 mils
Screen Pack   40-80-80-40 mesh

Extrusion Parameters	Set Conditions	Trial 1	Trial 2	Trial 3	Trial 4
Extruder Temperatures					
Zone 1	325°F (163°C)				
Zone 2	335°F (168°C)				
Die Temperatures					
Zone 1	350°F (177°C)				
Zone 2	360°F (182°C)				
Melt Temperature	401°F (205°C)				
Screw Speed	50 rpm				
Back Pressure	3100 psi				
Output	16.8 lb/hr				
Film Speed	25 ft/min				
Blow Up Ratio	2.25				
Layflat	8.8 in				
Thickness	1.6 mil				
Frostline Height	inches	12	12	12	
Cooling Air Temp.	75 °F				
Temp. of Withdrawn Air	°F		99	95	
Cocurrent Flow Rate	103 ft^3/min				
Countercurrent Flow Rate	varied ft^3/min	0	126	162	
Film Temp. Above Plenum (22 in above die) °F		232	236	228	
Film Temp. Below Plenum (12 in above die) °F		240	240	240	
Rows of Openings on Shroud	0 open 5 closed				
Plenum Position	highest (covers two uppermost rows of openings) (16 - 22 in above die)				

EXTRUSION CONDITIONS

Material — U.C. DFDY 3312 HP-LDPE
Extruder — 1 inch diameter, 24:1 L/D screw
Die — 2.5 inch spider
Die Gap — 23 mils
Screen Pack — 40-80-80-40 mesh

Extrusion Parameters	Set Conditions	Trial 1	Trial 2	Trial 3	Trial 4
Extruder Temperatures					
Zone 1	325°F (163°C)				
Zone 2	335°F (168°C)				
Die Temperatures					
Zone 1	350°F (177°C)				
Zone 2	360°F (182°C)				
Melt Temperature	401°F (205°C)				
Screw Speed	50 rpm				
Back Pressure	3100 psi				
Output	16.8 lb/hr				
Film Speed	25 ft/min				
Blow Up Ratio	2.25				
Layflat	8.8 in				
Thickness	1.6 mil				
Frostline Height	inches	12	12	12	12
Cooling Air Temp.	75 °F				
Temp. of Withdrawn Air	Not measured				
Cocurrent Flow Rate	103 ft^3/min				
Countercurrent Flow Rate	varied ft^3/min	200	268	200	268
Film Temp. Above Plenum (22 in above die) °F		225	225	226	225
Film Temp. Below Plenum (12 in above die) °F		240	240	240	240
Rows of Openings on Shroud	varied	2 open(near plenum) 3 closed(near die)		2 open(near die) 3 closed(near plenum)	
Plenum Position	highest (covers two uppermost rows of openings) (16 - 22 in above die)				

EXTRUSION CONDITIONS

Material   U.C. DFDY 3312 HP-LDPE
Extruder   1 inch diameter, 24:1 L/D screw
Die   2.5 inch spider
Die Gap   23 mils
Screen Pack   40-80-80-40 mesh

Extrusion Parameters	Set Conditions	Trial 1	Trial 2	Trial 3	Trial 4
Extruder Temperatures					
Zone 1	325°F (163°C)				
Zone 2	335°F (168°C)				
Die Temperatures					
Zone 1	350°F (177°C)				
Zone 2	360°F (182°C)				
Melt Temperature	401°F (205°C)				
Screw Speed	50 rpm				
Back Pressure	3100 psi				
Output	16.8 lb/hr				
Film Speed	25 ft/min				
Blow Up Ratio	2.25				
Layflat	8.8 in				
Thickness	1.6 mil				
Frostline Height	inches	12	12	11	11
Cooling Air Temp.	75 °F				
Temp. of Withdrawn Air	F	90	85		91
Cocurrent Flow Rate	varied ft^3/min	103	103.	123	123
Countercurrent Flow Rate	varied ft^3/min	200	272	0	162
Film Temp. Above Plenum (22 in above die) °F		220	204	211	210
Film Temp. Below Plenum (12 in above die) °F		240	240	240	240
Rows of Openings on Shroud	varied	0 open,	5 closed	5 open,	0 closed
Plenum Position	highest (covers two uppermost rows of openings) (16 - 22 in above die)				

EXTRUSION CONDITIONS

Material U.C. DFDY 3312 HP-LDPE
Extruder 1 inch diameter, 24:1, L/D screw
Die 2.5 inch spider
Die Gap 23 mils
Screen Pack 40-80-80-40 mesh

Extrusion Parameters	Set Conditions	Trial 1	Trial 2	Trial 3	Trial 4
Extruder Temperatures					
Zone 1	$325^\circ F$ ($163^\circ C$)				
Zone 2	$335^\circ F$ ($168^\circ C$)				
Die Temperatures					
Zone 1	$350^\circ F$ ($177^\circ C$)				
Zone 2	$360^\circ F$ ($182^\circ C$)				
Melt Temperature	$401^\circ F$ ($205^\circ C$)				
Screw Speed	50 rpm				
Back Pressure	3100 psi				
Output	16.8 lb/hr				
Film Speed	25 ft/min				
Blow Up Ratio	2.25				
Layflat	8.8 in				
Thickness	1.6 mil				
Frostline Height	inches	11	11	11	11
Cooling Air Temp.	75 $^\circ F$				
Temp. of Withdrawn Air	Not measured				
Cocurrent Flow Rate	123 ft^3/min				
Countercurrent Flow Rate	varied ft^3/min	0	162	0	162
Film Temp. Above Plenum (22 in above die) $^\circ F$		226	224	225	224
Film Temp. Below Plenum (12 in above die) $^\circ F$		240	240	240	240
Rows of Openings on Shroud	varied	2 open(near plenum) 3 closed (near die)		2 open(near die) 3 closed(near plenum)	
Plenum Position	Highest (covers two uppermost rows of openings) (16 - 22 in above die)				

EXTRUSION CONDITIONS

Material   U.C. DFDY 3312 HP-LDPE
Extruder   1 inch diameter, 24:1 L/D screw
Die   2.5 inch spider
Die Gap   23 mils
Screen Pack   40-80-80-40 mesh

Extrusion Parameters	Set Conditions	Trial 1	Trial 2	Trial 3	Trial 4
Extruder Temperatures					
Zone 1	325°F (163°C)				
Zone 2	335°F (168°C)				
Die Temperatures					
Zone 1	350°F (177°C)				
Zone 2	360°F (182°C)				
Melt Temperature	401°F (205°C)				
Screw Speed	50 rpm				
Back Pressure	3100 psi				
Output	16.8 lb/hr				
Film Speed	25 ft/min				
Blow Up Ratio	2.25				
Layflat	8.8 in				
Thickness	1.6 mil				
Frostline Height	inches	11	11	11	11
Cooling Air Temp.	75 °F				
Temp. of Withdrawn Air	Not measured.				
Cocurrent Flow Rate	123 ft^3/min				
Countercurrent Flow Rate	varied ft^3/min	200	272	200	272
Film Temp. Above Plenum (22 in above die) °F		225	224	225	225
Film Temp. Below Plenum (12 in above die) °F		240	240	240	240
Rows of Openings on Shroud	varied	2 open(near plenum) 3 closed(near die)		2 open(near die) 3 closed(near plenum)	
Plenum Position	highest (covers two uppermost rows of openings) (16 - 22 in above die)				

EXTRUSION CONDITIONS

Material   U.C. DFDY 3312 HP-LDPE
Extruder   1 inch diameter, 24:1 L/D screw
Die   2.5 inch spider
Die Gap   23 mils
Screen Pack   40-80-80-40 mesh

Extrusion Parameters	Set Conditions	Trial 1	Trial 2	Trial 3	Trial 4
Extruder Temperatures					
Zone 1	325°F (163°C)				
Zone 2	335°F (168°C)				
Die Temperatures					
Zone 1	350°F (177°C)				
Zone 2	360°F (182°C)				
Melt Temperature	401°F (205°C)				
Screw Speed	50 rpm				
Back Pressure	3100 psi				
Output	16.8 lb/hr				
Film Speed	24 ft/min				
Blow Up Ratio	2.25				
Layflat	8.8 in				
Thickness	1.6 mil				
Frostline Height	inches	11	11	11	
Cooling Air Temp.	75 °F				
Temp. of Withdrawn Air	°F	86	82	82	
Cocurrent Flow Rate	123 ft³/min				
Countercurrent Flow Rate	varied ft³/min	200	268	272	
Film Temp. Above Plenum (22 in above die) °F		209	210	208	
Film Temp. Below Plenum (12 in above die) °F		240	240	240	
Rows of Openings on Shroud	5 open 0 closed				
Plenum Position	highest (covers two uppermost rows of openings) (16 - 22 in above die)				

EXTRUSION CONDITIONS

Material U.C. DFDY 3312 HP-LDPE
Extruder 1 inch diameter, 24:1 L/D screw
Die 2.5 inch spider
Die Gap 23 mils
Screen Pack 40-80-80-40 mesh

Extrusion Parameters	Set Conditions	Trial 1	Trial 2	Trial 3	Trial 4
Extruder Temperatures					
Zone 1	325°F (163°C)				
Zone 2	335°F (168°C)				
Die Temperatures					
Zone 1	350°F (177°C)				
Zone 2	360°F (182°C)				
Melt Temperature	401°F (205°C)				
Screw Speed	50 rpm				
Back Pressure	3100 psi				
Output	16.8 lb/hr				
Film Speed	25 ft/min				
Blow Up Ratio	2.25				
Layflat	8.8 in				
Thickness	1.6 mil				
Frostline Height	inches	11	11	11	
Cooling Air Temp.	75 °F				
Temp. of Withdrawn Air	°F		100	93	
Cocurrent Flow Rate	123 ft^3/min				
Countercurrent Flow Rate	varied ft^3/min	0	126	285	
Film Temp. Above Plenum (22 in above die) °F		215	218	209	
Film Temp. Below Plenum (12 in above die) °F		240	240	240	
Rows of Openings on Shroud	0 open 5 closed				
Plenum Position	highest (covers two uppermost rows of openings) (16 - 22 in above die)				

EXTRUSION CONDITIONS

Material | U.C. DFDY 3312 HP-LDPE
Extruder | 1 inch diameter, 24:1 L/D screw
Die | 2.5 inch spider
Die Gap | 23 mils
Screen Pack | 40-80-80-40 mesh

Extrusion Parameters	Set Conditions	Trial 1	Trial 2	Trial 3	Trial 4
Extruder Temperatures					
Zone 1	325°F (163°C)				
Zone 2	335°F (168°C)				
Die Temperatures					
Zone 1	350°F (177°C)				
Zone 2	360°F (182°C)				
Melt Temperature	401°F (205°C)				
Screw Speed	50 rpm				
Back Pressure	3100 psi				
Output	16.8 lb/hr				
Film Speed	25 ft/min				
Blow Up Ratio,	2.25				
Layflat	8.8 in				
Thickness	1.6 mil				
Frostline Height	inches	11	11	11	
Cooling Air Temp.	75 °F				
Temp. of Withdrawn Air	°F 90	87	86		
Cocurrent Flow Rate	123 ft^3/min				
Countercurrent Flow Rate	varied ft^3/min 200	268	272		
Film Temp. Above Plenum (22 in above die) °F		198	192	190	
Film Temp. Below Plenum (12 in above die) °F		240	240	240	
Rows of Openings on Shroud	0 open 5 closed				
Plenum Position	highest (covers two uppermost rows of openings) (16 -22 in above die)				

APPENDIX C

Equipment Drawings

Figure C7: Solid Cylindrical Shroud.

10.4in. Diameter

24in. Height

Side View

10.4 inch
Cylindrical Diameter

Top View

12.4in. Flare Diameter
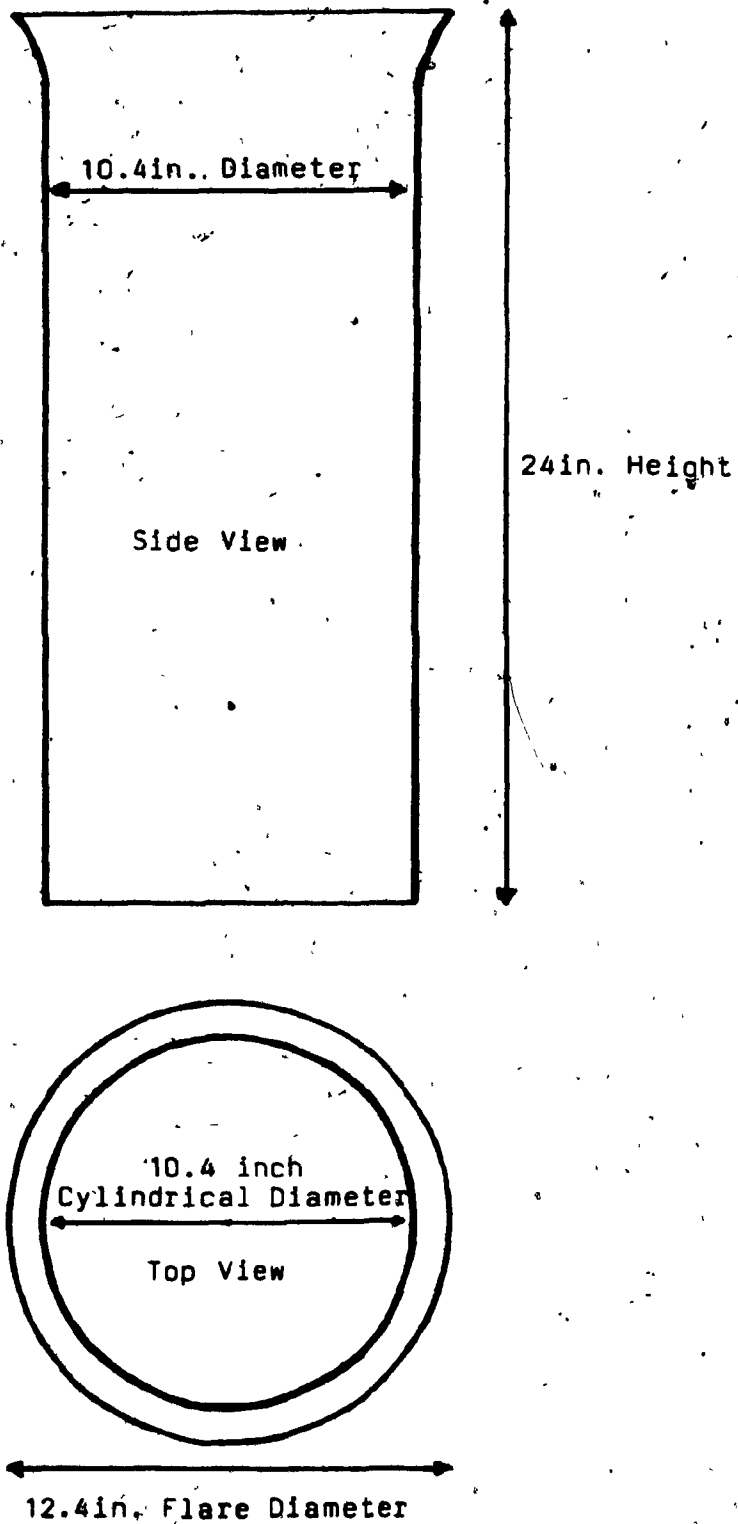
Figure C2: Modified Cylindrical Shroud.
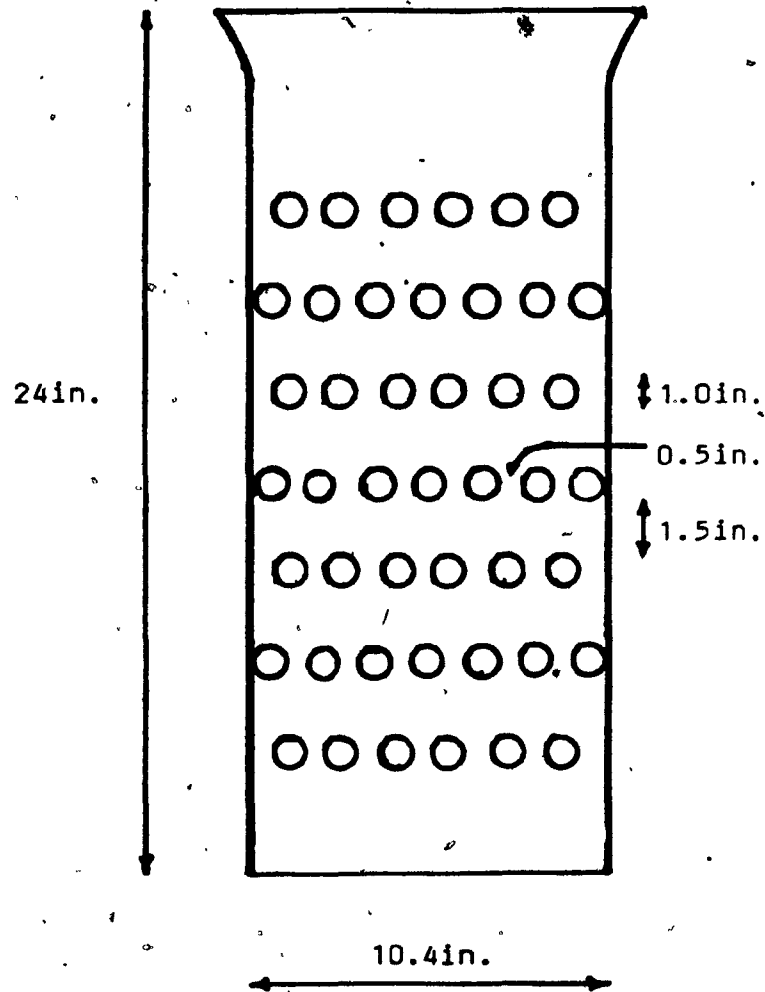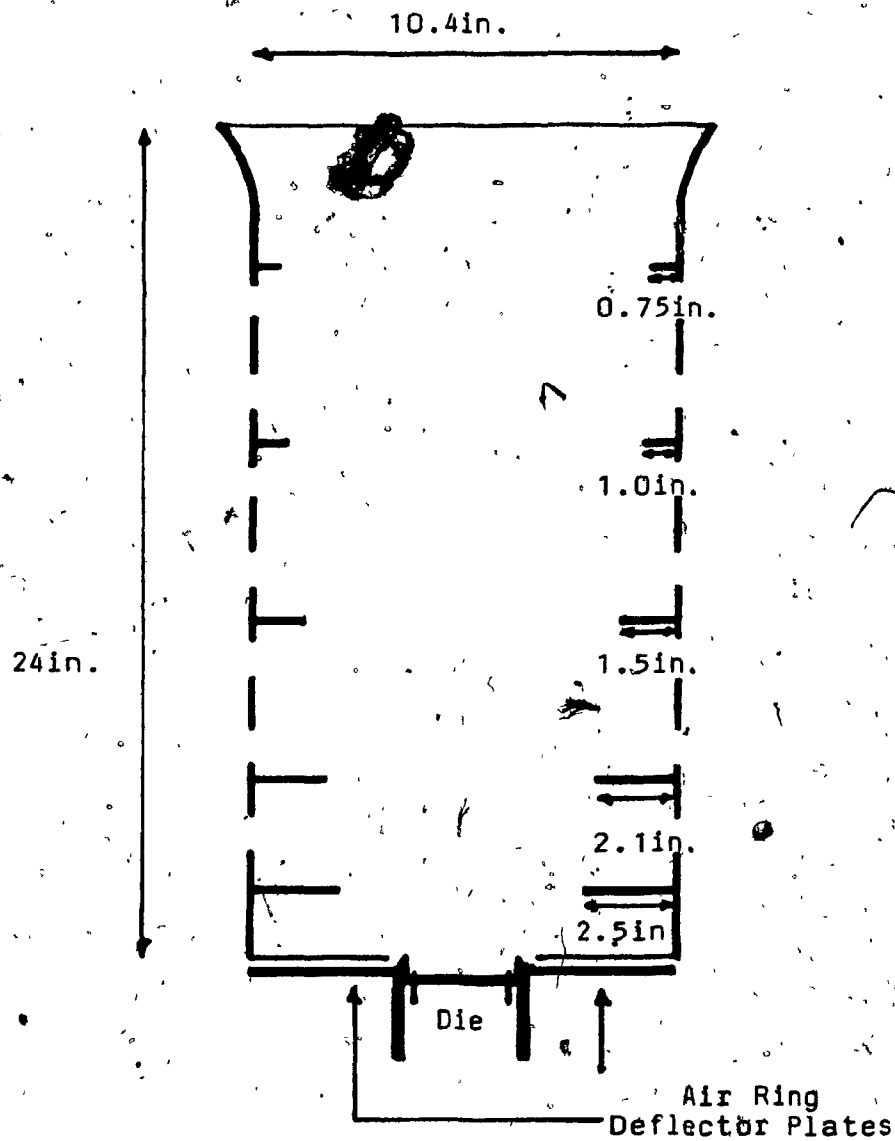
Figure C3: Cutaway View of Cylindrical Shroud
Showing Deflector Plates
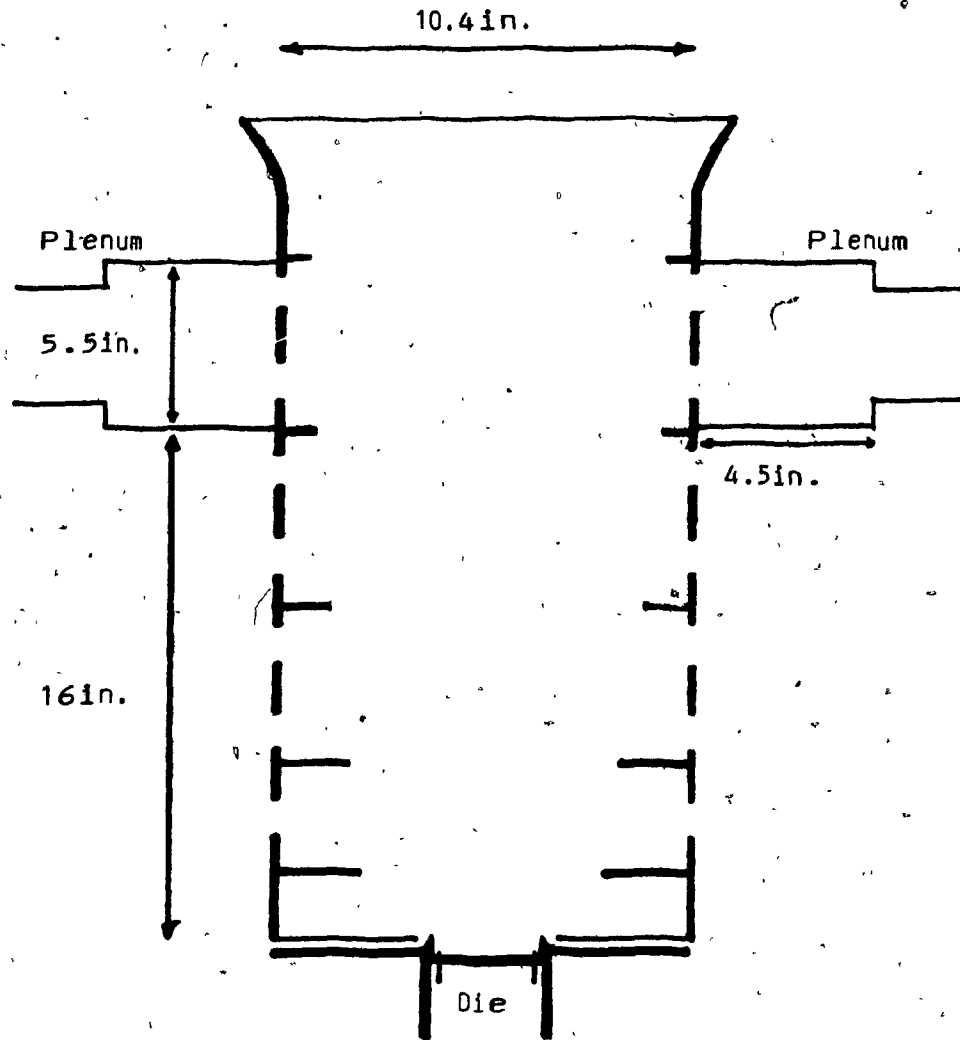
Figure C4: Cutaway View of Cylindrical Shroud
Showing Cooling Air Withdrawl Plenum

APPENDIX D

Dependent Variable Measurements

APPENDIX D1

Air Flow Rate Determination

Cocurrent Cooling

Number of Readings from Duct Wall	Pitot Tube Position from Duct Wall (inches)	Cases 1 and 3		Cases 8 and 9	
		Δl (mm)	U (ft/s)	Δl (mm)	U (ft/s)
1	0.10	4.75	8.67	7.0	10.53
2	0.42	5.5	9.33	7.75	11.08
3	0.84	6.25	9.95	8.5	11.6
4	1.19	6.5	10.14	8.75	11.77
5	1.99	7.0	10.53	9.0	11.94
6	3.51	7.0	10.53	9.5	12.27
7	4.31	6.5	10.14	9.25	12.10
8	4.76	6.0	9.74	8.75	11.77
9	5.08	5.5	9.33	8.0	11.26
10	5.40	4.25	8.2	7.0	10.53
Total Flow Rate ($Q = \overline{U}$ × Duct Area)		103 cfm		123 cfm	

Note: Δl is the distance that manometer fluid has risen in a slanted arm manometer. To obtain velocity the equation $U = (2(\Delta l \sin\Phi)\rho_m g / \rho_{air})^{\frac{1}{2}}$ is used. (See Section 5.5.)

Countercurrent Cooling Cases 3 and 10

Number of Readings	Pitot Tube Position from Duct Wall (inches)	Traverse 1		Traverse 2		Traverse 3		Traverse 4	
		Δl(mm)	U(ft/s)	Δl(mm)	U(ft/s)	Δl(mm)	U(ft/s)	Δl(mm)	U(ft/s)
1	0.10	2.0	5.63	5.0	8.90	6.0	9.75	7.0	10.53
2	0.38	7.0	10.53	6.0	9.75	7.0	10.53	9.0	11.94
3	0.77	19	17.35	16	15.92	13	14.35	16	15.92
4	1.09	22	18.67	19	17.35	18	16.89	20	17.80
5	1.81	22	18.67	27	20.68	28	21.06	22	18.67
6	3.20	21	18.24	28	21.06	23	19.09	20	17.80
7	3.92	21	18.24	20	17.35	21	18.24	21	18.24
8	4.24	15	15.41	18	16.89	19	17.35	16	15.92
9	4.62	7.0	10.53	18	16.89	18	16.89	16	15.92
10	4.91	5.0	8.90	5.0	8.90	8.0	11.26	10	12.59

Average Total Flow Rate = 126 cfm

Note: The identical Pitot tube positions from the duct wall were used in all countercurrent cooling flow rate determinations that appear in the following three tables.

Countercurrent Cooling Cases 4 and 11

Traverse 1		Traverse 2		Traverse 3		Traverse 4	
Δl(mm)	U(ft/s)	Δl(mm)	U(ft/s)	Δl(mm)	U(ft/s)	Δl(mm)	U(ft/s)
7	10.53	12	13.78	21	18.24	24	19.50
11	13.20	14	14.89	20	17.80	26	20.29
15	15.40	19	17.35	27	20.68	30	21.80
19	17.35	24	19.50	29	21.43	34	23.21
29	21.43	24	19.48	34	23.21	41	25.48
64	31.84	58	30.31	38	24.53	48	27.57
77	34.92	62	31.34	44	26.40	30	21.80
46	26.99	35	23.55	26	20.29	14	14.89
26	20.29	20	17.80	20	17.80	12	13.79
21	18.24	15	15.41	15	15.41	1	3.98

Average Velocity = 19.79 ft/s

Average Total Flow Rate = 162 cfm

Countercurrent Cooling Cases 5 and 12

| Traverse 1 | | Traverse 2 | | Traverse 3 | | Traverse 4 | |
Δl(mm)	U(ft/s)	Δl(mm)	U(ft/s)	Δl(mm)	U(ft/s)	Δl(mm)	U(ft/s)
2	5.36	16	15.92	23	19.09	35	23.55
10	12.59	19	17.35	30	21.80	40	25.17
13	14.35	16	15.92	32	22.51	41	25.48
20	17.80	24	19.50	33	22.86	43	26.10
43	26.10	39	24.86	28	21.06	46	26.99
81	35.82	57	30.05	50	28.14	47	27.86
100	39.80	78	35.15	53	28.97	33	22.86
110	41.74	90	37.76	53	28.97	20	17.80
54	29.25	89	37.55	55	29.52	15	15.41
14	14.89	73	34.00	44	26.40	5	8.90

Average Velocity = 24.38 ft/s

Average Total Flow Rate = 200 cfm

Countercurrent Cooling Cases 6 and 13

Traverse 1		Traverse 2		Traverse 3		Traverse 4	
Δl(mm)	U(ft/s)	Δl(mm)	U(ft/s)	Δl(mm)	U(ft/s)	Δl(mm)	U(ft/s)
10	12.59	15	15.41	69	33.06	100	39.80
15	15.40	22	18.67	73	34.01	102	40.20
16	15.92	36	23.88	66	32.33	94	38.59
24	19.50	47	27.29	59	30.57	91	38.00
65	32.09	66	32.33	44	26.40	84	36.48
142	47.42	104	40.59	85	36.69	55	29.52
189	54.72	151	48.91	98	39.40	50	28.14
210	57.68	179	53.25	100	39.80	27	20.68
69	33.06	160	50.34	118	43.23	18	16.89
13	14.35	133	45.90	94	38.59	9	11.94

Average Velocity = 32.84 ft/s

Average Total Flow Rate = 268 cfm

Countercurrent Cooling Cases 7 and 14

Traverse 1		Traverse 2		Traverse 3		Traverse 4	
Δl(mm)	U(ft/s)	Δl(mm)	U(ft/s)	Δl(mm)	U(ft/s)	Δl(mm)	U(ft/s)
11	13.20	17	16.41	71	33.54	108	41.36
15	15.41	24	19.50	77	34.92	111	41.93
15	15.41	40	25.17	69	33.06	98	39.40
25	19.90	51	28.42	62	31.34	94	38.59
68	32.82	72	33.77	47	27.29	86	36.91
152	49.07	110	41.74	92	38.17	55	29.52
200	56.29	159	50.19	103	40.39	25	19.90
220	59.03	186	54.28	105	40.78	20	17.80
82	36.04	174	52.50	123	44.14	17	16.41
10	12.59	136	46.41	97	39.20	6	9.75

Average Velocity = 33.3 ft/s

Average Total Flow Rate = 272 cfm

APPENDIX D2

Surface Temperature Measurements

Cocurrent Cooling

Height Above Die (inches)	Case 1 Cooling Conditions		Case 8 Cooling Conditions	
	Surface Temperature (°F)	Temperature Gradiant (dT_s/dz)	Surface Temperature (°F)	Temperature Gradiant (dT_s/dz)
3.4	384.0	1.20	380.0	1.32
4.0	375.0	1.60	370.0	1.87
5.4	343.7	2.48	322.0	4.36
6.0	326.1	2.44	298.5	3.30
7.0	309.5	2.40	275.2	1.88
8.0	286.4	1.86	257.0	1.09
9.0	270.5	1.23	241.0	0.68
10	255.7	1.04	240.6	0.36
11	240.9	0.49	240.0	0.00
12	240.1	0.20	240.0	0.00
13	240.4	0.00	238.3	0.16
14	240.2	0.00	236.2	0.23
15	239.2	0.00	231.6	0.40
16	239.0	0.15	228.6	0.49
17	236.0	0.28	224.0	0.53
18	231.0	0.45	218.6	0.62
19	224.6	0.55	212.0	0.62
20	219.0	0.55	205.0	0.58
21	216.0	0.44	200.0	0.49
22	211.8	0.27	196.8	0.38
23	207.5	0.24	193.5	0.33
24	204.5	0.22	188.0	0.26
25	203.0	0.21	185.9	0.20
26			184.7	0.09
27			183.7	0.09

Countercurrent Cooling

Surface Temperatures (°F) Under Different Cooling Conditions

Height Above Die (inches)	Case 2	Case 3	Case 4	Case 5	Case 6	Case 7
5.38	340.7	344.0	340.7	342.5	342.5	343.2
7.31	301.6	304.5	302.3	302.7	304.5	305.0
9.75	267.2	268.3	267.2	269.4	268.3	268.9
13.9	240.4	241.0	269.4	241.0	239.5	239.9
22.0	231.5	236.4	241.0	220.4	208.6	207.4
23.0	228.0	234.0	225.3	213.7	199.2	199.2
26.0	219.0	227.2	211.6	193.8	177.3	176.1
27.0	215.4	224.3	206.7	186.5	171.2	168.8

Countercurrent Cooling

Surface Temperatures (°F) Under Different Cooling Conditions

Height Above Die (inches)	Case 9	Case 10	Case 11	Case 12	Case 13	Case 14
5.38	320.0	323.1	318.3	316.4	321.3	317.9
7.31	272.4	276.3	270.0	268.9	272.7	268.2
9.75	239.5	239.5	239.6	239.8	239.5	240.3
13.9	238.7	239.5	239.6	239.8	239.5	236.1
22.0	215.0	219.4	208.6	198.4	192.0	190.8
23.0	211.9	216.0	203.9	193.8	185.4	184.0
26.0	201.0	211.5	191.0	179.1	166.9	166.0
27.0	198.0	209.8	186.5	173.5	160.8	160.0

APPENDIX D3

Film Bubble Shape

Measurements of Film Bubble Shape

Cooling Condition	Height Above Die (inches)	Bubble Radius (inches)	Angle (θ) that Tangent to Bubble Surface makes with Bubble Centerline
	0.00	1.25	5.0
	4.88	1.85	9.0
Case 1	7.13	2.19	9.0
	12.13	2.73	3.5
	14.38	2.85	0.0
	0.00	1.25	5.5
	4.88	1.85	9.0
Case 2	7.13	2.18	9.0
	12.13	2.72	3.5
	14.38	2.90	2.0
	0.00	1.25	4.5
	5.0	1.83	8.0
Case 4	7.13	2.16	9.0
	11.88	2.68	2.0
	14.38	2.86	0.0
	0.00	1.25	4.5
	5.0	1.80	8.0
Case 5	7.13	2.14	9.0
	11.88	2.72	4.0
	14.38	2.88	0.0
	0.00	1.25	5.0
	4.88	1.79	7.5
Case 6	7.13	2.10	8.5
	12.13	2.60	4.0
	14.38	2.74	0.0
	0.00	1.25	4.5
	4.88	1.79	7.5
Case 7	7.13	2.09	8.5
	12.13	2.60	4.0
	14.38	2.74	0.0

Measurements of Film Bubble Shape

Cooling Condition	Height Above Die (inches)	Bubble Radius (inches)	Angle (Θ) that Tangent to Bubble Surface makes with Bubble Centerline
Case 8	0.00	1.25	7.0
	5.00	2.15	9.0
	7.13	2.40	6.5
	11.88	2.75	2.0
	14.38	2.82	0.0
Case 9	0.00	1.25	6.0
	5.00	2.14	9.0
	7.13	2.40	6.5
	11.88	2.75	2.0
	14.38	2.83	0.0
Case 10	0.00	1.25	4.0
	5.00	2.11	10.0
	7.13	2.37	6.5
	11.88	2.75	2.0
	14.38	2.84	0.0
Case 11	0.00	1.25	4.0
	5.00	2.08	10.0
	7.13	2.37	6.5
	11.88	2.74	1.5
	14.38	2.84	0.0
Case 12	0.00	1.25	4.0
	5.00	2.07	9.5
	7.13	2.36	6.5
	11.88	2.74	1.0
	14.38	2.78	0.0
Case 13	0.00	1.25	4.0
	5.00	2.08	10.0
	7.13	2.35	6.0
	11.88	2.73	1.0
	14.38	2.77	0.0
Case 14	0.00	1.25	4.0
	5.00	2.07	9.5
	7.13	2.33	6.0
	11.88	2.71	1.0
	14.38	2.77	0.0

APPENDIX D4

Air Temperature Measurements

Case 1 Cooling Condition

Height Above Die	Radial Distance from Bubble Surface (inches)					
2.38 inches	0.3	0.5	1.0	2.0	3.0	4.0
Air Temperature(°C)	36.5	30.4	27.5	27.3	27.0	26.8
5.25 inches	0.2	0.6	0.8	1.8	2.8	3.8
Air Temperature(°C)	36.4	33.6	31.2	28.2	27.6	27.5
7.5 inches	0.6	1.2	2.2	3.2		
Air Temperature(°C)	34.6	30.7	29.0	28.3		
9.88 inches	0.5	1.2	2.2	3.2	4.2	
Air Temperature(°C)	35.2	31.2	30.1	29.2	28.8	
12.88 inches	0.5	1.1	2.1	3.1	4.1	
Air Temperature(°C)	34.4	31.6	30.4	29.5	29.3	
22.38 inches	0.5	1.0	2.0	3.0	4.0	
Air Temperature(°C)	34.4	32.0	31.3	30.3	29.7	
27.13 inches	0.2	1.0	2.0	3.0	4.0	
Air Temperature(°C)	39.6	31.2	30.3	29.9	29.3	

Case 2 Cooling Condition

Height Above Die	Radial Distance from Bubble Surface (inches)				
4.5 inches	0.4	1.5	2.5	3.9	7.0
Air Temperature(°C)	51.2	36.2	36.3	36.2	33.1
7.0 inches	0.5	1.1	2.1	3.1	6.6
Air Temperature(°C)	44.8	38.0	36.5	34.6	33.6
12.4 inches	0.5	1.5	2.5	6.0	
Air Temperature(°C)	43.7	38.4	34.1	32.4	
22.0 inches	0.5	1.0	2.0	5.5	
Air Temperature(°C)	47.8	41.0	38.9	32.0	
27.0 inches	0.5	1.5	2.5	6.0	
Air Temperature(°C)	47.4	43.8	41.8	32.4	

Case 3 Cooling Condition

Height Above Die	Radial Distance from Bubble Surface (inches)				
4.5 inches	0.4	1.5	2.5	3.5	7.0
Air Temperature(°C)	49.8	36.0	36.1	36.2	32.7
7.0 inches	0.5	1.2	2.2	3.2	6.7
Air Temperature(°C)	47.5	38.0	36.5	34.6	33.6
12.4 inches	0.6	1.6	2.6	6.1	
Air Temperature(°C)	41.3	36.0	32.2	30.8	
22.0 inches	0.1	1.1	2.1	5.6	
Air Temperature(°C)	55.0	29.2	29.2	28.8	
27.0 inches	0.5	1.5	2.5	6.0	
Air Temperature(°C)	37.9	29.2	29.1	29.1	

Case 5 Cooling Condition

Height Above Die	Radial Distance from Bubble Surface (inches)					
4.5 inches	0.4	0.7	1.5	2.5	3.5	7.0
Air Temperature(°C)	46.5	38.4	35.4	35.5	36.0	31.7
7.0 inches	0.5	1.2	2.2	3.2	6.7	
Air Temperature(°C)	42.8	37.4	35.6	32.2	32.2	
12.4 inches	0.2	0.5	1.5	2.5	6.0	
Air Temperature(°C)	49.4	41.8	35.6	33.1	32.2	
22.0 inches	0.2	1.1	2.1	5.6		
Air Temperature(°C)	38.9	29.3	30.3	30.3		
27.0 inches	0.4	1.4	2.4	5.9		
Air Temperature(°C)	36.3	29.3	29.3	28.8		

Case 6 Cooling Condition

Height Above Die	Radial Distance from Bubble Surface (inches)					
4.5 inches	0.5	1.1	1.6	2.6	3.6	7.1
Air Temperature(°C)	42.7	36.0	35.3	35.7	35.8	33.6
7.0 inches	0.5	1.2	2.2	3.2	6.7	
Air Temperature(°C)	42.2	36.0	34.0	30.3	32.2	
12.4 inches	0.5	1.0	1.5	2.5	6.0	
Air Temperature(°C)	41.1	36.5	33.1	30.8	27.9	
22.0 inches	0.1	0.6	1.1	2.1	5.6	
Air Temperature(°C)	47.5	26.7	26.9	27.4	27.7	
27.0 inches	0.4	1.4	2.4	5.9		
Air Temperature(°C)	34.1	26.6	26.6	26.7		

Case 7 Cooling Condition

Height Above Die	Radial Distance from Bubble Surface (inches)					
4.5 inches	0.5	1.0	1.5	2.5	3.5	7.0
Air Temperature(°C)	42.1	36.2	34.3	34.1	34.1	28.4
7.0 inches	0.5	0.7	1.2	2.2	3.2	6.7
Air Temperature(°C)	42.5	39.9	36.0	33.6	29.8	29.8
12.4 inches	0.5	1.0	1.5	2.0	5.5	
Air Temperature(°C)	40.8	34.6	31.2	29.3	30.3	
22.0 inches	0.5	0.8	1.3	2.3	5.8	
Air Temperature(°C)	30.3	25.9	25.9	26.3	27.9	

Case 8 Cooling Condition

Height Above Die	Radial Distance from Bubble Surface (inches)					
2.38 inches	0.4	0.5	1.0	2.0	3.0	4.0
Air Temperature(°C)	35.5	31.1	29.5	27.4	28.0	28.2
5.25 inches	0.4	0.6	1.6	2.6	3.6	
Air Temperature(°C)	35.5	31.6	28.8	28.2	27.9	
7.5 inches	0.4	1.4	2.4	3.3		
Air Temperature(°C)	38.1	30.6	29.3	29.1		
9.88 inches	0.5	1.2	2.2	3.2	4.2	
Air Temperature(°C)	34.7	31.5	30.0	29.5	29.3	
12.88 inches	0.3	1.0	2.0	3.0	4.0	
Air Temperature(°C)	39.9	31.5	30.6	29.3	28.3	
22.38 inches	0.3	1.0	2.0	3.0	4.0	
Air Temperature(°C)	40.8	31.0	29.5	29.3	28.8	
27.13 inches	0.4	1.3	2.3	3.3	4.3	
Air Temperature(°C)	35.5	31.4	30.5	30.2	29.1	

Case 9 Cooling Condition

Height Above Die	Radial Distance from Bubble Surface (inches)				
4.5 inches	0.4	1.2	2.2	3.2	6.7
Air Temperature(°C)	51.3	37.0	37.4	37.0	33.2
7.0 inches	0.4	0.7	1.7	2.7	6.2
Air Temperature(°C)	48.0	39.4	37.0	34.1	32.7
12.4 inches	0.5	1.4	2.4	5.9	
Air Temperature(°C)	44.6	37.0	34.1	33.6	
22.0 inches	0.3	1.5	2.5	6.0	
Air Temperature(°C)	56.0	42.0	40.0	33.9	
27.0 inches	0.5	1.8	2.8	6.3	
Air Temperature(°C)	49.4	44.6	43.9	34.1	

Case 10 Cooling Condition

Height Above Die	Radial Distance from Bubble Surface (inches)				
4.5 inches	0.3	1.2	2.2	3.2	7.2
Air Temperature(°C)	47.9	37.0	36.5	36.5	33.0
7.0 inches	0.4	0.9	1.9	2.9	6.9
Air Temperature(°C)	46.9	39.1	37.7	37.2	35.8
12.4 inches	0.4	1.5	2.5	6.0	
Air Temperature(°C)	46.5	38.3	34.1	28.4	
22.0 inches	0.25	1.4	2.4	5.9	
Air Temperature(°C)	49.4	42.7	38.9	33.1	
27.0 inches	0.5	1.1	2.1	3.1	6.6
Air Temperature(°C)	46.5	43.7	43.2	43.2	33.2

Case 11 Cooling Condition

Height Above Die	Radial Distance from Bubble Surface (inches)				
4.5 inches	0.3	1.1	2.1	3.1	6.6
Air Temperature(°C)	47.5	37.0	36.6	36.8	33.4
7.0 inches	0.25	0.6	1.6	2.6	6.1
Air Temperature(°C)	50.8	39.3	37.1	35.8	33.4
12.4 inches	0.4	1.5	2.5	6.0	
Air Temperature(°C)	45.6	36.5	33.6	33.2	
22.0 inches	0.5	1.5	2.5	6.0	
Air Temperature(°C)	37.9	31.2	31.5	31.7	
27.0 inches	0.5	1.8	2.8	6.3	
Air Temperature(°C)	37.0	30.8	30.8	30.6	

Case 12 Cooling Condition

Height Above Die	Radial Distance from Bubble Surface (inches)				
4.5 inches	0.5	1.3	2.3	3.3	6.8
Air Temperature(°C)	40.5	36.3	36.4	36.8	32.2
7.0 inches	0.5	1.0	2.0	3.0	6.5
Air Temperature(°C)	44.3	38.6	37.0	32.9	32.2
12.4 inches	0.5	1.5	2.5	6.0	
Air Temperature(°C)	45.6	34.3	30.8	29.8	
22.0 inches	0.5	1.6	2.6	6.1	
Air Temperature(°C)	33.5	27.9	27.8	26.9	
27.0 inches	0.4	1.6	2.6	6.1	
Air Temperature(°C)	34.1	30.3	30.3	27.9	

Case 13 Cooling Condition

Height Above Die	Radial Distance from Bubble Surface				
4.5 inches	0.5	1.5	2.5	3.5	7.0
Air Temperature(°C)	42.7	35.5	35.5	35.8	30.3
7.0 inches	0.5	1.2	2.2	3.2	6.7
Air Temperature(°C)	45.5	37.7	35.4	31.2	31.2
12.4 inches	0.5	1.5	2.5	6.0	
Air Temperature(°C)	39.9	31.4	28.5	28.6	
22.0 inches	0.6	1.6	2.6	6.1	
Air Temperature(°C)	28.8	27.4	27.6	28.4	
27.0 inches	0.5	1.7	2.7	6.2	
Air Temperautre(°C)	33.1	27.5	27.8	27.8	

Case 14 Cooling Condition

Height Above Die	Radial Distance from Bubble Surface (inches)				
4.5 inches	0.5	1.5	2.5	3.5	7.0
Air Temperature(°C)	41.3	35.1	34.7	35.1	30.3
7.0 inches	0.5	1.1	2.1	3.1	6.6
Air Temperature(°C)	42.7	37.0	34.9	29.3	28.6
12.4 inches	0.4	1.3	2.3	5.8	
Air Temperature(°C)	41.8	31.2	27.4	25.4	
22.0 inches	0.2	0.9	1.9	5.4	
Air Temperature(°C)	33.6	26.4	26.9	26.9	
27.0 inches	0.5	1.4	2.4	5.9	
Air Temperature(°C)	32.0	27.1	27.1	27.3	

APPENDIX D5

Hot Wire Anemometer Calibration Data

and

Air Velocity Measurements

Explanation of Hot Wire Anemometer Calibration Equation

The macroscopic mechanical energy balance for steady
state incompressible flow, which is called Bernoulli's,
equation (29) has the following form:

$$\frac{P_1}{\rho_1} + \frac{U_1^2}{2} + g \cdot Z_1 + W = \frac{P_2}{\rho_2} + \frac{U_2^2}{2} + g \cdot Z_2 + F$$

where subscripts 1 and 2 refer to the position of measurement
in Figure 5.11 and:

W work done by an external source

F friction-heating term

P pressure of fluid

Z distance from a given point

U velocity of fluid

g acceleration due to gravity,

This equation was rearranged to yield:

$$(\frac{P_1}{\rho_1} - \frac{P_2}{\rho_2}) + g \cdot (Z_1 - Z_2) + \tfrac{1}{2} \cdot (U_1^2 - U_2^2) = F - W$$

and the following assumptions were made to further simplify
it:

1) At point 1 the velocity U_1 is negligible.

2)   The pressure at point 2 (P_2) is equal to the local atmospheric pressure.

3)   The fluid has constant density ($\rho_1 = \rho_2 = \rho_{air}$).

4)   The gravity 'head' term $g(Z_1 - Z_2)$ is neglegible.

5). No 'pump' work is done.

6). The air is flowing out through a frictionless nozzle at position 2.

Using these assumptions and solving for U_2 results in:

$$U_2 = \left(\frac{2 \cdot (P_1 - P_{atm})}{\rho_{air}}\right)^{\frac{1}{2}}$$

The term $P_1 - P_{atm}$ was measured with a slanted arm manometer and can be rewritten in terms of the length the manometer fluid has risen in the slanted arm:

$$U_2 = \left(\frac{2 \cdot (\Delta l \sin\Phi \, \rho_{mano} \cdot g)}{\rho_{air}}\right)^{\frac{1}{2}}$$

Average Velocity and Output Voltage Data Used to Determine a Corrected Voltage Term (V_0^*) at Zero Velocity and the Exponent of the Transfer Function (Equation 4)

Slanted Arm Manometer Position						Average Output Velocity / Voltage			$(\frac{V}{V_0^*})^2 - 1$	$(\frac{V}{V_0^*})^2 - 1$	$(\frac{V}{V_0^*})^2 - 1$
1:10		1:5		1:2							
Δl_{mm}	$U_{ft/s}$	Δl_{mm}	$U_{ft/s}$	Δl_{mm}	$U_{ft/s}$	ft/s	m/s	Voltage	(s = 0.925)	(s = 1.0)	(s = 0.9)
0	0	0	0	0	0	0	0	2.77	0.17	0	
2.0	6.05	1.25	6.69	0.5	6.37	6.37	1.94	3.40	0.76	-0.51	0.86
5.0	9.57	3.0	10.4			9.97	3.04	3.57	0.94	0.66	1.05
10.0	13.5	5.5	14.0			13.8	4.20	3.72	1.11	0.80	1.23
19.5	18.9	10.5	19.4	4.5	19.1	19.1	5.83	3.88	1.30	0.96	1.42
18.5	18.4	10.3	19.2	4.5	19.1	18.9	5.76	3.90	1.32	0.98	1.45
36.5	25.9	19.5	26.4	8.0	25.5	26.0	7.90	4.04	1.49	1.13	1.63
48.5	29.8	25.0	29.9	10.5	29.2	29.6	9.03	4.14	1.62	1.23	1.76
116	46.1	59.0	45.9	25.0	45.0	45.7	13.9	4.38	1.93	1.50	2.09
		109	62.4	45.0	60.4	61.4	18.7	4.59	2.21	1.75	2.39
		131	68.4	53.0	65.6	67.0	20.4	4.65	2.30	1.82	2.48
		183	80.9	74.0	77.5	79.2	24.1	4.76	2.46	1.95	2.65
				99.5	89.9	89.9	27.4	4.87	2.62	2.09	2.82
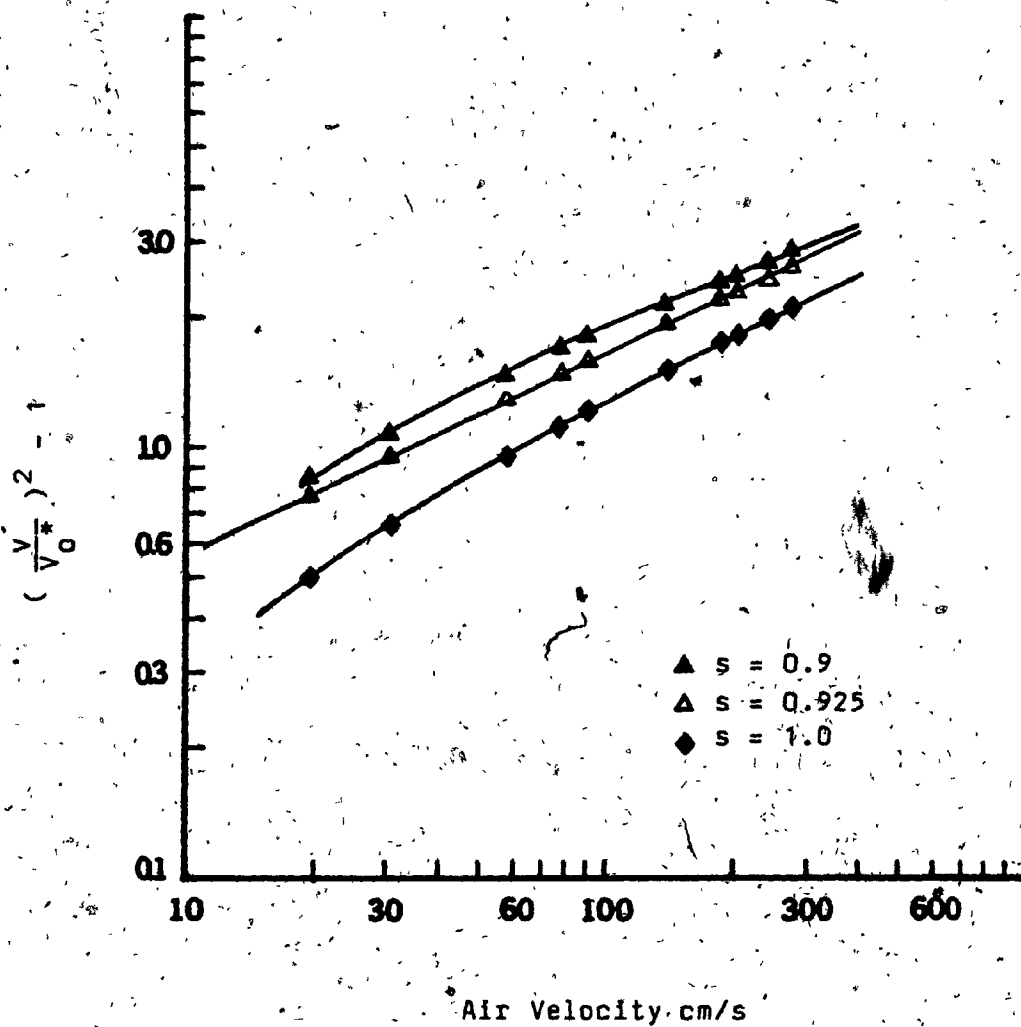
Figure D51: Determination of an Empirical Constant s
             (where $V_0^* = V_0(s)$).

Average Velocity versus Linearized and Unlinearized Output Voltage

Average Velocity		Linearized Output Voltage	Unlinearized Output Voltage	Slanted Arm Manometer Position					
				1:10		1:5		1:2	
ft/s	m/s			Δl_{mm}	$U_{ft/s}$	Δl_{mm}	$U_{ft/s}$	Δl_{mm}	$U_{ft/s}$
0	0	0	2.77	0	0	0	0	0	0
6.42	1.96	1.96	3.49	2.25	6.42				
9.00	2.75	2.77	3.61	4.0	8.56	2.5	9.45		
10.0	3.06	3.13	3.65	5.5	10.0				
12.2	3.71	3.75	3.72	7.75	11.9	4.3	12.4		
14.8	4.52	4.52	3.79	12	14.8				
17.1	5.22	5.17	3.86	15.5	16.9	8.5	17.4		
19.4	5.90	5.90	3.91	20	19.1	10.5	19.4	4.75	19.6
21.1	6.41	6.35	3.95	23	20.5	13	21.6		
25.8	7.86	7.84	4.06	35.5	25.5	19	26.1		

Air Velocity Measurements

Air Velocity Measurements under Cocurrent Cooling in meters/second

Height Above Die (inches) — Radial Distance From Bubble (inches)

		Height Above Die (inches)	0.3	0.5	0.6	0.7	0.8	1.0	1.4	1.9	2.4	2.9	3.4	4.0	5.0	5.5	6.5
Case 1 Cooling Conditions		24.9	1.65	1.71	1.71		1.70	1.68	1.66	1.59		1.32	1.29	1.10	0.78	0.57	0.38
		19.9	2.14	2.15	2.20		2.24	2.22	2.10	2.03	1.88	1.72	1.44	1.25	0.85	0.58	0.33
		14.3	2.65	2.73	2.80		2.83	2.78	2.75	2.60	2.41	2.03	1.77	1.41	0.95	0.50	0.25
		11.8		3.99		4.06	4.06	3.96	3.83	3.55	2.95	2.48	1.61	1.11	0.60	0.33	0.25
		7.7		5.55	5.40		4.71	4.15	3.43	2.55	1.60	1.00	0.65	0.35	0.25		
		4.3			6.50	6.15	5.35	4.15	2.80	1.62	0.60		0.30				
		2.1			8.60	8.28	4.80	1.80	0.72			0.30					
Case 8 Cooling Conditions		24.9	1.93	1.97	2.10		2.10	2.09	1.98	1.95	1.76	1.57	1.39	1.20	0.90	0.72	0.65
		19.9	2.25	2.30	2.31		2.36	2.30	2.22	2.16	1.90	1.75	1.50	1.28	0.95	0.62	0.40
		14.3	2.78	2.81	2.89		2.93	2.88	2.82	2.75	2.50		2.10	1.35	0.60		
		11.8	4.20	4.25	4.35		4.35	4.30	4.15	3.52	2.93	2.10	1.57		0.85	0.50	
		7.7		6.28	6.17		5.70	5.05		3.43		1.33		0.60			
		4.3			7.10	6.80	5.95	4.52	3.06	1.75	0.83		0.45		0.30		
		2.1			9.43	8.00		4.05	1.05	0.80			0.35				

-D5-8-

Air Velocity Measurements (m/s) 1.0 inch above Die

Cooling Condition	Radial Distance from Film Bubble (inches)					
	0.5	0.6	0.7	0.8	1.0	2.0
Case 2	9.25	8.28	6.55	4.62	2.35	0.25
Case 6	9.25	8.30	6.60	4.70	2.35	0.25
Case 9	9.90	8.20	5.90	3.50	2.36	0.25
Case 13		9.75	7.80	5.66	2.36	0.25

Air Velocity Measurements (m/s) 9.8 inches above Die

Cooling Condition	Radial Distance from Film Bubble (inches)			
	0.5	0.6	0.7	0.8
Case 2	3.60	3.41	3.20	2.94
Case 4	3.55	3.37	3.11	2.92
Case 5	3.43	3.20	3.03	2.80
Case 6	3.10	2.93	2.86	2.65
Case 9	4.89	4.70	4.46	4.03
Case 11	4.76	4.70	4.42	4.05
Case 12	4.72	4.65	4.30	4.03
Case 13	4.54	4.31	4.00	3.60

Air Velocity Measurements (m/s) 23.1 inches above Die

Cooling Condition	Radial Distance from Film Bubble (inches)														
	0.3	0.35	0.4	0.45	0.6	0.8	1.0	1.2	1.4	1.5	1.7	1.8	1.9	2.0	2.3
Case 2	0.96		0.97		1.10	1.11	1.09	1.09	0.97		0.80			0.68	
Case 4	0.90		1.02		1.13	1.29	1.53	1.60	1.60		1.70		1.70		
Case 5	1.28		1.36		2.55	3.43	3.60	3.70		3.70		3.90			4.45
Case 6		3.45		4.00	5.63	5.95	6.05		6.24		6.40			6.90	7.70
Case 9	1.27		1.32		1.34	1.35	1.35	1.34	1.30		1.18			1.00	
Case 11	0.65		0.77		1.05	1.26	1.38	1.45	1.46		1.50			1.55	1.57
Case 12	1.22		1.36		2.35	3.35	3.55	3.60	3.70		3.70			3.90	4.35
Case 13	2.80		3.70		5.70	6.20	6.22	6.22	6.23		6.40			6.80	7.60

Air Velocity Measurements (m/s) 29.6 inches above Die

Cooling Condition	Radial Distance from Film Bubble (inches)									
	0.3	0.5	0.7	1.0	1.5	2.0	2.5	3.0	3.5	4.0
Case 2 (probe turned down, sensor 24 in. above die)			0.60	0.75	0.87	0.89	0.88	0.80		
Case 4	0.10	0.10	0.10	0.10	0.10	0.12	0.14	0.14	0.14	0.13
Case 5	0.10	0.09	0.10	0.10	0.16	0.21	0.21	0.22	0.22	0.20
Case 6	0.22	0.21	0.21	0.25	0.30	0.34	0.36	0.38	0.39	0.36
Case 9 (probe turned down, sensor 24 in. above die)			0.62	0.78	0.89	0.91	0.94	0.90		
Case 11	0.08	0.07	0.07	0.08	0.10	0.11	0.11	0.12	0.12	0.12
Case 12	0.12	0.11	0.12	0.14	0.18	0.19	0.20	0.20	0.21	0.20
Case 13	0.24	0.23	0.21	0.24	0.31	0.35	0.37	0.37	0.37	0.36

Air Velocity Measurements (m/s) 33.3 inches above die with sensor pointed downward and 38.8 inches above die with sensor turned upward

Cooling Condition	Height of Sensor above Die	Radial Distance from Film Bubble (inches)										
		0.3	0.4	0.5	0.7	1.0	1.5	2.0	2.5	3.0	3.5	4.0
Case 2	33.3	0.41	0.43	0.44	0.47	0.51	0.53	0.56	0.56	0.56	0.55	0.50
	38.8	0.03	0.04	0.04	0.04	0.05	0.07	0.08	0.09	0.10		0.10
Case 4	33.3	0.11	0.10	0.10	0.10	0.11	0.12	0.12		0.12		
	38.8	0.05	0.05	0.04	0.04	0.04		0.04				
Case 5	33.3	0.11	0.11	0.10	0.09	0.10	0.10		0.10			
	38.8	0.03	0.03	0.03	0.03	0.03		0.04		0.04		
Case 6	33.3	0.06	0.05	0.05	0.05			0.05				
Case 9	33.8	0.35	0.37	0.39	0.43	0.47	0.55	0.58	0.61	0.60	0.58	0.52
	38.8	0.05	0.04	0.04	0.05	0.05	0.06	0.07	0.07	0.08		
Case 11	33.3	0.08	0.09	0.09	0.09	0.10	0.10	0.10		0.11		
	38.8	0.03	0.03	0.03	0.03	0.04		0.04				
Case 12	33.3	0.08	0.08	0.08	0.08	0.08	0.08					
	38.8	0.03	0.03	0.03	0.03	0.03		0.03		0.03		
Case 13	33.3	0.06	0.06	0.06	0.07	0.07		0.07		0.06		

Calculation of Continuity of Mass Under the Cocurrent and Combination Cooling Conditions Measured in Figure 6.19.

The density of cooling air was assumed constant under the conditions of Cases 2 and 6 and Cases 9 and 13. Preservation of continuity within the cylindrical shroud was demonstrated by calculating the volumetric flow rate for each cooling condition. The equation $Q = U \times A$ was used, where Q is the volumetric flow rate, U the average air velocity (obtained from the measurements shown in Figure 6.19) and A the annular area between film bubble and obstruction plate at 9.8 inches above the die. The results of these calculations are shown in the following table:

Cooling Condition	Film Bubble Diameter (inches)	Obstruction Plate Diameter (inches)	Annular Area (feet^2)	Average Velocity Across Annular Area (ft/s)	Volumetric Flow Rate (cfm)	Differences in Calculated Flow Rates Between Cases 2 and 6 and Cases 9 and 13
Case 2	4.86	7.25	0.158	10.8	102	
						4 %
Case 6	4.59	7.25	0.172	9.5	98	
Case 9	5.26	7.25	0.136	14.8	121	
						6 %.
Case 13	5.18	7.25	0.140	13.5	114	

APPENDIX D6

Film Thickness Measurements

and

Thermal Analysis Data

Measurements of Film Thickness at Various Distances from the Die

Overall Average Thickness (mils)	Height Above Die (inches)	Cooling Condition					
		Case 1			Case 8		
		Average Thickness	Standard Deviation	Sample Size	Average Thickness	Standard Deviation	Sample Size
12.1	2	13.67	2.22	9	10.53	4.97	9
6.9	3	8.03	0.81	19	5.73	0.83	18
4.9	4	5.29	0.73	22	4.45	0.61	22
3.7	5	3.86	0.74	26	3.47	0.73	25
3.1	6	3.19	0.68	29	3.01	0.73	29
2.7	7	2.85	0.67	30	2.56	0.76	31
2.4	8	2.49	0.63	29	2.36	0.69	32
2.2	9	2.23	0.64	32	2.07	0.67	33
2.0	10	2.03	0.58	33	1.89	0.52	34
1.8	11	1.88	0.55	32	1.74	0.45	34
1.7	12	1.81	0.56	35	1.63	0.43	34
1.7	13	1.76	0.54	35	1.63	0.37	36
1.7	14	1.74	0.57	35	1.63	0.34	36
1.6	15	1.70	0.40	36	1.63	0.29	36
1.6	16	1.67	0.36	36	1.63	0.28	35
1.6	17				1.63	0.33	33

Emissivity as a Function of Film Thickness
(from reference 27)

Film Thickness (mil)	Emissivity
2.20	0.299
3.12	0.060
4.81	0.422
5.71	0.455
8.79	0.556
11.88	0.612

Thermal Analysis Results

The following equation was used to calculate specific
heats from a differential thermal analysis specrtum:

$$\frac{dH}{dt} = m \cdot C_p \cdot \frac{dT}{dt}$$

or

$$C_p = \frac{\Delta H / \Delta t}{\Delta T / \Delta t \cdot (m)}$$

where:

Cp	specific heat
H	enthalpy
m	mass of sample
T	temperature

Substitution of values from the DTA thermogram into the
above equation allowed the following table to be generated:

Calculated Specific Heat Values as a Function of Temperature

Temperature (°C)	Specific Heat (cal/g °C) (at $\Delta T/\Delta t$ = 20 °C/min)
53.7	0.64
57.4	0.66
62.9	0.72
66.6	0.72
72.1	0.81
75.8	0.85
81.3	0.88
85.0	0.92
90.5	0.99
94.2	1.07
99.7	1.21
103.4	1.39
109.3	2.07
108.9	2.14
112.6	1.68
118.1	0.96
121.8	0.75
127.3	0.64
131.0	0.62
136.5	0.61
140.2	0.61
146.3	0.60

APPENDIX D7

Heat Transfer Coefficient Calculations

Sample Calculation of Heat Transfer Coefficient

A heat balance over an element of film bubble was given in Equation 6:

$$\dot{m}\, C_p\, \cos\theta\, dT_s/dz + \dot{m}\, H_c\, \cos\theta\, dX_c/dz =$$
$$\Pi D\, [\, h\, (T_s - T_c) + e\, K\, (T_s^4 - T_a^4)\,] \quad (6)$$

The above equation was rearranged to solve for the heat transfer coefficient h outside the frostline region.

$$h = \frac{\dfrac{\dot{m}\, C_p\, \cos\theta\, dT_s/dz}{\Pi D} - e\, K\, (T_s^4 - T_a^4)}{T_s - T_c}$$

The following values were used to obtain the local heat transfer coefficient at 6 inches above the die under cooling conditions of Case 1.

$$
\begin{aligned}
\dot{m} &= 7590\ \text{g/hr} \quad (0.28\ \text{lb/min}) \\
C_p &= 0.6\ \text{cal/g}\,^\circ\text{C} \\
\theta &= 9.0^\circ \\
D &= 0.1\ \text{m} \quad (4\ \text{inches}) \\
T_s &= 436.6\ \text{K} \quad (326\,^\circ\text{F}) \\
T_c &= 297.0\ \text{K} \quad (75\,^\circ\text{F}) \\
T_a &= 297.0\ \text{K} \quad (75\,^\circ\text{F}) \\
z &= 0.15\ \text{m} \quad (6\ \text{inches}) \\
dT_s/dz &= 5.7\,^\circ\text{C/cm} \\
e &= 0.37 \\
K &= 1.355 \times 10^{-12}\ \text{cal/s cm}^2\ \text{K}^4
\end{aligned}
$$

Substitution of these values in the above equation yields:

$$h = \cfrac{\cfrac{(7590 \text{ g/hr})(0.6 \text{ cal/g C})(0.001 \text{ kcal/cal})(\cos 9)(510 \text{ C/m})}{\Pi(0.1 \text{ m})}}{(436.6 \text{ K} - 297.0 \text{ K})} -$$

$$\cfrac{(0.37)(1.355 \times 10^{-8} \text{ cal/s m}^2 \text{ K}^4)(0.001 \text{ kcal/cal})(3600 \text{ s/hr})}{(436.6 \text{ K} - 297.0 \text{ K})} \text{ x}$$

$$\cfrac{[(436.6 \text{ K})^4 - (297.0 \text{ K})^4]}{(436.6 \text{ K} - 297.0 \text{ K})}$$

$$h = 55.9 \text{ kcal/hr m}^2 \text{ K}$$

Contributions of Terms in Heat Transfer Coefficient Calculations
at 22 and 27 inches above the die

$$h = \frac{\dot{m}\, C_p \cos\theta\, (dT/dz)}{\Pi D\, (T_s - T_c)} - \frac{e\, \dot{K}\, (T_s^4 - T_a^4)}{T_s - T_c} \qquad (6)$$

Cooling Condition	Percent Contribution of Term: $\dot{m}\, C_p \cos\theta\, (dT_s/dz)(1/T_s - T_c)$		Percent Contribution of Term: $e\, K\, (T_s^4 - T_a^4)(1/T_s - T_c)$	
	22 inches	27 inches	22 inches	27 inches
Case 1	86%	60%	14%	40%
Case 2	85%	80%	15%	20%
Case 8	89%	70%	11%	30%
Case 9	87%	84%	13%	16%

Calculated Heat Transfer Coefficients at Various
Distances from the Die

Height Above Die (inches)	Case 1 Cooling Conditions Heat Transfer Coefficient (kcal/hr m²K)	Case 8 Cooling Conditions Heat Transfer Coefficient (kcal/hr m²K)
2.0		23.3
3.0	24.2	33.1
3.4	31.0	35.0
4.0	41.6	51.5
4.5	54.5	60.3
5.4	54.4	60.5
6.0	55.9	60.7
7.0	48.8	61.7
8.0	45.4	55.4
9.0	41.9	51.5
10.0	37.8	47.0
11.0	34.7	
12.0		
13.0		Frostline Region
14.0	Frostline Region	
15.0		
16.0		28.6
17.0	19.6	26.0
18.0	18.9	24.5
19.0	17.6	23.2
20.0	15.9	22.0
21.0	15.6	19.0
22.0	14.4	18.0
23.0	12.8	16.5
24.0	10.9	14.8
25.0	7.6	10.8
26.0	6.1	8.4
27.0	5.0	6.3

Calculated Heat Transfer Coefficients Under Cocurrent and Combination
Cooling Conditions at Various Distances from the Die

Height Above Die (inches)	Heat Transfer Coefficients (kcal/hr m^2 K)					
	Case 2	Case 3	Case 4	Case 5	Case 6	Case 7
22	10.3	6.7	13.4	20.7	25.1	25.3
23	10.5	7.8	14.7	21.5	26.2	26.2
26	10.7	8.9	16.0	21.3	30.0	30.3
27	10.9	9.0	16.3	22.2	31.3	32.1

Calculated Heat Transfer Coefficients Under Cocurrent and Combination
Cooling Conditions at Various Distances from the Die

Height Above Die (inches)	Heat Transfer Coefficients (kcal/hr m^{2}K)					
	Case 9	Case 10	Case 11	Case 12	Case 13	Case 14
22	13.7	8.8	17.0	22.5	27.6	27.8
23	13.0	8.4	17.1	22.3	27.8	28.2
26	13.0	6.5	15.8	20.9	27.6	27.9
27	12.8	6.0	15.9	21.6	28.8	29.1

Heat Transfer Coefficients and Cooling Air Velocities
at Various Distances from the Die

Height Above Die (inches)	Case 1 Cooling Conditions		Case 8 Cooling Conditions	
	h (kcal/hr m^{2}K)	U (m/s) 0.5 inches from film	h (kcal/hr m^{2}K)	U (m/s) 0.5 inches from film
3.0	24.2	7.85	33.1	8.85
3.4	31.0	7.60	35.0	8.60
4.0	41.6	7.25	51.5	8.20
4.5	54.5	7.00	60.3	7.85
5.4	54.4	6.50	60.5	7.30
6.0	55.5	6.20	60.7	6.90
7.0	48.8	5.70	61.7	6.30
8.0	45.4	5.20	55.4	5.80
9.0	41.9	4.75	51.5	5.25
10.0	37.8	4.35	47.0	4.80
11.0	34.7	4.00		
12.0				
13.0			Frostline Region	
14.0	Frostline Region			
15.0				
16.0			28.6	2.90
17.0	19.6	2.50	26.0	2.70
18.0	18.9	2.35	24.5	2.52
19.0	17.6	2.25	23.2	2.40
20.0	15.9	2.15	22.0	2.25
21.0	15.6	2.05	19.0	2.10
22.0	14.4	1.95	18.0	2.00
23.0	12.8	1.90	16.5	1.95
24.0	10.9	1.85	14.8	1.90
25.0	7.6	1.80	10.8	1.85
26.0	6.1	1.77	8.4	1.82
27.0	5.0	1.75	6.3	1.79

Calculated Nusselt and Reynolds Numbers
at Various Distances from the Die

Height Above Die (inches)	Case 1 Cooling Conditions			Case 8 Cooling Conditions		
	L (inches)	Nu	Re	L (inches)	Nu	Re
6.0	0.0	0.0	0.0			
7.0	1.0	54.4	230	0.0	0.0	0.0
8.0	2.0	101.2	420	1.0	68.8	234
9.0	3.0	140.1	575	2.0	123.6	424
10.0	4.0	168.7	702	3.0	157.3	581
11.0	5.0	193.3	807	4.0		
12.0	6.0			5.0		
13.0	7.0			6.0	Frostline Region	
14.0	8.0	Frostline Region		7.0		
15.0	9.0			8.0		
16.0	10.0			9.0	286.9	1054
17.0	11.0	240.6	1110	10.0	289.9	1090
18.0	12.0	251.0	1138	11.0	300.8	1119
19.0	13.0	255.5	1181	12.0	311.1	1163
20.0	14.0	248.6	1215	13.0	318.7	1181
21.0	15.0	260.2	1241	14.0	269.9	1187
22.0	16.0	257.4	1259	15.0	301.2	1211
23.0	17.0	243.1	1304	16.0	295.2	1259
24.0	18.0	218.1	1344	17.0	280.5	1304
25.0	19.0	161.5	1381	18.0	216.7	1344
26.0	20.0	135.0	1429	19.0	177.2	1396
27.0	21.0	116.9	1483	20.0	141.0	1445

Calculated Crystallinity Values over the Frostline Region

Height Above Die (inches)	Case 1 Cooling Conditions		Case 8 Cooling Conditions	
	dXc/dz	Percent Crystallinity	dXc/dz	Percent Crystallinitty
9.0		0		0
10.0		0	0.051	5
11.0	0.052	5	0.047	10
12.0	0.036	9	0.045	14.5
13.0	0.034	12	0.041	18.5
14.0	0.032	15.5	0.038	22
15.0	0.029	18.5	0.035	25.5
16.0	0.027	22	0.031	28.5
17.0	0.024	24		

This analysis assumes that crystallization starts at the frostline region, that is, the molten portion of the film bubble is predominantly amorphous.

APPENDIX E

Error Analysis

Error Analysis

If a calculated result, y, is dependent on the variables x_1, x_2, ...x_n, then the uncertainty, e_y, in the calculated result is given by:

$$e_y = [(\frac{\partial y}{\partial x_1} e_1)^2 + (\frac{\partial y}{\partial x_2} e_2)^2 + \ldots (\frac{\partial y}{\partial x_n} e_n)^2]^{\frac{1}{2}}$$

where e_1, e_2, ...e_n are the uncertanties in the variables x_1, x_2, ...x_n.

The above equation is applied to the appropriate expressions employed in the calculation of the various measured quantities shown in the following sections.

Air Flow Rates

The experimental error of the distance-manometer fluid has risen in a slanted-arm (Δl) was estimated to be 5%.

Velocity a distance
y from the wall of
the pipe

$$U_y = F\,(2.\Delta l\,\sin\theta\,\rho_m\,g/\rho_{air})^{\frac{1}{2}}$$

$$e_{U_y} = F\cdot(2\cdot\sin\theta\cdot\rho_m\cdot g\,/\,\rho_{air})^{\frac{1}{2}}\cdot(\tfrac{1}{2}\cdot\Delta l^{-\frac{1}{2}})\cdot e_{\Delta l}$$

$$e_{U_y} = (0.98)\cdot[(2)\cdot\sin(5.8)\cdot(62.2)\cdot(32.2)\,/\,(0.072)]^{\frac{1}{2}}\cdot$$
$$(0.5)\cdot(0.016)^{-\frac{1}{2}}\cdot(0.05)$$

Percentage error $= \dfrac{14}{126} \times 100 = 11\%$

Surface Temperature Measurements

The experimental error in measuring film surface temperature was estimated to be 5° F by the manufacturer(31). This corresponds to an error of four percent (5/125 = 0.04).

The reproducibility of these measurements was five percent.

Unrestrained Shrinkage

The experimental errors in the various measured quantities were estimated to be:

Variable	Error
Initial diameter (Di)	2.5 %
Final diameter (Df)	2.5 %

Percent Unrestrained Shrinkage = $((D_i - D_f)/D_f)100$

$$e_{Shrinkage} = [(100 \cdot \frac{D_f}{D_i^2} \cdot e_{D_i})^2 + (100(1 - \frac{1}{D_i}) \cdot e_{D_f})^2]^{\frac{1}{2}}$$

$$e_{Shrinkage} = [[(100) \cdot \frac{(1.9)}{(2^2)} \cdot (0.025)]^2 + [(100) \cdot (1 - \frac{1}{2}) \cdot (0.025)]^2]^{\frac{1}{2}}$$

$$e_{Shrinkage} = 1.72$$

Percent unrestrained shrinkage error = $\frac{1.72}{75} \times 100 = 2.3\%$

Elmendorf Tear

The experimental errors in the various measured quantities were estimated to be:

Variable	Error
Elmendorf apparatus scale reading (S)	1 %
Film thickness (b)	2 %

Elmendorf tear result = $(S)16/b$

$$e_{\substack{Elmendorf \\ Tear}} = [(\frac{16}{b} \cdot e_{\substack{Tear \\ Value}})^2 + (\frac{Tear\ Value}{b^2} \cdot 16 \cdot e_b)^2]^{\frac{1}{2}}$$

$$e_{\substack{Elmendorf \\ Tear}} = [(\frac{16}{1.5} \cdot (0.0\blacksquare))^2 + (\frac{20 \cdot (16)}{(1.5)^2} \cdot (0.02))^2]^{\frac{1}{2}}$$

$$e_{\substack{Elmendorf \\ Tear}} = 8.1$$

Percentage error $= \frac{8.1}{143} \times 100 = 5.7\%$

Sonic Velocity

The experimental errors in measuring sonic velocity were estimated to be two percent (49).

The reproducibility of these measurements were five percent.

Birefringence

The experimental errors in the various measured quantities were estimated to be:

Variable	Error
Phase difference	7.0×10^{-5} um
Film thickness (b)	2.5 um

$$\text{Birefringence} = \text{Phase difference}/b$$

$$e_{\text{Birefringence}} = \left[\left(\frac{1}{b} \cdot e_{\text{Phase Change}}\right)^2 + \left(-\frac{\text{Phase Change}}{b^2} \cdot e_b\right)^2\right]^{\frac{1}{2}}$$

$$e_{\text{Birefringence}} = \left[\left(\frac{1}{45.7} \cdot (7.0 \times 10^{-5})\right)^2 + \left(\frac{(40 \times 10^{-3})}{(45.7)^2} \cdot (2.5)\right)^2\right]$$

$$e_{\text{Birefringence}} = 4.79 \times 10^{-5}$$

$$\text{Percent error} = \frac{4.79 \times 10^{-5}}{4.49 \times 10^{-4}} \times 100 = 11\%$$

The reproducibility of the birefringence measurement was found to be 15%.

APPENDIX G

Physical Property Measurements

APPENDIX G1

Unrestrained Shrinkage

Unrestrained Shrinkage

Cooling Condition	Sample Number	Percent Shrinkage MD	TD
Case 1	1	75	10
	2	70	20
	3	70	10
	4	65	14
	5	70	14
Case 2	1	70	20
	2	55	10
	3	65	25
	4	65	25
	5	70	10
	6	70	5
	7	65	20
	8	65	5
Case 3	1	65	10
	2	70	15
	3	65	10
	4	60	25
	5	65	10
	6	65	15
	7	70	20
	8	60	15
Case 4	1	65	15
	2	70	20
	3	70	25
	4	70	20
	5	70	25
	6	70	10
	7	70	10
	8	70	15

Cooling Condition	Sample Number	Percent Shrinkage	
		MD	TD
Case 5	1	70	15
	2	70	20
	3	70	10
	4	70	15
	5	70	25
	6	65	20
	7	70	20
	8	65	15
Case 6	1	65	10
	2	75	15
	3	75	10
	4	65	20
	5	70	25
	6	75	25
	7	70	15
	8	70	30
Case 7	1	75	10
	2	70	10
	3	75	10
	4	70	15
	5	70	25
	6	70	15
	7	70	10
	8	65	25
Case 8	1	70	15
	2	75	10
	3	65	15
	4	70	20
	5	70	0
	6	70	20
	7	70	0
	8	75	10

Cooling Condition	Sample Number	Percent Shrinkage	
		MD	TD
Case 9	1	75	5
	2	70	20
	3	75	20
	4	70	5
	5	70	15
	6	70	5
	7	75	15
	8	65	20
Case 10	1	75	0
	2	75	10
	3	80	20
	4	75	20
	5	75	15
	6	75	25
	7	75	15
	8	70	5
Case 11	1	75	10
	2	70	20
	3	70	20
	4	70	0
	5	75	15
	6	70	20
	7	75	5
	8	75	0
Case 13	1	75	10
	2	75	20
	3	75	10
	4	75	25
	5	75	20
	6	75	15
	7	75	5
	8	75	10

Cooling Condition	Sample Number	Percent Shrinkage	
		MD	TD
Case 14	1	75	15
	2	70	10
	3	75	15
	4	75	20
	5	70	15
	6	70	5
	7	75	10
	8	70	10

APPENDIX G2

Elmendorf Tear

Elmendorf Tear

Cooling Condition	Sample Number	Elmendorf Tear (g/mil)	
		MD	TD
Case 1	1	165	238
	2	155	212
	3	161	219
	4	160	201
	5		208
	6		199
Case 2	1	160	215
	2	184	253
	3	155	232
	4	141	172
	5	168	210
	6		216
Case 3	1	191	215
	2	137	219
	3	154	256
	4	128	271
	5	155	194
	6	173	209
Case 4	1	166	232
	2	192	249
	3	160	225
	4	160	218
	5	128	201
	6	154	225

Cooling Condition	Sample Number	Elmendorf Tear (g/mil)	
		MD	TD
Case 5	1	164	221
	2	176	217
	3	139	222
	4	142	190
	5	109	256
	6		197
Case 6	1	143	213
	2	123	229
	3	145	192
	4	92	216
	5	182	213
	6	154	211
Case 7	1	124	213
	2	190	201
	3	139	194
	4	142	216
	5	165	225
	6	143	204
Case 8	1	118	213
	2	160	190
	3	108	225
	4	92	213
	5	186	236
	6	111	198
Case 9	1	156	244
	2	143	228
	3	179	224
	4	176	213
	5	204	200
	6	143	232

Cooling Condition	Sample Number	Elmendorf Tear (g/mil) MD	TD
Case 10	1	104	160
	2	76	274
	3	186	204
	4	202	228
	5	112	183
Case 11	1	163	213
	2	154	221
	3	194	229
	4	134	240
	5	135	199
	6	152	216
Case 12	1	130	210
	2	140	193
	3	200	197
	4	133	242
	5	155	197
	6	151	244
Case 13	1	142	214
	2	147	251
	3	203	223
	4	158	218
	5	153	239
	6	208	265
Case 14	1	72	199
	2	180	225
	3	179	229
	4	200	214
	5	170	238
	6	165	244

APPENDIX G3

Sonic Velocity and Birefringence

Sonic Velocity and Birefringence

Cooling Condition	Sample Number	Sonic Velocity (km/s)		Birefringence $(x\ 10^{2})$
		MD	TD	
*Case 1	1	1.66	1.69	3.65
	2	1.63	1.66	3.43
	3	1.71	1.69	4.50
	4	1.63	1.72	4.50
	5	1.64	1.73	4.62
	6	1.68	1.69	1.34
	7	1.67	1.74	2.32
	8	1.64	1.78	3.90
	9	1.66	1.77	1.02
	10	1.71	1.72	1.05
Case 2	1	1.78	1.78	4.62
	2	1.64	1.85	2.57
	3	1.73	1.85	5.87
	4	1.73	1.73	5.02
	5	1.62	1.73	6.51
	6	1.55	1.74	2.73
	7	1.74	1.85	3.92
	8	1.55	1.89	-6.35
	9	1.78	1.91	5.37
	10	1.78	1.81	3.13
Case 3	1	1.67	1.86	7.04
	2	1.66	1.73	6.60
	3	1.73	1.74	10.33
	4	1.71	1.82	7.00
	5	1.71	1.86	3.94
	6	1.73	1.78	2.61
	7	1.69	1.87	3.81
	8	1.68	1.85	3.58
	9	1.78	1.73	2.45
	10	1.64	1.76	2.83

Cooling Condition	Sample Number	Sonic Velocity (km/s)		Birefringence ($\times 10^4$)
		MD	TD	
Case 4	1	1.78	1.80	2.03
	2	1.73	1.86	2.86
	3	1.70	1.80	6.05
	4	1.73	1.80	4.85
	5	1.73	1.80	4.46
	6	1.73	1.80	3.41
	7	1.63	1.82	3.16
	8	1.78	1.77	4.85
	9	1.78	1.68	-1.15
	10	1.73	1.85	-2.95
Case 5	1	1.70	1.70	2.37
	2	1.70	1.81	4.23
	3	1.67	1.73	6.51
	4	1.67	1.83	5.00
	5	1.69	1.73	6.33
	6	1.73	1.76	2.82
	7	1.78	1.81	2.53
	8	1.73	1.86	1.80
	9	1.66	1.85	1.51
	10	1.70	1.79	-3.12
Case 6	1	1.56	1.78	2.99
	2	1.52	1.86	3.38
	3	1.69	1.78	5.00
	4	1.64	1.80	5.61
	5	1.72	1.74	3.77
	6	1.57	1.78	2.32
	7	1.67	1.77	3.52
	8	1.57	1.78	5.17
	9	1.60	1.74	2.65
	10	1.66	1.78	3.49

Cooling Condition	Sample Number	Sonic Velocity (km/s)		Birefringence $(\times 10^4)$
		MD	TD	
Case 7	1	1.69	1.73	7.71
	2	1.67	1.73	5.05
	3	1.70	1.75	6.42
	4	1.66	1.66	5.42
	5	1.70	1.84	3.44
	6	1.66	1.73	1.48
	7	1.71	1.66	4.23
	8	1.67	1.66	1.61
	9	1.59	1.66	1.42
	10	1.62	1.73	1.42
Case 8	1	1.61	1.69	4.73
	2	1.59	1.71	4.78
	3	1.69	1.72	4.83
	4	1.67	1.77	4.72
	5	1.63	1.66	7.48
	6	1.65	1.70	2.87
	7	1.63	1.68	1.56
	8	1.60	1.67	3.13
	9	1.70	1.68	1.57
	10	1.70	1.73	3.40
Case 9	1	1.69	1.73	4.18
	2	1.66	1.74	4.77
	3	1.66	1.75	9.63
	4	1.69	1.73	5.96
	5	1.66	1.76	4.40
	6	1.66	1.71	2.07
	7	1.63	1.67	2.90
	8	1.66	1.77	6.60
	9	1.67	1.68	3.07
	10	1.64	1.73	2.65

Cooling Condition	Sample Number	Sonic Velocity (km/s)		Birefringence $(\times 10^4)$
		MD	TD	
Case 10	1	1.60	1.69	7.33
	2	1.58	1.69	5.17
	3	1.62	1.69	6.06
	4	1.67	1.70	3.38
	5	1.65	1.68	4.30
	6	1.60	1.68	4.13
	7	1.67	1.67	4.51
	8	1.62	1.69	3.83
	9	1.55	1.69	4.74
	10	1.65	1.69	-1.88
Case 11	1	1.71	1.86	4.85
	2	1.67	1.74	3.85
	3	1.67	1.80	7.66
	4	1.66	1.76	3.54
	5	1.69	1.86	4.93
	6	1.67	1.73	2.01
	7	1.71	1.75	1.09
	8	1.69	1.69	1.60
	9	1.67	1.71	4.18
	10	1.68	1.73	2.78
Case 12	1	1.69	1.73	3.70
	2	1.71	1.77	3.51
	3	1.63	1.77	7.98
	4	1.70	1.76	7.40
	5	1.66	1.68	3.47
	6	1.67	1.65	3.04
	7	1.71	1.75	2.29
	8	1.64	1.85	3.51
	9	1.71	1.78	1.80
	10	1.66	1.74	1.80

Cooling Condition	Sample Number	Sonic Velocity (km/s)		Birefringence $(x \cdot 10^4)$
		MD	TD	
Case 13	1	1.44	1.67	3.55
	2	1.62	1.77	3.53
	3	1.55	1.61	5.32
	4	1.63	1.68	4.99
	5	1.63	1.77	5.32
	6	1.63	1.67	1.56
	7	1.44	1.66	4.00
	8	1.53	1.58	1.25
	9	1.58	1.71	2.45
	10	1.51	1.67	1.00
Case 14	1	1.64	1.73	4.89
	2	1.64	1.68	6.83
	3	1.62	1.67	5.05
	4	1.55	1.70	3.32
	5	1.57	1.71	4.21
	6	1.57	1.71	4.21
	7	1.59	1.67	3.90
	8	1.55	1.69	4.00
	9	1.65	1.69	3.73
	10	1.59	1.64	2.15